Event-related and resting-state oscillatory dynamics in the healthy ageing brain: how EEG-age and MEG-age can be used as markers of general brain functioning

Thomas Martin James

Doctor of Philosophy

Aston University

December 2024

Aston University

Event-related and resting-state oscillatory dynamics in the healthy ageing brain: how EEG-age and MEG-age can be used as markers of general brain functioning

Thomas Martin James

Doctor of Philosophy

2024

Abstract

With an ageing global population, the number of older adults with deleterious age-related changes in the brain, including dementia, will continue to increase unless we can make progress in the early detection and treatment of such conditions. This thesis presents a set of research projects that have used EEG and MEG to advance our understanding of oscillatory dynamics in the ageing human brain. First, the Firefly Model (FM) of short-term, event-related oscillatory dynamics was tested. The FM offered an empirically credible, alternative explanation of information processing that relies on systematic oscillatory phase synchronisation and frequency slowing. Second, inspired by the aphorism, 'All models are wrong, but some are useful', the FM was used to develop a new phase-based metric – time of synchronisation gradient, $t_{synch}G$ – for tracking age-related changes in the brain. This $t_{synch}G$ metric was established as a new EEG-estimate of brain age, with EEG-age significantly correlating with chronological age, before being estimated in MEG for the first time. Thereafter, long-term, resting-state oscillatory dynamics were examined, with peak alpha frequency (PAF) and alternative amplitude-based EEG-age estimates examined as distinct methods of tracking age-related changes in the brain. Using multivariate methods to analyse the broad EEG power spectrum (0.1 Hz to 45 Hz), the resting-state EEG-age and chronological age were also correlated strongly, and EEG-age was a more accurate estimate and accounted for more variance in chronological age than well-established PAF estimates of age. In summary, new phase, frequency, and amplitude metrics are introduced as estimates of brain age, framed as markers of general brain functioning. This thesis offers novel contributions to our understanding of the ageing human brain and how to detect and track deleterious age-related changes. There is substantial scope for research projects to build on these foundations, particularly in enhancing the signal-to-noise ratio of the newly established metrics.

Keywords: Ageing brain; Age-related changes; Brain age; Chronological age; EEG; General brain functioning; Human lifespan; Information processing; MEG; Oscillatory dynamics.

Acknowledgements

Thank you to my mum, Linda James, and partner, Bethan Sykes; I am so grateful for your support and encouragement in the highs and lows, and I could not have completed this PhD without you. Thank you to all the teachers, colleagues, friends, and other family members who supported me into and throughout this PhD journey. Thank you to my previous and current associate supervisors, Dr Carol Holland, Dr Charlotte Hartwright, Prof Klaus Kessler, and Dr Caroline Witton, and thank you to Dr Sian Worthen for your support with MEG. Last but certainly not least, thank you to my primary supervisor, Prof Adrian Burgess. You have been a source of inspiration, life-affirming wit, and wisdom; thank you for your supervision and friendship.

List of contents

List of abbreviations 7

Chapter 1: An introduction to this PhD thesis 11
1.1 Why is this thesis examining oscillatory dynamics in the ageing brain? 11
1.2 The aims of this thesis 14
1.3 An outline of the chapters of this thesis 16

Chapter 2: A review of the EEG and MEG methods and analyses used in this thesis 17
2.1 EEG and MEG signal detection methods 18
2.1.1 EEG methodology 18
2.1.2 MEG methodology 22
2.2 EEG and MEG data analyses: measuring event-related oscillatory dynamics 26
2.2.1 Evoked and induced changes in the EEG and MEG 26
2.2.2 The Firefly Model of synchronisation through cross-frequency phase modulation: introducing the time of synchronisation gradient ($t_{synch}G$) 34
2.3 EEG and MEG data analyses: measuring resting-state oscillatory dynamics 40
2.3.1 Peak alpha frequency 40
2.3.2 Introducing alternative metrics in resting-state paradigms 43

Chapter 3: Testing the Firefly Model of synchronisation through cross-frequency phase modulation: establishing $t_{synch}G$ 45
3.1 Introduction 45
3.2 Methods 47
3.2.1 Participants 47
3.2.2 EEG recording 48
3.2.3 Data preparation 49
3.2.4 Signal analysis 50
3.3 Results 52
3.3.1 Replication of the Firefly Model 53
3.3.2 Estimating $t_{synch}G$ 63
3.3.3 Differences in $t_{synch}G$ between conditions and modality 64
3.4 Discussion 66

Chapter 4: Estimating chronological age from the EEG: event-related oscillatory dynamics in the healthy ageing brain 70
4.1 Introduction 70
4.2 Methods 72
4.2.1 Participants 72
4.2.2 EEG recording 73
4.2.3 Data preparation 73
4.2.4 Signal analysis 74
4.3 Results 74
4.3.1 Correlations between chronological age, NART-IQ, and cognitive performance 75
4.3.2 Estimating chronological age with components of the ERP 77
4.3.3 Estimating chronological age as EEG-age with $t_{synch}G$ 86
4.3.4 Correlations between EEG-age, NART-IQ, and cognitive performance 89
4.4 Discussion 92

Chapter 5: Estimating chronological age from the MEG: event-related oscillatory dynamics in the healthy ageing brain 99
5.1 Introduction 99
5.2 Methods 101
5.2.1 Participants 101
5.2.2 MEG recording 102
5.2.3 Data preparation 103
5.2.4 Signal analysis 104
5.3 Results 105
5.3.1 Application of the Firefly Model in MEG 106
5.3.2 Estimating $t_{synch}G$ in MEG 116
5.3.3 Differences in chronological age, NART-IQ, and cognitive performance between age groups 119
5.3.4 Differences in P3b peaks and $t_{synch}G$ between age groups 119
5.4 Discussion 124

Chapter 6: Estimating chronological age from the EEG: resting-state oscillatory dynamics in the healthy ageing brain 127
6.1 Introduction 127
6.2 Methods 129
6.2.1 Participants 129
6.2.2 EEG recording 130

6.2.3 Data preparation 130
6.2.4 Signal analysis 131
6.3 Results 135
6.3.1 Correlations between chronological age, NART-IQ, and cognitive performance. 135
6.3.2 Topographical variation of PAF estimated by the N-PAF method 135
6.3.3 Comparing D-PAF, M-PAF, C-PAF, and K-PAF 137
6.3.4 Estimating chronological age with PAF 139
6.3.5 Estimating chronological age as EEG-age with PLS regression 141
6.3.6 Correlations between EEG-age, NART-IQ, and cognitive performance 146
6.4 Discussion 148

Chapter 7: General discussion 153
7.1 An overview of the main findings of this PhD thesis 153
7.2 A look into the future of EEG-age and MEG-age 155
7.3 The overall conclusions of this PhD thesis 160

List of references 162

List of abbreviations

AAM	asymmetric amplitude modulation model
AD	alzheimer's disease
$AdjR^2$	adjusted r-squared
AM	autoregressive method
ANT	ant neuro (private limited company)
AO	auditory oddball
ARCHA	aston research centre for health in ageing
AS	auditory standard
AU-REC	aston university research ethics committee
BHR	bayesian hierarchical regression
BLR	bayesian linear regression
C-PAF	corcoran's peak alpha frequency
CA	chronological age
CL	correlation limit
CRT	choice reaction time
CRUNCH	compensation-related utilisation of neural circuits hypothesis
CV	coefficient of variation
D-PAF	direct estimate of peak alpha frequency
DC-EEG	direct current electroencephalography
EC	eyes closed
EEG	electroencephalography
EEG-age	'brain age' estimated via EEG
EM	evoked model
EMD	empirical mode decomposition

EO	eyes open
EOG	electrooculogram
ERD	event-related desynchronisation
ERF	event-related field
ERP	event-related potential
ERS	event-related synchronisation
FCRT	four-choice reaction time
FFT	fast-fourier-transform
FIR	finite impulse response
FM	firefly model
GDS-15	geriatric depression scale-15
HAM	hamming-windowed method
HAN	hanning-windowed method
HEOG	horizontal electrooculogram
HLS	college of health and life sciences
HPI	head position indicator
HT	hilbert transform
IAS	internal active shielding
ICA	independent components analysis
IHN	aston institute of health and neurodevelopment
IMF	intrinsic mode function
IQ	intelligence quotient
ISD	intra-individual standard deviation
JZS	jeffreys-zellner-siow prior
K-PAF	klimesch's peak alpha frequency
M-PAF	modelled peak alpha frequency

MCI	mild cognitive impairment
MEG	magnetoencephalography
MEG-age	‘brain age’ estimated via MEG
MINQUE	minimum norm quadratic unbiased estimator
MRI	magnetic resonance imaging
MSR	magnetically shielded room
N-PAF	naïve peak alpha frequency
NART	national adult reading test
NEH	neural efficiency hypothesis
OPMs	optically pumped magnetometers
PAF	peak alpha frequency
PCC	pearson correlation coefficient
PLS	partial least squares
PLV	phase-locking value
PRM	phase reorganisation model
PSP	postsynaptic potential
qEEG	quantitative electroencephalography
QMCI	quick mild cognitive impairment screen
R-PLS	recursive weighted-partial least squares
RMSE	root-mean-square error
ROI	region of interest
RT	reaction time
SCI	subjective cognitive impairment
SNR	signal-to-noise ratio
SQUIDS	superconducting quantum interference devices
SSS	signal space separation

SVD	singular value decomposition
tSSS	temporal signal space separation
t_{synch}	time of synchronisation
$t_{synch}G$	time of synchronisation gradient
VE	virtual electrode
VEOG	vertical electrooculogram
VIP	variable importance in projection score
VO	visual oddball
VS	visual standard
VSH	von stein and sarnthein hypothesis
WAIS	wechsler adult intelligence scale
WD	wavelet denoising

Chapter 1: An introduction to this PhD thesis

1.1 Why is this thesis examining oscillatory dynamics in the ageing brain?

With an ageing global population, the number of older adults with deleterious age-related changes in the brain, including dementia, will continue to increase unless we can make progress in the early detection and treatment of such conditions. In the UK alone, the percentage of older adults aged 85+ years is forecast to increase from 2.5% of the total population (approximately 1.6 million people) to 3.5% (approximately 2.6 million people) over the next 15 years (Office for National Statistics, 2024). In turn, the prevalence of dementia is forecast to increase to 1.6 million by 2040, comprising one in six people in their 80s and one in three of those aged 90+ years (Dementia UK, 2023). With an increase in the prevalence of dementia comes an increase in the cost of dementia, which is estimated to increase from £42 billion in 2024 to £90 billion by 2040 (Alzheimer's Society, 2024a, 2024b). However, an estimated 65% of people living with dementia will remain undiagnosed (Alzheimer's Society, 2024a) and, consequently, not receive appropriate support or targeted intervention at early stages of disease onset and progression (Robinson et al., 2015). Stimulated by the evidence that people are living longer with an ageing population but a declining birth rate, and the projected increases in the requirement and cost of care provision, charities and other formal bodies in the UK have recently called for an acceleration of efforts towards early, accurate, and accessible diagnosis of deleterious age-related changes. For example, the Alzheimer's Society (2024a, p. 14) has reported on dementia and the pressing need for "screening to identify more cases earlier" through the "use of imaging".

Early, accurate, and accessible detection and tracking of dementia would be life-changing for many people, because around 45% of dementia cases worldwide could be delayed or even prevented with targeted intervention on fourteen modifiable risk factors across the lifespan (Livingstone et al., 2020, 2024). These risk factors include less education in early life (accounting for approximately 5% of cases), hearing loss and high low-density lipoprotein cholesterol during midlife (accounting for approximately 7% of cases respectively), and social isolation in later life (accounting for approximately 5% of cases). There is also substantial funding for the development of new drugs to treat dementia and slow the speed of its progression, such as Lecanemab (van Dyck et al., 2023) and Donanemab (Sims et al., 2023) for Alzheimer's Disease (AD). However, early, accurate, and accessible detection and tracking of pre-cursor stages of dementia could mitigate the need for expensive drugs that have negative side effects (Alzheimer's Society, 2024b). For example, many of the fourteen modifiable risk factors for dementia are also predictive of Mild Cognitive Impairment (MCI; Apostolo et al., 2016; Jekel et al., 2015). MCI is a confirmed pre-

cursor stage to dementia, particularly AD, and progression is estimated to occur in 15-41% of MCI cases (Davis et al., 2018; Gauthier et al., 2006; Geslani et al., 2005; Ritchie, 2004). The remaining cases either maintain an MCI diagnosis or revert to healthy age-related changes (Lonie et al., 2010; Sanz-Blasco et al., 2021). In summary, deleterious age-related conditions such as dementia or MCI are not inevitable and may not remain untreatable either. However, for lifestyle and drug interventions to be effective in preventing, delaying, or reverting deleterious age-related changes, interventions need to be implemented at the optimal point in time. This is only going to be possible with the development of early, accurate, and accessible detection and tracking of deleterious changes in a person's neural and cognitive integrity.

Electroencephalography (EEG), a tool for measuring electrical activity of the brain (e.g., oscillatory dynamics; outlined in Chapter 2), is relatively accessible and affordable from both clinician and patient perspectives when compared to other imaging methods such as Magnetic Resonance Imaging (MRI) and Magnetoencephalography (MEG). As a result of this affordability and accessibility, EEG is widely regarded as a candidate for unlocking the early and accurate detection and tracking of deleterious age-related changes in the brain (e.g., Dauwels et al., 2010a; Koenig et al., 2020; Poil et al., 2013; Popa et al., 2020). EEG is an established assessment tool in other clinical contexts, such as sleep disorders and epilepsy (Mushtaq et al., 2024; Popa et al., 2020; Tatum et al., 2018), but, at the time of writing, there are no clinical EEG protocols for the diagnosis and management of dementia. This is in part due to a lack of optimised, standardised EEG protocols for maximising signal-to-noise ratio (SNR) and reliable findings in ageing studies, but also due to an incomplete understanding of age-related changes in the EEG and how they are related to cognitive performance. Over the past 25 years, many neurocognitive and neurobiological theories of ageing have emerged in attempts to explain age-related changes in neural and cognitive integrity from a predominantly brain imaging perspective, which has included EEG (see Ebaid & Crewther, 2020, Grady, 2012, and McDonough et al., 2022, for reviews). Two distinct theoretical frameworks persist in deficit versus benefit models. The deficit framework considers dedifferentiation, which comprises diminishing distinctiveness and selectivity of cortical and cognitive processing with increasing age (Koen & Rugg, 2019), and noise, which comprises decreasing SNR and processing efficiency, perhaps related to increasing intra-individual variability and decreasing fidelity in processing with increasing age (Cremer & Zeef, 1987; Voytek et al., 2015a, 2015b). The benefit framework considers compensation, reserve, and maintenance (Cabeza et al., 2018; Stern, 2012), all of which can mitigate age-related declines in task performance. Compensation is the recruitment of neural and cognitive resources to meet task demands, with the levels of compensation often

proportional to chronological age. Reserve is the presence of neural and cognitive resources, and maintenance is the preservation of those resources.

Early empirical evidence for the deficit framework's dedifferentiation and noise processes relied largely on behavioural and fMRI methodologies. For example, sensory acuity tests (e.g., visual and auditory) and cognitive tasks (e.g., perceptual speed, verbal fluency, reasoning and memory) had stronger correlations at the intraindividual level with increasing chronological age, interpreted as cognitive performance dedifferentiation (Baltes & Lindenberger, 1997). In turn, age-dependent neural dedifferentiation was operationalised in fMRI as a signal change, driven by reduced specificity or sensitivity with increasing age, in localised areas that are known to be selective to specific stimuli (e.g., less selective signal in the parahippocampal place area to houses, lateral occipital cortex to objects, and fusiform face area to faces; Park et al., 2004, 2012), both in cross-sectional and longitudinal ageing studies (McDonough et al., 2022). Age-related decreases in SNR, including increases in both task-unrelated and resting-state neural activity, and an increase in intraindividual response variability in neural metrics, have also been reported in fMRI (Logan et al., 2002) and EEG (Voytek et al., 2015a). For example, EEG researchers have explicitly described changes in trial-averaged peak amplitude and latency metrics with age, accompanied by increased variability (i.e., noise) in the underlying neural responses on a trial-by-trial basis (MacDonald et al., 2009; Polich, 2007; Van Dinteren et al., 2014). Empirical evidence for the compensation, reserve and maintenance processes of the benefit framework has also relied largely on behavioural measures (e.g., cognitive reserve; Stern, 2012) and MRI imaging (e.g., structural and functional brain reserve; Aron et al., 2022; Reuter-Lorenz et al., 2001, 2014).

Both deficit and benefit models are still being refined based on new evidence from brain imaging studies, including EEG. For example, Pichot et al. (2022) reported a range of age-dependent and age-invariant relationships between neural noise (operationalised as a flattening of the 1/f exponent of the frequency power spectrum with age) and neural dedifferentiation (operationalised as scene-selective and face-selective peak amplitude reductions and latency increases with age) in the EEG. This mixture of age-dependent and age-invariant relationships suggests that the deficit processes and their outcomes may depend on variables such as task, stimulus category, and the underlying neural network, and that the relationship between the deficit processes may also change with age. Nevertheless, it still holds that "many cognitive processes and their neurophysiological correlates are not accounted for by current theories. Indeed, the claim that '[EEG] is still mainly an empirical science' (Zhadin, 1984) is as true now as it was 30 years ago" (Cohen & Gulbinaite, 2014, p. 7). Whilst there is certainly extensive literature on the effects of ageing on the EEG (further

outlined in Chapter 2), the empirical evidence is often neither explicitly nor neatly explained by the particulars of the deficit and benefit models (see Ebaid & Crewther, 2020, Grady, 2012, and McDonough et al., 2022, for reviews). Therefore, no comprehensive amalgamation of the deficit and benefit theories has been forthcoming to explain all the observed relationships between chronological age, brain functioning, and cognitive performance, particularly in the realm of EEG.

For the context of this thesis, using two newly collected EEG and MEG datasets, fundamental mechanistic age-related changes can be drawn from the sum of the ostensibly distinct theoretical deficit and benefit models and their supporting empirical evidence; namely, a changing distribution of cortical processing with changing processing efficiency across the lifespan, which can be used to interpret age-related changes in the EEG and beyond (outlined in Chapter 2). Indeed, empirical attempts to predict conversion from normal ageing to MCI and AD with EEG changes combined with other metrics have provided encouraging results in academic research settings, with good sensitivity and specificity (Apostolo et al., 2016; Dauwels et al., 2010a; Huang et al., 2000; Poil et al., 2013; Snaedal et al., 2012; Weiner et al., 2022). This suggests that EEG metrics could be developed for the early and accurate detection and tracking of deleterious age-related changes in clinical settings, such as part of an optimised form of triangulated diagnosis (Hackfort & Birkner, 2011) and disease management (e.g., combined with blood and plasma tests, DNA-mapping, neuropsychological and cognitive tasks, self-report questionnaires, and interviews with family members). In summary, whilst establishing EEG for use in a clinical, ageing context is an ambitious project, where EEG is unlikely to be a sole solution in any case, EEG could well accelerate our progress towards the early, accurate, and accessible diagnosis of deleterious age-related changes such as dementia. Several unanswered questions need addressing first though, which informed the aims of this PhD thesis.

1.2 The aims of this thesis

There were three broad aims of this thesis, which could be achieved concurrently; namely, 1) to advance our understanding of event-related and resting-state EEG and MEG, 2) to advance our understanding of age-related changes in the brain with EEG and MEG, and 3) to establish EEG and MEG metrics that have the potential to track those age-related changes over time. The hope was that the outcomes of this thesis would take us closer to realising an early, accurate, and accessible diagnosis of deleterious age-related changes. Specifically, the vision was to establish a way of estimating ‘brain age’ as a marker of general brain functioning. If it were possible to reliably estimate an individual’s chronological age based on the EEG, then this brain age – coined EEG-age – could be compared with actual chronological age and any discrepancy between the two might reflect some age-

related condition, based on either protective or deleterious changes. For example, using good normative data, the number of standard deviations above or below the mean EEG-age for the person's chronological age could be a useful biomarker for mild cognitive impairment or early dementia.

Developing neuroimaging biomarkers is not a particularly novel venture (e.g., Dauwels et al., 2010a; Franke & Gaser, 2019; Hofmann et al., 2022; Koenig et al., 2020; Poil et al., 2013; Snaedal et al., 2012) and follows in the traditions of Roy John's Neurometrics (John et al., 1977). Furthermore, several attempts have been made to operationalise an EEG-age concept in all but name by using machine learning to identify age-related electrophysiological components from a plethora of popular EEG metrics (e.g., Al Zoubi et al., 2018; Sun et al., 2019). However, this thesis aimed to take a more targeted approach, using alternative data analyses that may provide more robust, holistic estimates of brain age in samples of healthy adults. The approach to using an EEG-age metric was like that pioneered by Miloš Matoušek, Ingemar Petersén, and Jiri Wackermann (Matoušek & Petersén, 1973; Wackermann & Matoušek, 1998). However, this thesis aimed to incorporate larger age-balanced samples of exclusively healthy adults from across the chronological age range. It would also use more sophisticated procedures and analyses that can inspect phase, frequency and amplitude separately as distinct aspects of the EEG and MEG. Finally, this thesis would consider proxy measures of general cognitive integrity alongside brain age, to probe the cognitive performance outcomes of age-related deficit and benefit processes (e.g., dedifferentiation and noise versus reserve).

The reasoning for a restricted focus on healthy adults was multifaceted, comprising a desire to set a strong foundation for future research in sub-clinical and clinical populations, but also largely due to practical limitations. A core practical limitation was that data collection took place in and around the COVID-19 pandemic, which caused major, multiple revisions to the original plans for this PhD thesis. For example, COVID-19 eliminated access routes to sub-clinical and clinical participants, as well as significantly delaying and impacting the data collection with healthy samples. However, this unavoidable situation presented an opportunity to re-focus on developing a deeper understanding of fundamental oscillatory dynamics in the ageing human brain, whilst at the same time establishing novel ways of tracking age-related changes in the brain. The hope is that future research, post-pandemic, can use this thesis as a foundation to build on with targeted populations and optimised methods and analysis pipelines.

1.3 An outline of the chapters of this thesis

Chapter 1 outlines the context and aims of this PhD thesis: 1) to advance our understanding of event-related and resting-state EEG and MEG, 2) to advance our understanding of age-related changes in the brain with EEG and MEG, and 3) to establish EEG and MEG metrics that have the potential to track those age-related changes over time. **Chapter 2** provides an extensive overview of the EEG and MEG data, methods, and analyses used to achieve the aims of this thesis. Specifically, traditional EEG and MEG metrics, as proxies of general brain functioning, and their complex relationships with age and cognitive performance are outlined. Thereafter, alternative, novel metrics that are interrogated by this thesis are introduced. This chapter provides a comprehensive foundation that is built upon across the subsequent experimental chapters of the thesis.

Chapter 3 advances our understanding of the oscillatory dynamics in event-related EEG by testing the Firefly Model (FM) of synchronisation through cross-frequency phase modulation (Burgess, 2012). This determines whether the FM offers an empirically credible, alternative explanation of information processing and multiscale neural network communication, which can be used to inform the development of a new phase-based metric for the explanation and tracking of age-related changes in the brain. **Chapter 4** develops and applies the new phase-based metric in a healthy ageing sample from across the chronological age range, to explain and track age-related changes in the brain with EEG. **Chapter 5** advances our understanding of the oscillatory dynamics in event-related MEG by again testing the FM, but it also applies the new phase-based metric in two different groups of young and older adults to further explain and track age-related changes in the brain with MEG. **Chapter 6** extends the hunt for a robust new way to track age-related changes in the brain to a resting-state paradigm. Alternative frequency and novel amplitude metrics are established and applied in a healthy ageing sample from across the chronological age range, again to advance our understanding of EEG but also to explain age-related changes in the brain and track them with a brain age metric.

Chapter 7 provides a general discussion and summary of the research findings presented in this thesis. It outlines the novel contributions that have advanced our understanding of the ageing human brain and how to detect and track age-related changes in the brain via EEG and MEG, but it also identifies what remains inconclusive and highlights multiple targets for future research. It concludes that there is substantial scope for research projects to build on the foundations set by this thesis, particularly in enhancing the SNR of the newly established metrics in the hope of one day establishing an early, accurate, and accessible way of detecting and tracking deleterious age-related changes and conditions, such as dementia, with EEG and MEG.

Chapter 2: A review of the EEG and MEG methods and analyses used in this thesis

Table 2.1 provides a concise summary of each section of Chapter 2, outlining the organisation and purpose of the content to support efficient engagement with this chapter and wider thesis, specifically the EEG and MEG datasets, methods, and analyses that are applied and developed in the subsequent experimental chapters.

Table 2.1

An outline of the organisation of Chapter 2, split into sections organised in line with the different methodological approaches reviewed, and in a way that mirrors the narrative progression (including rationale therein) of the subsequent experimental chapters.

	Content	Purpose	Context
Section 2.1.1	Overview of EEG data collection	Introducing EEG and the ANT Neuro EEG system used to collect the EEG dataset for this thesis	Supports Chapters 3, 4, 6 and 7 – different parts of the same EEG dataset are used in all these chapters
Section 2.1.2	Overview of MEG data collection	Introducing MEG and the Elekta Neuromag® TRIUX MEG system used to collect the MEG dataset for this thesis	Supports Chapters 5 and 7
Section 2.2.1	Overview of evoked and induced event-related methods and analyses in EEG/MEG	Introducing the classic ERP/ERF and ERD/ERS analysis approaches applied to the event-related EEG and MEG datasets in this thesis	Supports Chapters 3, 4, 5 and 7
Section 2.2.2	Overview of the extension of evoked and induced approaches in this thesis	Introducing the novel t_{synch} and $t_{synch}G$ analysis approaches applied to the event-related EEG and MEG datasets in this thesis	Supports Chapters 3, 4, 5 and 7

Section 2.3.1	Overview of resting-state methods and analyses in EEG	Introducing the classic PAF analysis approaches applied to the resting-state EEG dataset in this thesis	Supports Chapters 6 and 7
Section 2.3.2	Overview of the extension of resting-state approaches in this thesis	Introducing the M-PAF and novel PLS analysis approaches applied to the resting-state EEG dataset in this thesis	Supports Chapters 6 and 7

2.1 EEG and MEG signal detection methods

2.1.1 EEG methodology

EEG is a tool for measuring electrical activity of the brain. It is renowned for its millisecond temporal resolution in non-invasive quantification of dendritic postsynaptic potentials (PSPs). PSPs are changes in the membrane potential (cf. action potential) of postsynaptic receptors caused by neurotransmitters in the synaptic cleft. Temporally synchronous PSPs of spatially aligned pyramidal cells in the tens or hundreds of thousands, termed open field dipoles, cause an alteration in the electrical charge of extracellular fluid. The extracellular current undergoes volume conduction, which is transmission through the surrounding conducting medium to reach the scalp, before passing via an effective bridge of conductive gel, which reduces signal impedance, to electrodes that are temporarily attached to the scalp. Cutting-edge EEG hardware circumvents the use of conductive gel, but the gold-standard EEG procedures and most hardware vendors still recommend the application of conductive gel per electrode to minimise signal impedance. The raw EEG signal is recorded as fluctuations in voltage (i.e., μV, microvolts) over time, calculated from the difference in electrical potential between an active electrode and reference electrode(s). The signal is amplified, and the continuous analogue fluctuation is converted to a digital representation via sampling and interpolation between the sampled data points (see Buzsaki et al., 2012, Jackson & Bolger, 2014, and Luck, 2014, for overviews of EEG signal detection). Quantitative analysis of the EEG signals recorded at the electrodes is known as sensor space analysis, and the signals, termed complex oscillations, may not accurately represent the precise spatial nature of the underlying neuronal activity owing to volume conduction (Van den Broek et al., 1998; cf., source space analysis, which requires intricate estimation of the neuronal sources underlying the sensor level signals; e.g., Hamalainen & Sarvasm, 1989).

This thesis utilises sensor space analysis, where the academic field of quantitative EEG (qEEG) can examine oscillatory changes in the metrics of amplitude, frequency, and phase. EEG amplitude, measured as voltage (μV) or power (dB) that is proportional to μV^2 (Lyons, 2011), can be thought of as the strength of oscillatory activity (Cohen, 2014). However, amplitude is affected by a range of other inter-individual and intra-individual factors such as the thickness of the skull and scalp (Lehtinen et al., 1996), and signal impedance (Ferree et al., 2001; Van den Broek et al., 1998). Furthermore, when humans sit at rest with their eyes closed, the EEG power spectrum is distributed such that the power at each frequency is approximately proportional to the reciprocal of the frequency (Power $\propto$ 1/frequency) plus a peak in power in the alpha 7-13 Hz frequency band (He, 2014; Lopes da Silva, 2013; Pritchard, 1992). The broadband frequency distribution of the awake human EEG is commonly split into bands (Buzsaki & Draguhn, 2004; Burgess, 2019), and whilst filtered bandwidth and frequency bandings differ between researchers and experiments (Lopes da Silva, 2013; Newson & Thiagarajan, 2019), five example bands are Delta (e.g., 1-4 Hz), Theta (e.g., 4-7 Hz), Alpha (e.g., 7-13 Hz), Beta (e.g., 13-30 Hz), and Gamma (e.g., >30 Hz). There is no one universally agreed interpretation of frequency bands (Cohen & Gulbinaite, 2014), but the differing oscillatory frequencies can be thought of as differing neuronal networks, with the scale of the network inversely proportional to the frequency (Von Stein & Sarnthein, 2000). EEG phase can be converted from radians (Rad) to degrees (°) or represented as unit vectors on a circle (Cohen, 2014). Phase can be thought of as the position on an oscillation at a specific point in time, which is useful for judging synchronisation between oscillations. For example, the phase-locking value (PLV) can be calculated, which is a measure of phase synchrony between oscillations across trials, ranging from 0, no synchrony, to 1, perfect synchrony (Lachaux et al., 1999). Figure 2.1 provides a visualisation of amplitude, frequency, and phase to consolidate the meaning of each metric in the context of EEG, because they are key metrics that will be discussed and applied in subsequent sections of this review chapter and the later experimental chapters.

Figure 2.1

A circular representation of amplitude, frequency, and phase metrics in EEG. Amplitude is the distance (i.e., the magnitude) and direction (positive or negative; cf. polarity) of the black point from the central origin (measured in μV). Frequency is the rate at which the black point moves around the circle (measured in Hz). Phase is the angle of intersection at the black point's origin with the imaginary axis (measured in Rad).

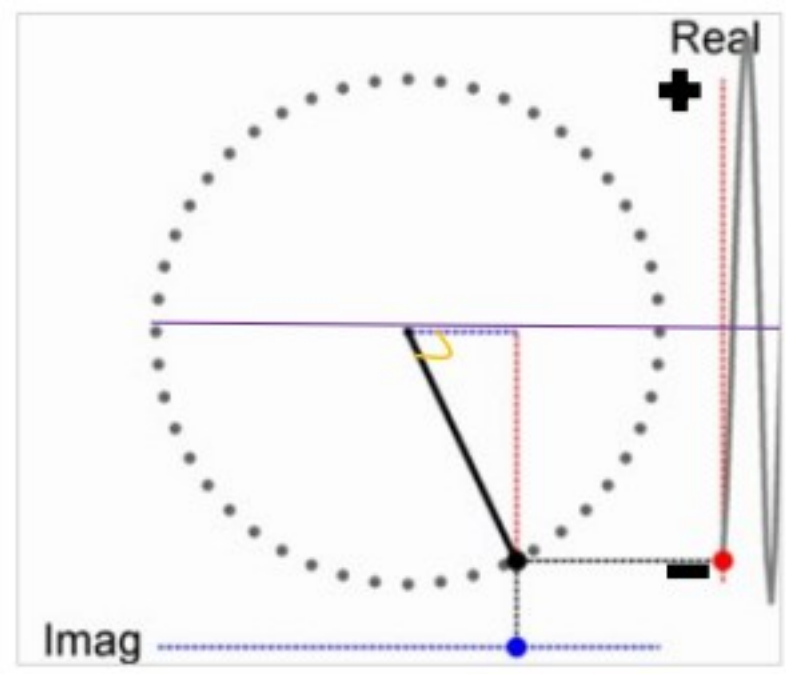

A portable ANT Neuro (ANT) direct current EEG (DC-EEG) recording system was used to collect a new EEG dataset for this thesis, comprising sixty participants who completed both event-related and resting-state paradigms. Further details on this EEG dataset and respective paradigms can be found later in Chapter 2 and in the EEG experimental chapters (signposted in Table 2.1). This EEG system comprised an ANT eego™ amplifier (EE-215; with an input impedance of >1 GΩs) and ANT eego™ recording software suite (version 1.7.0), which was run on an Intel Dell Venue 8 Pro 5855 tablet with a Windows 10 operating system. The sampling rate (SR) was 500 Hz, with a 24-bit resolution and a 0 (i.e., DC point) to 130 Hz signal bandwidth set by the manufacturer (i.e., 0.26 × SR). Participants wore a 64-channel ANT Waveguard Originals EEG cap, comprising sintered Ag/AgCl electrodes arranged in a 10/10 layout (Jurcak et al., 2007) and with coaxial noise-shielded cabling. The electrode positioning and terminology of the ANT Waveguard Originals EEG cap, which was used to collect the EEG dataset used in chapters 3, 4, and 6 of this thesis, are outlined in Figure 2.2 to support consistency across future studies and comparability with the wide range of different caps that are used in EEG research. AFz and CPz electrodes were the ground and online reference electrodes respectively, set as default

for the ANT eego™ by the manufacturer, but data was re-referenced to the common average (i.e., subtracting the average of all electrodes from each electrode) offline before the main analyses. Conductive OneStep Cleargel was applied to each electrode via a blunt syringe to reduce impedance levels. Optimal cut-off levels for impedance when using the high-impedance ANT EEG system are reported as lying between 40 kΩs (Ferree et al., 2001) and 50 kΩs (Kaneko et al., 2021), with a workable maximum of 200 kΩs. Four additional electrodes were applied to each participant, allowing for bipolar electrooculogram (EOG) recordings of vertical eye movements (VEOG; two electrodes, one placed above the right eyebrow and another beneath the right eye) and horizontal eye movements (HEOG; two electrodes, one placed on the right temple area and another on the left temple area). This EEG, VEOG, and HEOG recording setup remained identical for each participant, with room temperature kept at about 20°C and a low level of ambient light.

Figure 2.2

The positioning and terminology of the electrodes of the 64-channel ANT Waveguard Originals cap used to collect the EEG dataset for this thesis (from ANT Neuro).

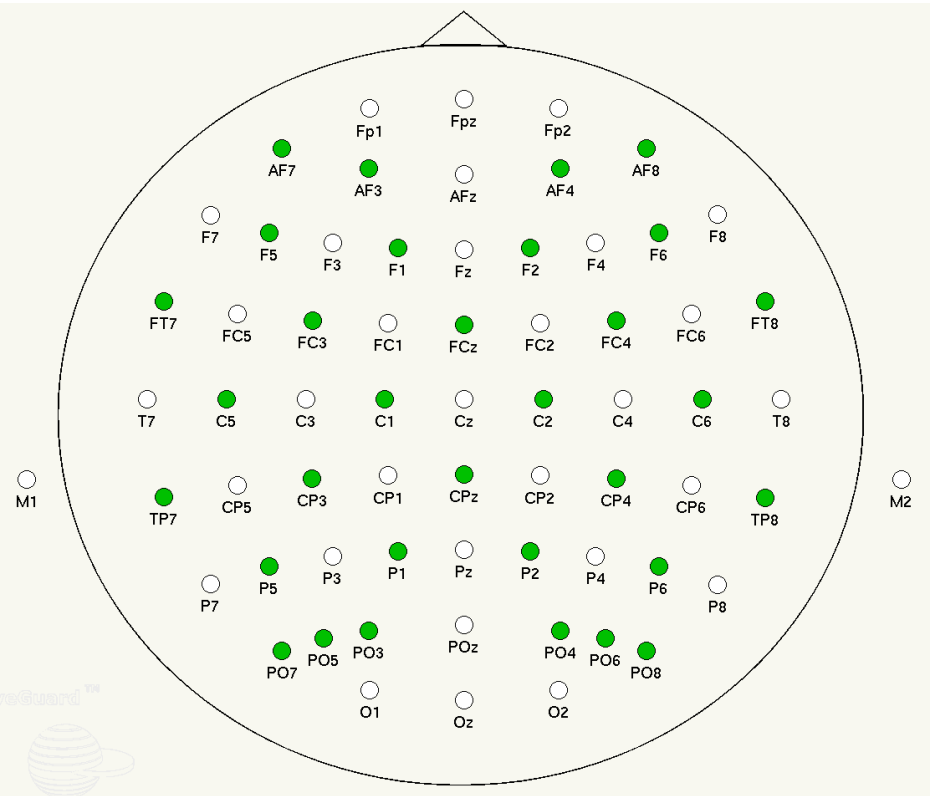

2.1.2 MEG methodology

MEG is a tool for measuring magnetic activity of the brain. Like EEG, MEG is also renowned for its millisecond temporal resolution in non-invasive quantification of dendritic PSPs, but the biophysical and technical foundations of MEG signal detection are distinct from EEG (see Cohen, 1972, Hämäläinen et al., 1993, Hillebrand & Barnes, 2002, and Vrba & Robinson, 2001, for overviews of MEG signal detection). The temporally synchronous PSPs over spatially aligned pyramidal cells cause an alteration in magnetic fields that do not rely on volume conduction to reach the scalp and pass unimpeded to reach nearby MEG sensors. MEG is sensitive to tangential source dipoles, which are oriented anterior-posterior or left-right thus the magnetic fields pass through the scalp, rather than radial source dipoles, which are oriented superior-inferior (cf. Fleming's right-hand rule of electromagnetism). The sensors used in all MEG experiments presented in this thesis are called superconducting quantum interference devices (SQUIDs). SQUIDs are superconducting loops containing Josephson junctions (i.e., magnetic flux to voltage convertors) that measure magnetic field fluctuations over time. Superconductivity, which is a state of zero electrical resistance, is maintained by housing the SQUIDs in liquid helium at a temperature of -269 °C.

The raw MEG signal is transformed through pick-up coils, which are antennae-like devices that extend the range of signal detection and mitigate environmental noise, before reaching the SQUIDs through inductive coupling coils. The pick-up coils used in all MEG experiments presented in this thesis are called magnetometers (i.e., single coils) and planar gradiometers, which are counter-wound coils on a flat horizontal axis thus environmental noise that appears equal yet opposite at both coils will cancel out. Magnetometers measure total magnetic flux in tesla (T), whereas planar gradiometers measure the gradient of the source magnetic field as the difference in magnetic flux in tesla per distance unit (i.e., T/cm). This means there is a different pattern of SNR and amplitude scaling in the final signals when comparing magnetometers and gradiometers, which has caused debate over how to use each type of sensor within MEG analyses (Garces et al., 2017). The difference in SNR and scaling needs to be remembered when using standardised units across magnetometers and planar gradiometers (e.g., 10^{-15} T, which is femtotesla, fT). After being recorded by SQUIDs, the continuous analogue fluctuation is converted to a digital representation via sampling and interpolation. Like EEG, analysis of the complex oscillations can follow sensor space and source space approaches (Hillebrand et al., 2005), with the focus being on sensor space in this thesis, to examine oscillatory changes in amplitude, frequency, and phase.

A stationary Elekta Neuromag® TRIUX DC-MEG recording system was used to collect a new event-related MEG dataset for this thesis, as outlined and analysed in Chapter 5. This data collection was controlled via the Elekta Neuromag® recording software suite running on a PC with a Linux operating system. The sampling rate (SR) was 1000 Hz, with a 24-bit resolution and a 0 (i.e., DC point) to 330 Hz signal bandwidth set by the manufacturer (i.e., 0.33 × SR). Participants sat with their heads carefully, comfortably positioned to touch the top of the MEG helmet, which comprised 102 magnetometers and 204 planar gradiometers. These coils were housed as triple sensor units of one magnetometer per two gradiometers within a magnetically shielded room (MSR) that reduces external magnetic interference, which is orders of magnitude larger than the magnetic fields originating from the brain. Figure 2.3 provides a schematic of the triple sensor units, and Figure 2.4 visualises the positioning and terminology of the Elekta Neuromag® TRIUX MEG sensors, which were used to collect the MEG dataset used in Chapter 5 of this thesis, to support consistency across future studies and comparability with the different setups that are used in MEG research. Four additional electrodes were applied to each participant, allowing for bipolar VEOG and HEOG recordings implemented in the same way as in the EEG procedure. This MEG, VEOG, and HEOG recording setup remained identical for each participant, with room temperature kept at about 20°C and a low level of ambient light.

Figure 2.3

A schematic of the Elekta Neuromag® TRIUX MEG triple sensor units, comprising one magnetometer, shown as the red outline on the far right, per two planar gradiometers shown as the red outlines on the far left and centre, used to collect the MEG dataset for this thesis (from Elekta, now MEGIN).

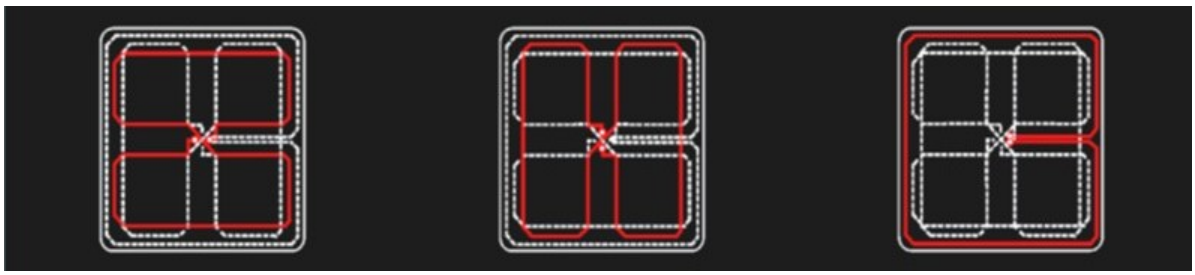

Figure 2.4

The positioning and terminology of the Elekta Neuromag® TRIUX MEG sensors for the magnetometers (NM306mag.lay) and planar gradiometers (NM306planar.lay) respectively, both used to collect the MEG dataset for this thesis (from Elekta, now MEGIN).

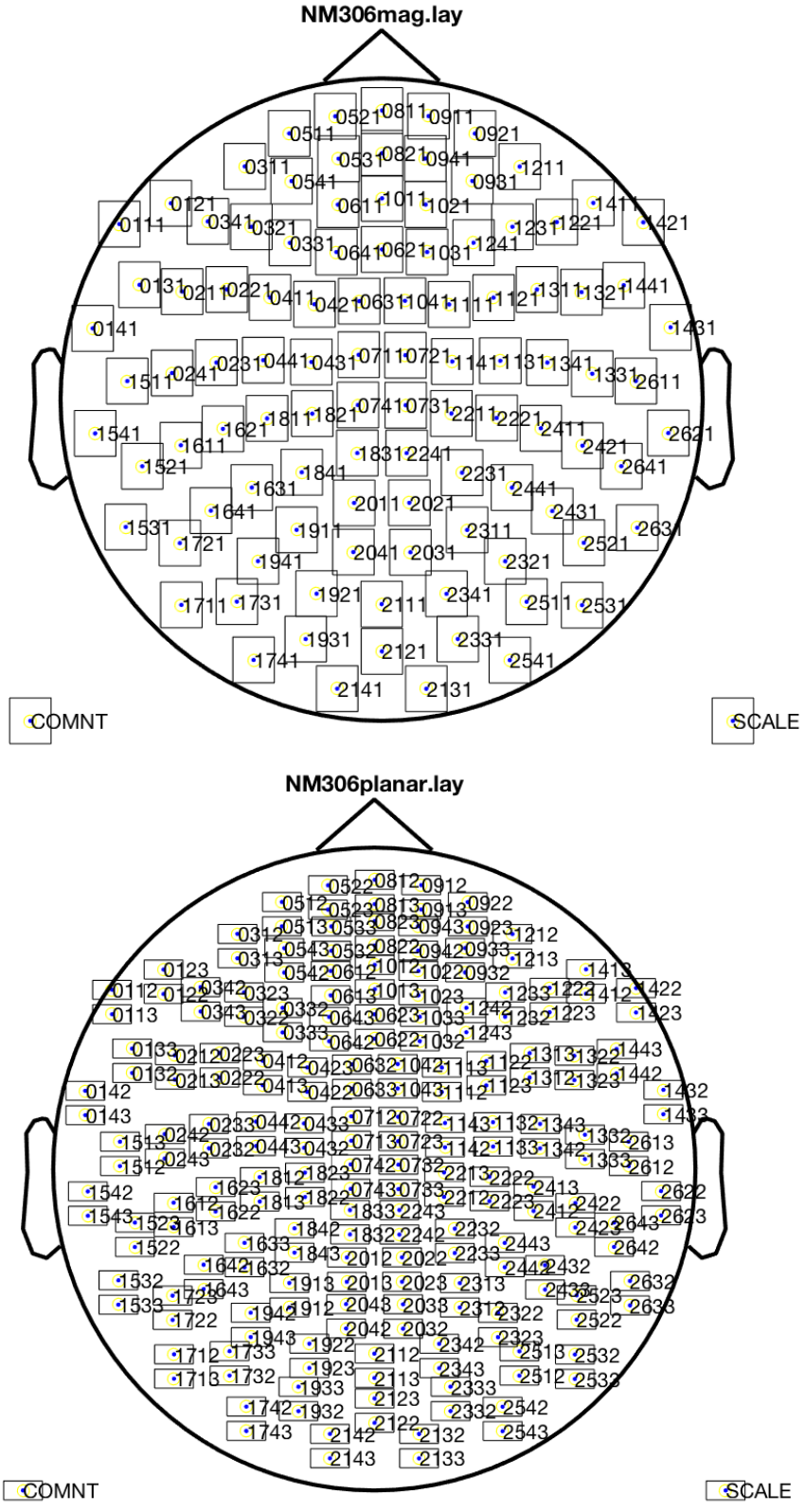

The Elekta Neuromag® TRIUX DC-MEG recording system uses an interference suppression software called MaxFilter™ (version 2.2) because the vendor-supplied MSR uses only a single shell of interleaved mu-metal and aluminium layers (termed MaxShield™) thus is thinner than MSRs provided with alternative MEG systems (De Tiege et al., 2008). This 'lightweight' MSR was designed to make MEG more suitable for clinical environments, because MaxShield™ is less expensive and more compact than other MSRs, with a faster build time and reduced impact on existing infrastructure. However, the use of MaxShield™ means that the MEG signal is more susceptible to environmental noise that reduces analytical sensitivity by reducing SNR and introducing signal errors. Therefore, MaxFilter™ is provided alongside MaxShield™ as a solution to this need for additional interference suppression. MaxFilter™ is a software that uses an algorithm called signal space separation (SSS; Taulu et al., 2004, 2005, 2006) to discern components of the MEG signal that originate from the environment surrounding the MEG sensor array (i.e., the external subspace, magnetic interference) rather than inside the MEG sensor array (i.e., the internal biomagnetic subspace, pure brain signal). By considering these two linearly independent subspaces, SSS decomposes the MEG signal into separate components and omits the external magnetic interference via a reconstruction of the internal pure brain signal from components corresponding to just the biomagnetic subspace.

To further enhance SNR, SSS also permits head movement correction when head position indicator (HPI) coils have been attached to the participant in a defined layout (e.g., three coils across the forehead and two further coils, one behind each ear around the mastoid area; an Elekta Neuromag® TRIUX HPI coil set was used in Chapter 5). After attaching the HPI coils, head digitisation is completed to provide a model sphere that estimates the participant's head shape. This involves recording 3 cardinal landmarks – nasion, left pre-auricular, and right pre-auricular – before a surface outline of the head, including forehead, eyebrows, cheekbones, and nose (a Fasttrack Polhemus system was used in Chapter 5). During the MEG recording, the HPI coils send continuous (cHPI) sinusoidal signals at 300-330 Hz for a MEG sampling rate of 1000 Hz. This data allows for the implementation of a motion correction algorithm in MaxFilter™, which uses amplitudes of the cHPI signals to model the sphere's movement from the sensor movement relative to the MEG dewar (proceeds with a 10 ms amplitude estimation step function within 200 ms estimation windows). The algorithm compensates for head movement identified outside a 0.98 goodness of fit limit (with a 5 mm coil fitting error limit) by realigning the recorded magnetic field distribution. This realignment is performed via interpolation and extrapolation based on a model of the magnetic field distribution if the head had not moved from baseline

coordinates of the cHPI signals, estimated using spherical harmonic functions (Stolk et al., 2013).

Temporal signal space separation (tSSS) is an extension of SSS that can remove temporally correlated internal and external components from the data, with a subspace correlation coefficient limit set at 0.9 (proceeds with a data buffer of 10 seconds). The working assumption of tSSS is that internal components that are strongly correlated with external components can be regarded as large artefacts that are powerful enough to have leaked to the external subspace so are unlikely to be originating from the brain (Taulu & Simola, 2006). The vendor advises the application of tSSS when there are signals in the raw data that are orders of magnitude larger than signals likely to be originating from the brain (e.g., dental metalwork artefacts). An additional vendor-supplied interference suppression tool of internal active shielding (IAS) was not used in this thesis, because IAS, which relies on feedforward and feedback electronics' interference suppression from additional active sensors located outside and inside the MSR, results in nonstandard raw data that can be incompatible with analysis pipelines and software.

2.2 EEG and MEG data analyses: measuring event-related oscillatory dynamics

2.2.1 Evoked and induced changes in the EEG and MEG

Event-related EEG and MEG involve the examination of oscillatory changes after an event (e.g., presentation of a stimulus). Evoked and induced changes are two quantifications of event-related activity, historically treated as distinct processes that require time domain and frequency domain analysis respectively (see Cohen, 2014, and Luck, 2014, for overviews of event-related changes). Induced changes, comprising event-related synchronisation (ERS) and event-related desynchronisation (ERD), are characterised by increases and decreases respectively in ongoing power (Pfurtscheller & Lopes da Silva, 1999). ERS and ERD are said to be 'time-locked' to the event because the power changes appear after event onset, and these induced changes are often reported within isolated frequency bands. For example, Berger (1929) reported an ERD in the alpha frequency band when participants transitioned from eyes closed to eyes open. Klimesch et al. (2007b) proposed that alpha ERD signifies increased cognitive processing after the allocation of attention (i.e., ERS reflects increased inhibition) and is thus related to cognitive performance. It has also been suggested that this alpha ERD may change with age (Klimesch, 1999), but the underlying mechanisms and meaning of event-related changes in mean oscillatory power are yet to be confirmed both in and out of an ageing context. For example, there are widely reported changes in the frequency of the mean peak in power in the alpha frequency band (termed peak alpha frequency, PAF) across the lifespan (more on PAF later in Chapter 2), as well as a rapidly growing interest in age-related changes in aperiodic, non-oscillatory

1/f-like exponent (function slope) and offset (y-axis crossing point) background activity (e.g., Finley et al., 2024). Taken alongside other inter-individual and intra-individual differences that affect SNR, such as physiological noise (e.g., muscle movement artefacts) and neuronal response variability that may increase with age and dilute the averaged amplitude (Cremer & Zeef, 1987; Voytek et al., 2015a), changes in both PAF and aperiodic activity could help to explain changes in alpha power (Donoghue et al., 2020, 2021; Merkin et al., 2023; Voytek, 2015b). In summary, induced power changes and their relationships with age and cognitive performance are complex, and conclusions on their meaning cannot be drawn without caution and consideration of a wide variety of factors.

Alpha is by no means the only frequency band that has been assigned specific functional specialisation in the context of induced amplitude changes. For example, the delta band has been linked with homeostatic and motivational processes (Knyazev, 2012), theta with memory encoding (Klimesch, 1999) and intelligence (Jausovec & Jausovec, 2000), beta with sensorimotor activity (Engel & Fries, 2010), and gamma with construction of object representations (Tallon-Baudry & Bertrand, 1999) and meditative zen (Lutz et al., 2004). However, other researchers have proposed that apparent functional specialisation may be a misinterpretation and a by-product of popular band-based analysis; instead, the whole frequency spectrum could be considered in parallel for a deeper interrogation of multiscale, cross-frequency interactions that might reflect fundamental neuronal network communication and information processing (e.g., Burgess, 2012; Cohen & Gulbinaite, 2014; Newson & Thiagarajan, 2019). Frequency bands may remain segregated at resting to prevent unnecessary cross-frequency interference, possibly with a golden ratio between the means of adjacent frequencies such that phase synchronisation is mathematically impossible (i.e., 1:1.618; Pletzer et al., 2010). However, perhaps events cause synchronisation in the activity of different frequency bands, with a systematic pattern of cross-frequency coupling across the whole broadband frequency range that can be interpreted as a travelling wave that represents the transition from resting state to information processing (Canolty, & Knight, 2010; Klimesch, 2018; Palva & Palva, 2007; Rodriguez-Larios & Alaerts, 2019). This interpretation aligns with Von Stein and Sarnthein's (2000) hypothesis (VSH) that post-stimulus high-frequency interactions (e.g., beta and gamma) reflect localised network communication and post-stimulus low-frequency interactions (e.g., alpha and theta) reflect widespread network communication, irrespective of cognitive faculty but implicating bottom-up versus top-down processing respectively. An explanatory mechanism for a travelling wave of information processing and network communication across the full frequency spectrum and how it underpins event-related changes has been proposed by Burgess (2012) in the Firefly Model (FM). The FM will be outlined in full after an introduction to

evoked event-related changes, because the FM was constructed in part to explain evoked changes, but it can also explain induced changes at the same time.

Evoked changes, termed event-related potentials (ERPs) in EEG and event-related fields (ERFs) in MEG, are simply trial-averaged waveforms plotted over time. These evoked waveforms are consistent in both when they occur (i.e., they are time-locked to the event) and their shape post-stimuli (i.e., they are phase-locked to the event). Different ERP and ERF waveforms have been reported alongside different sensory and cognitive events (see Cohen, 2014, and Luck, 2014, for overviews of event-related changes). The components of an ERP/ERF waveform have historically been characterised by peak amplitude polarity, latency of the amplitude peak, and location of the peak over the sensors. For example, the 'P3b' is a particularly well-defined ERP and ERF component appearing after onset of an oddball stimulus. The term 'oddball' comes from the stimulus in question, which the participant is asked to pay attention to, having an irregular onset rate, such as one out of five stimuli, and positioned within a sensory stream of alike 'standard' stimuli that have a regular onset rate, such as the remaining four out of five stimuli (Comerchero & Polich, 1999; Picton, 1992; Squires et al., 1975; Sutton et al., 1965). P3b is characterised by a large positive (P) polarity amplitude deflection, with its peak presenting at around 300 ms (3) post-stimulus and located at central-parietal electrodes (b). The N2 is another example component of the same trial-averaged waveform arising in oddball attention paradigms, seen as a negative polarity amplitude deflection, with its peak presenting at around 200ms post-stimulus and being visible at central-parietal electrodes (Luck, 2014).

In a similar way to the attempts to assign functional specialisation to induced power changes within discrete frequency bands, attempts have been made to interpret the components of ERPs and ERFs as having discrete functional specialisation (Neuper & Pfurtscheller, 2001; Woodman, 2010). For example, it has been proposed that the P3b component might reflect endogenous context updating of schemas in line with task demands (Donchin, 1981) or inhibition of extraneous processing to enhance attention and/or working memory processes (Polich, 2007; Polich & Criado, 2006; cf., Klimesch et al., 2007b). This is in part due to P3b's peak amplitude appearing to be proportional to cognitive performance (Bell et al., 2021; Porcaro et al., 2019), leading to the proposal that a reduction in amplitude may reflect a decline in task-specific cognitive resources and atrophy of underlying brain networks (Polich, 2007; Van Dinteren et al., 2014). Age-related changes have also been examined, with P3b peak amplitude typically decreasing in healthy ageing (Polich, 1996, 1997) and in age-related conditions such as mild cognitive impairment and dementia (Dauwels et al., 2010a; Hedges et al., 2016; Jiang et al., 2015; Porcaro et al., 2019). However, it is still not confirmed whether this mean amplitude reduction is driven by latency

jitter in the estimated single-trial peaks, which might be caused by an increasing variability of intra-individual neural response with increasing age (McDowell et al., 2003). For example, the latency jitter hypothesis was rebuffed after the inversely proportional age-peak amplitude relationship remained when statistically correcting for latency jitter (Walhovd et al., 2008). In summary, there is currently no conclusive answer on the meaning of ERP and ERF peak amplitudes and their relationships with age and cognitive performance, very much like the lack of clarity around induced changes.

Peak amplitude is not the only metric that can be used to characterise the components of ERPs and ERFs. P3b mean peak latency (i.e., the timing of the peak amplitude) also reliably increases alongside healthy ageing (Polich, 1996, 1997) and deleterious age-related conditions (Dauwels et al., 2010a; Duncan et al., 2009). Additionally, P3b latency is inversely proportional to cognitive performance (Howe et al., 2014; Pavarini et al., 2018), but whether this is a 'direct' (e.g., increased variability in the underlying brain activity) or an 'indirect' relationship (e.g., reflecting the effects of atrophy in regional cortical thickness) remains to be confirmed (e.g., Fjell et al., 2005, 2007, 2009). Still, it has been proposed that latency changes might reflect an age-related decline in the speed of controlled attention and/or working memory processing efficiency, linked to altered neural network integrity (e.g., loss or change of neural structure and cognitive resources) and communication efficiency, such as the increased variability in task performance and underlying neural functioning (MacDonald et al., 2009; Polich, 2007; Van Dinteren et al., 2014). Yet again though, any relationship between age, brain functioning, and cognitive performance is going to be complex and masked by numerous factors, such as those outlined by the deficit and benefit models of ageing. These relationships are made yet more opaque by a lack of understanding of the implicated cognitive faculties, such as attention and memory, and how they are represented in the brain in the first place (Cohen & Gulbinaite, 2014; Salthouse, 2010, 2016). As a result, it has been recommended to take a general, multiscale system-level interpretation of brain functioning and cognitive performance when analysing EEG data in attempts to establish metrics for application in clinical domains such as dementia (e.g., Koenig et al., 2020).

Compounding the difficulty in defining the meaning of event-related changes and their relationships with cognitive performance and chronological age, there has also been no unanimous agreement on an explanatory mechanism underlying the formation of evoked waveforms. A dichotomy persists; are ERPs new activity caused by the event and distinct from ongoing EEG activity, or reflecting phase modulations of the ongoing EEG? This dichotomy has been fuelled by the existence of two, longstanding theoretical models: the Evoked Model (EM) versus the Phase Reorganisation Model (PRM) respectively (see

Burgess, 2012, Klimesch, 2018, Sauseng et al., 2007, and Yeung et al., 2004, for overviews of these two models). The EM claims that ERPs comprise new time-locked and phase-locked EEG activity that is initially embedded within ongoing, spontaneous background activity yet is distinct from that activity. The distinct ERP signals are unveiled by averaging over trials, with each superimposed component of an ERP originating from discrete neuronal sources with distinct timecourses and oscillatory dynamics. In short, a new event causes a cascade of new brain activation, revealed by averaging out irrelevant ongoing brain activity over trials. Figure 2.5 provides a visual characterisation of the EM's explanation of ERPs, to establish its explanatory mechanism and permit greater clarity in how it differs from the PRM outlined next. This characterisation aligns with the functional specialisation perspectives on event-related changes in the EEG (Jervis et al., 1983; Makinen et al., 2005; Mazaheri & Jensen, 2006; Shah et al., 2004).

Figure 2.5

A visual representation of the EM with EEG data, with a) and b) showing the trial-averaged waveform excluding any superimposed signal, c) and d) showing the trial-averaged waveform of just the signal without any background noise, and e) and f) showing the trial-averaged waveform including signal superimposed on the irrelevant background noise (from Burgess, 2012).

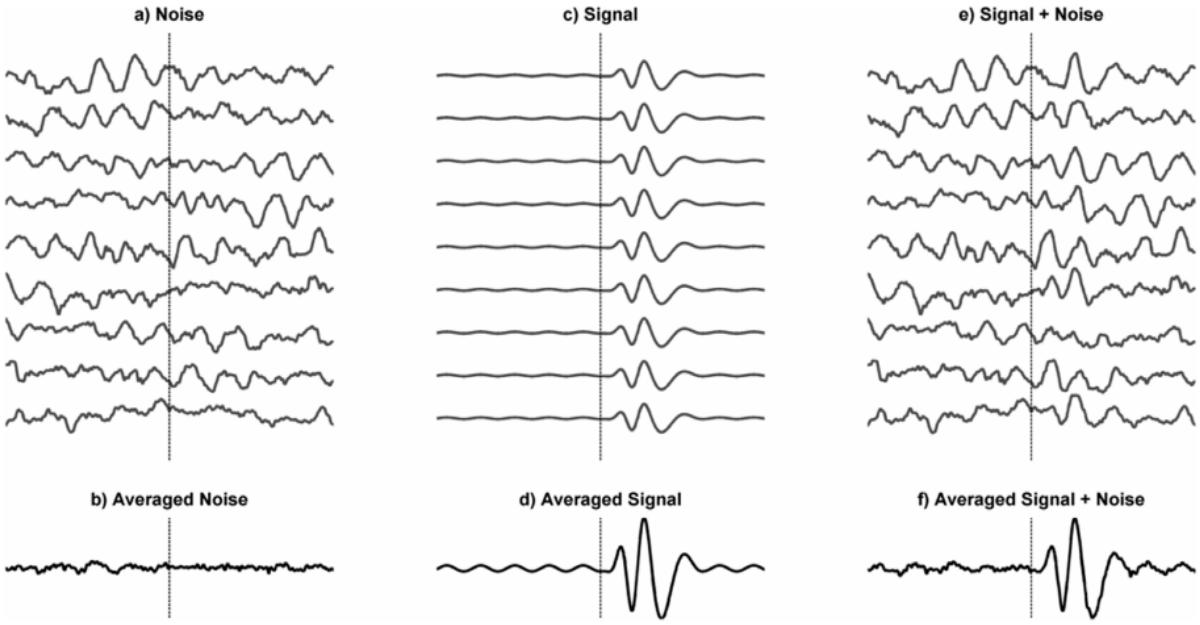

In contrast to the EM, the PRM proposes that an ERP is a by-product of averaging time-locked convergence in phase angles of the ongoing EEG, with each component reflecting different facets of that ongoing EEG. This convergence can be visualised as oscillations' peaks and troughs aligning and summating to produce an ERP. Figure 2.6 provides a visual characterisation of the PRM's explanation of ERPs, to establish its explanatory mechanism and permit greater clarity in how it differs from the EM outlined previously. This characterisation aligns with the general, multiscale system-level perspectives on event-related changes in the EEG. The PRM explains common ERP shapes by differences in the ongoing EEG (e.g., amplitude and frequency) and a varying time course in underlying phase alignment (e.g., latency). Therefore, ongoing activity is treated as a systematically modulated signal rather than spontaneous background noise. Whilst the EM and PRM originated as two discrete theories governed by their contrasting characterisations of ERPs (Sayers et al., 1974), the EM and PRM terminology has grown into umbrella categories that house numerous alternative models (see Burgess, 2012, Klimesch, 2018, Sauseng et al., 2007, and Yeung et al., 2004, for overviews of alternative models under these umbrella categories).

The Asymmetric Amplitude Modulation model (AAM; Mazaheri & Jensen, 2008) is a third, alternative model, which does not easily fit into either EM or PRM categories. It attempts to explain ERPs with a model developed on the asymmetric fluctuation in the alpha band's peaks and troughs. Specifically, it is proposed that the peaks are more strongly modulated than the troughs, which will result in a waveform deflection when multiple trials are averaged. Figure 2.7 provides a visual characterisation of the AAM's explanation of ERPs, to establish its explanatory mechanism and permit greater clarity in how it differs from the EM and PRM outlined previously. Whilst aligning with PRMs by implicating ongoing EEG/MEG activity, the AAM model attributes amplitude modulation, rather than phase modulation, as the core mechanism underlying the existence of ERPs (or ERFs in MEG).

Figure 2.6

A visual representation of three variants of the PRM with EEG data, with a) an instant phase reset in the on-going EEG, averaging over trials as an ERP, b) a gradual phase modulation with frequency increase in the on-going EEG, also averaging over trials as an ERP, and c) a gradual phase modulation with frequency slowing in the on-going EEG, again averaging over trials as an ERP (from Burgess, 2012).

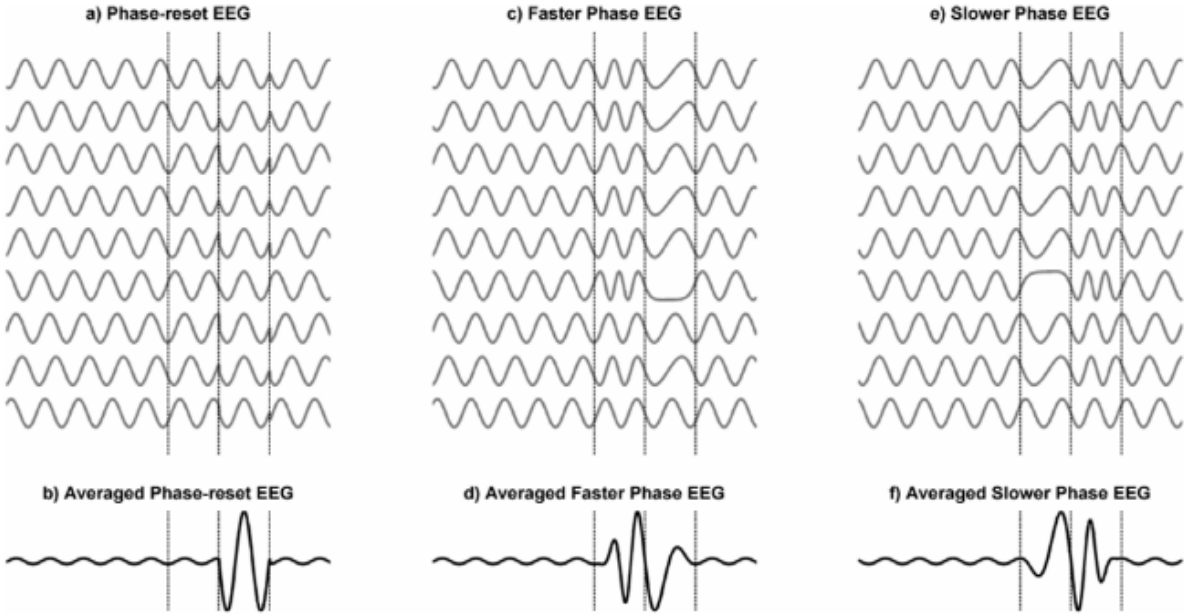

Figure 2.7

A visual representation of the AAM with MEG data, with A & C showing a symmetrical event-related change in amplitude of the on-going MEG averaging over trials to no ERF, and B & D showing an asymmetrical event-related change in amplitude of the on-going MEG, where peaks are more strongly modulated than troughs, averaging as an ERF deflection (from Mazaheri & Jensen, 2008).

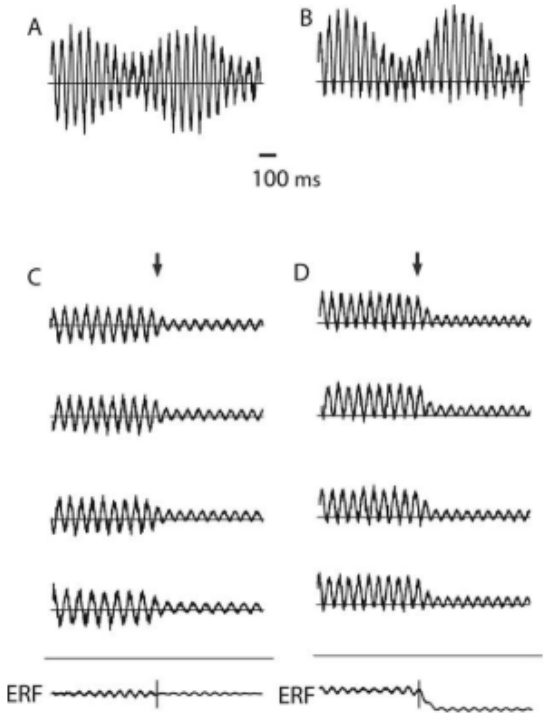

There are notable limitations of the EM. For example, predicted global amplitude increases post-stimulus have not materialised (Sayers et al., 1974), yet ongoing EEG pre-stimulus is related to component magnitude post-stimulus (Fellinger et al., 2011). The EM struggles to explain how EEG in the pre-stimulus period predicts post-stimulus amplitudes (Makinen et al., 2005; Klimesch et al., 2006). Another limitation of the EM is that it provides no accepted, mechanistic explanation of the traditional waveform shapes of event-related EEG. The EM attempts to explain the varying shapes by variability in sources, time course, and dynamics, which has proven very hard to test (Burgess, 2012). The AAM model does not provide a complete explanation of the shape and timing of event-related waveforms either, particularly beyond changes in alpha. That said, limitations also hampered the original PRM. For example, it proposed that ERPs only emerge from multiple trials with equivalent starting frequencies (i.e., phase reorganisation between trials, not within trials). This cannot explain the existence of single-trial ERPs (Jung et al., 1999, 2001; Makeig et al., 2002). Thereafter, researchers have proposed many contrasting, mutually exclusive versions of the

PRM in attempt to overcome limitations in the initial PRM (e.g., Barry, 2009; Basar, 1999; Fell et al., 2004; Fuentemilla et al., 2006; Hanslmayr et al., 2007; Klimesch et al., 2007c; Makeig et al., 2002; Ritter & Becker, 2009; Sayers et al., 1974, to name a few).

Over most of the contrasting PRM models, there is no clear explanation of when and how phase reorganisation occurs. For example, is there an instant phase reset or a gradual phase alignment? And how is this phase modulation represented in the frequency domain? This is an important discrepancy, because frequency is the change in phase over time, thus a wholly convincing PRM needs to explain how ERPs are created within the context of narrowband and broadband frequency changes. For example, does narrowband instantaneous frequency increase or decrease with phase modulation? And how does phase modulation progress across the broadband frequency range? Because EMs, PRMs, and the AAM do not provide a complete explanatory mechanism of evoked waveforms, an alternative PRM model called the Firefly Model (FM) was created (Burgess, 2012).

2.2.2 The Firefly Model of synchronisation through cross-frequency phase modulation: introducing the time of synchronisation gradient (t_{synch}G)

The FM proposes a markedly different mechanism to explain both evoked and induced changes in the EEG. This mechanism is a gradual slowing in the frequency domain of ongoing EEG that is concurrent with phase alignment. Specifically, the timing of this phase modulation is frequency dependent, with evidence, in the form of empirical EEG data and simulation models, supporting a systematic, cross-frequency phase locking (Lachaux et al., 1999) that progresses downwards through the broadband frequency range over time (Burgess, 2012). The timing of maximal phase alignment (i.e., time of synchronisation, t_{synch}) is proposed to occur in a power law curve across the broadband frequency range, starting at high frequencies (e.g., gamma) and working downwards towards delta. All narrowband instantaneous frequency dips are followed by a gradual rebound for phase desynchronization that represents a return to resting frequency segregation to prevent unnecessary cross-frequency interference. Figure 2.8 provides a visual characterisation of the FM's explanation of ERPs, to establish its explanatory mechanism and permit greater clarity in how it differs from the EM, other PRMs, and AAM outlined previously. This FM will form the crux of future experimental chapters 3, 4, and 5. Therefore, when considering the outstanding question of how phase modulation is represented in the frequency domain, the FM provides clear answers: that instantaneous frequency gradually decreases for phase alignment, and this fundamental mechanism follows a systematic pattern across the broadband frequency range over time.

Figure 2.8

A visual representation of the FM in both frequency domain (top panel) and time domain EEG data (bottom panel, including a) and b) inserts). In the frequency domain, the red line represents the averaged post-stimulus power spectrum, dotted blue lines represent the shift in the power spectrum as the ongoing EEG slows down to synchronise for various degrees of phase disparity over trials, and the blue line represents the averaged pre-stimulus power spectrum. In the time domain, the blue lines of insert a) represent post-event phase modulation with frequency slowing observed in oscillatory activity across base frequencies, and the red lines of insert a) represent the same oscillatory activity with no event-related change. T_{synch}, the timing of maximal phase alignment, is modelled as a power law curve, where latency is inversely proportional to frequency, before desynchronisation and a rebound to resting state. Insert b) shows the trial-averaged ERP from the post-event phase modulations via frequency slowing shown in the blue lines of insert a) (from Burgess, 2012).

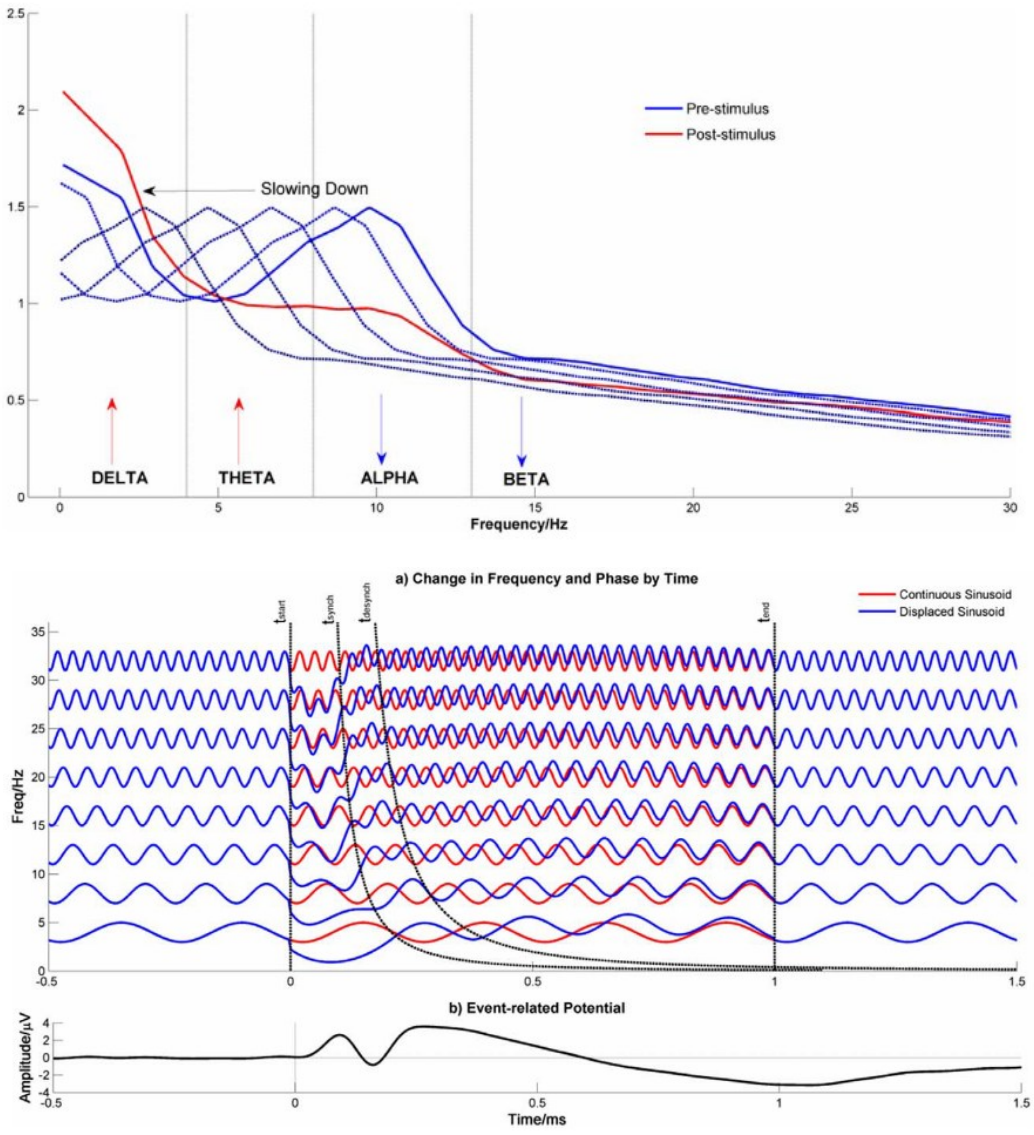

Therefore, the FM (Burgess, 2012) explains evoked changes by proposing that ERP components are caused by the ongoing EEG phase convergence (i.e., peak-peak and trough-trough summation) of different, decreasing source frequencies across time. Unlike other PRMs, this mechanism also allows for single-trial ERPs (Jung et al., 1999, 2001) and logically aligns with the VSH (Von Stein & Sarnthein, 2000), which had characterised EEG frequency as being inversely proportional to scale. The ERP waveform may, therefore, reflect task-relevant transition from resting state, to localised network communication (i.e., early high-frequency phase synchronisation), to widespread communication (i.e., late low-frequency synchronisation). In turn, the FM aligns with the suggestions that ERPs might be best characterised as travelling waves of multiscale, cross-frequency interactions in brain activity (e.g., Alexander et al., 2013; Klimesch, 2018; Klimesch et al., 2007a). In summary, the FM attempts to resolve limitations with previous PRMs by providing a specific mechanism to explain when and how phase modulation occurs, which accounts for ERPs' shape and timing and explains how ERPs are created within the context of narrowband and broadband frequency changes.

The FM (Burgess, 2012) explains induced changes with the same explanatory mechanism of synchronisation through cross-frequency phase modulation. For example, theta ERS and alpha ERD are reliable induced changes (Klimesch, 1999; Pfurtscheller & Lopes da Silva, 1999). These changes have previously been isolated to each frequency band and interpreted as representing distinct functional specialisations (e.g., alpha for attention processes, and theta for memory processes; Klimesch, 1999; Klimesch et al., 2007b). However, the FM proposes that theta ERS reflects the slowing of alpha band activity into the theta band, and alpha ERD the slowing of beta band activity into the alpha band. Given that the FM posits no global changes in amplitude from pre-stimulus to post-stimulus periods, pre-stimuli averaged power spectra show higher alpha power than theta power, with alpha power shifting into theta post-stimulus. Pre-stimuli averaged power spectra also show lower beta power than alpha power, with beta power shifting into alpha post-stimulus. A delta ERS can be explained with the smearing of alpha power across lower frequencies. This smear is determined by the extent of frequency slowing that is required to reach a target phase over multiple trials, and the proportion of ongoing EEG responding to an event. Assuming that trial-to-trial baseline phase is random, the required frequency slowing for t_{synch} is set by each trial's baseline phase. The more often a large frequency dip is required, the more alpha smear into the delta band, thus the delta ERS is amplified by averaging over trials. However, Burgess (2012) clarified that it is unlikely that all the ongoing EEG will respond to an event, although determining the exact quantity will be a complex task likely influenced by many inter-individual, intra-individual, and task demand factors. That said, by

assuming approximately 50% of ongoing EEG responded to an event, Burgess was able to satisfactorily model the empirical data of a visual recognition paradigm in twenty healthy young adults. Consequently, the lower the proportion of ongoing EEG that responds to an event (and the lower the SNR), the smaller the recorded trial-averaged dip in frequency. These explanatory mechanisms of varying frequency slowing, response proportions, and measurement noise with averaging smear may also explain why there is no direct translation of the pre-stimuli power spectrum to lower frequency bands post-stimuli, but there is usually a partial transition of ongoing power from high to low frequency when comparing pre-stimulus and post-stimulus power spectra across many tasks.

To summarise the impact of the FM, it is a new PRM that provides a distinctive explanatory mechanism for event-related changes in the EEG. This mechanism can explain when phase aligns and how it aligns in the context of changes in frequency, whilst also proposing that evoked and induced changes can be considered as fundamentally related phenomena. Burgess (2012, p. 20) summarised that the FM 'may prove to be a useful guide in helping us move from a focus on surface features of the ERP, such as amplitude and latency of peaks, towards a study of the true deep structure of event-related changes in the EEG'. Indeed, the FM encourages healthy caution in assigning discrete functional specialisation to peaks of ERP components, particularly later-latency components, and induced power changes. Instead, events cause changes in all ongoing frequency band activity, thus frequency is not rigidly fixed despite having a preferred resting rate, and these changes may represent task-relevant information processing and communication across neural networks, where high frequency/early ERP components reflect localised network communication and low frequency/late ERP components reflect widespread network communication. The FM does not only provide a theoretical explanation of induced and evoked changes though. Empirical measurement of the underlying cross-frequency phase modulation mechanism could provide alternative metrics that may improve our understanding of the EEG, but also of age-related changes in the EEG and, in turn, how to detect and track deleterious age-related changes. At the time of writing, an examination of the FM's explanatory mechanism in an ageing context had never been done before.

Empirical mode decomposition (EMD) allows for a data-driven and adaptive decomposition of a complex oscillation into discrete intrinsic mode functions (IMFs), which are core components of the original signal (Huang et al., 1998; Sweeney-Reed & Nasuto, 2007; Sweeney Reed et al., 2018). EMD uses a data reduction, interpolation-sifting procedure, which involves identifying maxima and minima of the source signal to interpolate cubic spline fits. These fits permit the calculation of a mean to subtract from the original signal, and this procedure produces the IMF components when repeated consecutive times

on each mean until the mean of the interpolation is monotonic (see Burgess, 2012, and Cohen, 2014, for overviews of the EMD procedure). Figure 2.9 provides a visual representation of the EMD procedure when applied to EEG data, but the same procedure can be applied to MEG data. EMD will form a key part of the analyses of both EEG and MEG datasets in future experimental chapters 3, 4, and 5. A key advantage of combining EMD with the Hilbert transform is that instantaneous metrics (i.e., time-varying, not stationary) can be estimated across the broadband frequency range without the requirement to predetermine frequency bands (Cong et al., 2009; Burgess, 2012). That is, the IMFs extracted per trial reflect naturally occurring, distinct frequency components, and the Hilbert transform can be applied to each IMF to provide analytic signals (i.e., comprising both real and imaginary components) for the estimation of the instantaneous measures of amplitude, frequency, and phase per component (Bruns, 2004; Cohen, 2014). The FM characterises time of maximal PLV (Lachaux et al., 1999) per IMF as t_{synch}. In other words, t_{synch} is the timepoint where phase, within a frequency component (represented as the IMF's mean baseline frequency), is most similar across trials in event-related paradigms. t_{synch} is a prime new metric to allow for interrogation of the deep structure of event-related changes across chronological age. Specifically, across a widespread frequency range (i.e., across ordinal IMFs), it is possible to examine whether a systematic, gradual frequency slowing occurs with phase alignment over time. Having estimated t_{synch} in a range of different frequency components, it will be possible to perform model fitting across the IMFs' t_{synchs}, which will provide a novel metric coined the time of synchronisation gradient, $t_{synch}G$.

Figure 2.9

A visual representation of EMD, from the raw EEG through the data reduction, interpolation-sifting procedure via identifying maxima and minima of the source signal, interpolating cubic spline fits, calculating a mean to subtract from the original signal to give the IMF (a), then repeating the procedure (b and c) until the mean of the interpolation is monotonic, so either nonincreasing or nondecreasing (from Burgess, 2012).

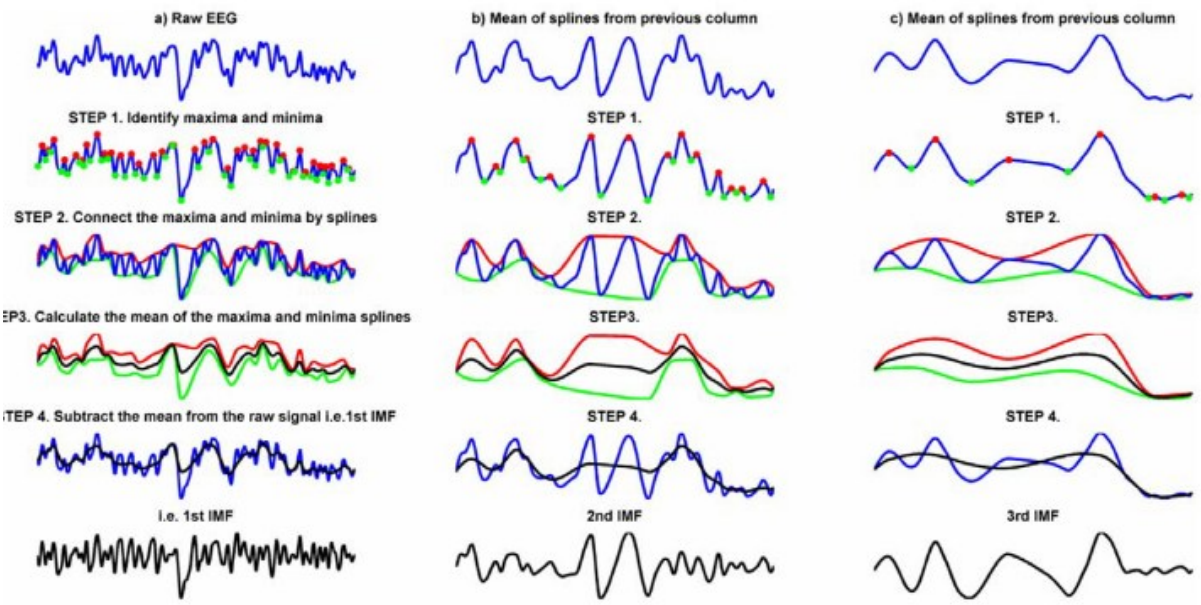

The new $t_{synch}G$ metric can be thought of as a direct empirical measurement of the underlying cross-frequency phase modulation mechanism proposed by the FM to underpin the formation of evoked and induced changes. In other words, $t_{synch}G$ is a quantification of the timecourse of information processing and communication through neural networks of increasing scale, such that the flatter (more positive) the gradient, the slower or more variable (e.g., inefficient) the multiscale communication. If the FM holds up to empirical scrutiny, $t_{synch}G$ could not only advance our understanding of age-related changes in the brain at a deeper structural level, but it could also be developed into a new way to track age-related changes in the brain. For example, $t_{synch}G$ could be used to estimate 'brain age' as EEG-age, which could then be compared with actual chronological age and any discrepancy between the two might reflect some deleterious age-related change or even condition (e.g., MCI). The new EEG dataset and MEG dataset collected for this thesis have enabled the interrogation of these event-related changes in the context of ageing, spanning Chapters 3, 4, and 5 (signposted in Chapter 1 and Table 2.1).

2.3 EEG and MEG data analyses: measuring resting-state oscillatory dynamics

Declaration of prior use: a substantial portion of this subsection has been submitted as part of a preprint on PsyArXiv and for publication in the journal Psychophysiology.

2.3.1 Peak alpha frequency

When humans sit at rest with their eyes closed (i.e., in a 'resting state'), the EEG power spectrum is distributed such that the power at each frequency is approximately proportional to the reciprocal of the frequency (Power $\propto 1/f$) plus a peak in power in the alpha frequency band (He, 2014; Lopes da Silva, 2013; Pritchard, 1992). The frequency of the peak in power (i.e., peak alpha frequency, PAF) increases rapidly through childhood, reaching 10 to 11 Hz in early adulthood, before gradually declining to an average of 8 to 9 Hz by 80 years of age. The change in mean PAF across the human lifespan is arguably the best-established EEG-correlate of age and has been reported not only from the visual inspection of relatively small numbers of EEG recordings (Duffy et al., 1984; Dustman et al., 1993; Hughes & Cayaffa, 1977; Mizukami & Katada, 2018; Obrist, 1954; Stroganova et al., 1999) but also in multiple studies using large sample sizes and automated algorithms (Aurlien et al., 2004; Chiang et al., 2011; Finley et al., 2022; Hashemi et al., 2016; John et al., 1980; Lodder & van Putten, 2011; Merkin et al., 2023; Samson-Dollfuss & Goldberg, 1979). PAF's short-term test-retest reliability (e.g., between days, weeks, and months) has been reported as good-to-excellent in adults (Joffe et al., 2021; Näpflin et al., 2007; Popov et al., 2023; Salinsky et al., 1991), suggesting that PAF is a stable electrophysiological measure across short intervals in adulthood. Longitudinal studies further confirmed the rapid increase in PAF from the earliest months of life through childhood and adolescence (Cragg et al., 2011; Freschl et al., 2022; Lindsley, 1939; Schaworonkow & Voytek, 2021; Soroko et al., 2014) before a steady, linear decline in PAF from early adulthood onwards (Kondacs & Szabó, 1999). However, longitudinal studies of PAF across adulthood are less common and typically follow participants for only a few years. In summary, although we cannot be sure what any individual's PAF trajectory may be, we can be quite confident of how the population-level PAF changes with age.

Brain-ageing phenomena are often associated with changes in cognitive functioning, as already demonstrated with event-related changes in the EEG, and PAF is no exception. PAF remains positively correlated with scores on a range of tests of cognitive abilities (e.g., attention, processing speed, and memory) even when samples are age-matched, such that lower PAF predicts worse performance and may reflect inferior information processing (Angelakis et al., 2004a; Angelakis et al., 2004b; Bornkessel et al., 2004; Clark et al., 2004;

Rathee et al., 2020; Surwillo, 1961; Trammell et al., 2017). Grey and white brain matter both deteriorate with advancing age (Grady, 2012; Hofmann et al., 2022), and a tranche of recent neuroanatomical evidence suggests that changes in the structure of white matter, particularly of thalamocortical networks, play a crucial role in both the slowing of PAF and age-related decline in cognitive functioning (Bells et al., 2017; Hindriks et al., 2015; Hughes & Crunelli, 2005; Minami et al., 2020; Valdés-Hernández et al., 2010). Understandably then, PAF is lower in persons with age-related conditions such as mild cognitive impairment (Babiloni et al., 2011; Jelic et al., 2000; Prichep et al., 2006) and dementia (Babiloni et al., 2021; Klimesch et al., 1990; Neto et al., 2015; Penttilä et al., 1985). It has been suggested that PAF may be an electrophysiological marker of general intellectual capacity, 'g' (Grandy et al., 2013), or that it reflects specific aspects of cognition such as processing speed (Ociepka et al., 2022). When considering what are theorised to be fundamental mechanistic changes of the ageing human brain (outlined in Chapter 1 as a wider distribution of cortical processing with decreasing efficiency across the adult lifespan), a slowing in PAF could well be reflecting a transition to larger, perhaps less specialised neural networks, assuming that the scale of the network is indeed inversely proportional to the frequency (Von Stein & Sarnthein, 2000). However, the recurring caveat on interpreting relationships between chronological age, neural function, and cognitive performance is again highly pertinent; these relationships will be complex and are not yet fully understood. In summary, a decline in PAF is an oft-reported, normal brain-ageing phenomenon that likely reflects changes in neural and cognitive integrity, although no specific mechanism or interpretation has been established beyond reasonable doubt, just like with the event-related changes in the EEG.

Currently, there are also practical limitations in using PAF as a proxy to track age-related changes in integrity. One limitation is that the frequency resolution of a typical EEG power spectrum is poor. A widely used method to estimate the EEG power spectrum, Welch's method (Welch, 1967), involves splitting an EEG recording into short, stationary, artefact-free segments, performing the Fast Fourier Transform (FFT) on each segment, and averaging. The frequency parameters depend on the sampling rate of the EEG recording and the length of the segments, which, given typical values (e.g., 500 Hz and 4 seconds), will give a frequency resolution no better than about 0.25 Hz. With the average decline in PAF estimated at around 1 to 2 Hz over six decades, a frequency resolution of 0.25 Hz is sufficient to detect relatively large changes in PAF across the lifespan. Alternative methods of estimating the EEG power spectrum, such as autoregressive methods (AMs), are rarely used even though they offer the advantages of higher frequency resolution and smoother EEG power spectra (Gersch, 1970). AMs estimate the EEG power spectrum by regressing each value of the EEG time series onto a set number of past values. This number, called the

model order, determines the period of the lowest frequency detectable, and a higher model order allows for better frequency resolution (Takalo et al., 2005). As a statistical approach, AMs model error in the data, which enables them to produce smoother EEG spectra than conventional methods, and this should improve the ability to interrogate and track fine-grained changes in PAF.

Another limitation in using PAF to track age-related changes is that there is no consensus as to the best way to estimate PAF, because, as Corcoran et al. (2018) suggest, defining PAF "poses a nontrivial challenge, and may rely on subjective assessments or arbitrary criteria" (p. 2). In other words, there is no 'true' PAF, but there is a set of well-established, distinct approaches to estimating PAF. A researcher who defines PAF as the frequency of maximum power in the EEG spectrogram (i.e., the Naïve Peak Alpha Frequency method, N-PAF) is faced with several problems. One is that the N-PAF method offers no guidance on how to handle cases where there may be two or more peaks in the alpha frequency range, nor where there are no peaks at all (Chiang et al., 2008; Olejarczyk et al., 2017). Another problem is that PAF varies across scalp sites (Mahjoory et al., 2020; Quinn et al., 2021), although the extent of this topographical variation and its relationship to the SNR in the EEG spectrogram remains undetermined. One way to deal with within-subject variation is by calculating the arithmetic mean PAF, which requires taking an average of the estimates of PAF obtained from different scalp locations or calculating a single estimate of PAF from the EEG power spectrum averaged across scalp locations. A third issue is that the N-PAF method assumes fixed frequency bounds (e.g., 7 to 13 Hz for alpha frequency), which is questionable given that PAF varies with age, and misdefined boundaries can cause problems due to the exclusion of alpha peaks or inclusion of peaks that are not alpha (Donoghue et al., 2020, 2021; Haegens et al., 2014). A complete method for estimating PAF should be able to readily deal with any number of peaks, within-subject variance, and individual differences in the alpha frequency band. No existing method meets all these criteria, but several other demonstrably useful ways of estimating PAF do exist.

These alternative methods to estimate PAF include the Corcoran-PAF (C-PAF) method, proposed by Corcoran et al. (2018), which involves identifying the PAF from the smoothed EEG log(power) spectra across multiple channels, taking the average weighted by channels' SNR. The Klimesch-PAF (K-PAF) method, first proposed by Klimesch et al. (1990, 1993) and adapted by Corcoran et al. (2018), is based on the centre-of-gravity of the individually defined alpha band. Corcoran et al. (2018) have shown that both the K-PAF and C-PAF methods can estimate PAF in nearly all participants. Furthermore, in simulations where there was a single peak, both methods outperformed N-PAF, and C-PAF was superior to K-PAF in cases of low SNR.

2.3.2 Introducing alternative metrics in resting-state paradigms

The Modelled-PAF (M-PAF) method is another alternative, curve-fitting approach to estimating PAF, previously used as an automatic algorithm in large-scale studies. It involves modelling the EEG power spectrum as one or more frequency bands (typically assumed to follow a Gaussian distribution) superimposed on a 1/f slope (Chiang et al., 2011; Lodder & van Putten, 2011). The mean frequency of the Gaussian distribution used to represent the alpha frequency is taken as the estimate of PAF. The N-PAF, K-PAF, C-PAF, and M-PAF methods are not free from assumptions, and each method requires some user input. For example, C-PAF requires pre-defined alpha bounds and a minimum value for the power of alpha peaks. M-PAF involves fitting a non-linear model, and solving the model requires the user to pre-define boundaries for the parameters. These parameters include the upper and lower limits of the mean and standard deviation of the Gaussian that represents the alpha frequency band. Once the parameters are set though, PAF can be estimated without further user intervention. One advantage of M-PAF is it can be readily extended to frequency bands other than alpha and incorporates the 1/f slope, thus both periodic (e.g., traditional oscillatory bands) and aperiodic (e.g., non-oscillatory 1/f slope) components of the EEG power spectrum can be considered (Donoghue et al., 2020). M-PAF could also be implemented alongside AM and singular value decomposition (SVD) to further improve SNR of the PAF estimate. SVD (Harner, 1990) deconstructs an EEG input into a linear combination of components and, when used to improve the SNR of EEG by data reduction, emphasises features of the EEG that are consistent across electrodes in an individual. This is comparable to creating a weighted-mean EEG dataset, where the weighting is by the common variance across electrodes.

One way to circumvent the difficult choices required when estimating PAF is to consider a distinct metric that, at the time of writing, has not previously been used to estimate chronological age but could improve SNR and provide a robust assessment of age-related changes in the EEG. That metric is a quantification of age-related changes across the broad EEG power spectrum using a multivariate method called Partial Least Squares (PLS) regression. PLS, which can be thought of as a combination of principal component analysis and regression, is particularly useful where the independent predictor variables are highly correlated, as they invariably are with spectral data. Widely used for analysing spectral data in Chemistry (Wold et al., 2001), PLS has been used with EEG data too, particularly event-related potential data (Lobaugh et al., 2001; McIntosh & Lobaugh, 2004), with multiple tutorials now available on how to run PLS-based analyses with different types of neuroimaging data (e.g., Alin et al., 2009; Krishnan et al., 2011). PLS regression is used when independent predictor variables can be represented as a two-dimensional matrix (e.g.,

participant-by-spectra); this makes it possible, for example, to analyse the relationship between spectral data from multiple participants and chronological age in the same analysis. In summary, PLS regression is an alternative, multivariate approach to probing amplitude across broad power spectra, with EEG-age as the outcome estimate of brain age. Like $t_{synch}G$ can be considered an insight into the deep structure of event-related changes in the brain, PLS regression analysis of the broad frequency spectrum can be considered a more holistic and distinct measure of the resting state brain compared to targeting discrete frequency bands and PAF respectively.

There is extensive literature on the effects of ageing on the EEG, particularly PAF, but here, in a reversal of convention, we wanted to use the EEG, interrogating both the broad power spectrum and the frequency of the peak in power, to estimate chronological age. EEG-age and PAF-age are distinct metrics but can be compared in their ability to estimate chronological age, with the fact that they are distinct as a reason to make the comparison. The applied motivation for this approach was the same as for interrogating peak components of ERPs and $t_{synch}G$ in an event-related context; an individual's brain age might act as a proxy of their general brain functioning. If it were possible to reliably estimate an individual's chronological age based on their M-PAF and/or broad EEG power spectrum, then this EEG-age could be compared with actual chronological age and any discrepancy between the two might reflect some age-related condition, either protective or deleterious. The next four experimental chapters apply $t_{synch}G$, M-PAF, and PLS-derived EEG-age to advance our understanding of event-related and resting-state EEG and MEG, to advance our understanding of age-related changes in the brain, and to establish new ways to track age-related changes over time. The new EEG dataset collected for this thesis has enabled the interrogation of resting-state oscillatory dynamics in the context of ageing in Chapter 6 (signposted in Chapter 1 and Table 2.1).

Chapter 3: Testing the Firefly Model of synchronisation through cross-frequency phase modulation: establishing $t_{synch}G$

3.1 Introduction

The creation of the FM was a step towards a unified understanding of event-related changes in the EEG. It explains both evoked and induced changes with a mechanism of systematic, gradual frequency slowing of ongoing EEG that is concurrent with phase alignment (Burgess, 2012). By measuring the phase alignment with a PLV (Lachaux et al., 1999), the timing of maximal phase alignment (i.e., t_{synch}) is proposed to occur in the form of a power law curve across the broadband frequency range, starting at high frequencies (e.g., gamma and beta) and working downwards towards lower frequencies (e.g., theta and delta) over time. Evidence to support the existence of this cross-frequency phase modulation mechanism came from both empirical data and simulation modelling (Burgess, 2012). The results were interpreted under the VSH (Von Stein & Sarnthein, 2000), where the scale of the network is proposed to be inversely proportional to the frequency, and linked to synchronisation processes that have been shown to exist in the natural world and the cortex of animals, such as macaque as well as humans (e.g., Geisler et al., 2010; Lowet et al., 2017; Neda et al., 2000; O'Keefe & Reece, 1993; Singer, 2018; Woolnough et al., 2022). Additionally, the complementary grand theories of travelling waves and multiscale interactions (Alexander et al., 2013; Cohen & Gulbinaite, 2014; Klimesch, 2018), comprising the hypothesis that cross-frequency synchronisation underpins thalamocortical network communication (Ribary et al., 2019; Voytek et al., 2015b), have gained further traction in recent years. The FM, therefore, provides a unified explanation of both evoked and induced changes and, in turn, a plausible explanation of information processing and communication through neuronal networks of increasing scale over time. The model also aligns with increasingly popular general, multiscale system-level perspectives on event-related changes in the EEG.

Compared to what Burgess (2012, p. 20) considered to be 'surface features' such as ERS/ERD in discrete frequency bands and the amplitude and latency changes in discrete peaks of ERPs, the FM may allow for the study of 'the true deep structure of event-related changes'. Indeed, $t_{synch}G$, the gradient across multiple t_{synch} at different mean instantaneous frequencies, is a quantification of the FM's explanatory mechanism. For example, the flatter (more positive) the gradient, the slower or more variable (e.g., inefficient) the multiscale communication. This novel metric has the potential to improve our understanding of the ageing human brain and how to detect and track age-related changes. At the time of writing, the FM and $t_{synch}G$ had never been examined in the context of healthy ageing. This is likely

because there is a pressing need to first demonstrate the replicability of the FM model's empirical representation, to support that it offers an empirically credible explanation of event-related changes via systematic oscillatory phase synchronisation and frequency slowing. It is well known that EEG data are noisy, that EEG data analysis has many researcher degrees of freedom, and that, in turn, successful replication is a fundamental characteristic of science (Cohen, 2014; Luck, 2014; Pavlov et al., 2021). However, there are also more specific theoretical and practical reasons to attempt a replication study in this case.

Burgess (2012) recruited twenty adults with a mean age of 26 years (*SD* = 5.6, *Range* = 19-41) to complete a demanding visual recognition memory task, and did not report any evidence of controlling for health and normal levels of cognitive performance in this young sample of limited size. Furthermore, whilst there was clear evidence for cross-frequency phase modulation over time, there was no differentiation between the different conditions of the visual recognition memory task (e.g., New Faces versus Old Faces). This lack of explanatory power may have been caused by a methodological issue rather than a fundamental flaw in the FM though, where the difference in task demands between the experimental conditions were too subtle given the analytical context. Another unanswered question arises from the lack of comparisons between sensory modalities in the original proof-of-principle for the FM. For example, visual and auditory ERPs show distinct waveforms and attributes in their peaks, such as a later peak latency in visual P3b (e.g., Bennington & Polich, 1999; Comerchero & Polich, 1999). In summary, it is unknown whether the FM replicates across different ERPs, particularly those from attention paradigms with lower task demands than the original visual recognition memory paradigm. Furthermore, it is unknown whether the FM's explanatory mechanism can differentiate between different conditions with more substantial differences between them, and then between visual and auditory modalities too. An oddball attention paradigm would allow for comparisons within and between sensory modality (i.e., visual and auditory) and condition (i.e., oddball and standard), with the conditions of auditory oddball (AO), auditory standard (AS), visual oddball (VO), and visual standard (VS). This approach also makes good, applied sense with the end goal being to use $t_{synch}G$ to track age-related changes in the brain. Simpler tasks, such as the oddball attention paradigm compared to the visual recognition memory task, would be more suitable in clinical contexts (Duncan et al., 2009) and across a range of different patient populations (e.g., blind and deaf).

Our objective was to determine whether the FM is an empirically credible, alternative explanation of event-related EEG that has the potential to be used in an ageing context. This would not only advance our understanding of event-related EEG (aim #1 of this thesis), but also set the foundation for further study to improve our understanding of age-related

changes in the brain (aim #2 of this thesis) and, potentially, how to track deleterious age-related changes (aim #3 of this thesis). First, we wanted to replicate frequency and phase modulations as the explanatory mechanism of event-related changes in the EEG. Based on Burgess (2012), we predicted that changes in instantaneous frequency and PLV would be negatively cross-correlated, with post-stimulus frequency slowing concurrent with increasing PLV. Second, we sought to explore the ability to estimate a $t_{synch}G$ metric. Based on the FM and the VSH, it was predicted that modelling t_{synch} across ordinal IMFs (i.e., cross-frequency) would follow a power law curve to reflect the systematic, gradual spread of information processing and communication across neural networks of increasing scale (thus decreasing frequency) over time. If the power law curve followed the predicted direction of t_{synch} frequency being inversely proportional to latency, this power law curve would be transformed into a linear space where a negative log-log polynomial line would provide the time of synchronisation gradient, $t_{synch}G$. Finally, we wanted to see if $t_{synch}G$ differed across conditions (oddball versus standard) and modalities (auditory versus visual) in an oddball attention paradigm. It was predicted, based on there being differences in the ERP waveforms between different conditions and sensory modalities, that there would be differences in $t_{synch}G$ too.

3.2 Methods

3.2.1 Participants

Sixty healthy adults (24 men, 36 women; 5 left-handed, 55 right-handed) volunteered to participate from across the chronological age range (*M* = 49 years, *SD* = 17.9, *Range* = 20 to 78). Having reached our resource limit for this EEG dataset, collected for use in Chapters 3, 4, and 6 of this thesis, sensitivity power analyses were conducted for the key age relationships of interest (signposted in Chapter 2). Because the age relationships are not considered in this chapter, the sensitivity power analyses are presented in Chapters 4 and 6 instead, where the age relationships are considered (i.e., see the Participants subsections of Chapters 4 and 6 for event-related and resting-state respectively). All participants were recruited via Aston University's advertising portals, which includes the Aston Research Centre for Health in Ageing (ARCHA) panel that comprises older adults from around the UK who volunteer to take part in studies at Aston University. This study received a favourable opinion from Aston University's Research Ethics Committee (AU-REC) and was carried out in accordance with the Declaration of Helsinki and the British Psychological Society Code of Human Research Ethics. Written informed consent was obtained from each participant, and they were reimbursed £15 for their participation.

All participants actively reported having no experience of traumatic brain injury, no diagnosis of neurological or psychiatric disorder, and no known cognitive impairment.

Participants were also screened for depression via the Geriatric Depression Scale-15 (GDS-15; Sheikh & Yesavage, 1986) and cognitive impairment via the Quick Mild Cognitive Impairment Screen (QMCI; O'Caoimh & Molloy, 2017). The QMCI is a paper-based, quick-to-administer assessment of general cognitive ability, comprising validated cut-off scores for normal cognitive functioning, mild cognitive impairment, and dementia (O'Caoimh et al., 2017). Two individuals (aged 59 and 78) scored just below the optimal unadjusted cut-off score for cognitive impairment (<62). However, when accounting for their chronological age and number of years in education, both participants scored above their optimal adjusted cut-off score (<60 and <54 respectively). Six individuals (aged 24, 24, 32, 38, 52, and 59) scored on or just above the cut-off score for mild depression (≥5) on the GDS-15, and two individuals (aged 44 and 68) scored on or just above the cut-off score for moderate depression (≥10). No participants scored ≥12, indicating no cases of severe depression.

3.2.2 EEG recording

EEG was recorded while participants completed auditory oddball (AO and AS conditions) and visual oddball (VO and VS conditions) paradigms. The EEG setup used for data collection is outlined in Chapter 2 of this thesis. With a mean electrode impedance of 11.51 kΩs (*SD* = 10.03, *Range* = 0.06 to 90.75) and 11.58 kΩs (*SD* = 10.10, *Range* = 0.03 to 112.12) for the auditory and visual paradigms respectively, most electrodes had similar impedances that were less than the reported optimal cut-offs of 40 kΩs (Ferree et al., 2001; i.e., 98% of 3780 electrodes per paradigm respectively) and 50 kΩs (Kaneko et al., 2021; i.e., 99% of 3780 electrodes per paradigm respectively) for the high-impedance ANT EEG system. A mastoid electrode (M1) reached the highest impedance, although this was still below the workable maximum of 200 kΩs (Ferree et al., 2001).

The order of the auditory and visual paradigms was counterbalanced across participants, within each decade of age. Participants closed their eyes during the auditory paradigm and listened to recurrent tones of 500 Hz for the standard condition and 1000 Hz for the oddball condition. These tones had a rise and fall of 10 ms and were presented at approximately 60 dbSPL. In the visual paradigm, participants saw the letter O for the standard condition and the letter X for the oddball condition. These letters were matched on point size (35), colour (white, on a black background), and font (Calibri), and presented at the centre of the screen. A central fixation point was presented for two seconds at the beginning of each visual block. The oddball presentation was pseudo-randomised at a rate of 20% in sets of five stimuli (i.e., one oddball and four standards). In both visual and auditory paradigms, participants saw or heard one practice set before completing the experimental blocks, where there were 60 oddball stimulus presentations and 240 standard stimulus presentations split over 3 experimental blocks. The number of oddball presentations

within each consecutive block was fixed at 22, 17, and 21 for the auditory paradigm, and 25, 16, and 19 for the visual paradigm. Participants were asked to keep a mental count of how many oddballs they encountered per block and were questioned on that number at the end of each block. One trial lasted 2 seconds, with 1 second before stimulus onset and 1 second from stimulus onset. All stimuli were presented for 150 ms, meaning there was an interstimulus interval of 1850 ms. Participants rested between blocks and between visual and auditory paradigm recordings.

The oddball attention paradigms were designed and presented on E-prime Professional (Version 2.0). Stimulus onset triggers were sent from E-prime to the EEG system via a Windows 7 Lenovo ThinkCentre PC's parallel port. Stimuli were presented on a 22" 1680x1050 Philips LCD monitor (Brilliance 220BW9; Brightness = 49; Contrast = 50; 9300K colour temperature). Participants were sat approximately 60 cm from screen to head. Two speakers (Dell, Model A215) sat approximately 65 cm from the participants, with participants sitting centrally between both speakers. The room layout was kept identical for each participant, with lighting turned up during rest periods and dimmed during the paradigms via a programmable dimmer.

3.2.3 Data preparation

Data were exported as EEProbe (.cnt/.evt) files, and the ANT eego™ recording software's in-built data preparation montage was not applied to avoid phase distortion from the Butterworth infinite impulse response filter (Widmann et al., 2015). Saved on secure cloud storage (Box, version 2.9.369), EEG data (.set/.fdt) was imported into MATLAB (R2021a) for offline analysis with EEGLAB (2021.0; Delorme & Makeig, 2004) and purpose-built code. First, EEG was demeaned, filtered between 0.1 Hz to 100 Hz, and segmented from -1000 ms to +1000 ms around stimulus onset with a 200 ms pre-stimulus absolute mean baseline correction. The filter was a one-pass finite impulse response (FIR; zero-phase and hamming-windowed; Widmann et al., 2015) to avoid phase distortion. Having linearly detrended the EOG data, Gratton EOG correction (Gratton et al., 1983) was applied to all epochs, which uses regression to estimate and apply blink and eye movement correction factors to subtract EOG artefacts from the EEG. Whilst Gratton EOG correction may remove a small proportion of brain activity from the data, it was implemented as a lighter touch data cleaning compared to methods such as independent components analysis (ICA). It is not clear whether ICA distorts phase relations, potentially differentially across frequencies (Montefusco-Siegmund et al., 2013; Thatcher, 2012), and whether it is worth the added complexity and user input, particularly in a clinical context, for the average improvement in SNR (Delorme, 2023).

Data were referenced to the average reference (excluding the noisy, high-impedance level mastoids), with CPz reconstituted and trials comprising values outside -120 to +120 μV rejected. Consequently, for the AO condition, a mean of 5 trials were rejected (*SD* = 8.69, *Range* = 0 to 44). For the AS condition, a mean of 18 trials were rejected (*SD* = 29.72, *Range* = 0 to 175). For the VO condition, a mean of 8 trials were rejected (*SD* = 10.57, *Range* = 0 to 56). For the VS condition, a mean of 31 trials were rejected (*SD* = 39.78, *Range* = 0 to 217). Data preparation was completed without reference to demographic data, such as chronological age, but we later checked whether age and the number of rejected trials were correlated, and they were significantly positively correlated (AO: $r = .30$, $p = .022$; AS: $r = .31$, $p = .016$; VO: $r = .35$, $p = .007$; VS: $r = .36$, $p = .005$). From here on, a central-parietal electrode region of interest (ROI) was used in the hope of enhancing SNR (fifteen electrodes: C3, Cz, C4, CP1, CP2, P3, Pz, P4, C1, C2, CP3, CP4, P1, P2, and CPz; Figure 2.2). The fifteen-electrode ROI was informed by P3b topography and published recommendations for oddball attention paradigms (Huffmeijer et al., 2014; Riha et al., 2020; Squires et al., 1975; Polich, 2007).

3.2.4 Signal analysis

Pre-stimulus and post-stimulus power spectra (-1000 ms and +1000 ms around stimulus onset respectively) were estimated in three alternative ways. First, an AM power spectral density estimation was used with the covariance method of model order 128 that covers a span of 256 milliseconds (128×2; MATLAB function ‘pcov.m’), which allows for the estimation of spectral density values from 0.1 to 45 Hz at a resolution of 0.1 Hz. Frequencies above 45 Hz were excluded from analysis because of their low SNR, including the United Kingdom’s 50 Hz mains electricity noise. Second, spectral analysis followed the traditional Welch FFT-method implemented in MATLAB function ‘pwelch.m’ with a 512-millisecond Hanning-tapered window with 50% overlap (HAN). Third, spectral analysis followed the traditional Welch FFT-method implemented in EEGLAB function ‘spectopo.m’ with a 512-millisecond Hamming-tapered window (HAM). To prevent the highest power values at low frequencies from biasing the visualisations, the EEG power spectrum was converted to amplitude by taking the square root and then the logarithm (base 2) to create a $\log_2(amplitude)$ spectrum (Burgess, 2019). ERPs were calculated by averaging across the baseline-corrected trials, and then filtered with a low-pass at 30 Hz using the same FIR as specified earlier and trimmed between -200 ms pre-stimulus and 800 ms post-stimulus.

IMFs were produced via the EMD of an SVD of the channel-by-epoch EEG data. SVD (Harner, 1990) deconstructs an EEG input into a linear combination of components and, when used to improve the SNR of EEG by data reduction, emphasises features of the EEG that are consistent across electrodes in an individual. This is comparable to creating a

weighted-mean EEG dataset, where the weighting is by the common variance across electrodes. In the current context, the first extracted component only just accounted for the majority of variance per participant (e.g., *M* = 53% variance, *SD* = 12%, *Range* = 32% to 83%), so where the variance accounted for by the first component was below 85%, additional components were included in a multi-component reconstruction of a weighted-mean epoch. The threshold of 85% was chosen as a middle ground between too few components (i.e., an incomplete representation of the true signal) and too many components (i.e., overfitting) bearing in mind this data reduction was performed at the epoch level. It sat between a published rule of thumb of keeping between 70% to 90% of variance when aiming for a conservative improvement in SNR (Falini, 2022). In total, IMFs were produced for the original EEG data (i.e., at 500 Hz SR) as well as an additional five downsampled datasets at 373 Hz, 281 Hz, 211 Hz, 157 Hz, and 113 Hz respectively. This method of using prime-numbered downsamples at three-quarters of the source frequency results in different mean baseline frequencies per IMF of the respective EMD. Therefore, running an EMD on multiple downsampled datasets incorporates a greater range of the broadband frequency range, but also means that there will be enough data points to ensure a valid model fitting of $t_{synch}G$ thereafter.

For each ordinal IMF per epoch, the Hilbert transform was used to provide an analytic signal. This analytic signal allowed for calculation of instantaneous phase, with Euler's formula representing complex numbers (both real and imaginary parts) as points on a circle as in Figure 2.1 (Cohen, 2014). The PLV (Lachaux et al., 1999) was calculated as the absolute mean phase vector at each time point (2 ms) across epochs, with the higher the PLV the greater the phase synchrony across trials. Instantaneous frequency was estimated from the gradient of the unwrapped phase averaged across epochs, using a continuous wavelet transform (derived from Gaussian family smoothing function; Luo et al., 2006) in attempt to minimise amplified noise from numerical dedifferentiation (Burgess, 2012). For completeness, amplitude was calculated from the mean amplitude envelope, and the evoked signal from the mean of each IMF.

The peak PLV per ordinal IMF, located between 50 ms to 500 ms post-stimulus, represents t_{synch} (Burgess, 2012). Calculating t_{synch} for each IMF allows for model fitting of $t_{synch}G$ with the MATLAB Curve Fitting Toolbox (v3.5.13). A non-linear least squares power law curve was fit via the Levenberg-Marquardt method using default starting points and a Least Absolute Residuals robust fitting approach to minimise the effect of outliers. A linear least squares polynomial straight line was also fit after log-log transformation of the t_{synch} data points per frequency by time, and a Bisquare robust fitting approach was used to minimise the effect of outliers. Modelling was completed across all IMFs' t_{synch} points per

participant, and all the grand average IMFs' t_{synch} points after averaging across participants' frequency and PLV data. Because the first IMF is poorly estimated (Burgess, 2012) and often contains high-frequency noise (e.g., the United Kingdom's 50 Hz mains electricity noise), it was omitted from analyses.

3.3 Results

Table 3.0 provides a concise summary of this Results section, outlining its organisation and purpose of the content to support efficient engagement with this chapter and to clarify how it contextualises future chapters.

Table 3.0

An outline of the organisation of this Results section, split into sections organised in line with the different analytical approaches covered, and in a way that deliberately mirrors the narrative progression (including rationale therein).

	Content	Purpose	Context
Section 3.3.1	Event-related power spectra and ERPs, and IMFs and cross-correlations between instantaneous metrics	Preliminary checks, visual and statistical, to ensure that widely reported event-related changes in the EEG were present in the current dataset, a necessary precursor to examining whether the FM is an empirically credible, alternative explanation of event-related EEG. Thereafter, replication of patterns of event-related change in instantaneous measures of EEG as predicted by the FM and reported by Burgess (2012).	Supports Chapters 4, 5, and 7
Section 3.3.2	Estimating $t_{synch}G$ from EEG data	Model fitting $t_{synch}G$ with both power law and log-log polynomial fits as proof-of-principle to establish the $t_{synch}G$ metric for later use in an ageing context.	Supports Chapters 4, 5, and 7

Section 3.3.3	Differences in $t_{synch}G$ between modalities and conditions	Analysing differences in $t_{synch}G$ between auditory and visual modality ERPs and oddball and standard conditions of those ERPs, as well as the interaction between modality and condition.	Supports Chapters 4, 5, and 7

3.3.1 Replication of the Firefly Model

First, the power spectra of the pre-stimulus and post-stimulus periods were visually inspected as part of preliminary checks to ensure that widely reported event-related changes in the EEG were present in the current dataset, a necessary precursor to examining whether the FM is an empirically credible, alternative explanation of event-related EEG. The oddball spectra showed the expected clear reductions in high-frequency power (i.e., alpha band upwards) and increases in low-frequency power (i.e., theta band downwards) from pre-stimulus to post-stimulus periods in the AO condition (as shown in Figure 3.1.1) and VO condition (as shown in Figure 3.1.3). The changes in the oddball conditions' power spectra were presented irrespective of the estimation method used (i.e., AM, HAN, or HAM). There was a marginal increase in low-frequency power from pre-stimulus to post-stimulus periods in the AS condition (as shown in Figure 3.1.2) and VS condition (as shown in Figure 3.1.4), and a reduction in alpha in the VS condition too. However, these changes in the standard condition's power spectra were not as substantial as the changes seen in the oddball conditions' power spectra, and the changes were dependent on the estimation method used.

Figure 3.1.1

Pre-stimulus (red line) and post-stimulus (blue line) AO EEG spectra per estimation method (AM, HAN, and HAM) averaged over electrodes and participants, with 95% confidence intervals shaded the same colours respectively to visualise overlaps and differences between the pre- and post- spectra.

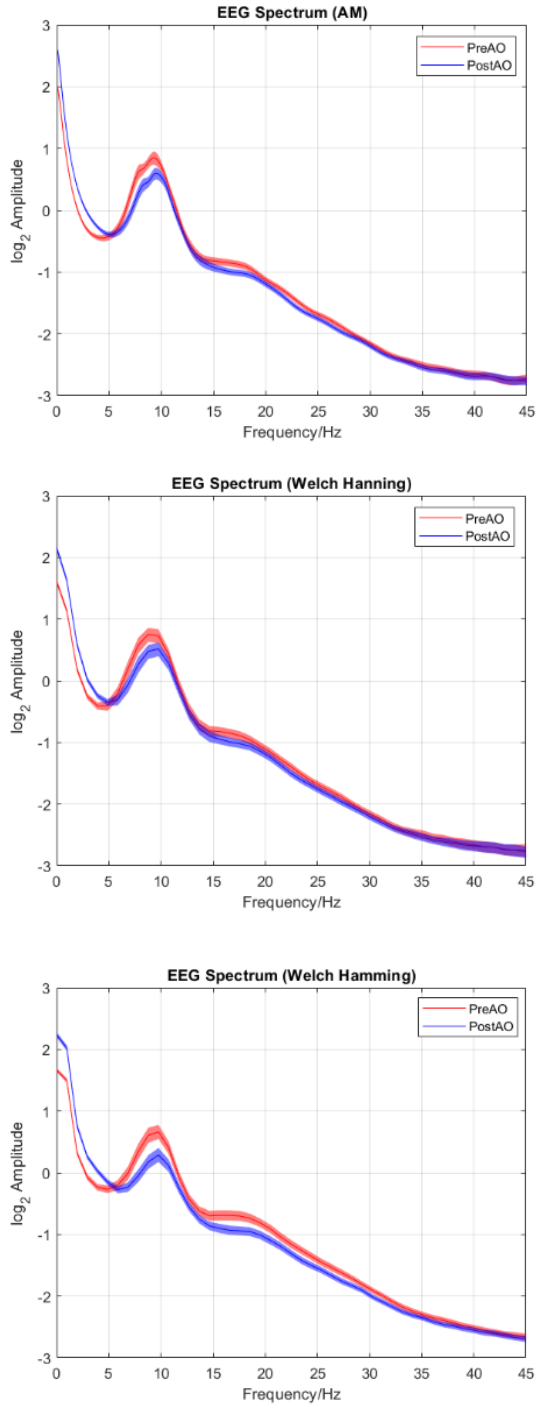

Figure 3.1.2

Pre-stimulus (red line) and post-stimulus (blue line) AS EEG spectra per estimation method (AM, HAN, and HAM) averaged over electrodes and participants, with 95% confidence intervals shaded the same colours respectively to visualise overlaps and differences between the pre- and post- spectra.

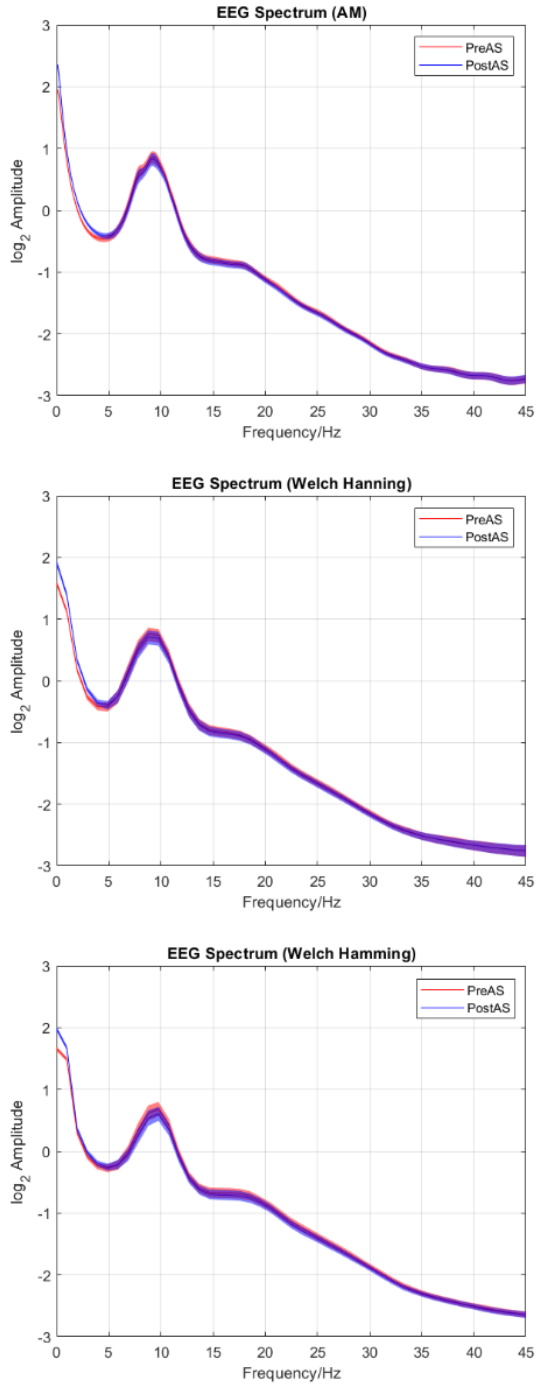

Figure 3.1.3

Pre-stimulus (red line) and post-stimulus (blue line) VO EEG spectra per estimation method (AM, HAN, and HAM) averaged over electrodes and participants, with 95% confidence intervals shaded the same colours respectively to visualise overlaps and differences between the pre- and post- spectra.

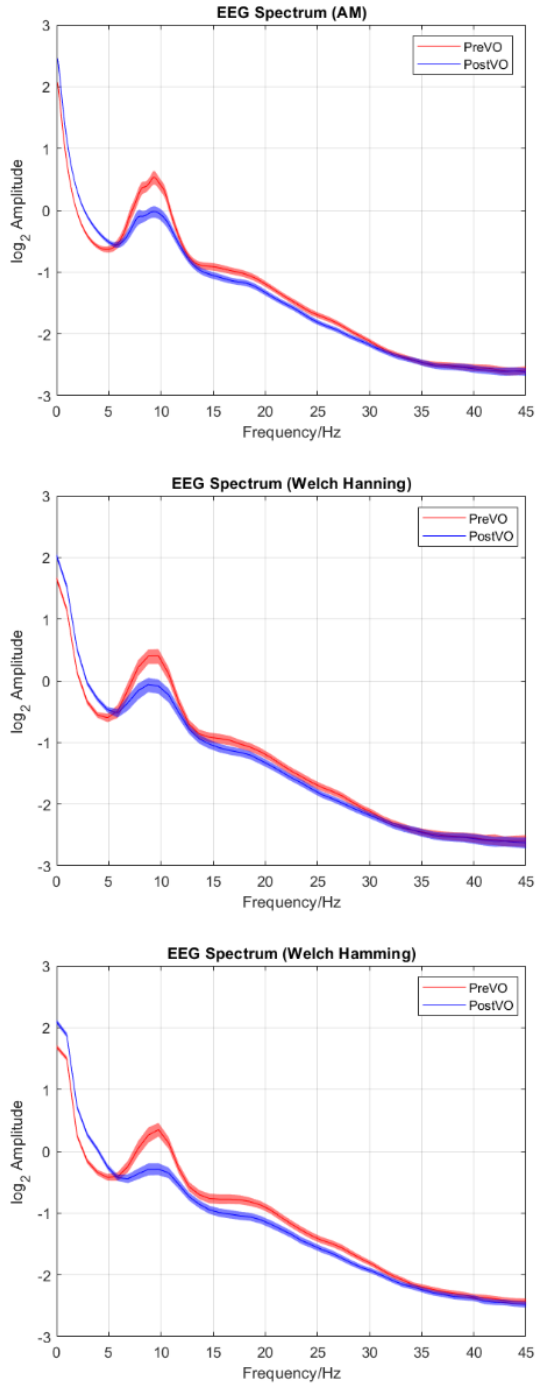

Figure 3.1.4

Pre-stimulus (red line) and post-stimulus (blue line) VS EEG spectra per estimation method (AM, HAN, and HAM) averaged over electrodes and participants, with 95% confidence intervals shaded the same colours respectively to visualise overlaps and differences between the pre- and post- spectra.

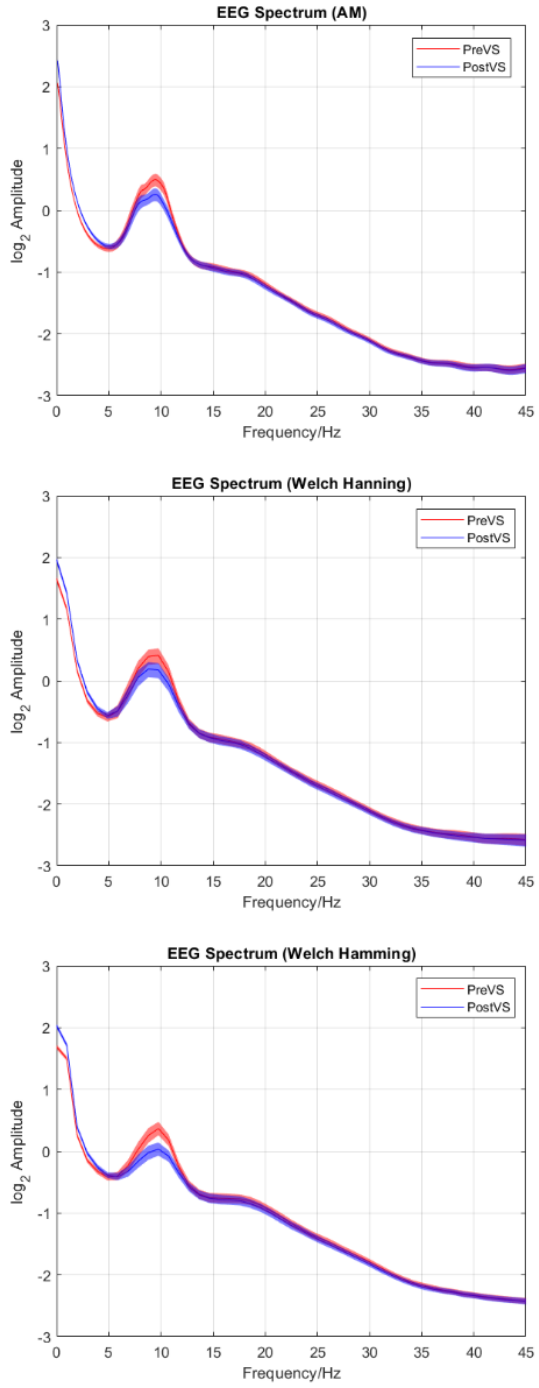

Second, the ERPs were visually inspected as part of further preliminary checks to ensure that widely reported event-related changes in the EEG were present in the current dataset, a necessary precursor to examining whether the FM is an empirically credible, alternative explanation of event-related EEG. The ERPs showed clear oddball-related components for the AO and VO conditions and not the AS and VS conditions (as shown in Figure 3.2). For example, the N2 and P3b components are clear to the eye, with the VO peaks having a general delay compared to the AO peaks (e.g., an approximately 30 ms delay for the mean visual P3b peak). There was a constant negative offset of approximately -1 μV for visual compared to auditory ERPs, but amplitude components were not compared between modalities here.

Figure 3.2

EEG ERPs for the AO-AS conditions (black-magenta lines) and VO-VS conditions (red-cyan lines) averaged over electrodes and participants, with 95% confidence intervals shaded the same colours respectively to visualise overlaps and differences between the conditions.

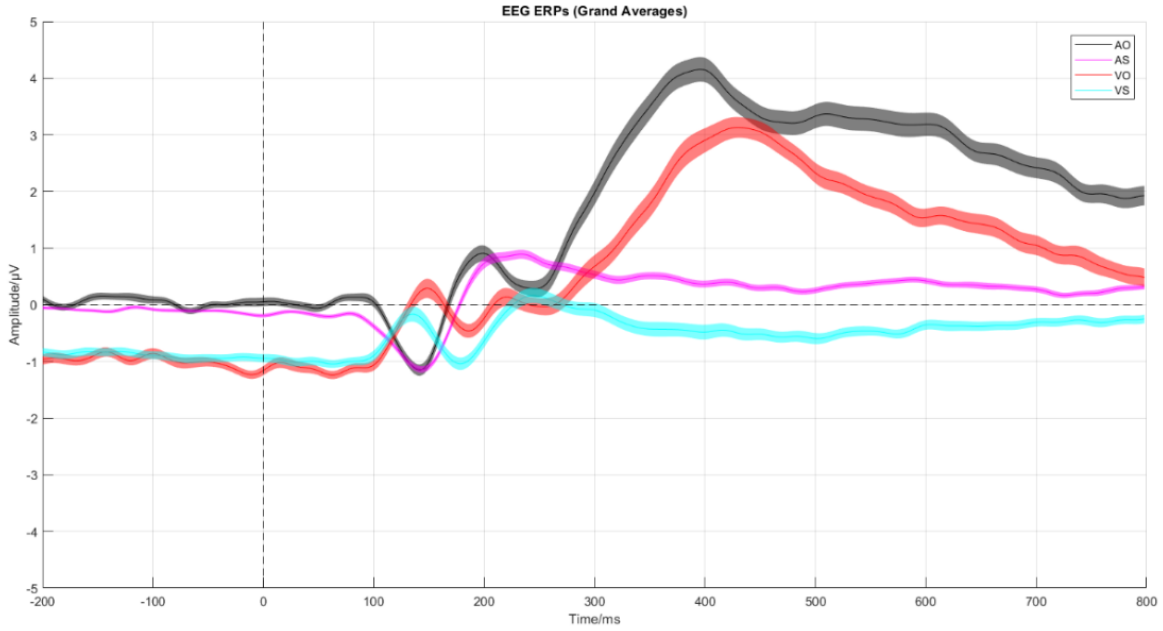

Third, the IMFs were visually inspected to identify replication in the patterns of event-related change in instantaneous measures of EEG as predicted by the FM and reported by Burgess (2012). The IMFs showed that increases in PLV were temporally aligned with decreases in instantaneous frequency post-stimulus (as shown in Figure 3.3). t_{synch} per IMF followed a clear trend across time with earlier t_{synch} the higher the frequency, which was also evident in the pattern across IMFs' instantaneous frequency troughs. Late IMFs (i.e., low frequencies) showed long latency modulations and omitted the rebound, which can be accounted for by the long period and limited window size per epoch; indeed, a reason for

implementing a long ISI between trials was to minimise the impact of overlapping activity per trial. For amplitude, there was often a small, short-duration increase before a deeper, prolonged dip and rebound that also increased in latency per ordinal IMF. This change was most clear in the AO condition, but also in IMF4 across conditions and modalities. For the evoked signal, W-shapes were evident, which widened with each ordinal IMF. The overarching pattern of post-stimulus modulations, with the peak latency and width of modulations increasing with each IMF (i.e., with decreasing mean baseline frequency), was more consistent for the AO condition than the VO condition, and more pronounced and systematic in the oddball conditions than the standard conditions.

Figure 3.3

An example output from EMD showing the time course of phase synchrony (PLV, red line), frequency (FRQ, red line), amplitude (AMP, red line), and evoked response (EVO, red line) for IMFs 2-6 (in descending order) of one downsample (281 Hz), averaged over participants per condition; the dotted lines represent 95% confidence intervals of the measurement in the -200 ms to 0 ms baseline period to visualise crosses of the red line (i.e., change in the metric of interest), and the blue dots represent t_{synch} for PLV and the point of lowest frequency for FRQ.

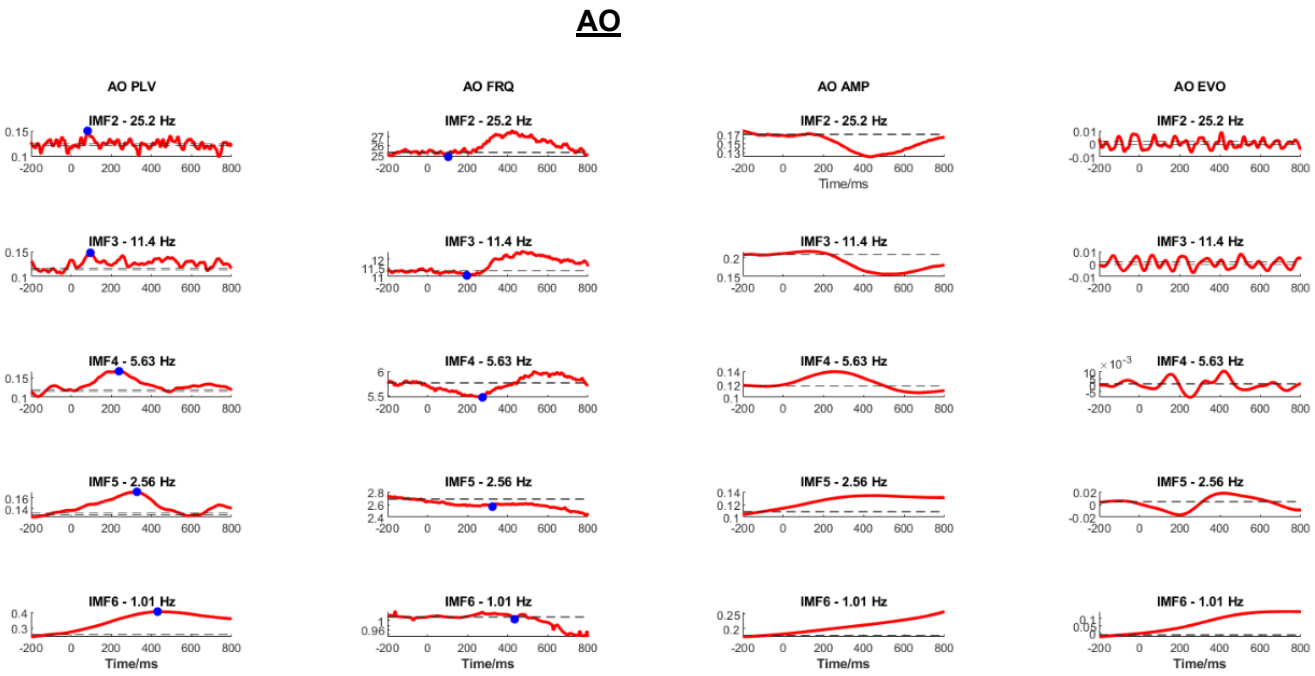

AS

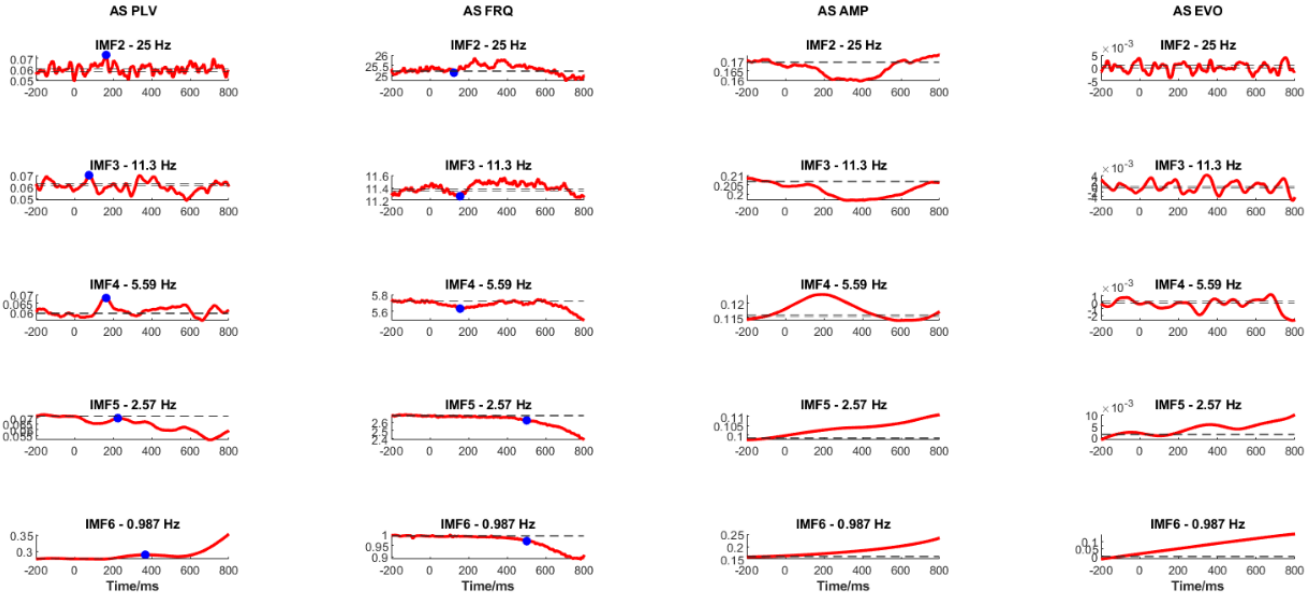
AS PLV
AS FRQ
AS AMP
AS EVO
IMF2 - 25 Hz
IMF3 - 11.3 Hz
IMF4 - 5.59 Hz
IMF5 - 2.57 Hz
IMF6 - 0.987 Hz
Time/ms

VO

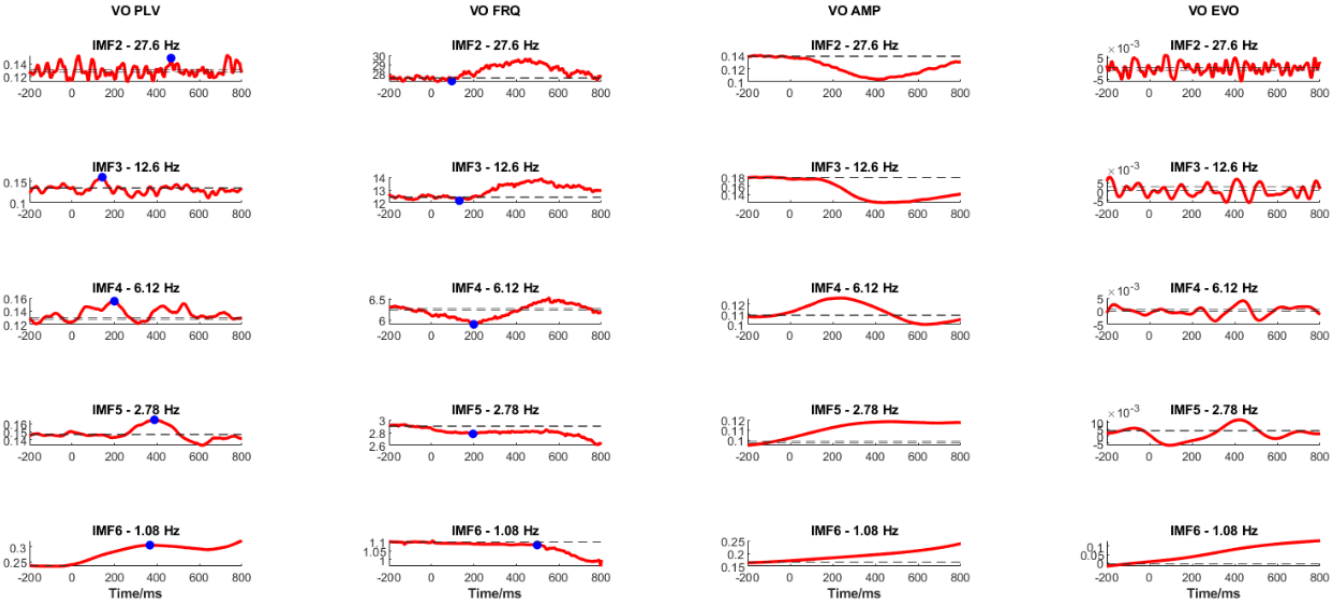
VO PLV
VO FRQ
VO AMP
VO EVO
IMF2 - 27.6 Hz
IMF3 - 12.6 Hz
IMF4 - 6.12 Hz
IMF5 - 2.78 Hz
IMF6 - 1.08 Hz
Time/ms

VS

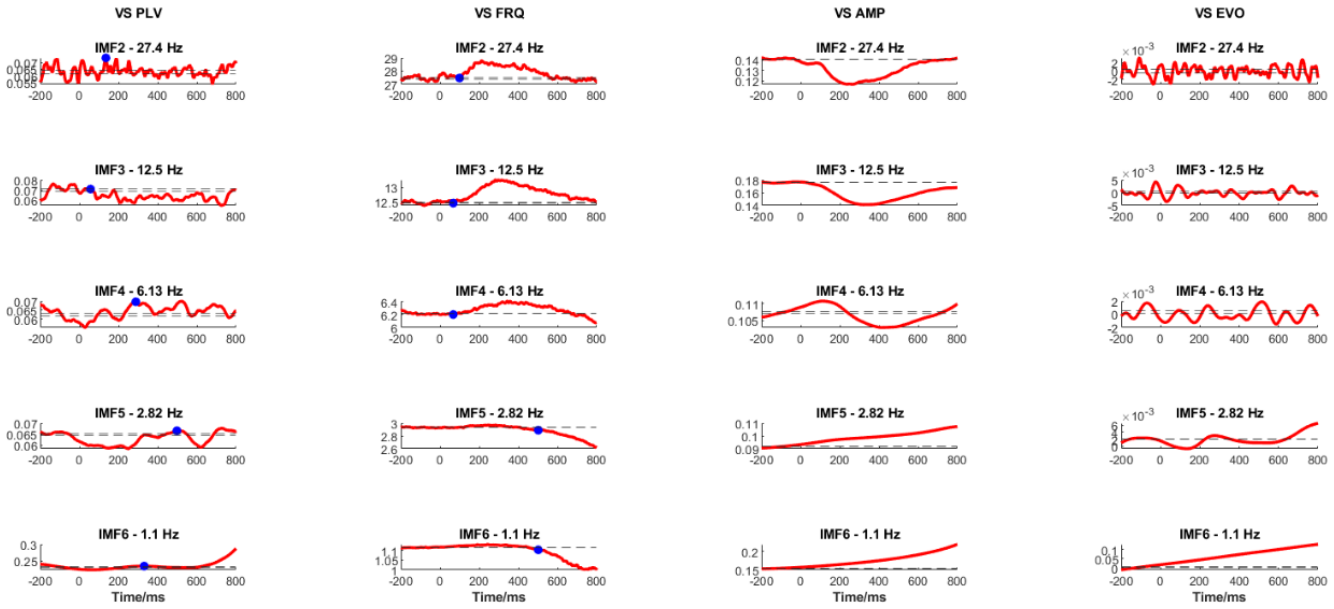

Finally, cross-correlations at zero lag were calculated between PLV and instantaneous frequency, again to identify replication in the patterns of event-related change in instantaneous measures of EEG as predicted by the FM and reported by Burgess (2012). These Pearson Correlation Coefficient (PCC) cross-correlations were calculated on each downsampled IMFs' PLV and frequency data averaged across all participants. The resultant cross-correlation coefficients and mean baseline frequencies were then averaged across equivalent IMFs to efficiently visualise the overarching trends. There were clear negative cross-correlations (as shown in Table 3.1.1) in IMFs 2 and 3 across all conditions and modalities, and in IMFs 4 and 5 for the AO condition. IMF1 averaged at around a 50 Hz baseline frequency, which supports the exclusion of IMF1 from other analyses. Due to mode mixing in EMD where averaged ordinal IMFs do not always contain equivalent or single frequencies (e.g., IMF2 containing a mix of beta and alpha, IMF3 a mix of alpha and theta, IMF4 a mix of theta and delta), thus blurring the relationships, average cross-correlations were also calculated for discrete frequency bands of beta (13-30 Hz), alpha (7-13 Hz), theta (4-7 Hz), and delta (1-4 Hz). This banding used the mean baseline frequencies per IMF across downsamples, and was implemented to make the negative cross-correlations clearer (as shown in Table 3.1.2).

Table 3.1.1

Cross-correlation coefficients (PCC) at zero lag, averaged over downsamples, between PLV and frequency of the IMFs per condition in the time range 0 ms to 500 ms, with mean baseline frequency/Hz and SD shown in brackets (M, SD).

IMF	AO	AS	VO	VS
1	.21	.01	-.22	-.01
	(52.03, 19.10)	(51.55, 19.18)	(53.83, 18.88)	(53.29, 18.76)
2	-.10	-.16	-.12	-.24
	(21.96, 6.96)	(21.49, 6.74)	(24.10, 7.33)	(23.39, 6.82)
3	-.29	-.11	-.48	-.25
	(9.94, 2.79)	(9.84, 2.68)	(11.04, 3.13)	(10.79, 2.85)
4	-.76	-.20	.04	.19
	(4.79, 1.43)	(4.84, 1.40)	(5.23, 1.55)	(5.25, 1.47)
5	-.49	.37	.27	-.09
	(2.16, 0.75)	(2.20, 0.77)	(2.37, 0.81)	(2.38, 0.80)
6	.40	.43	.34	.26
	(0.80, 0.35)	(0.78, 0.35)	(0.88, 0.31)	(0.86, 0.37)

Table 3.1.2

Cross-correlation coefficients (PCC) at zero lag, averaged over downsamples, between PLV and frequency of set frequency bands taken from IMFs per condition in the time range 0 ms to 500 ms, with mean baseline frequency/Hz and SD shown in brackets (M, SD)

Band	AO	AS	VO	VS
Beta	-.17	-.15	-.06	-.17
	(24.03, 4.72)	(23.51, 4.57)	(26.29, 4.78)	(25.53, 4.36)
Alpha	-.14	-.13	-.45	-.41
	(10.93, 1.81)	(10.80, 1.74)	(12.16, 1.99)	(11.87, 1.80)
Theta	-.76	-.27	-.14	.28
	(5.63, 0.48)	(5.67, 0.46)	(6.14, 0.52)	(5.81, 0.92)
Delta	-.41	.31	.13	-.03
	(2.14, 0.89)	(2.31, 0.88)	(2.23, 1.00)	(2.06, 0.88)

3.3.2 Estimating $t_{synch}G$

The gradient across t_{synch} points (i.e., $t_{synch}G$) was estimated with both power law curve and log-log polynomial straight-line models. The power law curve gradient was better evidence as a proof-of-principle for the systematic delay in latency of t_{synch} points across ordinal IMFs, with far higher adjusted R^2 values (adjR^2). However, the log-log polynomial straight-line gradient was more easily interpreted as a single number, thus preferred as the final $t_{synch}G$ metric for ease of use in future analyses and applications. Figure 3.4.1 visualises both power and polynomial $t_{synch}G$s for the AO and AS conditions, and Figure 3.4.2 visualises the power and polynomial $t_{synch}G$s for the VO and VS conditions, as proof-of-principle to establish the $t_{synch}G$ metric for use in an ageing context in the following chapters.

Figure 3.4.1

Model fitting $t_{synch}G$ with both power law (Pcurve, left side) and log-log polynomial (Lline, right side) fits for the AO condition (black lines) and AS condition (pink lines), modelled across all downsamples' t_{synch} points per condition (black and pink dots for AO and AS conditions respectively), with PLV and frequency data averaged over participants.

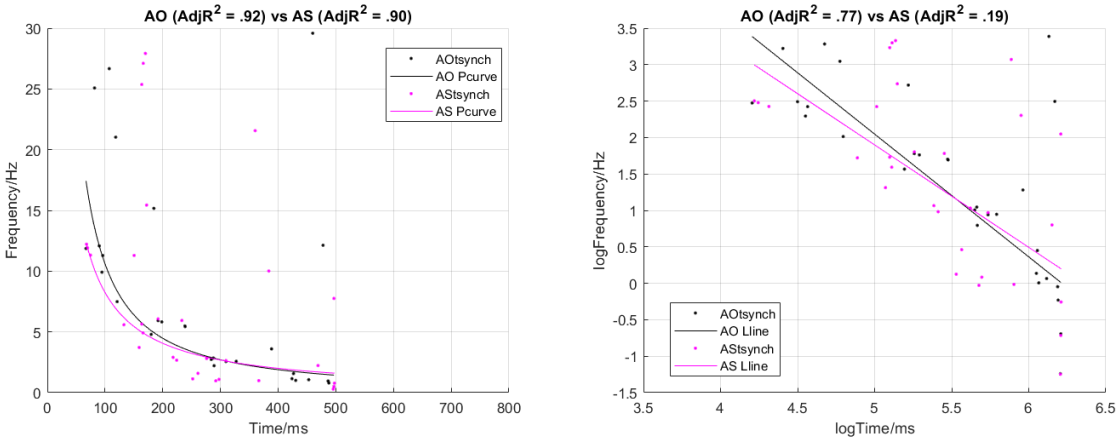

Figure 3.4.2

Model fitting $t_{synch}G$ with both power law (Pcurve, left side) and log-log polynomial (Lline, right side) fits for the VO condition (black lines) and VS condition (pink lines), modelled across all downsamples' t_{synch} points per condition (black and pink dots for VO and VS conditions respectively), with PLV and frequency data averaged over participants.

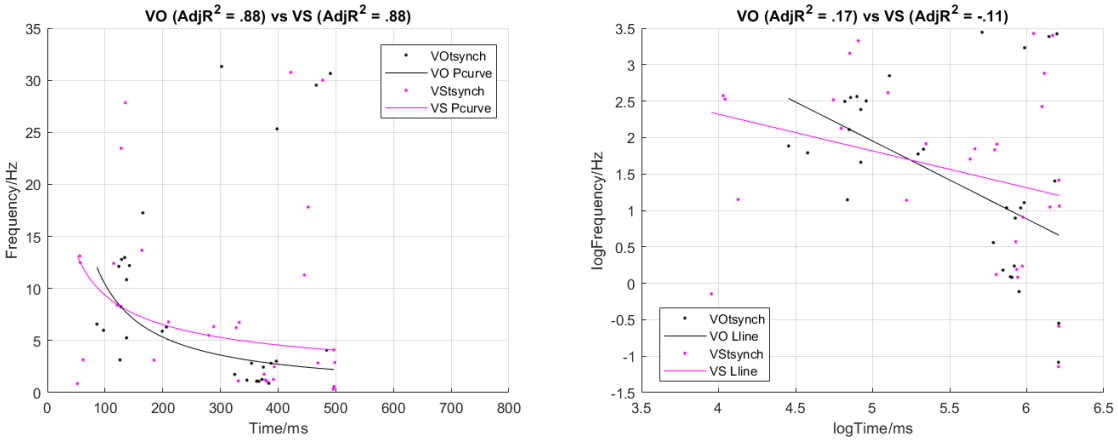

3.3.3 Differences in $t_{synch}G$ between conditions and modality

A two-way within-subjects factorial ANOVA was conducted to examine the main effects of condition (oddball versus standard) and modality (auditory versus visual), as well as any interaction between these factors, using the log-log version of $t_{synch}G$ per individual. The main effect of condition was significant ($F(1,59) = 7.58$, $p = .008$, $\eta^2_p = 0.11$), where the oddball gradient (*M* = -0.42, *SD* = 0.53, *Range* = -2.13 to 0.80, *95% CI* [-0.55, -0.28]) was steeper than the standard gradient (*M* = -0.19, *SD* = 0.40, *Range* = -1.06 to 0.61, *95% CI* [-0.29, -0.09]). Additionally, the modality main effect was significant ($F(1,59) = 8.83$, $p = .004$, $\eta^2_p = 0.13$), where the auditory gradient (*M* = -0.42, *SD* = 0.42, *Range* = -1.52 to 0.79, *95% CI* [-0.53, -0.31]) was steeper than the visual gradient (*M* = -0.19, *SD* = 0.49, *Range* = -1.25 to 0.93, *95% CI* [-0.32, -0.06]).

The interaction effect between condition and modality was also significant ($F(1,59) = 4.38$, $p = .041$, $\eta^2_p = 0.07$). Specifically, there was no difference between standard auditory (*M* = -0.21, *SD* = 0.56, *Range* = -1.53 to 1.12, *95% CI* [-0.36, -0.07]) and standard visual (*M* = -0.17, *SD* = 0.61, *Range* = -1.67 to 1.10, *95% CI* [-0.33, -0.01]), but there was a difference between oddball auditory (*M* = -0.62, *SD* = 0.68, *Range* = -3.67 to 0.87, *95% CI* [-0.80, -0.45]) and oddball visual (*M* = -0.21, *SD* = 0.74, *Range* = -2.16 to 1.63, *95% CI* [-0.40, -0.02]). Also, there was no difference between oddball visual (*M* = -0.21, *SD* = 0.74, *Range* = -2.16 to 1.63, *95% CI* [-0.40, -0.02]) and standard visual (*M* = -0.17, *SD* = 0.61, *Range* = -1.67 to 1.10, *95% CI* [-0.33, -0.01]), but there was a difference between oddball auditory (*M*

= -0.62, *SD* = 0.68, *Range* = -3.67 to 0.87, *95% CI* [-0.80, -0.45]) and standard auditory (*M* = -0.21, *SD* = 0.56, *Range* = -1.53 to 1.12, *95% CI* [-0.36, -0.07]).

Both the main effect and interaction descriptive data of the two-way within-subjects factorial ANOVA are presented visually in Figure 3.5. This aims to clarify the differences in $t_{synch}G$ seen between ERPs of different modality (i.e., auditory versus visual) and condition (i.e., oddball versus standard), with steeper $t_{synch}G$ in auditory and oddball conditions respectively, as well as the difference in $t_{synch}G$ between oddball and standard conditions depending on the auditory modality of the paradigm (i.e., oddball $t_{synch}G$ steeper only in the auditory modality).

Figure 3.5

Line plot visualisations of the significant condition (oddball < standard; O_S) and modality (auditory < visual; A_V) main effects on $t_{synch}G$, and the significant interaction effect of condition and modality, with dots as means and bars as the 95% confidence intervals to show overlaps and differences (n = 60).

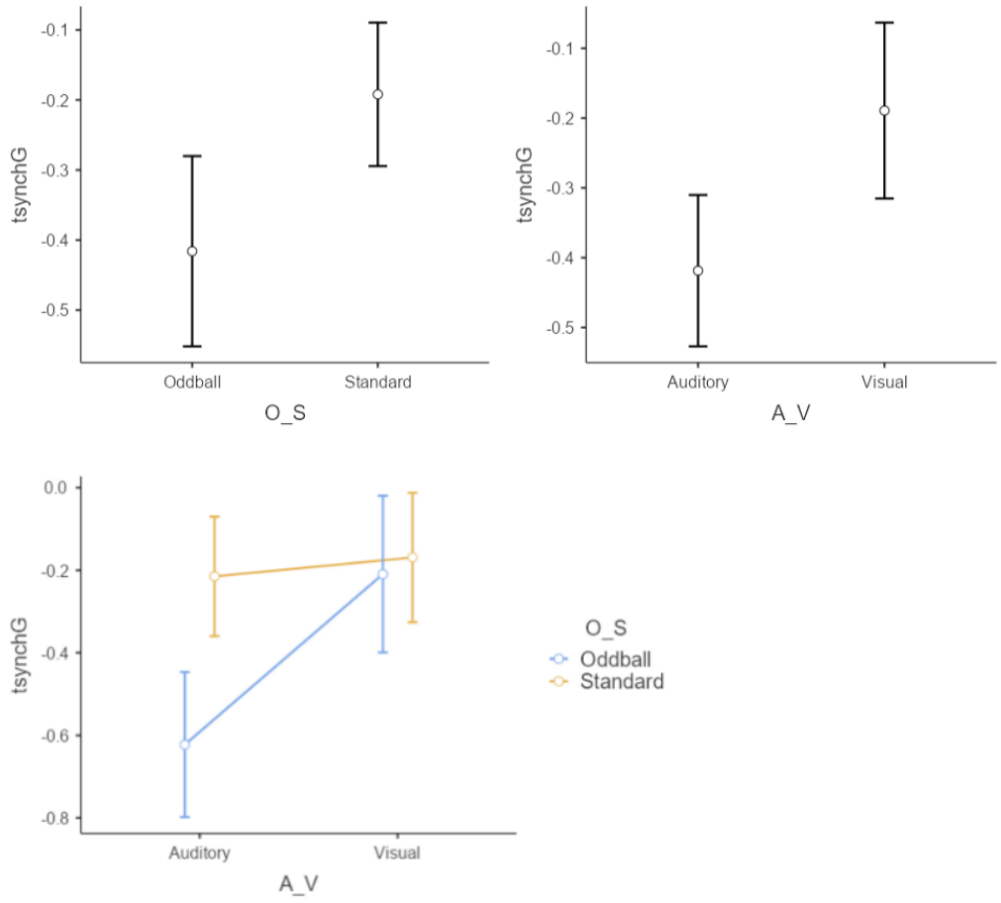

3.4 Discussion

Our objective was to determine whether the FM is an empirically credible, alternative explanation of event-related EEG that has the potential to be used in an ageing context. This would not only advance our understanding of event-related EEG, but also set the foundation for further study to improve our understanding of age-related changes in the brain and, potentially, how to track deleterious age-related changes. First, we wanted to replicate frequency and phase modulations as the explanatory mechanism of event-related changes in the EEG. The negative PCC cross-correlations seen between instantaneous frequency and PLV in Burgess (2012) were replicated in this study, with post-stimulus instantaneous frequency slowing concurrent with increasing PLV across multiple IMFs. This finding supports the existence of a systematic, gradual slowing in the frequency domain of ongoing EEG that is concurrent with phase alignment, thus suggesting that the FM does offer an empirically credible explanation of event-related information processing in the EEG. There were also expected changes in power spectra and shapes of ERP waveforms, supporting the conclusion that the oddball attention paradigms were successfully implemented across modalities, and supporting the validity of the prior interpretation of the patterns across IMFs and cross-correlations.

Second, we sought to explore the ability to estimate a novel $t_{synch}G$ metric. Based on the FM and the VSH, it was predicted that modelling t_{synch} across ordinal IMFs (i.e., cross-frequency) would follow a power law curve to reflect the systematic, gradual spread of information processing and communication across neural networks of increasing scale (thus decreasing frequency) over time. Power law curves emerged and accurately modelled the pattern of t_{synch} across a set of decreasing mean baseline frequencies over time. In turn, log-log polynomial lines were produced as the new metric of $t_{synch}G$ (i.e., the gradient of the model fit). The linear gradient is one number that is more interpretable and usable than the complex, multiple power law gradients, although it should be noted that the linear fits were less accurate than the power law fits. This finding supports that the power curve model better reflects the systematic, cross-frequency phase modulation mechanism.

Finally, we wanted to see if $t_{synch}G$ differed across conditions (oddball versus standard) and modalities (auditory versus visual) in an oddball attention paradigm. It was predicted, based on there being differences in the ERP waveforms between different conditions and sensory modalities, that there would be differences in $t_{synch}G$ too. $t_{synch}G$ is a direct measure of the FM's explanatory mechanism that underpins the formation of evoked and induced changes. Therefore, $t_{synch}G$ can be thought of as a quantification of the timecourse of information processing and communication through neural networks of increasing size. For example, the flatter (more positive) the gradient, the slower or more

variable (i.e., inefficient) the communication. In the current study, the oddball $t_{synch}G$ was steeper than the standard $t_{synch}G$. So, this can be interpreted as a faster timecourse of neural network communication for the oddball condition. However, it might be the case that the oddball gradient reflects rigid task demands with naturally more efficient information processing and communication across neural networks. In contrast, the standard gradient was trending towards a gradient closer to zero due to reflecting far less homogenous activity over trials, because the standard condition does not require a strict set of behavioural and cognitive responses. These conclusions are supported by the power spectrum comparisons for pre-stimulus and post-stimulus periods, where there were clear and consistent changes in the oddball conditions but not the standard conditions. The auditory $t_{synch}G$ was also steeper than the visual $t_{synch}G$, which can be interpreted in an analogous way, where the auditory gradient may be a purer measure of more efficient processes; there may also be better SNR in the auditory condition. The general conclusion is that the FM does account for differences in an oddball attention paradigm's ERP in terms of condition and modality, but the meaning behind the differences remains unclear. The significant interaction further elaborates on these main effects and their interpretation, however.

The interaction effect between condition and modality showed the key differences in $t_{synch}G$ as being between oddball auditory and oddball visual, and oddball auditory and standard auditory. There were no differences between standard auditory and standard visual, or oddball visual and standard visual. Indeed, there were clear auditory oddball patterns across the data visualisation, which were less clear in standard conditions and the visual modality of both conditions. A potential interpretation of this interaction is that the SNR in the auditory conditions is better than the visual conditions (Bennington & Polich, 1999; Polich, 1996), alongside the distinction in measurement noise and event-related neurophysiology between auditory eyes closed and visual eyes open conditions (Barry & De Blasio, 2017), which is borne out in the different ERP waveforms and power spectra per modality. To summarise, the AO condition's $t_{synch}G$ is the most statistically sensitive, highest SNR metric, perhaps due to the nature of the task demands and intrinsic measurement noise, but also due to the nature of the underlying efficiency of the brain activity, particularly when compared to the standard condition. Additionally, the electrode ROI was informed by recommendations on increasing the SNR of the P3b component of the oddball ERP. In future, incorporating a larger number of electrodes and different ROIs or full scalp (Delorme, 2023) for other ERPs, modalities and conditions should improve our understanding of the differences in $t_{synch}G$ between different methodologies.

Whilst the results of this study provide support for the FM, there are still unanswered questions. First, the exact shape of the post-stimulus power spectra as predicted by the FM

does not perfectly match that of the empirical data. For example, there is only a marginal transition of the peak alpha frequency post-stimulus towards lower frequencies in some of the power spectra, whereas the FM proposes global frequency slowing with no change in amplitude. Also, the size of the decrease in instantaneous frequency alongside amplitude changes seen across IMFs were small, and sometimes even negligible. However, a possible interpretation of these disparities is that due to the task demands being minimal in an oddball paradigm, particularly in the standard conditions, only a small proportion of the EEG responded to the event (Burgess, 2012). When combined with averaging smear, alpha smear and latency jitter, measurement noise and the electrode ROI, there will likely have been a dilution of the visible changes in frequency. That said, there remains uncertainty as to whether there is an amplitude change that is not implicated and accounted for by the FM, but that would be by models such as the AAM (Mazaheri & Jensen, 2008). And there is no answer forthcoming on how best to account for empirical evidence that contradicts the VSH's conceptualisation of the scale of the neural network being inversely proportional to the frequency (e.g., apparent large-scale communication in the gamma frequency range; Doesburg et al., 2008; Pesaran et al., 2008; Siegel et al., 2008). In general, this reinforces the requirement to amalgamate models based on empirical evidence to best explain the complexity of the EEG (Cohen & Gulbinaite, 2014).

There are also concerns around how noisy the estimates of $t_{synch}G$ are. Indeed, it is well-known that the baseline variability in EEG metrics is high, particularly at an individual level (Burgess & Gruzelier, 1993). In the current context, first, instantaneous variables are innately noisy to quantify. This is particularly the case for frequency, where numerical differentiation increases the noise of a signal (Luo et al., 2006). This may further explain why the frequency dips were minimal across some of the IMFs in the current study, and why they were originally lower than anticipated in Burgess (2012). Second, EMD has several intrinsic limitations that will augment noise and likely contribute to unreliable measures at the individual level. For example, a specific ordinal IMF may not include directly comparable and/or single frequencies (i.e., mode mixing) across trials, tasks, electrodes, and participants. These issues undermine extensive averaging for univariate analyses and are further amplified by noisy recordings thus signal intermittency (Gao et al., 2008; Huang et al., 1999), which are common in EEG. Finally, $t_{synch}G$ was not always modelled as expected, especially for the standard conditions. For example, a minority of participants' $t_{synch}G$ were greater than 0, which would not be readily explained by the FM. Instead, this would likely implicate problematic SNR alongside limited task demands in the current paradigm, and an arguably suboptimal ROI for the standard conditions. That is, participants with gradients greater than zero could be reflecting what would be flatter but still negative gradients with

optimised SNR. It is also the case that there will inevitably be limited SNR for oddball trials, given they must be deviant in comparison to the standard condition. Sixty trials has been the minimum number recommended for a suitably powered experimental manipulation (Huffmeijer et al., 2014). The number of oddball trials per participant in the current study was on average lower than sixty after data cleaning. These SNR issues are also augmented in older adults, where measurement noise becomes more common and challenging, as shown by the significant correlations between age and the number of trials removed during data cleaning. Therefore, it perhaps comes as little surprise that EEG metrics share a similar level of undesirable variability that is so intrinsic to the underlying methodology and analytical techniques.

Whilst caveated by the current SNR of $t_{synch}G$ at the individual level, the overarching findings remain informative, and it is now for future research to optimise the methodological and analytical pipelines to improve the SNR. Indeed, future research will need to disentangle SNR from meaningful changes in $t_{synch}G$ if it is to have utility for clinical settings. However, this chapter can conclude that the FM offers an empirically credible, alternative explanation of event-related EEG that relies on systematic oscillatory phase synchronisation and frequency slowing. In summary, there were three broad aims of this thesis, which could be achieved concurrently; namely, 1) to advance our understanding of event-related and resting-state EEG and MEG, 2) to advance our understanding of age-related changes in the brain with EEG and MEG, and 3) to establish EEG and MEG metrics that have the potential to track those age-related changes over time. This first experimental chapter has advanced our understanding of event-related EEG and established $t_{synch}G$ as a novel metric that can be used to advance our understanding of age-related changes in the brain and perhaps track age-related changes over time. Inspired by the well-known aphorism, ‘All models are wrong, but some are useful’, the focus of this thesis will now turn to whether $t_{synch}G$ could be useful in an ageing context. Oddball paradigms and their ERPs are already used in ageing studies and clinical contexts (Dauwels et al., 2010a; Duncan et al., 2009; Howe et al., 2014; Vecchio & Maatta, 2011), so the first test will be whether $t_{synch}G$ correlates with chronological age, and how that correlation compares with the correlations between ERPs’ peak metrics and chronological age. Cognitive performance could also be considered, and whether $t_{synch}G$ reflects any known protective and/or deleterious changes associated with ageing. Not only will this research improve our understanding of age-related changes in the brain, namely age-related changes in event-related EEG, but set the foundation for using $t_{synch}G$ in an applied way, such as to detect and track deleterious age-related changes.

Chapter 4: Estimating chronological age from the EEG: event-related oscillatory dynamics in the healthy ageing brain

4.1 Introduction

After the findings of Burgess (2012) and Chapter 3 of this thesis, the FM has now been supported by replicable empirical findings that largely align with the original simulation modelling. These converging results suggest that the FM is a true candidate for explaining event-related changes in the EEG. Inspired by the well-known aphorism of 'All models are wrong, but some are useful', this thesis will now consider whether $t_{synch}G$ could be useful in an ageing context. It is hoped that $t_{synch}G$ can advance our understanding of age-related changes in the brain, and, in turn, help to detect and track deleterious changes early, accurately, and in an accessible way. There is already extensive literature on the effects of ageing on the event-related EEG, as outlined in Chapter 2. For example, mean P3b peak amplitude typically decreases in healthy ageing (Polich, 1996, 1997; Van Dinteren et al., 2014) and in age-related conditions such as mild cognitive impairment and dementia (Dauwels et al., 2010a; Hedges et al., 2016; Porcaro et al., 2019). Whereas mean P3b peak latency reliably increases alongside healthy ageing (Polich, 1996, 1997; Van Dinteren et al., 2014) and deleterious age-related conditions (Dauwels et al., 2010a; Duncan et al., 2009). These age-related changes are reliable at the population-level, but there is not a widely recognised mechanistic explanation of them, which is partly due to not having had a complete mechanistic explanation of the event-related EEG itself. The FM has now defined that explanatory mechanism, but this has never been applied to an ageing context. Furthermore, the sheer complexity of any relationships between age, cognitive performance, and brain activity, particularly at the individual level, has meant that no previous theories or general interpretation of age-related changes (e.g., the deficit and/or benefit models) has been established beyond reasonable doubt.

In accordance with the FM, $t_{synch}G$ is a direct measure of cross-frequency phase modulation underpinning the formation of ERPs, such as the widely studied waveform occurring in oddball attention paradigms. When the FM is interpreted in alignment with theories such as the VSH (Von Stein & Sarnthein, 2000), ERPs can be thought of as a travelling wave of information processing and neural network communication that spreads out over time to incorporate more and more of the cortex whilst reducing in frequency. Therefore, $t_{synch}G$ is a metric that may enable us to study, as Burgess (2012, p. 20) put it, 'the true deep structure of event-related changes in the EEG' compared to 'surface features of the ERP, such as amplitude and latency of peaks'. This interpretation suggests that $t_{synch}G$ will provide a meaningful, new perspective on age-related changes in information processing

and communication in the brain, and take us closer to a specific, mechanistic explanation. Taking inspiration from previous findings with ERPs across the lifespan, $t_{synch}G$ should correlate with chronological age in a way that reflects age-related changes in components of the ERP if the FM is a true candidate for explaining event-related changes in the EEG.

In an applied ageing context, $t_{synch}G$ but also well-defined peak amplitude and latency components of ERPs could be compared on their ability to estimate chronological age. The applied motivation for this approach is that an individual's brain age might act as a proxy of their general brain functioning, whereby a discrepancy between chronological age and EEG-estimated age could prove clinically informative by implicating deleterious conditions. At the time of writing, $t_{synch}G$ has not previously been used to examine age-related changes in the brain with an applied focus of estimating chronological age. However, it is also important to examine the relationship of $t_{synch}G$ with cognitive performance, as it has been shown that ERP components such as P3b peak amplitude and latency are related to cognitive performance in and out of an ageing context (Bell et al., 2021; Howe et al., 2014; Pavarini et al., 2018; Porcaro et al., 2019). Therefore, it will be informative to compare proxy measures of general cognitive integrity alongside EEG-estimated age to further probe previously established age-related processes that may impact cognitive performance (e.g., dedifferentiation and noise versus reserve). For example, $t_{synch}G$, due its consideration of multiscale interactions and reflection of deeper structures, may be a more holistic representation of changes in cognitive performance compared to discrete ERP components.

In summary, it would be amiss to treat the FM as a true candidate for explaining event-related changes in the EEG (aim #1 of this thesis) without showing that its fundamental explanatory mechanism – cross-frequency phase modulation that can be operationalised via $t_{synch}G$ – demonstrates an age-related shift (aim #2 of this thesis). Our objective was to use the new $t_{synch}G$ metric to estimate chronological age as EEG-age (aim #3 of this thesis). First, we wanted to compare the well-established N2 and P3b ERP components of the auditory and visual oddball attention paradigms on their ability to estimate age. Based on previous evidence, we predicted that peak amplitude would be negatively correlated with chronological age, and peak latency would be positively correlated with chronological age, and we aimed to determine which estimate correlated most strongly and provided the most accurate estimate of chronological age. Second, we sought to explore the potential of $t_{synch}G$ to estimate chronological age, with $t_{synch}G$ interpreted as a metric that may allow us to study the true deep structure of event-related changes in the form of multiscale information transfer and neural network communication across the brain. Third, we wanted to examine the relationships of ERP-estimated age and $t_{synch}G$ EEG-age with already established proxy measures of general cognitive integrity.

4.2 Methods

4.2.1 Participants

This is the same EEG dataset as previously used in Chapter 3, but now considering the relationships with age rather than collapsing data across age. As a brief recap of the demographics, sixty healthy adults (24 men, 36 women; 5 left-handed, 55 right-handed) volunteered to participate, which allowed for ten participants per decade of chronological age across six decades (*M* = 49 years, *SD* = 17.9, *Range* = 20 to 78). Having reached our resource limit, a sensitivity power analysis for a univariate positive correlation between P3b latency and age using Pearson's *r*, with an alpha of .05 and a beta of .2 [.1], calculated a minimum detectable effect size of .31 [.37] (calculated using G*Power, version 3.1.9.7; Faul et al., 2009). Participants had a mean of 17 years in formal education (*SD* = 4.0, *Range* = 7 to 27). Fifty-two participants identified as White, seven as Asian, and one as Black, with all participants recruited via Aston University's advertising portals, which includes the ARCHA Panel that comprises older adults from around the UK who volunteer to take part in studies at Aston University. This study received a favourable opinion from AU-REC and was carried out in accordance with the Declaration of Helsinki and the British Psychological Society Code of Human Research Ethics. Written informed consent was obtained from each participant, and they were reimbursed £15 for their participation.

All participants actively reported having no experience of traumatic brain injury, no diagnosis of neurological or psychiatric disorder, and no known cognitive impairment. Participants were screened for depression via the GDS-15 (Sheikh & Yesavage, 1986), as severe depression may confound measures of cognitive performance (Byers & Yaffe, 2011; Morimoto & Alexopoulos, 2013). Participants were also screened for cognitive impairment via the QMCI (O'Caoimh & Molloy, 2017). We included the QMCI not only as a screening tool though, where healthy adults should report scores that are isolated to the normal category rather than MCI or dementia categories, but as our estimate of general cognitive integrity, a proxy measure of dedifferentiation and noise, where higher scores represented higher general brain functioning (O'Caoimh et al., 2017). Ageing is associated with more than depression and detrimental changes in neural and cognitive integrity, and there are neurocognitive and neurobiological agents that provide protective benefits, like compensation, reserve, and maintenance. Therefore, participants also completed the National Adult Reading Test (NART; Nelson, 1982; Nelson & Willison, 1991), which is a well-established tool that was designed to be robust to early age-related decline in integrity (both normal decline and dementia; Maddrey et al., 1996; Nelson & McKenna, 1975; Nelson & O'Connell, 1978). Consequently, the NART-IQ is a good estimate of premorbid intelligence, which is positively correlated with the Wechsler Adult Intelligence Scale's WAIS-IQ score (a

large correlation coefficient of .69; Bright et al., 2018) but takes far less time to complete than the WAIS. We converted the raw NART scores to estimates of the Wechsler Adult Intelligence Scale score (WAIS-IV; Wechsler, 2008), called NART-IQ, via a validated conversion, NARTIQ = 126.41 - 0.9775 × NART errors (Bright et al., 2018). Overall, being more reflective of crystallised than fluid intelligence (Bright et al., 2002; Cattell, 1963), the NART-IQ was included as an efficient, proxy measure of mechanisms that support cognitive functioning, particularly reserve (Boyle et al., 2021), in contrast to the QMCI. Years in education is another such proxy measure, albeit with a weaker reported effect size than NART-IQ (Boyle et al., 2021; Bright et al., 2002).

4.2.2 EEG recording

The EEG setup used for data collection is outlined in Chapter 2 of this thesis. The EEG recording procedure that was used across the AO, AS, VO, and VS conditions of the oddball attention paradigm is outlined in Chapter 3 of this thesis. This study also involved a four-choice reaction time (FCRT) task that has often been used in ageing studies and provides a range of measures of processing speed and variability (Batterham et al., 2014; Deary et al., 2010; Dykiert et al., 2012). Participants saw arrows and had to respond as quickly and accurately as possible by pressing the corresponding arrow key on a Psychology Software Tools, Model 200A serial response box that allowed for a 0 millisecond debounce period. Participants were instructed to use their index and middle fingers of their left hand and right hand respectively (Deary et al., 2011) across the four arrows that were pointing left, right, upwards, and downwards. Participants first completed a practice session, consisting of four trials per arrow. There were two subsequent experimental blocks comprising 40 trials each block (i.e., 10 trials per arrow per block), and participants rested between these blocks. The arrows were pseudo-randomly presented '.bmp' files, matched for central positioning, size, and colour (white, on a black background). This FCRT paradigm was designed and presented on E-prime Professional (Version 2.0), and stimuli were presented on a 22" 1680x1050 Philips LCD monitor.

4.2.3 Data preparation

The EEG data preparation is outlined in Chapter 3 of this thesis. The FCRT data preparation involved calculating mean accuracy and the mean reaction time (RT), raw intra-individual standard deviation (ISD), coefficient of variation (CV; i.e., the intra-individual standard deviation divided by mean RT), and modelled ISD (i.e., the ISD estimated as standardised residuals from a regression model to account for mean RT). These were calculated from cleaned data after the removal of inaccurate trials and reaction times under or over two standard deviations from the mean (Berger & Kiefer, 2021), which resulted in the removal of 4% of the trials on average (*SD* = 1%, *Range* = 1% to 8%). Except for accuracy

and mean RT, with the latter metric being an estimate of processing speed, raw ISD, CV, and modelled ISD are all estimates of intra-individual variability in FCRT performance.

4.2.4 Signal analysis

Classic ERPs were calculated as outlined in Chapter 3 of this thesis. Additionally, to explore the impact of SVD on ERPs, SVD-ERPs were also calculated from the channel-by-ERP decompositions to emphasise features of the ERP that were consistent across channels in an individual. In the current context, the first extracted component accounted for a majority of variance in a majority of participants (AO: *M* = 85% variance, *SD* = 11%, *Range* = 44% to 97%; AS: *M* = 68% variance, *SD* = 11%, *Range* = 41% to 90%; VO: *M* = 78% variance, *SD* = 12%, *Range* = 53% to 95%; VS: *M* = 70% variance, *SD* = 14%, *Range* = 43% to 96%). The resulting ERPs, from both classic and SVD estimation methods, were filtered with a low pass at 30 Hz using the same FIR as specified in Chapter 3 of this thesis. The P3b component was identified by searching for the peak positive amplitude within a latency range of 250 ms to 500 ms post-stimulus. The N2 component was identified by searching for the peak negative amplitude within a latency range of 200 ms to 400 ms post-stimulus. These latency ranges were informed by published recommendations for the oddball attention paradigm's ERP (Luck, 2014; Polich, 1996; Duncan et al., 2009). The method used for estimating $t_{synch}G$ is outlined in Chapter 3 of this thesis.

4.3 Results

Table 4.0 provides a concise summary of this Results section, outlining its organisation and purpose of the content to support efficient engagement with this chapter and to clarify how it contextualises future chapters.

Table 4.0

An outline of the organisation of this Results section, split into sections organised in line with the different analytical approaches covered, and in a way that deliberately mirrors the narrative progression (including rationale therein).

	Content	Purpose	Context
Section 4.3.1	Correlations between chronological age, NART-IQ, and cognitive performance	Preliminary checks of the ageing sample's age and cognitive characteristics to identify replications, confounds, and considerations that may impact later analyses.	Supports Chapters 5 and 7

Section 4.3.2	Estimating chronological age with components of the ERP	Using widely reported components, such as peak amplitude and latency measures of N2 and P3b, to estimate chronological age.	Supports Chapters 5 and 7
Section 4.3.3	Estimating chronological age as EEG-age with $t_{synch}G$	Using the novel measure of $t_{synch}G$ to estimate chronological age.	Supports Chapters 5 and 7
Section 4.3.4	Correlations between EEG-age, NART-IQ, and cognitive performance	Analysing the relationships between different estimates of age, and relationships with pre-validated measures of deficit and benefit framework processes.	Supports Chapters 5 and 7

4.3.1 Correlations between chronological age, NART-IQ, and cognitive performance

The mean NART-IQ was 115 (*SD* = 5.8, *Range* = 102 to 125), indicating that the sample was generally above average and less varied in premorbid intelligence than the general population. There was also a significant positive correlation between NART-IQ and chronological age ($r = .54$, $p < .001$), which reflects the high premorbid intelligence (e.g., reserve) of older adult volunteers on the ARCHA Panel. The mean score of cognitive performance on the QMCI was 77.0 (*SD* = 7.4, *Range* = 61 to 93), indicating that the sample had normal cognitive functioning. Age was not significantly correlated with cognitive performance ($r = -.18$, $p > .05$), and NART-IQ was not significantly correlated with cognitive performance ($r = .12$, $p > .05$). The mean score of mood on the GDS-15 was 2 (*SD* = 2.6, *Range* = 0 to 11), indicating that the sample was presenting with normal mood on average. Chronological age ($r = -.07$, $p > .05$), cognitive performance ($r = -.16$, $p > .05$), and NART-IQ ($r = -.14$, $p > .05$) were not significantly correlated with mood. Participants had a mean of 17 years in formal education (*SD* = 4.0, *Range* = 7 to 27), and chronological age ($r = -.16$, $p > .05$), cognitive performance ($r = .01$, $p > .05$), NART-IQ ($r = .09$, $p > .05$), and mood ($r = -.14$, $p > .05$) were not significantly correlated with years in formal education.

The mean accuracy score on the FCRT was 96% (*SD* = 3%, *Range* = 81% to 100%), indicating that the sample was generally performing accurately. There was a significant positive correlation between accuracy and cognitive performance ($r = .37$, $p = .003$), which suggests that accuracy on the FCRT partly reflects general cognitive performance as measured by the QMCI. Accuracy on the FCRT was not significantly correlated with chronological age ($r = -.18$, $p > .05$), NART-IQ ($r = -.15$, $p > .05$), mood ($r = .08$, $p > .05$), or

years in formal education (r = .21, p > .05). The mean RT on the FCRT was 653 ms (*SD* = 166.4, *Range* = 403 to 1287), indicating that the sample was generally performing at an expected response speed compared to the general population (Der & Deary, 2006). There was a significant positive correlation between mean RT and chronological age (r = .56, p < .001), which demonstrates a slowing in RT with increasing age. Mean RT on the FCRT was not significantly correlated with NART-IQ (r = .15, p > .05), cognitive performance (r = -.15, p > .05), mood (r = -.03, p > .05), years in formal education (r = -.11, p > .05), or FCRT accuracy (r = -.12, p > .05).

When it comes to intra-individual variability in FCRT performance, the mean raw ISD on the FCRT was 165 ms (*SD* = 83.5, *Range* = 50 to 454), indicating that the sample had a wide range of intra-individual variability in RT (Der & Deary, 2006). The mean CV on the FCRT was 0.2 (*SD* = 0.1, *Range* = 0.1 to 0.4), and the mean modelled ISD was 0 (*SD* = 1.0, *Range* = -2 to 4), both again demonstrating the wide variability in the FCRT performance at an intra-individual level. There was a significant positive correlation between mean raw ISD and chronological age (r = .44, p < .001), which demonstrates a greater intra-individual variability in RT with increasing age. Mean raw ISD on the FCRT was not significantly correlated with NART-IQ (r = .08, p > .05), cognitive performance (r = -.15, p > .05), mood (r = .03, p > .05), years in formal education (r = -.12, p > .05), or FCRT accuracy (r = -.11, p > .05). There was a significant positive, near perfect correlation between mean raw ISD and mean RT (r = .92, p < .001), which supports examining metrics that disentangle mean RT from intra-individual variability.

There was a significant positive correlation between CV and chronological age (r = .30, p = .019), which demonstrates a greater intra-individual variability in RT with increasing age despite statistically controlling for mean RT. CV on the FCRT was not significantly correlated with NART-IQ (r = .01, p > .05), cognitive performance (r = -.16, p > .05), mood (r = .08, p > .05), years in formal education (r = -.13, p > .05), or FCRT accuracy (r = -.10, p > .05). However, there was still a significant positive correlation between CV and mean RT (r = .65, p < .001). To statistically disentangle mean RT from intra-individual variability in a more stringent way, modelled ISD was calculated and was not significantly correlated with chronological age (r = -.18, p > .05), NART-IQ (r = -.15, p > .05), cognitive performance (r = -.03, p > .05), mood (r = .14, p > .05), years in formal education (r = -.04, p > .05), or FCRT accuracy (r = -.01, p > .05).

4.3.2 Estimating chronological age with components of the ERP

Classic and SVD ERPs (as shown in Figure 4.1) were estimated to allow for the examination of relationships between chronological age and peaks of the N2 and P3b components of the oddball attention paradigm in both auditory and visual modalities. Chronological age was regressed onto the peak amplitude and peak latency of each oddball component for each estimation method per auditory and visual modality.

Figure 4.1

Classic ERPs, top panel, and SVD ERPs, bottom panel, comprising AO-AS conditions (black-magenta lines) and VO-VS (red-cyan lines) averaged over electrodes and participants, with 95% confidence intervals shaded the same colours respectively to visualise overlaps and differences between the conditions.

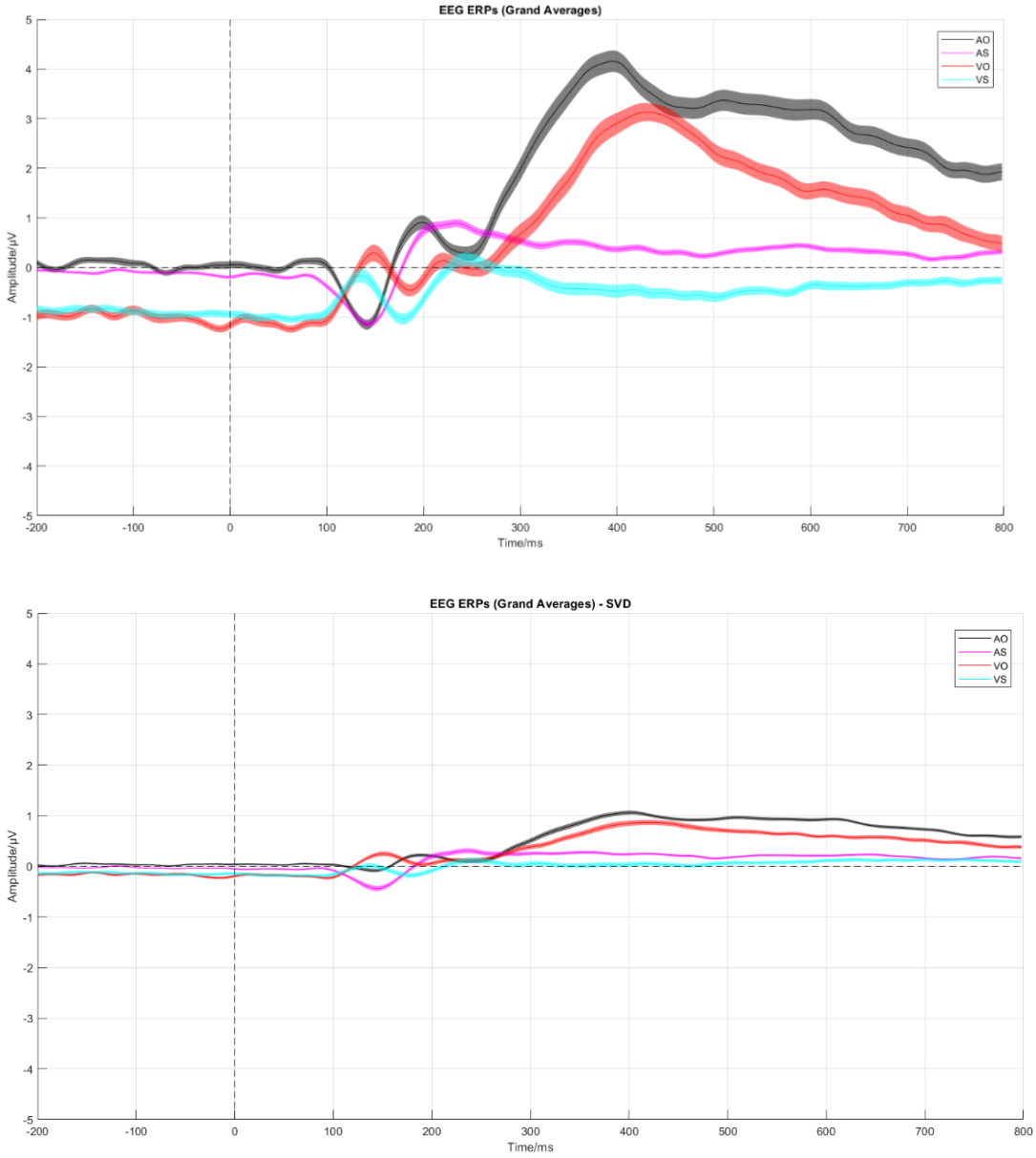

For the auditory modality, P3b and N2 peak amplitudes proved to be significant (p < .05) predictors of chronological age in both classic and SVD estimation methods (as visualised via scattergrams in Figure 4.2). P3b of the SVD method was the most accurate and strongest predictor of age, descriptively, according to RMSE and the correlation coefficient respectively. Using the Glass & Hopkins method (Glass & Hopkins, 1996; IBM Support, 2020) to compare the strengths of correlation coefficients between chronological age and amplitude for each component and estimation method, Table 4.1 shows that there were no significant differences in the strengths of the correlations except between P3b classic and P3b SVD estimation methods; P3b SVD amplitude was a significantly stronger correlate with chronological age. The regression of chronological age on P3b amplitude of the SVD method corresponded with a correlation of r = -.53 (or .53 with P3b-age) and accounted for approximately 26% of the variance in age (*RMSE* = 15.07). When regressing P3b amplitude onto chronological age (*RMSE* = 0.30), each decade of chronological age was associated with an expected change of 0.11 μV in amplitude ($P3b\ amplitude = -0.011 \times Age + 1.81$). When combining P3b and N2 amplitudes from SVD in a multiple regression (*RMSE* = 14.79), N2 amplitude did not significantly improve the model (F(1, 57) = 2.15, p > .05, *AdjR² change* = .03).

Figure 4.2

Scattergrams showing the linear relationship between peak amplitude (μV) and chronological age (years) for auditory P3b (top row) and auditory N2 (bottom row) oddball ERP components of classic (left side) and SVD (right side) estimation methods.

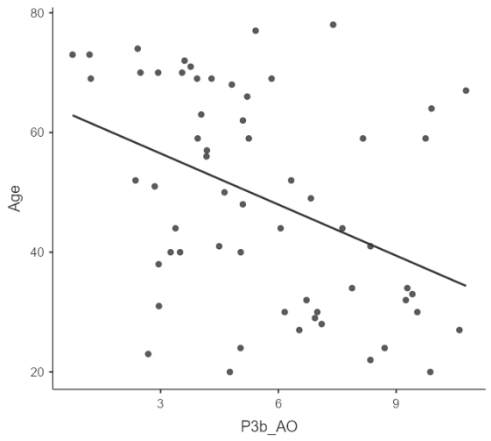

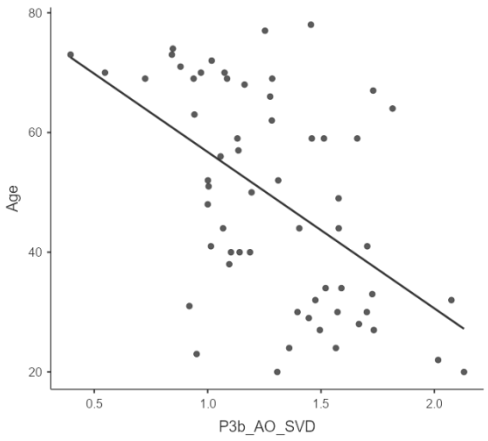

Age = -2.84 x P3b amplitude + 65.03

F = 11.73, *df* 1, 58 *p* = .001

r = -.41; *AdjR²* = 0.15; *RMSE* = 16.16

Age = -26.13 x P3b amplitude SVD + 82.88

F = 22.19, *df* 1, 58 *p* < .001

r = -.53; *AdjR²* = 0.26; *RMSE* = 15.07

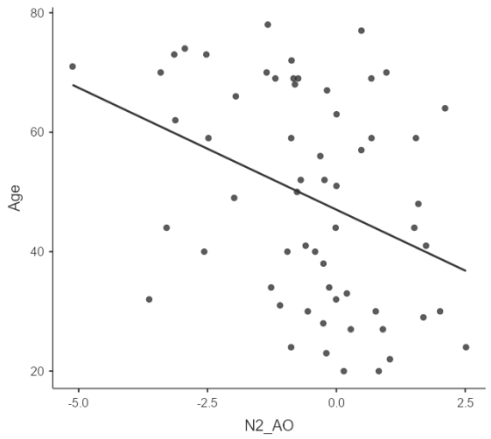

Age = -4.08 x N2 amplitude + 47.03

F = 8.85, *df* 1, 58 *p* = .004

r = -.36; $AdjR^2$ = 0.12; *RMSE* = 16.51

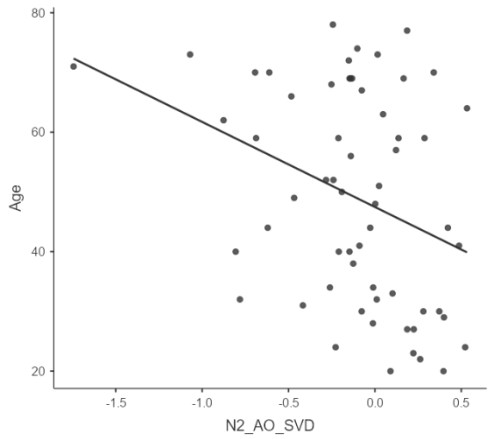

Age = -14.24 x N2 amplitude SVD + 47.47

F = 7.36, *df* 1, 58 *p* = .009

r = -.34; $AdjR^2$ = 0.10; *RMSE* = 16.69

Table 4.1

Differences between Pearson's r correlations of chronological age with AO peak amplitude, using the Glass & Hopkins method to formally compare the strengths of these correlation coefficients.

	P3b_Classic	P3b_SVD	N2_Classic	N2_SVD
P3b_Classic	-			
P3b_SVD	.12*	-		
N2_Classic	-.05	-.16	-	
N2_SVD	-.07	-.19	-.03	-

Note. The values represent the differences between the respective Pearson's *r* correlation coefficients (e.g., P3b_Classic – P3b_SVD); *p < .05

For the auditory modality, P3b and N2 peak latencies proved to be significant (p < .05) predictors of chronological age in both estimation methods (as visualised via scattergrams in Figure 4.3). P3b of the SVD method was the most accurate and strongest predictor of age, descriptively, according to RMSE and the correlation coefficient respectively. Using the Glass & Hopkins method (Glass & Hopkins, 1996; IBM Support, 2020) to compare the strengths of correlation coefficients between chronological age and latency for each component and estimation method, Table 4.2 shows that there were no significant differences in the strengths of the correlations. The regression of chronological age on P3b latency of the SVD method corresponded with a correlation of *r* = .28 and

accounted for approximately 6% of the variance in age (*RMSE* = 17.00). When regressing P3b latency onto chronological age (*RMSE* = 56.49), each decade of chronological age was associated with an expected change of 9.37 ms in latency ($P3b\ latency = 0.937 \times Age + 361.81$). When combining P3b and N2 latencies from SVD in a multiple regression (RMSE = 15.98), N2 latency significantly improved the model ($F(1, 57) = 7.53$, $p = .008$, $AdjR^2$ *change* = .11), thus warranting inclusion of both P3b (standardised estimate = 0.35) and N2 (standardised estimate = 0.33) peak latencies when predicting age ($Age = 0.10 \times P3b\ latency + 0.16 \times N2\ latency - 33.74$).

Figure 4.3

Scattergrams showing the linear relationship between peak latency (ms) and chronological age (years) for auditory P3b (top row) and auditory N2 (bottom row) oddball ERP components of classic (left side) and SVD (right side) estimation methods.

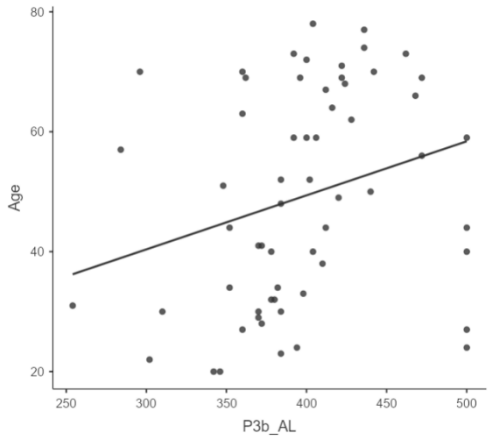

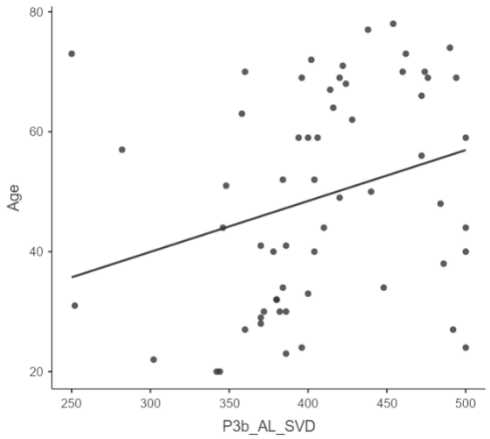

Age = 0.09 x P3b latency + 13.35

F = 4.52, *df* 1, 58 *p* = .038

r = .27; $AdjR^2$ = 0.06; *RMSE* = 17.07

Age = 0.08 x P3b latency SVD + 14.51

F = 5.01, *df* 1, 58 *p* = .029

r = .28; $AdjR^2$ = 0.06; *RMSE* = 17.00

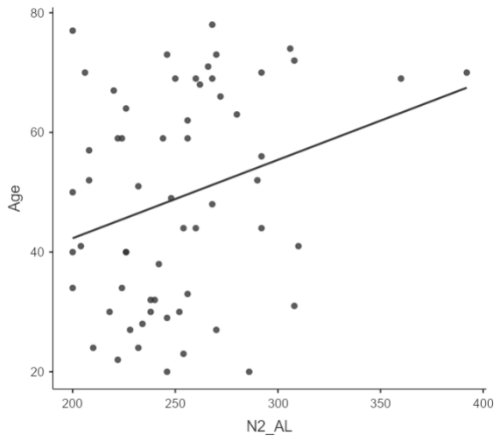

Age = 0.13 x N2 latency + 16.11

F = 4.88, *df* 1, 58 *p* = .031

r = .28; $AdjR^2$ = 0.06; *RMSE* = 17.02

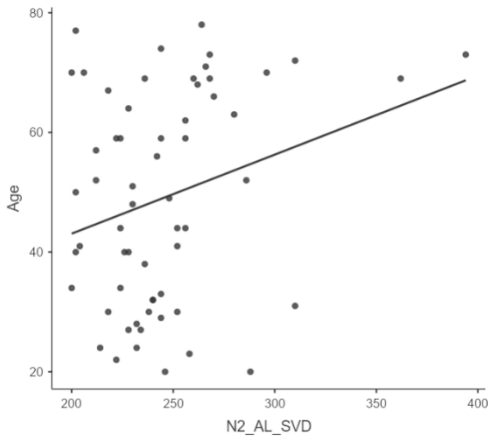

Age = 0.13 x N2 latency SVD + 16.66

F = 4.49, *df* 1, 58 *p* = .038

r = .27; $AdjR^2$ = 0.06; *RMSE* = 17.07

Table 4.2

Differences between Pearson's r correlations of chronological age with AO peak latency, using the Glass & Hopkins method to formally compare the strengths of these correlation coefficients.

	P3b_Classic	P3b_SVD	N2_Classic	N2_SVD
P3b_Classic	-			
P3b_SVD	-.01	-		
N2_Classic	-.01	.00	-	
N2_SVD	.00	.01	.01	-

Note. The values represent the differences between the respective Pearson's *r* correlation coefficients (e.g., P3b_Classic – P3b_SVD); there were no significant differences

For the visual modality, P3b and N2 peak amplitudes proved to be nonsignificant ($p > .05$) predictors of chronological age in both estimation methods (as visualised via scattergrams in Figure 4.4). N2 peak latencies also proved to be nonsignificant predictors of chronological age in both estimation methods (as visualised via scattergrams in Figure 4.5). However, P3b peak latencies proved to be significant predictors of chronological age in both estimation methods (as visualised via scattergrams in Figure 4.5), and P3b of the classic method was the most accurate and strongest predictor of age, descriptively, according to RMSE and the correlation coefficient respectively. The Glass & Hopkins method (Glass & Hopkins, 1996; IBM Support, 2020) was again used to compare the strengths of correlation

coefficients between chronological age and P3b peak latency on each estimation method. Table 4.3 shows that there were no significant differences in the strengths of the correlations except between P3b classic and N2 SVD estimation methods, where P3b classic latency was a significantly stronger correlate with chronological age. The regression of chronological age on P3b latency of the classic method corresponded with a correlation of *r* = .46 and accounted for approximately 20% of the variance in age (*RMSE* = 15.70). When regressing P3b latency onto chronological age (*RMSE* = 39.80), each decade of chronological age was associated with an expected change of 11.76 ms in latency ($P3b\ latency = 1.176 \times Age + 368.25$). As this is a correlational study, the distributions of all the ERP components' variables are provided in Table 4.4 and Table 4.5.

Figure 4.4

Scattergrams showing the linear relationship between peak amplitude (μV) and chronological age (years) for visual P3b (top row) and visual N2 (bottom row) oddball ERP components of classic (left side) and SVD (right side) estimation methods

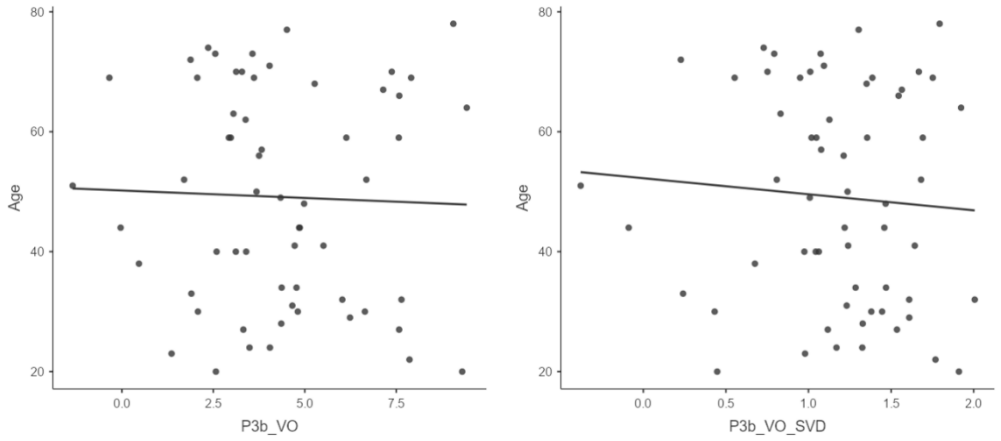

Age = -0.25 x P3b amplitude + 50.20

F = 0.06, *df* 1, 58 *p* = .801

r = -.03; *AdjR*^{2} = -0.02; *RMSE* = 17.71

Age = -2.67 x P3b amplitude SVD + 52.24

F = 0.30, *df* 1, 58 *p* = .583

r = -.07; *AdjR*^{2} = -0.01; *RMSE* = 17.67

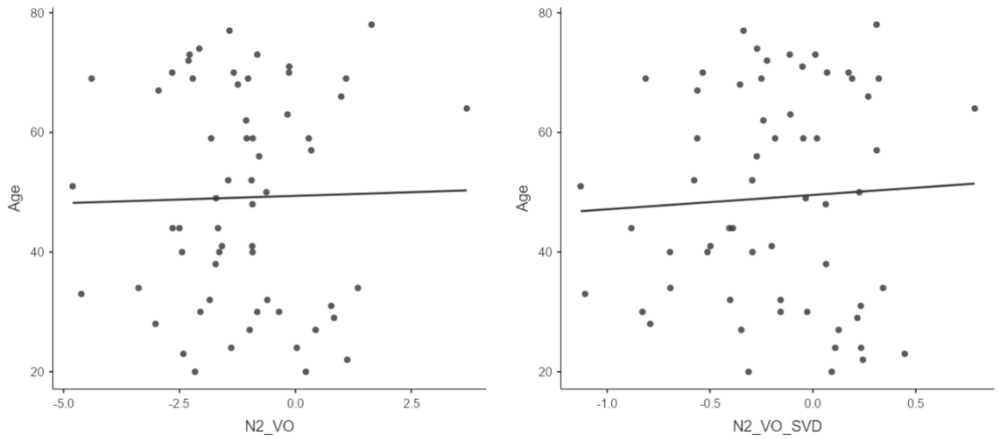

Age = 0.24 x N2 amplitude + 49.39 *F* = 0.03, *df* 1, 58 *p* = .872 *r* = .02; *AdjR*^{2} = -0.02; *RMSE* = 17.72	Age = 2.40 x N2 amplitude SVD + 49.55 *F* = 0.17, *df* 1, 58 *p* = .686 *r* = .05; *AdjR*^{2} = -0.01; *RMSE* = 17.70

Figure 4.5

Scattergrams showing the linear relationship between peak latency (ms) and chronological age (years) for visual P3b (top row) and visual N2 (bottom row) oddball ERP components of classic (left side) and SVD (right side) estimation methods

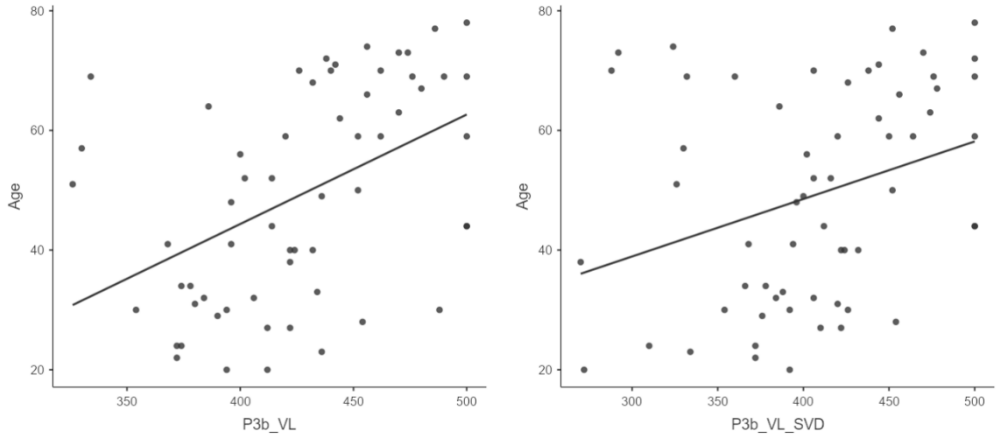

Age = 0.18 x P3b latency - 28.81 *F* = 15.70, *df* 1, 58 *p* < .001 *r* = .46; *AdjR*^{2} = 0.20; *RMSE* = 15.70	Age = 0.10 x P3b latency SVD + 10.10 *F* = 6.62, *df* 1, 58 *p* = .013 *r* = .32; *AdjR*^{2} = 0.09; *RMSE* = 16.79

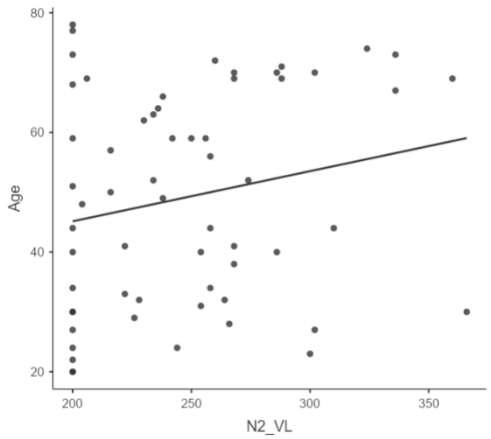

Age = 0.08 x N2 latency + 28.39

F = 2.61, *df* 1, 58 *p* = .112

r = .21; $AdjR^2$ = 0.03; *RMSE* = 17.34

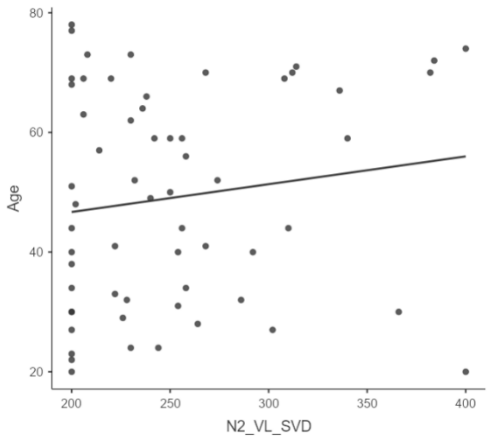

Age = 0.05 x N2 latency SVD + 37.41

F = 1.25, *df* 1, 58 *p* = .269

r = .15; $AdjR^2$ = 0.01; *RMSE* = 17.53

Table 4.3

Differences between Pearson's r correlations of chronological age with VO peak latency, using the Glass & Hopkins method to formally compare the strengths of these correlation coefficients.

	P3b_Classic	P3b_SVD	N2_Classic	N2_SVD
P3b_Classic	-			
P3b_SVD	.14	-		
N2_Classic	.26	.11	-	
N2_SVD	.32*	.18	.06	-

Note. The values represent the differences between the respective Pearson's *r* correlation coefficients (e.g., P3b_Classic – P3b_SVD); *p < .05

Table 4.4

Distribution of the P3b and N2 ERP components' peak amplitude per estimation method (classic and SVD) and modality (auditory and visual) across all participants (n = 60)

	M	SD	Range
P3b_Classic (auditory)	5.59	2.58	0.76 to 10.78
P3b_SVD (auditory)	1.29	0.36	0.40 to 2.13
P3b_Classic (visual)	4.34	2.39	-1.35 to 9.43
P3b_SVD (visual)	1.17	0.48	-0.38 to 2.01
N2_Classic (auditory)	-0.51	1.59	-5.12 to 2.52
N2_SVD (auditory)	-0.12	0.42	-1.74 to 0.53
N2_Classic (visual)	-1.14	1.55	-4.80 to 3.70
N2_SVD (visual)	-0.18	0.40	-1.13 to 0.79

Table 4.5

Distribution of the P3b and N2 ERP components' peak latency per estimation method (classic and SVD) and modality (auditory and visual) across all participants (n = 60)

	M	SD	Range
P3b_Classic (auditory)	396.97	53.36	254 to 500
P3b_SVD (auditory)	407.83	59.38	250 to 500
P3b_Classic (visual)	426.00	45.31	326 to 500
P3b_SVD (visual)	405.97	59.49	270 to 500
N2_Classic (auditory)	251.93	38.02	200 to 392
N2_SVD (auditory)	245.70	36.25	200 to 394
N2_Classic (visual)	247.40	44.26	200 to 366
N2_SVD (visual)	251.97	55.81	200 to 400

4.3.3 Estimating chronological age as EEG-age with $t_{synch}G$

The novel metric of $t_{synch}G$ was estimated to examine the relationship between chronological age and the explanatory mechanism for event-related changes in the EEG, which can be thought of as a quantification of information processing and communication across decreasing frequency (i.e., across neural networks of increasing size and complexity according to the VSH). Chronological age was regressed onto the $t_{synch}G$ for each condition per modality of the oddball attention paradigm.

The AO gradient proved to be the only significant ($p < .05$) predictor of chronological age (as visualised via scattergrams in Figure 4.6), with AS, VO, and VS gradients all nonsignificant ($p > .05$). The regression of chronological age on AO $t_{synch}G$ corresponded with a correlation of $r = .36$ and accounted for approximately 11% of the variance in age (*RMSE* = 16.54). When regressing $t_{synch}G$ onto chronological age (*RMSE* = 0.63), each decade of chronological age was associated with an expected change of 0.14 in gradient

elevation ($AO\ tsynchG = 0.014 \times Age - 1.29$). When removing potential participant outliers (under/over 1.5 times interquartile range of 25th and 75th percentiles) from the AO $t_{synch}G$ data, the prediction improved very slightly (as visualised via scattergram in Figure 4.7). The new regression of chronological age on AO $t_{synch}G$ corresponded with a correlation of *r* = .38 and accounted for approximately 13% of the variance in age (*RMSE* = 16.14). When regressing the cleaned $t_{synch}G$ onto chronological age (*RMSE* = 0.45), each decade of chronological age was associated with an expected change of 0.11 in gradient elevation ($AO\ tsynchG = 0.011 \times Age - 1.15$). As this is a correlational study, the distributions of the $t_{synch}G$ and the best EEG-age metrics are provided in Table 4.6 and Table 4.7 respectively.

Figure 4.6

Scattergrams showing the linear relationship between $t_{synch}G$ (gradient) and chronological age (years) for AO, AS, VO, and VS conditions of the oddball attention paradigm (n = 60)

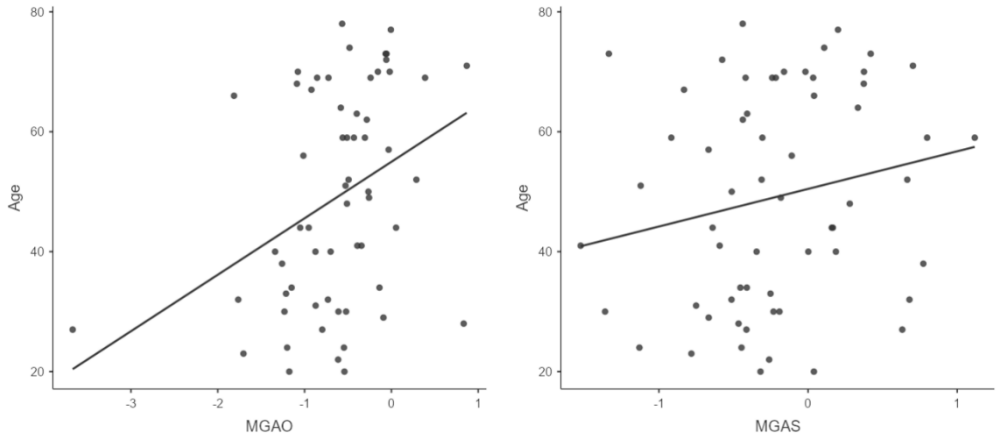

Age = 9.42 x AO $t_{synch}G$ + 54.98

F = 8.55, *df* 1, 58 *p* = .005

r = .36; $AdjR^2$ = 0.11; *RMSE* = 16.54

Age = 6.27 x AS $t_{synch}G$ + 50.46

F = 2.33, *df* 1, 58 *p* = .132

r = .20; $AdjR^2$ = 0.02; *RMSE* = 17.38

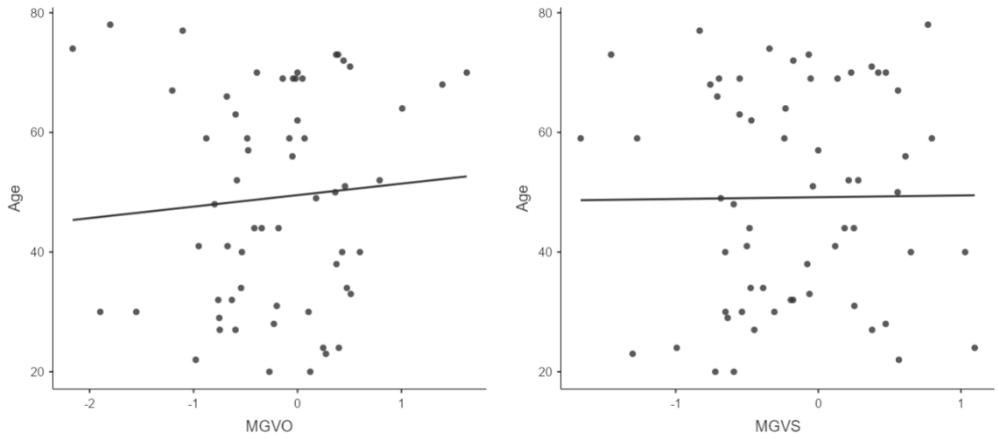

Age = 1.92 x VO $t_{synch}G$ + 49.52

F = 0.36, *df* 1, 58 *p* = .549

r = .08; $AdjR^2$ = -0.01; *RMSE* = 17.67

Age = 0.30 x VS $t_{synch}G$ + 49.17

F = 0.01, *df* 1, 58 *p* = .939

r = .01; $AdjR^2$ = -0.02; *RMSE* = 17.72

Figure 4.7

Scattergram showing the linear relationship between AO $t_{synch}G$ (gradient) and chronological age (years) with potential participant outliers removed from the AO $t_{synch}G$ data (outliers defined as under/over 1.5 times the interquartile range of 25th and 75th percentiles, n = 57)

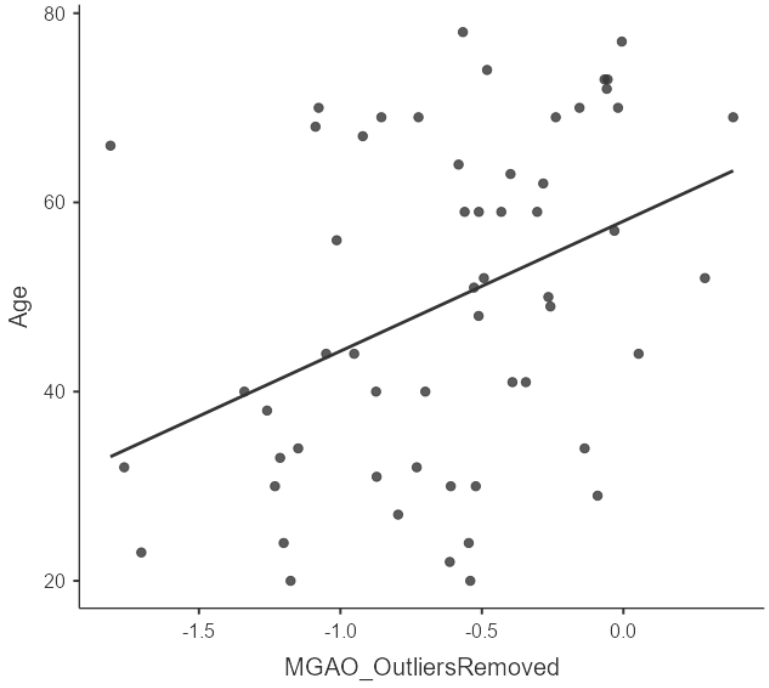

Age = 13.73 x AO $t_{synch}G$ + 58.02

F = 9.55, *df* 1, 55 *p* = .003

r = .38; $AdjR^2$ = 0.13; *RMSE* = 16.14

Table 4.6

Distribution of $t_{synch}G$ across conditions (oddball and standard) and modality (auditory and visual)

	M	SD	Range
AO $t_{synch}G$	-0.62	0.68	-3.67 to 0.87
AO $t_{synch}G$ (cleaned)	-0.62	0.49	-1.81 to 0.39
AS $t_{synch}G$	-0.21	0.56	-1.53 to 1.12
VO $t_{synch}G$	-0.21	0.74	-2.16 to 1.63
VS $t_{synch}G$	-0.17	0.61	-1.67 to 1.10

Note. n = 60 except for AO $t_{synch}G$ (cleaned), which was n = 57.

Table 4.7

Distribution of EEG-age for AO $t_{synch}G$ and P3b SVD amplitude, as the best predictors of chronological age per approach

	M	SD	Range
AO $t_{synch}G$ EEG-age	49	6.41	20 to 63
AO $t_{synch}G$ (cleaned) EEG-age	49	6.78	33 to 63
P3b SVD amplitude EEG-age	49	9.40	27 to 73

Note. n = 60 except for AO $t_{synch}G$ (cleaned), which was n = 57.

4.3.4 Correlations between EEG-age, NART-IQ, and cognitive performance

P3b peak amplitude age from the SVD method and AO $t_{synch}G$ age (i.e., EEG-age metrics) were chosen for the final stages of analysis because they produced the most accurate estimates of age, with the lowest RMSE, per approach. It was expected that QMCI would be negatively correlated with age, implicating deleterious age-related changes such as dedifferentiation and noise. In contrast, none of chronological age, P3b amplitude SVD age, nor AO $t_{synch}G$ age was significantly correlated with QMCI (as shown in Table 4.8). A

Bayesian Linear Regression (BLR) was used to evaluate null models against alternatives in predicting cognitive functioning with P3b amplitude age and AO t_{synch}G age, to judge the levels of evidence in favour of the null (H0) by using established cut-offs (Jeffreys, 1961; Wagenmakers et al., 2011). The default Jeffreys-Zellner-Siow (JZS) prior with an r scale of 0.354 was used due to this being the first time, at least to our knowledge, that this EEG-age procedure had been implemented. A BLR comparing a null model with a second model adding P3b amplitude age, in attempts to predict QMCI, reported BF01 = 3.45, providing substantial evidence in favour of H0. Next, a BLR comparing a null model with a second model adding AO t_{synch}G age, in attempts to predict QMCI, reported BF01 = 2.38, providing only anecdotal evidence in favour of H0 (Jeffreys, 1961; Wagenmakers et al., 2011). This suggests that AO t_{synch}G cannot be ruled out as a predictor of cognitive performance based on the current data.

A notable inconsistency between P3b amplitude age and AO t_{synch}G age was that t_{synch}G age was significantly correlated with NART-IQ (r = .31, p = .020), analogous to the correlation between chronological age and NART-IQ (r = .54, p < .001), but P3b amplitude SVD age was not significantly correlated with NART-IQ (r = .22, p > .05). To explore these inconsistencies further, partial correlations were run between ages and cognitive performance accounting for NART-IQ (as shown in Table 4.8). P3b amplitude age and AO t_{synch}G age remained not significantly correlated with cognitive performance (although the point estimates increased), but chronological age was now significantly negatively correlated with cognitive performance. In summary, these results cannot answer which estimate of brain age is the best proxy of general cognitive functioning. To examine this idea, it was expected that NART-IQ would positively correlate with QMCI, implicating protective processes that support cognitive functioning, particularly reserve. Indeed, NART-IQ and QMCI were significantly positively correlated when controlling for chronological age due to the age-NART-IQ bias (r = .26, p = .047). Additionally, mood and number of years in formal education were not significantly correlated with any of the EEG measures (p > .05), which is not overly surprising considering the relatively low levels of depression and small effect sizes when using years in education as a predictor variable.

Table 4.8

Pearson's r correlation coefficients of P3b SVD amplitude age (P3b), AO t_{synch}G age, and chronological age (CA) with QMCI

	P3b age	t_{synch}G age	CA
QMCI	-.06	-.14	-.18
QMCI (controlled for NART-IQ)	-.09	-.19	-.29*

Note. $*p < .05$

As an alternative perspective on event-related cognitive functioning, focusing more specifically on processing accuracy, speed, and intra-individual variability, the FCRT measures were examined. It was expected that FCRT measures would be correlated with age, implicating deleterious age-related changes such as dedifferentiation and noise, and this was the case for chronological age and P3b SVD amplitude age, but not AO t_{synch}G age (as shown in Table 4.9). To end, when controlling for both NART-IQ and chronological age, P3b amplitude age was no longer significantly correlated with FCRT metrics of RT ($r = .19$, $p > .05$) or raw ISD ($r = .14$, $p > .05$), which suggests that P3b amplitude is not best placed to estimate age-matched general cognitive functioning in the form of processing speed and variability.

Table 4.9

Pearson's r correlation coefficients of P3b SVD amplitude age (P3b), AO t_{synch}G age, and chronological age (CA) with FCRT metrics of accuracy, speed, and intra-individual variability

	P3b age	AO t_{synch}G age	CA
Accuracy	.05	-.10	-.18
Accuracy (controlled for NART-IQ)	.09	-.06	-.12
RT	.43***	.19	.56***
RT (controlled for NART-IQ)	.42**	.15	.57***
Raw ISD	.35**	.13	.44***
Raw ISD (controlled for NART-IQ)	.34**	.11	.47***
CV	.23	.04	.30*
CV (controlled for NART-IQ)	.23	.03	.35**
Modelled ISD	-.13	-.11	-.18
Modelled ISD (controlled for NART-IQ)	-.10	-.07	-.13

Note. $*p < .05$; $**p < .01$; $***p < .001$

4.4 Discussion

It would have been amiss to treat the FM as a true candidate for explaining event-related changes in the EEG without showing that its fundamental explanatory mechanism – cross-frequency phase modulation that can be operationalised via t_{synch}G – demonstrates an age-related shift. Therefore, our objective was to use the new t_{synch}G metric to estimate chronological age as EEG-age. First however, we wanted to compare the well-established N2 and P3b ERP components of the auditory and visual oddball attention paradigms on their ability to estimate age. We predicted that peak amplitude would be negatively correlated with chronological age, and peak latency would be positively correlated with chronological age. Irrespective of the estimation method used (i.e., classic or SVD) or ERP component examined (i.e., P3b or N2) in the auditory modality, peak amplitude was reliably negatively

correlated with chronological age. This finding is consistent with previous evidence that suggests an adult's gradual decline in mean amplitude is a normal brain-ageing phenomenon (Polich, 1996, 1997; Van Dinteren et al., 2014). Similarly, peak latency was reliably positively correlated with chronological age, which is again consistent with previous evidence that suggests an adult's gradual increase in mean latency is a normal brain-ageing phenomenon (Polich, 1996, 1997; Van Dinteren et al., 2014). However, except for a proportional relationship between P3b peak latency and chronological age, these relationships were not reported in the visual modality. This may be due to lower SNR in the visual paradigm (as previously outlined in Chapter 3; Barry & De Blasio, 2017; Bennington & Polich, 1999; Polich, 1996), and an inability to reliably identify peaks within the time window and ROI that was used in this study for identifying the visual N2 component. Whatever the reason however, the auditory modality has been providing greater SNR and more consistent results over both Chapter 3 and Chapter 4, thus may be more suited to clinical applications for tracking age-related changes in the brain where audition is maintained.

We also sought to determine which ERP component correlated most strongly and provided the most accurate estimate of chronological age. Although there were generally no statistically significant differences in the strength of the correlations with age, auditory P3b amplitude after SVD estimation was the best predictor of chronological age. This is unsurprising given the purpose of data reduction with SVD is to improve SNR, with the benefit of not requiring an unweighted averaging across electrode channels. However, it remains hard to interpret the meaning of this amplitude change, and equally as hard to contextualise it with ageing theory. With differing explanations (all outlined in Chapter 2) ranging from increasing variability of the underlying trial-to-trial peaks to a change in the underlying 1/f aperiodic component, from changes in the AAM mechanism to other intrinsic intra-individual and inter-individual changes in EEG noise (e.g., physiological and measurement) and the process of volume conduction, there is no clear interpretation. For example, Van Dinteren et al. (2014) suggest that changes in P3b amplitude may reflect a change in the power of neural activity or of available resources, but it could also link to a range of amalgamations of the benefit and deficit models of ageing too (e.g., increased neural noise alongside dedifferentiation; Cremer & Zeef, 1987; Koen & Rugg, 2019; Voytek et al., 2015a, 2015b).

Next, we sought to explore the potential of $t_{synch}G$ to estimate chronological age, with $t_{synch}G$ interpreted as a metric that may allow us to study the true deep structure of event-related changes in the form of multiscale information transfer and neural network communication across the brain. Chronological age was significantly estimated with AO $t_{synch}G$, but not AS $t_{synch}G$ or at all in the visual modality. This may be reflecting previously

noted particulars of the standard condition (e.g., reflecting far less homogenous activity over trials compared to the oddball condition; outlined in Chapter 3) and low SNR in the visual modality. Indeed, the lack of $t_{synch}G$ correlations in the visual modality could simply explain the lack of correlations in the ERP components; thus, $t_{synch}G$ reflected the overarching ERP findings very well. Whilst there was a significant correlation between P3b latency and age in the visual modality, this alone may not have been sufficient to affect a significant $t_{synch}G$ with age, given $t_{synch}G$ encompasses the whole structure of the ERP not just one component. Similarly, this may be why AO $t_{synch}G$ did not provide a markedly improved correlation between chronological age and estimated brain age compared to that seen with P3b and N2 latency components. The main conclusion thus far is that EEG-age estimated from ERP component peaks and $t_{synch}G$ can estimate chronological age with an expected error of around 16 years. However, it remains to be seen whether this EEG-age is sufficiently accurate to be useful, particularly at the individual level where the baseline variability in EEG metrics is greater thus making it more difficult to track meaningful change over time than at the group level (Burgess & Gruzelier, 1993). Indeed, there remains a concern with the underlying SNR when estimating $t_{synch}G$ at the individual level, as already outlined in Chapter 3. However, AO $t_{synch}G$ in its current form still positively correlated with chronological age, and in a direction that makes sense given the changes in the AO ERP components with increasing age (e.g., delayed peak latencies from a flatter gradient).

The proportional relationship between chronological age and AO $t_{synch}G$ can be interpreted in the context of the deficit theories of ageing, which posit a slowing of communication between neural networks with age due to increased ongoing neural noise that interferes with information transfer. This neural noise may originate from increased task-irrelevant neural activity and a baseline transition from efficient use of smaller, specialised networks to inefficient use of larger, general networks, which all aligns very well with a mechanistic explanation of increased $t_{synch}G$ (i.e., flattening of the gradient) with increasing age. Whilst only significant in the AO condition, the trend was consistent in the AS condition too, thus may become significant with greater analytical precision and power. Therefore, this shift in gradient may represent a slowing or greater inefficiency of information communication from resting state, through small, localised neural networks, to widespread networks. This interpretation could also explain age-related peak frequency slowing and downwards transition of power (Dauwels et al., 2011; Ishii et al., 2017; Klimesch, 1999; Scally et al., 2018; i.e., perhaps reflecting the network change), and reduced component amplitudes and prolonged component latencies within ERPs (Polich et al., 1985; Polich, 1996, 1997; Van Dinteren et al., 2014; i.e., perhaps reflecting the inefficient use, with high trial-by-trial variability).

Typical and atypical ageing has contrasting magnitudes of effect on event-related changes (Dauwels et al., 2010a, 2010b; Hedges et al., 2016), and the current sample proved to be a very healthy sample with a NARTIQ-chronological age bias. These factors substantiate why there was no real difference in the predictive power of ERP components and $t_{synch}G$, because there were likely no widespread and substantial age-related changes aside from those already represented by the P3b and N2 metrics. If anything then, the fact that the metrics show analogous results in this outstanding healthy ageing sample further supports that $t_{synch}G$ well explains ERPs and does so in one holistic metric rather than across multiple surface measures. Future work should examine subclinical and clinical populations from across the age range in comparison to healthy ageing, to see whether the patterns identified, such as a flattening of $t_{synch}G$, are indeed exaggerated or in any other way uniquely distinct compared to the healthy ageing track. In turn, researchers could examine how the flattening occurs across discrete IMFs, as the ageing process may 'start' at (i.e., pivot around) a particular IMF(s). Attempting to differentiate between healthy, subjective cognitive impairment (SCI; Jessen et al., 2020; Tales et al., 2014), MCI (Apostolo et al., 2016; Dauwels et al., 2010a), and dementia onset with the FM's metrics would be of particular clinical interest, as would longitudinal studies in each group rather than relying on cross-sectional approaches that limit our understanding to population-level conclusions.

Finally, we wanted to examine the relationships of ERP-estimated age and $t_{synch}G$ EEG-age with already established proxy measures of general cognitive integrity. Relationships between ERP components, chronological age, and cognitive functioning were already established, but $t_{synch}G$ had not previously been used to estimate EEG-age before. There were no significant correlations between general cognitive performance and ERP peaks or $t_{synch}G$, although the correlation coefficients were trending in the expected directions. Indeed, when analysing the relationship between cognitive performance and $t_{synch}G$ with Bayesian methods, there was only anecdotal evidence for the null, which suggests a statistical power issue rather than compelling evidence against the conjecture. That said, these findings are not consistent with previous evidence that suggests significantly decreased peak amplitude and increased peak latency measures, even with age-matched samples, likely reflects normal age-related changes in neural and cognitive integrity (e.g., dedifferentiation and noise as outlined by the deficit models of ageing). The significance of the ERP and $t_{synch}G$ correlations with cognitive performance did not change when controlling for NART-IQ either, although chronological age was significantly negatively correlated with cognitive performance.

The negative correlation between chronological age and cognitive performance could be expected with an ageing sample after statistically controlling for NART-IQ, because the

significant negative correlations between age and general cognitive performance were initially masked by the positive correlation between chronological age and premorbid IQ. That is, it is not an overly surprising result in this sample of healthy adults who displayed QMCI scores in the normal cognitive functioning range, because if the older adults were not scoring in the normal range, their levels of reserve, as proxied by the NART-IQ, would likely not be so high either. Further supporting this interpretation, NART-IQ and QMCI were modestly positively correlated after controlling for chronological age, because higher premorbid IQ, thus reserve as outlined by the benefit model of ageing, can support better cognitive functioning or at least the maintenance of normal functioning (Cabeza et al., 2018; Stern, 2012). The concurrent minor decline in cognitive functioning with chronological age, but not into an MCI range, was initially masking the relationship. In summary, normal age-related declines in cognitive functioning pull QMCI scores down, whilst an age-NART-IQ bias can pull older adults' QMCI scores up concurrently, which is why partial correlation analysis revealed the expected relationships for both age-QMCI (negative correlation) and NART-IQ-QMCI (positive correlation) given the current sample.

Clearly then, there was a sample bias in this study. Therefore, whilst AO $t_{synch}G$ was not significantly correlated with cognitive performance in this study with the current statistical power and SNR, one can still muse on a potential mechanism to explain the three aspects of chronological age, NART-IQ, and $t_{synch}G$ together. That is, higher innate neural efficiency may reflect a steeper gradient (i.e., faster, more efficient information communication across neural networks); higher age-related neural noise may reflect a flatter gradient (i.e., slower, less efficient information communication across neural networks). In the current sample, older participants had higher efficiency (proxied by increasing premorbid IQ) but also higher neural noise. When accounting for neural noise, participants' neural efficiency was highlighted; when accounting for neural efficiency, participants' neural noise was highlighted (i.e., more pronounced coefficients). Without accounting for either in this biased sample, neural efficiency blurred with neural noise and further concealed any relationships. Overall, AO $t_{synch}G$ may be a proxy measure of neural efficiency (with age-matched participants) and neural noise (with IQ-matched participants). That is, EEG-age derived from $t_{synch}G$, compared to ERP component peaks, may be a more comprehensive measure of general brain functioning and integrity due to its consideration of the deep structure of the EEG rather than discrete surface features. Furthermore, a subset of early neural developments that are damaging to general fluid cognitive functioning (e.g., decreased QMCI), or potentially indicative of future degradation once reaching a critical point, might be tracked when focusing in on discrete components (e.g., reflecting the deficit model of ageing, such as the beginnings of a wider transition to less efficient neural networks). In contrast, $t_{synch}G$

might provide a more comprehensive insight into general brain functioning and integrity that may reflect a range of both protective (e.g., reserve, benefit model) and deleterious (e.g., dedifferentiation and noise, deficit model) agents, general crystallised and fluid cognition.

The findings in this study cannot answer which estimate of brain age is the best proxy of general cognitive functioning, perhaps because there was a very weak distinction in general cognitive functioning across the age range in the current sample or because the metrics and methodology used do not fully account for the complexity involved. For example, other ageing theories, such as the Neural Efficiency Hypothesis (NEH; Doppelmayr et al., 2005; Grabner et al., 2006; Jausovec & Jausovec, 2000; Neubauer et al., 2004, 2005) posit that higher IQ (including premorbid, NART-IQ) partly reflects greater crystallised efficiency of neural network communication, whereby neural activation patterns are more refined and can account for early age-related decline. This may be particularly pertinent when participants are completing simple tasks that are not cognitively demanding, which aligns with the Compensation-related Utilisation of Neural Circuits Hypothesis (CRUNCH) model of ageing (Cappell et al., 2010; De Felice & Holland, 2018; Reuter-Lorenz & Cappell, 2008). The CRUNCH model proposes that changes in cognitive performance between age groups is far clearer in tasks with greater demands, where benefit mechanisms cannot make up for the age-related deficits. Therefore, future research should interrogate a range of tasks, from easy to hard in terms of their cognitive demands, as well as samples where there is no age-NART-IQ bias and where QMCI scores are not restricted to normal functioning.

This study purposely followed a general approach to the measurement (QMCI and NART) and interpretation (Koenig et al., 2020) of neural and cognitive integrity, but future studies could measure specific subcategories of fluid and crystallised intelligence (e.g., Ociepka et al., 2023). The proxy measures used in this study were not intended to be exhaustive but to provide a starting point in general brain functioning. Similarly, future studies could provide a systematic, thorough comparison of the different approaches to estimating the EEG metrics. This could include the wide array of different analytical approaches, such as area and fractional estimation of ERP components and t_{synch} (Luck, 2014) to improve SNR, whilst also elucidating concrete reasons for any differences observed within and between ERP-estimated and t_{synch}G-estimated age. Looking ahead then, it will be necessary to optimise methodology and analysis pipelines to establish good, large-scale normative data that makes it possible to estimate the EEG-age of individuals across the entire human lifespan, not just adulthood, with high reliability, validity, and precision. This would facilitate the identification of individuals with unusual discrepancies between their EEG-age and the normative EEG-age for their chronological age and condition. In working towards that end goal, the FM could also be tested in the context of MEG, whereby the

likeness of event-related changes to those in EEG encourages an analogous avenue of interrogation (Da Silva, 2018; David et al., 2006). Furthermore, EMD has its flaws as outlined in Chapter 3, but these might be less impactful in MEG due to the nature of MEG's signal detection and interference suppression tools (outlined in Chapter 5). Therefore, aside from providing a potentially complementary perspective on age-related changes in $t_{synch}G$ and its potential application in an ageing context, running a MEG study could add further empirical support for the FM in a completely new yet related context.

In summary, the three broad aims of this thesis were, 1) to advance our understanding of event-related and resting-state EEG and MEG, 2) to advance our understanding of age-related changes in the brain with EEG and MEG, and 3) to establish EEG and MEG metrics that have the potential to track those age-related changes over time. This chapter has successfully estimated $t_{synch}G$ and applied it to an ageing context; indeed, we have reported for the first time that chronological age can be estimated with the FM's $t_{synch}G$ metric. This has provided us with a better mechanistic understanding of age-related changes in the event-related brain, with change in the underlying frequency-phase modulations able to explain changes in the AO ERP waveform, both in and out of an ageing context. Therefore, $t_{synch}G$ has emerged as another phase-based variable (cf. Dauwels et al., 2010a, 2010b) that may be able to track age-related changes in the brain. However, the precision in which $t_{synch}G$ estimates healthy chronological age is not overly impressive in its current form and with the current dataset; there is still a way to go before these EEG metrics can be applied in the clinic or community. Nevertheless, we posit that EEG-age could be refined into a biomarker for neural and cognitive integrity, where a discrepancy between event-related EEG-age and chronological age could prove clinically informative by implicating protective or deleterious age-related change earlier than previously possible.

Chapter 5: Estimating chronological age from the MEG: event-related oscillatory dynamics in the healthy ageing brain

5.1 Introduction

Chapters 3 and 4 provided new evidence to support treating the FM as an empirically credible explanation of event-related changes in the EEG, both in and out of an ageing context. Having advanced our understanding of age-related changes in the EEG, $t_{synch}G$ has the potential to detect and track deleterious age-related changes in the brain, but optimisations need to be made first. The required optimisations include improving the SNR level of $t_{synch}G$, to disentangle suboptimal SNR from meaningful age-related changes. There are a wide range of complex methodological and analytical optimisations that will be discussed in Chapter 7, but one way to improve SNR would be altering parts of the procedure used to record event-related brain activity. Namely, incorporating more trials in the oddball condition of the auditory attention paradigm, which has already been providing the best SNR, and increasing the sensory impact of the oddball stimulus (e.g., a louder auditory dynamic). These relatively simple methodological changes have been shown to affect the SNR of the ERP components' peaks, such as increasing the effect size of the positive correlation between P3b peak latency and chronological age (e.g., Luck, 2014; Polich, 1996; Duncan et al., 2009), so they may affect $t_{synch}G$ too.

Another change would be switching from EEG to MEG. Our focus up to this point was on EEG due to its relative accessibility and affordability compared to other neuroimaging methods, thus being widely regarded as a candidate for unlocking the early and accurate diagnosis of deleterious age-related conditions (e.g., Dauwels et al., 2010a; Koenig et al., 2020; Poil et al., 2013; Popa et al., 2020). However, MEG could offer a complementary perspective on the credibility of the FM and complexity of age-related changes in the brain. This is because EEG and MEG are neurobiologically and analytically related (Cohen, 1972; Hamalainen et al., 1993), so event-related changes should be similar across these methods (cf. ERFs vs. ERPs; Lopes da Silva, 2013; David et al., 2006; Pfurtscheller & Lopes da Silva, 1999; Vrba & Robinson, 2001). For example, the P3b component of the ERP is seen in the MEG-equivalent ERF waveform of the oddball attention paradigm. Therefore, we posit that the FM and its explanatory mechanism of cross-frequency phase modulation can explain event-related changes recorded in MEG, but, at the time of writing, this had never been tested. Multimodal validations are persuasive ways to test models and their explanatory mechanisms (Huotilainen et al., 1998), so additional empirical evidence for the FM but in MEG rather than EEG would be very promising.

In addition to potentially offering further empirical support for the FM, MEG may also offer improved SNR due to practical differences concerning the signal detection and interference suppression tools. For example, the magnetic fields recorded by MEG pass through the head without confounds such as differential impedance levels, volume conduction, and scalp/skull thickness, which can distort the EEG signal in terms of spatial precision and SNR (Van den Broek et al., 1998). MEG does not require a reference either, so the risk of employing an invalid and potentially damaging reference is mitigated (e.g. averaging noise over all electrodes or distorting phase; Dien, 1998; Thatcher, 2012). MEG recordings also happen inside an MSR and comprise a greater number of sensors, thus a greater number of t_{synch} datapoints, and comprise planar gradiometers, which are all additional noise suppressors (Gross et al., 2012; Keil et al., 2014). Furthermore, there are potential benefits to SNR from MEG's analysis procedures (Gonzalez-Moreno et al., 2014), including sophisticated interference suppression techniques (e.g., SSS and tSSS), although it is unknown whether these techniques will cause artificial discrepancies in $t_{synch}G$, which is a gap in knowledge in and of itself. There is also a higher sampling rate in MEG and, due to less signal intermittency from noise, potentially less mode mixing in the EMD (Huang et al., 2003a, 2003b; Rilling & Flandrin, 2008), which could support a higher resolution and cleaner computation of instantaneous metrics (Luo et al., 2006). In summary, the FM had never been applied to event-related changes in the MEG (e.g., ERFs), in or out of an ageing context, but MEG could provide benefits to the SNR of $t_{synch}G$ due to its alternative methodological and analytical approaches compared to EEG.

Our objectives were to determine whether the FM is an empirically credible, alternative explanation of event-related MEG, and whether there is a difference in MEG-derived $t_{synch}G$ between two different age groups. This would not only further advance our understanding of event-related MEG (aim #1 of this thesis), but also our understanding of age-related changes in the brain (aim #2 of this thesis) and how $t_{synch}G$ might be applied in clinical settings (aim #3 of this thesis). First, we aimed to replicate frequency and phase modulations as the explanatory mechanism of event-related changes in the MEG. We predicted that changes in instantaneous frequency and PLV would be negatively cross-correlated, with post-stimulus frequency slowing concurrent with increasing PLV. Second, we sought to replicate a $t_{synch}G$ metric in MEG, but using both magnetometers and planar gradiometers together. It was predicted that modelling t_{synch} across ordinal IMFs would follow the same power law curve to reflect the systematic, gradual spread of activity across neural networks of increasing scale (thus decreasing frequency) over time. This power law curve would be transformed into a linear log-log polynomial line to provide $t_{synch}G$ for a comparison between healthy young adult and older adult age groups.

5.2 Methods

5.2.1 Participants

Twenty-two young (Y) healthy adults (6 men, 16 women; 2 left-handed, 20 right-handed; *M* = 23 years, *SD* = 5.9, *Range* = 18 to 37) and twenty-two older (O) healthy adults (10 men, 12 women; 22 right-handed; *M* = 72 years, *SD* = 3.9, *Range* = 63 to 78) volunteered to participate. There was a significant difference in chronological age ($t(42) = 32.13$, $p < .001$, $d = 9.69$) between the O and Y groups. Having reached our resource limit, a sensitivity power analysis for an independent groups test of difference between the Y and O groups using Cohen's d, with an alpha of .05 and a beta of .2 [.1], calculated a minimum detectable effect size of .76 [.89] (calculated using G*Power, version 3.1.9.7; Faul et al., 2009). The Y group had a mean of 16 years in formal education (*SD* = 4.1, *Range* = 5 to 25), and the O group also had a mean of 16 years in formal education (*SD* = 2.6, *Range* = 10 to 20). There was not a significant difference in years in formal education ($t(42) = 0.48$, $p = .630$, $d = 0.15$) between the O and Y groups. Fourteen young adults identified as White, two as Asian, three as Indian, and three as Black, whereas all twenty-two older adults identified as White. All participants were recruited via Aston University's advertising portals, which includes the ARCHA Panel that comprises older adults from around the UK who volunteer to take part in studies at Aston University. This study received a favourable opinion from AU-REC and was carried out in accordance with the Declaration of Helsinki and the British Psychological Society Code of Human Research Ethics. Written informed consent was obtained from each participant, and they were reimbursed a £15 Amazon voucher or course credit for their participation.

Participants were screened for depression via the GDS-15 (Sheikh & Yesavage, 1986), as severe depression may confound measures of cognitive performance (Byers & Yaffe, 2011; Morimoto & Alexopoulos, 2013). The mean score of mood on the GDS-15 was 2 (*SD* = 2.6, *Range* = 0 to 10) for the O group, and 3 (*SD* = 2.4, *Range* = 0 to 9) for the Y group, indicating that the samples were presenting with normal mood on average. No participants scored ≥12, indicating no cases of severe depression. There was not a significant difference in mood ($t(42) = -1.38$, $p > .05$, $d = -0.42$) between the O and Y groups. Participants were also screened for cognitive impairment via the QMCI (O'Caoimh & Molloy, 2017). As in Chapter 4, we included the QMCI not only as a screening tool, where healthy adults should report scores that are isolated to the normal category, but as our estimate of general cognitive integrity, a proxy measure of dedifferentiation and noise, where higher scores represented higher general brain functioning. Furthermore, participants also completed the NART (Nelson, 1982; Nelson & Willison, 1991), where NART-IQ is a good estimate of premorbid intelligence and positively correlated with the Wechsler Adult

Intelligence Scale's WAIS-IQ score (a large correlation coefficient of .69; Bright et al., 2018). We converted the raw NART scores to estimates of the Wechsler Adult Intelligence Scale score (WAIS-IV; Wechsler, 2008), called NART-IQ, via the same validated conversion as in Chapter 4, NARTIQ = 126.41 - 0.9775 × NART errors (Bright et al., 2018). Overall, being more reflective of crystallised than fluid intelligence (Bright et al., 2002; Cattell, 1963), the NART-IQ was included as an efficient, proxy measure of mechanisms that support cognitive functioning, particularly reserve (Boyle et al., 2021), in contrast to the QMCI.

5.2.2 MEG recording

MEG was recorded while participants completed an auditory oddball attention paradigm. The MEG setup used for data collection is outlined in Chapter 2 of this thesis. Participants closed their eyes during the recording and listened to recurrent tones of 500 Hz for the standard condition and 1000 Hz for the oddball condition. These tones had a rise and fall of 10ms and were presented at approximately 70 dbSPL, slightly louder than previous EEG studies but still at a safe auditory dynamic (International Telecommunication Union, 2019; Polich, 1996). The oddball presentation was pseudo-randomised at a rate of 20% in sets of five stimuli (i.e., one oddball and four standards). Participants heard one practice set before completing the experimental blocks, where there were 80 oddball stimulus presentations and 320 standard stimulus presentations across four experimental blocks. The number of trials was increased compared to the previous EEG studies, in the hope of keeping a greater number of oddball trials post-data cleaning. The number of oddball presentations within each consecutive block was fixed at 22, 17, 21, and 20 respectively. Participants were asked to keep a mental count of how many oddballs they saw per block and questioned at the end of each block. One trial lasted 2 seconds, with 1 second before stimulus onset and 1 second from stimulus onset. All stimuli were presented for 150 ms, meaning there was an interstimulus interval of 1850 ms. Participants rested between blocks. This was all deliberately kept equivalent thus comparable to the previous EEG studies. This experiment also included the FCRT task, implemented in the same way as outlined in Chapter 4 (Batterham et al., 2014; Dykiert et al., 2012).

The oddball and FCRT paradigms were designed and presented on E-prime Professional (Version 2.0). Stimuli onset triggers were sent from E-prime to the MEG system via a Windows 10 Lenovo ThinkCentre PC's parallel port. Auditory stimuli were presented via in-ear audio buds (Nicolet TIP-300s, which had been recommended by the vendor for use in MEG to minimise interference). FCRT stimuli were presented on a 22" 1920x1080 BENQ LCD monitor, where participants were sat approximately 60 cm from screen to head. MEG & FCRT room layouts were kept identical for each participant.

5.2.3 Data preparation

Raw data were first exported as FIF (.fif) files into MaxFilter™ (version 2.2) for both SSS and tSSS pre-processing as outlined in Chapter 2. These SSS and tSSS datasets were kept separate for later analysis, which was equivalent across these distinct pre-processing methods. However, this pre-processing revealed serious residual noise, most likely caused by undisclosed dental metalwork in one participant in the O group (P9) and two participants in the Y group (P8 & P16). This interference prohibited the use of these participants in subsequent analysis with the SSS data, but tSSS successfully mitigated this noise from the data, thus allowing for use of the full datasets in subsequent analysis with the tSSS data. This pre-processed MEG data was then imported into MATLAB (R2021a; .set/.fdt) for offline analysis with FIELDTRIP (2021; Oostenveld et al., 2011) and purpose-built code.

The maxfiltered MEG datasets, comprising separate SSS and tSSS datasets per age group of O and Y, were demeaned, filtered between 0.1 to 100 Hz, and segmented from -1000ms to +1000ms around stimulus onset with a 200ms pre-stimulus absolute mean baseline correction. The filter was a one-pass FIR (zero-phase and hamming-windowed; Widmann et al., 2015) to align with the filter used with previous EEG data. Additional data cleaning comprised the removal of trials containing clipped data (i.e., signal with a constant flat value due to being outside the amplifier range, often caused by excess sensor noise), jump data (i.e., caused by SQUID instabilities, such as flux traps), and serious eye blink and eye movement artefacts detected by the VEOG and HEOG bipolar arrays with the default 'ft_artifact_eog' function. Thereafter, trials comprising values outside -3 to +3 z-values were rejected per magnetometer and planar gradiometer respectively. Consequently, for the auditory oddball-SSS-O age group (i.e., AO-SSS-O; this shorthand will also be used for each condition), a mean of 19 trials were rejected (*SD* = 10.06, *Range* = 4 to 45). For AO-tSSS-O, a mean of 16 trials were rejected (*SD* = 10.33, *Range* = 4 to 45). For AS-SSS-O, a mean of 65 trials were rejected (*SD* = 32.36, *Range* = 21 to 149). For AS-tSSS-O, a mean of 56 trials were rejected (*SD* = 29.65, *Range* = 19 to 145). For AO-SSS-Y, a mean of 21 trials were rejected (*SD* = 9.74, *Range* = 11 to 51). For AO-tSSS-Y, a mean of 19 trials were rejected (*SD* = 7.77, *Range* = 6 to 40). For AS-SSS-Y, a mean of 79 trials were rejected (*SD* = 44.55, *Range* = 27 to 232). For AS-tSSS-Y, a mean of 70 trials were rejected (*SD* = 32.55, *Range* = 27 to 170).

This data preparation was completed without reference to demographic data, such as chronological age, but we later checked whether there were differences between the O and Y age groups on the number of rejected trials; there were not according to independent t-tests (AO-SSS: $p > .05$; AO-tSSS: $p > .05$; AS-SSS: $p > .05$; AS-tSSS: $p > .05$). From here on, a central-parietal electrode ROI was used for the magnetometers and planar

gradiometers respectively, to align with the scalp locations and rationale used in the EEG studies to enhance SNR of the classic P3b component. For the magnetometers, this was 'MEG0731', 'MEG2211', 'MEG2221', 'MEG2241', 'MEG2231', 'MEG2441', 'MEG2021', 'MEG2311', 'MEG0741', 'MEG1821', 'MEG1811', 'MEG1831', 'MEG1841', 'MEG1631', 'MEG2011', and 'MEG1911' (Figure 2.4). For the planar gradiometers, this was 'MEG0732', 'MEG0733', 'MEG2212', 'MEG2213', 'MEG2222', 'MEG2223', 'MEG2242', 'MEG2243', 'MEG2232', 'MEG2233', 'MEG2442', 'MEG2443', 'MEG2022', 'MEG2023', 'MEG2312', 'MEG2313', 'MEG0742', 'MEG0743', 'MEG1822', 'MEG1823', 'MEG1812', 'MEG1813', 'MEG1832', 'MEG1833', 'MEG1842', 'MEG1843', 'MEG1632', 'MEG1633', 'MEG2012', 'MEG2013', 'MEG1912', 'MEG1913' (Figure 2.4). FCRT data preparation followed the same process as outlined in Chapter 4, comprising the removal of inaccurate trials and reaction times under or over 2 standard deviations, which resulted in a mean removal of 5% and 4% of trials respectively for the O and Y groups (*SD* = 2% and 1% respectively, *Range* = 1% to 9% and 3% to 6% respectively).

5.2.4 Signal analysis

Classic ERFs were calculated by averaging across the baseline-corrected trials for magnetometers and gradiometers separately, and converted to fT units. SVD was not implemented on the ERFs, in part due to the prior use of SSS and tSSS interference suppression procedures, and because noise level and the number of rejected trials were similar between age groups, but also because it offered minimal additional value to peak latency analyses in the previous EEG studies. The resulting ERFs were filtered with a low pass at 30 Hz using the same FIR as specified earlier and trimmed between -200 ms pre-stimulus and 800 ms post-stimulus. The P3b component was identified by searching for the peak positive amplitude within a latency range of 250 ms to 500 ms post-stimulus, to further align with the EEG studies and as already shown to be the most influential ERP component.

Estimation of $t_{synch}G$ followed the same process as outlined in Chapter 3. The only difference for application in MEG was that t_{synch} was estimated for magnetometers and planar gradiometers separately first, due to their differing pattern of SNR and amplitude scaling in the SVD, then t_{synch} points from each sensor type were combined for model fitting to estimate $t_{synch}G$. Modelling was completed across all IMFs' t_{synch} points per participant, and all the grand average IMFs' t_{synch} points after averaging across participants' instantaneous frequency and PLV data. Additionally, the downsampled Hz were different to previous EEG studies due to using a higher SR of 1000 Hz in this MEG study. Therefore, IMFs were produced for the original MEG data (1000 Hz) as well as an additional five downsampled datasets, at 751 Hz, 563 Hz, 421 Hz, 317 Hz, and 239 Hz respectively.

5.3 Results

Table 5.0 provides a concise summary of this Results section, outlining its organisation and purpose of the content to support efficient engagement with this chapter and to clarify how it contextualises Chapter 7.

Table 5.0

An outline of the organisation of this Results section, split into sections organised in line with the different analytical approaches covered, and in a way that deliberately mirrors the narrative progression (including rationale therein).

	Content	Purpose	Context
Section 5.3.1	ERFs, IMFs, and PCCs between instantaneous metrics	Preliminary checks to ensure that widely reported event-related changes in the MEG were present in the current dataset, plus replication of patterns in instantaneous measures of MEG as predicted by the FM and reported by Burgess (2012), and in the EEG dataset of Chapter 3.	Supports Chapter 7
Section 5.3.2	Estimating $t_{synch}G$ from MEG data	Model fitting $t_{synch}G$ with a log-log polynomial fit across different MEG sensor types and with different pre-processing estimation methods as proof-of-principle to establish the $t_{synch}G$ metric for use in an ageing context.	Supports Chapter 7
Section 5.3.3	Differences in $t_{synch}G$ between age group and estimation method	Analysing differences in $t_{synch}G$ between younger and older adults and SSS and tSSS pre-processing estimation methods, as well as the interaction between age group and estimation method.	Supports Chapter 7

5.3.1 Application of the Firefly Model in MEG

First, the ERFs were visually inspected as part of preliminary checks to ensure that widely reported event-related changes in the MEG were present in the current dataset. The ERFs from the SSS (as shown in Figure 5.1.1) and tSSS (as shown in Figure 5.1.2) pre-processing estimation methods per sensor type of magnetometer and planar gradiometer presented clear oddball-related components (e.g., P3b) for the AO conditions and not the AS conditions. A latency delay in peak P3b of the O group compared to the Y group is also already visible for the grand averages.

Figure 5.1.1

For the SSS estimation method, Y AO-AS (black-pink lines) and O AO-AS (blue-red lines) ERFs averaged over sensors and participants per sensor type (magnetometers in the top panel, and planar gradiometers in the bottom panel), with 95% confidence intervals shaded the same colours respectively to visualise overlaps and differences between the conditions.

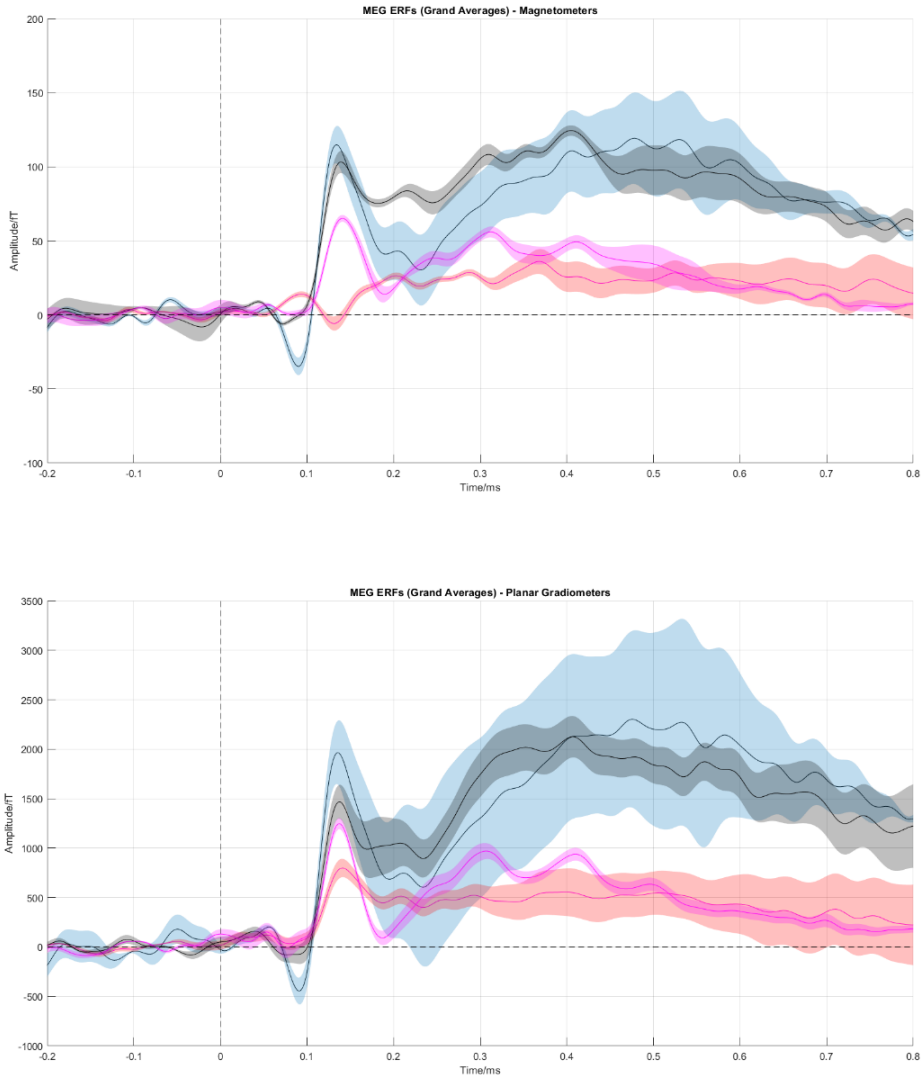

Figure 5.1.2

For the tSSS estimation method, Y AO-AS (black-pink lines) and O AO-AS (blue-red lines) ERFs averaged over ROI sensors and participants per sensor type (magnetometers in the top panel, and planar gradiometers in the bottom panel), with 95% confidence intervals shaded the same colours respectively to visualise overlaps and differences between the conditions.

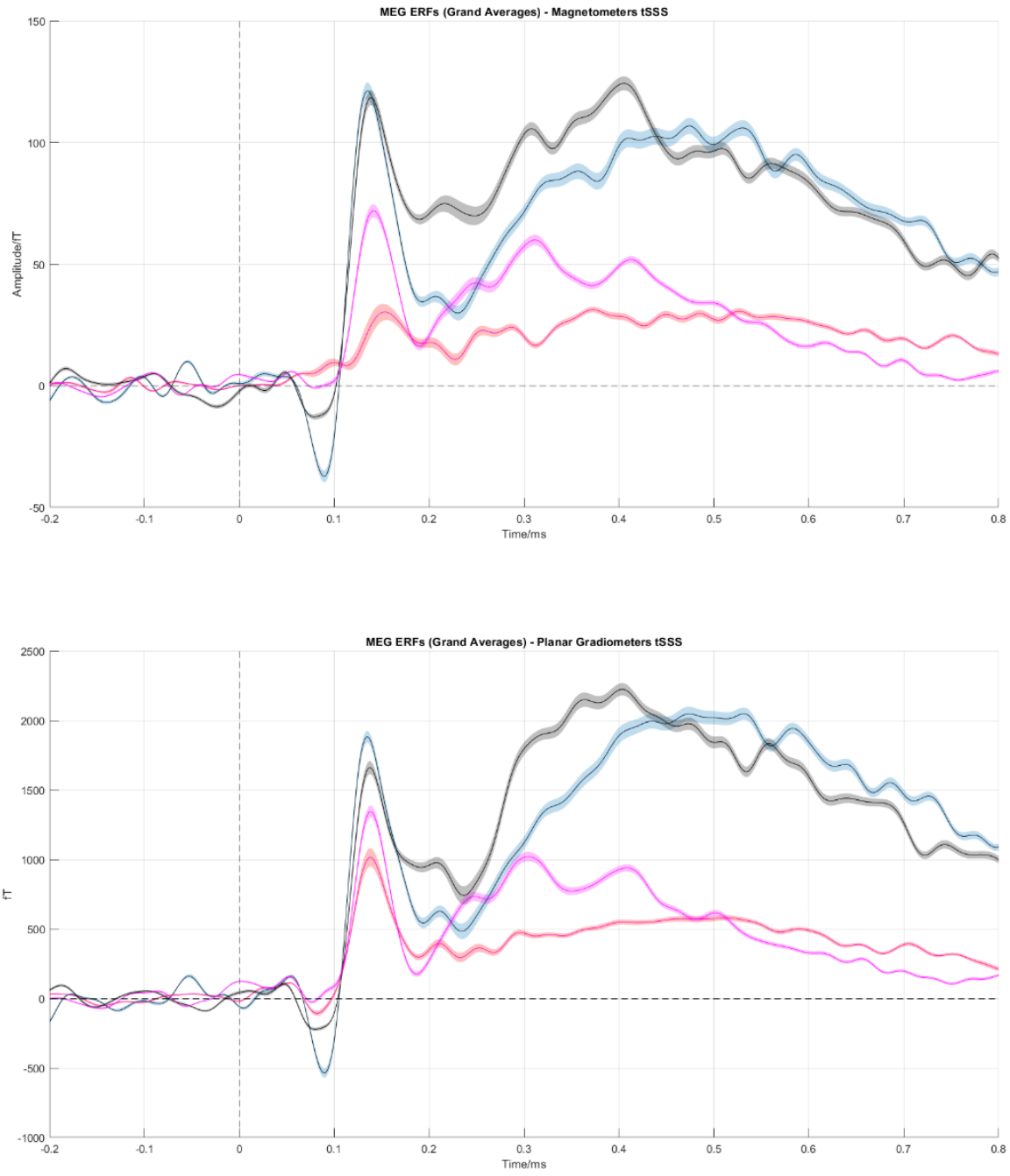

Thereafter, the IMFs were also visually inspected to identify replication in the patterns of event-related change in instantaneous measures of MEG as predicted by the FM, and reported by Burgess (2012) and in Chapter 3 of this thesis. For magnetometers and planar gradiometers (as shown in Figure 5.1.3 and Figure 5.1.4 respectively), the IMFs showed that increases in PLV were temporally aligned with decreases in instantaneous frequency post-stimulus. t_{synch} per IMF followed a clear trend across time with earlier t_{synch} the higher the frequency, which was also evident in the pattern across IMFs' instantaneous frequency troughs. Late IMFs (i.e., low frequencies) showed long latency modulations and omitted the rebound, which can be accounted for by the long period and limited window size per epoch; indeed, a reason for implementing a long ISI between trials was to minimise the impact of overlapping activity per trial. For amplitude, there was often a small, short-duration increase before a deeper, prolonged dip and rebound that also increased in latency per ordinal IMF. For the evoked signal, W-shapes were evident, which widened with each ordinal IMF. The overarching pattern of post-stimulus modulations, with the peak latency and width of modulations increasing with each IMF (i.e., with decreasing mean baseline frequency), was more pronounced and systematic in the oddball conditions than the standard conditions.

Figure 5.1.3

An example output from EMD on the AO-SSS-O data (top panel = magnetometers, M; bottom panel = planar gradiometers, PG) showing the time course of phase synchrony (PLV, red line), frequency (FRQ, red line), amplitude (AMP, red line), and evoked response (EVO, red line) for IMFs 2-6 (in descending order) of the base sampling rate (1000 Hz), averaged over participants per condition; the dotted lines represent 95% confidence intervals of the measurement in the -200 ms to 0 ms baseline period to visualise crosses of the red line (i.e., change in the metric of interest), and the blue dots represent t_{synch} for PLV and the point of lowest frequency for FRQ.

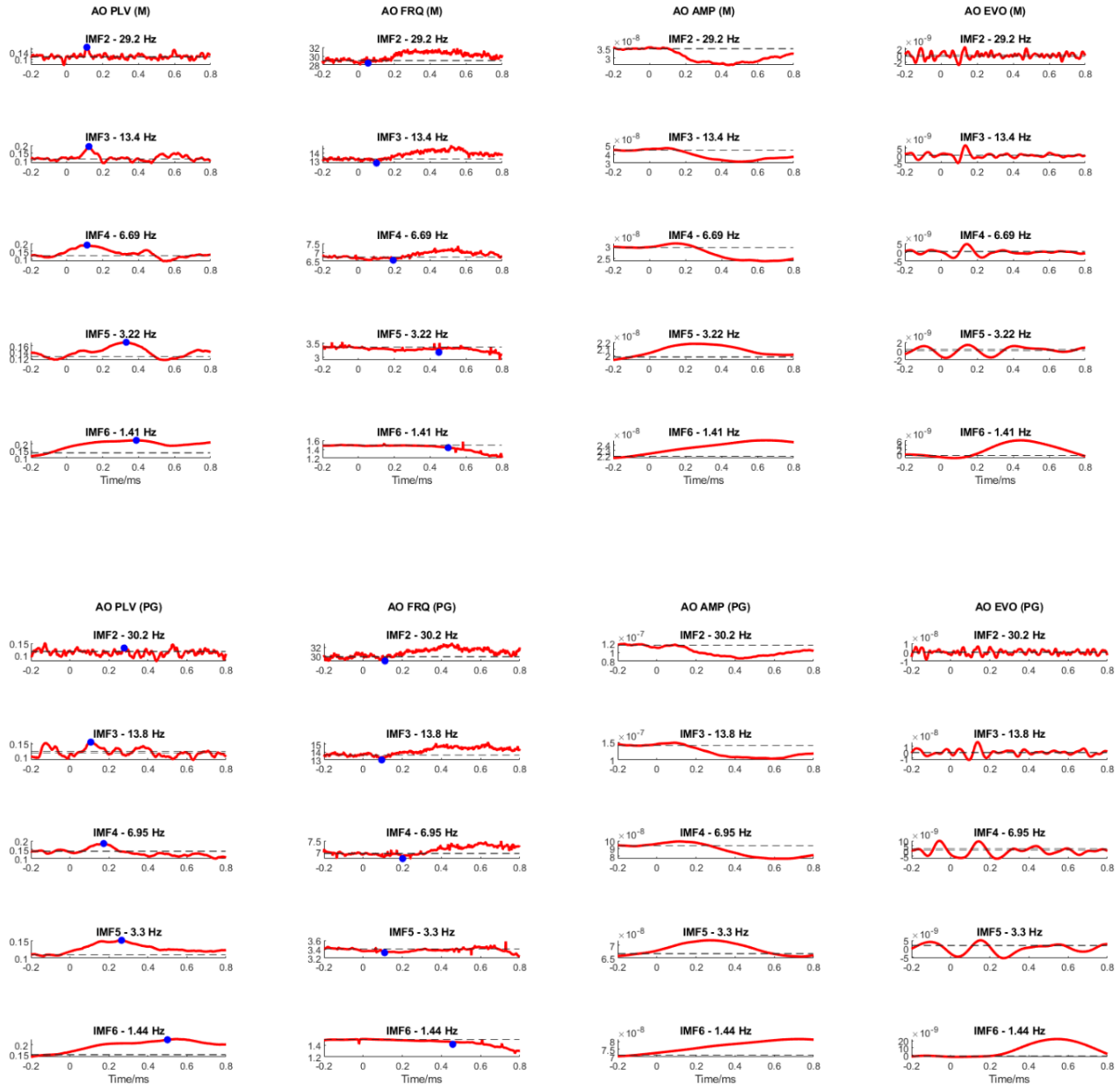

Figure 5.1.4

An example output from EMD on the AO-tSSS-O data (top panel = magnetometers, M; bottom panel = planar gradiometers, PG) showing the time course of phase synchrony (PLV, red line), frequency (FRQ, red line), amplitude (AMP, red line), and evoked response (EVO, red line) for IMFs 2-6 (in descending order) of the base sampling rate (1000 Hz), averaged over participants per condition; the dotted lines represent 95% confidence intervals of the measurement in the -200 ms to 0 ms baseline period to visualise crosses of the red line (i.e., change in the metric of interest), and the blue dots represent t_{synch} for PLV and the point of lowest frequency for FRQ.

Next, the cross-correlations at zero-lag were calculated between PLV and instantaneous frequency, again to identify replication in the patterns of event-related change in instantaneous measures of MEG as predicted by the FM, and reported by Burgess (2012) and in Chapter 3 of this thesis. These PCC cross-correlations were calculated on each downsampled IMFs' PLV and frequency data averaged across participants. The resultant cross-correlation coefficients and mean baseline frequencies were then averaged across equivalent IMFs to efficiently visualise the overarching trends (just like the ERF waveforms, the cross-correlations in magnetometers and planar gradiometers were similar, as later visualised with t_{synch}Gs, thus averaged across). There were again clear negative cross-correlations between PLV and frequency (as shown in Tables 5.1.1 and 5.1.3).

Cross-correlations were also calculated again for discrete frequency bands of beta (13-30 Hz), alpha (7-13 Hz), theta (4-7 Hz), and delta (1-4 Hz), based on the mean baseline frequencies per IMF across sensor types and downsamples (Tables 5.1.2 and 5.1.4). There were clear and similar negative cross-correlations in both SSS and tSSS estimation methods, particularly for frequencies within the theta range across all conditions, but also for beta, alpha, and delta ranges across most conditions. Generally, the AO cross-correlations were more robust than the AS cross-correlations across age and estimation method. The related power law curves for t_{synch} were also visually inspected for replication of Chapter 3's findings per condition, sensor type, and estimation method, showing there were clear curves for AO but not AS (as shown in Figure 5.2.1 and Figure 5.2.2).

Table 5.1.1

For the SSS method in Y and O groups, average cross-correlation coefficients (PCC) at zero lag between PLV and frequency of the IMFs per condition in the time range 0 to 500 ms, with mean baseline frequency/Hz and SD shown in brackets (M, SD).

IMF	AO-Y	AO-O	AS-Y	AS-O
1	-.07	.07	-.03	-.10
	(68.81, 5.04)	(68.31, 5.26)	(68.56, 5.04)	(67.80, 5.27)
2	-.27	-.36	-.03	-.07
	(29.90, 1.88)	(29.04, 1.73)	(29.72, 1.90)	(28.17, 1.68)
3	-.05	-.56	-.15	.15
	(13.27, 0.73)	(13.31, 0.73)	(13.15, 0.73)	(12.98, 0.68)
4	-.50	-.73	-.43	-.66
	(6.49, 0.35)	(6.60, 0.37)	(6.51, 0.36)	(6.54, 0.35)
5	-.21	-.05	.00	.04
	(3.13, 0.18)	(3.17, 0.19)	(3.12, 0.20)	(3.18, 0.18)
6	-.07	-.47	-.90	.42
	(1.35, 0.11)	(1.39, 0.11)	(1.34, 0.11)	(1.40, 0.10)

Table 5.1.2

For the SSS method in Y and O groups, average cross-correlation coefficients (PCC) at zero lag between PLV and frequency of set frequency bands taken from IMFs per condition in the time range 0 to 500 ms, with mean baseline frequency/Hz and SD shown in brackets (M, SD).

Band	AO-Y	AO-O	AS-Y	AS-O
Beta	-.09	-.46	-.03	.05
	(18.82, 7.29)	(20.55, 7.61)	(19.09, 7.35)	(22.74, 7.42)
Alpha	-.28	-.68	-.37	.01
	(12.20, 0.48)	(12.23, 0.47)	(12.32, 0.58)	(12.34, 0.57)
Theta	-.50	-.73	-.43	-.66
	(6.49, 0.35)	(6.60, 0.37)	(6.51, 0.36)	(6.54, 0.35)
Delta	-.14	-.26	-.45	.23
	(2.24, 1.01)	(2.28, 1.01)	(2.23, 1.01)	(2.29, 1.01)

Table 5.1.3

For the tSSS method in Y and O groups, average cross-correlation coefficients (PCC) at zero lag between PLV and frequency of the IMFs per condition in the time range 0 to 500 ms, with mean baseline frequency/Hz and SD shown in brackets (M, SD).

IMF	AO-Y	AO-O	AS-Y	AS-O
1	-.02	.00	.03	-.12
	(69.31, 5.00)	(68.77, 5.24)	(69.22, 5.03)	(68.21, 5.25)
2	-.27	-.10	.03	.09
	(29.95, 1.83)	(29.25, 1.71)	(29.85, 1.85)	(28.31, 1.64)
3	-.37	-.43	.12	-.38
	(13.21, 0.70)	(13.49, 0.73)	(13.13, 0.68)	(13.09, 0.67)
4	-.24	-.80	-.41	-.81
	(6.46, 0.35)	(6.67, 0.37)	(6.49, 0.33)	(6.59, 0.34)
5	-.35	-.39	.22	-.02
	(3.10, 0.18	(3.20, 0.18)	(3.12, 0.17)	(3.20, 0.18)
6	-.28	-.42	-.84	-.13
	(1.36, 0.10)	(1.42, 0.10)	(1.38, 0.09)	(1.42, 0.09)

Table 5.1.4

For the tSSS method in Y and O groups, average cross-correlation coefficients (PCC) at zero lag between PLV and Frequency of set frequency bands taken from IMFs per condition in the time range 0 to 500 ms, with mean baseline frequency/Hz and SD shown in brackets (M, SD).

Band	AO-Y	AO-O	AS-Y	AS-O
Beta	-.32	-.30	.07	-.08
	(17.94, 6.89)	(20.17, 7.65)	(18.70, 7.34)	(22.37, 7.56)
Alpha	-.43	-.44	.20	-.45
	(12.15, 0.42)	(12.43, 0.50)	(12.14, 0.44)	(12.30, 0.55)
Theta	-.24	-.80	-.41	-.81
	(6.46, 0.35)	(6.67, 0.37)	(6.49, 0.33)	(6.59, 0.34)
Delta	-.32	-.41	-.31	-.08
	(2.23, 0.99)	(2.31, 1.01)	(2.25, 0.99)	(2.31, 1.01)

Figure 5.2.1

Model fitting $t_{synch}G$ with power law fits (red line) for both magnetometer (left side) and planar gradiometer (right side) sensor types, modelled across t_{synch} points (blue dots) for all the O group's conditions of estimation method (SSS versus tSSS) and condition (AO versus AS), from grand averages over participants' frequency and PLV data.

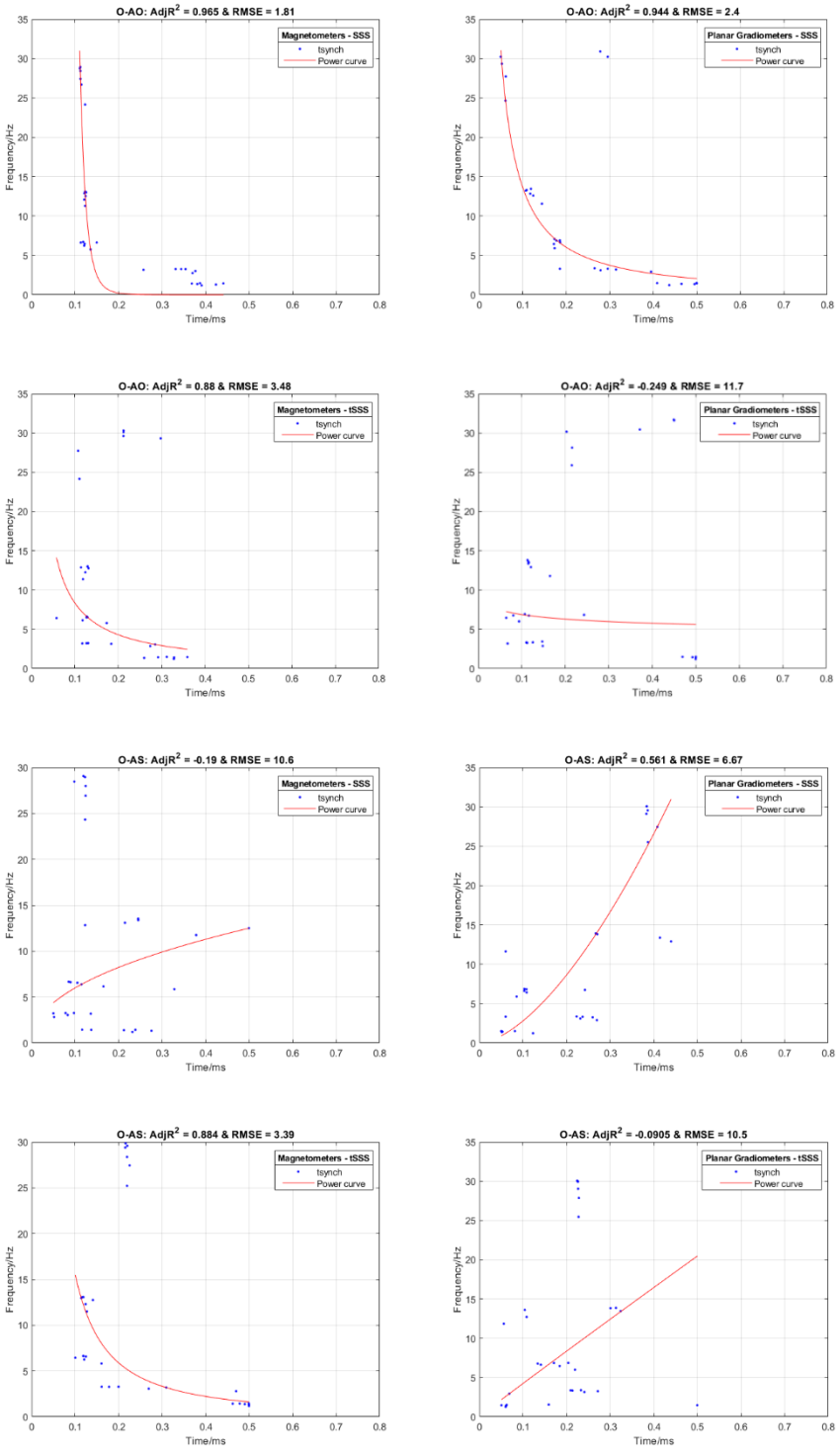

Figure 5.2.2

Model fitting $t_{synch}G$ with power law fits (red line) for both magnetometer (left side) and planar gradiometer (right side) sensor types, modelled across t_{synch} points (blue dots) for all the Y group's conditions of estimation method (SSS versus tSSS) and condition (AO versus AS), from grand averages over participants' frequency and PLV data.

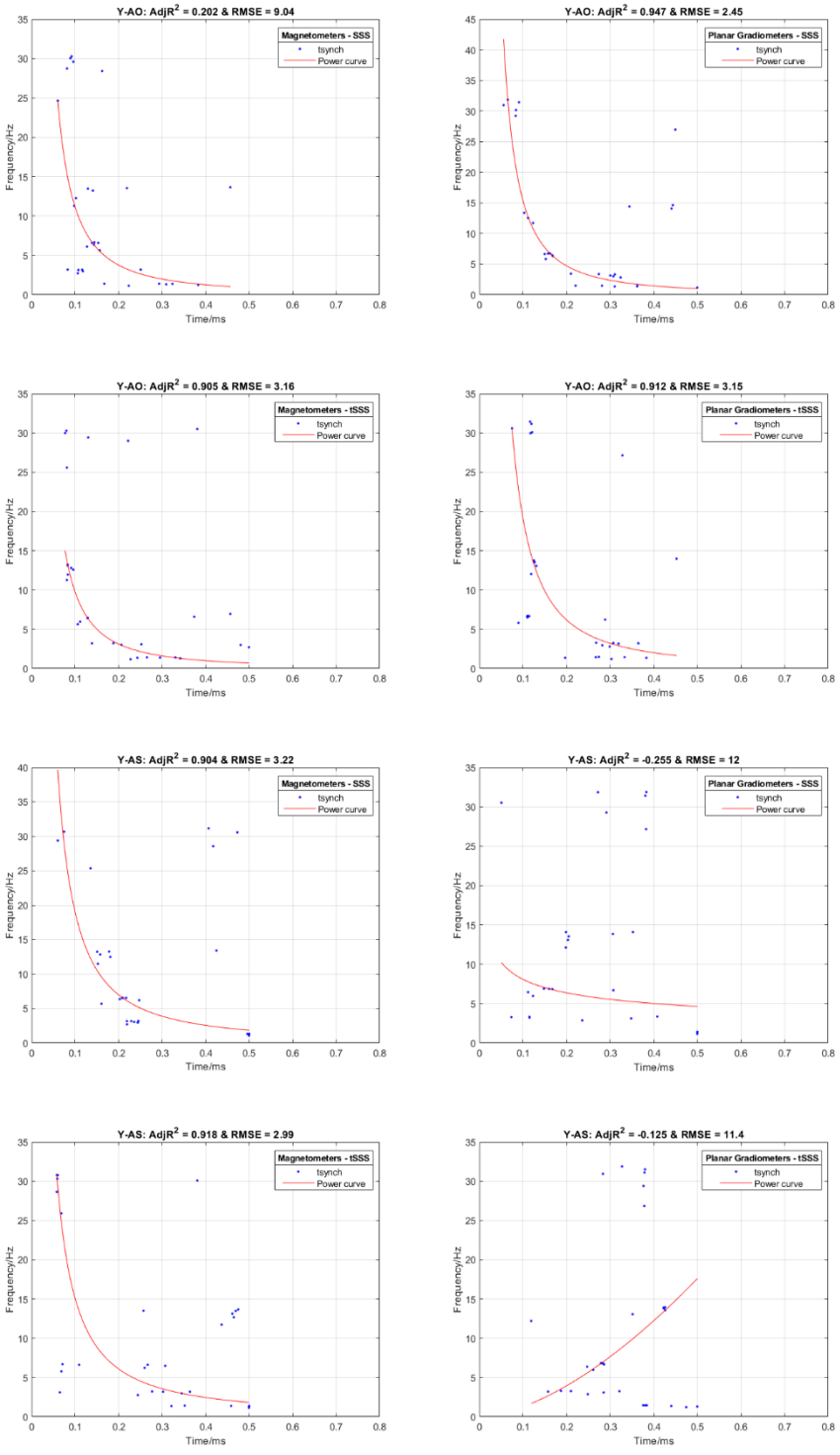

5.3.2 Estimating $t_{synch}G$ in MEG

The gradient across t_{synch} points (i.e., $t_{synch}G$) was again estimated as the log-log polynomial straight-line model across all t_{synch} points from IMF2 to IMF6, following the approach outlined and justified in Chapters 3 and 4 of this thesis, and modelled per age group for each estimation method. Figures 5.4.1 and 5.4.2 visualise the polynomial $t_{synch}Gs$ for each age group (O versus Y) and pre-processing estimation method (SSS versus tSSS), with underlying data averaged across participants and then modelled across all downsamples' t_{synch} points per condition from magnetometers and planar gradiometers together. This combination was to provide additional points for the modelling with the aim of a more robust fit and greater SNR. This approach is supported by Garces et al. (2017) and sensors generally showing comparable patterns across $t_{synch}G$ estimates for the AO condition of interest (as first shown in Figures 5.3.1 for SSS and 5.3.2 for tSSS). Notably, the grand average $t_{synch}Gs$ for older adults demonstrated a slightly flatter gradient than younger adults when data were agglomerated in this way (as shown in Figures 5.4.1 and 5.4.2).

Figure 5.3.1

For the SSS estimation method, model fitting $t_{synch}G$ with log-log polynomial fits (Lline, black = AO condition, pink = AS condition) for O (top row) and Y (bottom row) age groups per estimation method in magnetometers (left side) and planar gradiometers (right side).

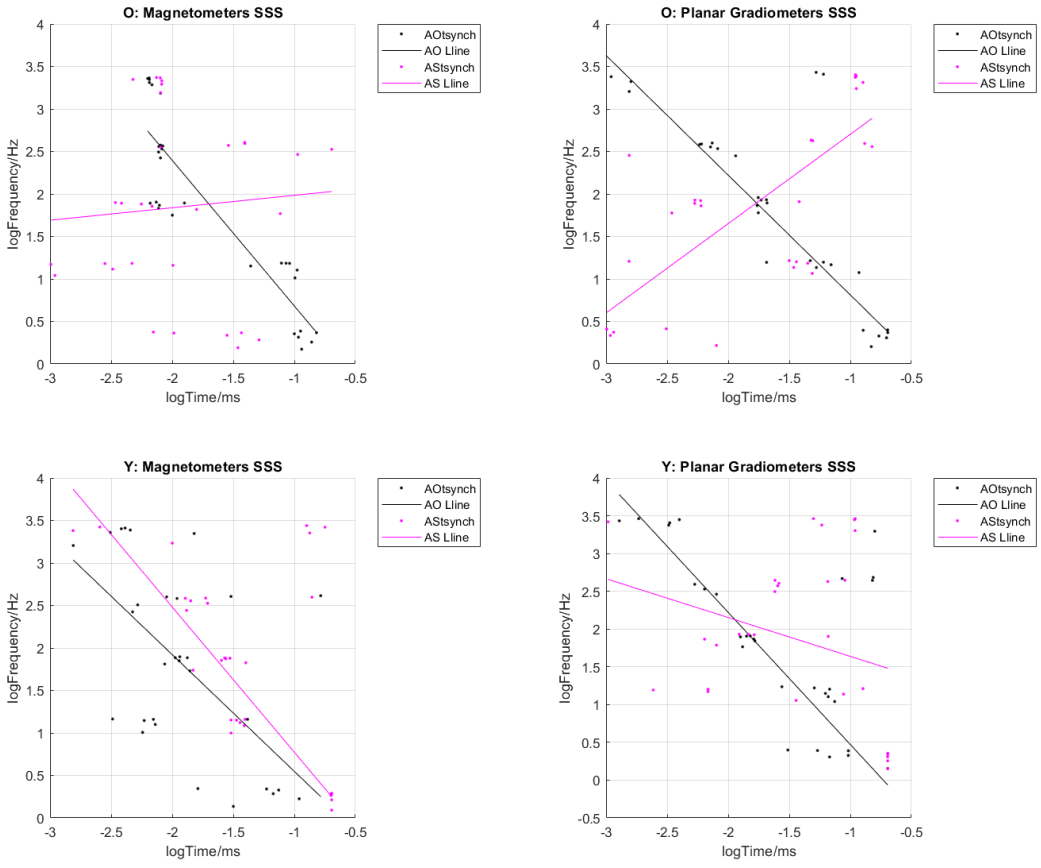

Figure 5.3.2

For the tSSS estimation method, model fitting $t_{synch}G$ with log-log polynomial fits (Lline, black = AO condition, pink = AS condition) for O (top row) and Y (bottom row) age groups per estimation method in magnetometers (left side) and planar gradiometers (right side) separately.

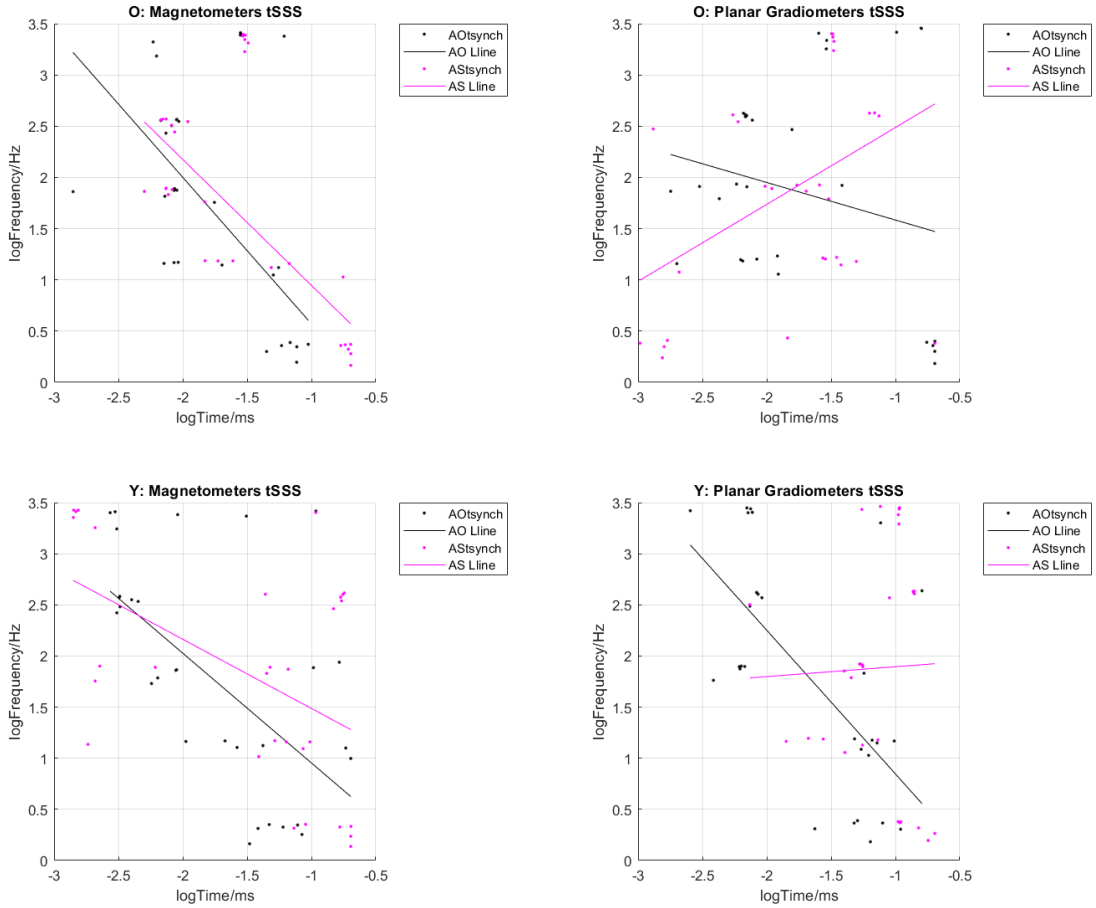

Figure 5.4.1

For the SSS method, model fitting $t_{synch}G$ with log-log polynomial fits for AO (left side) and AS (right side) conditions per age group (Y = purple line and black dots; O = red line and blue dots) across all sensors' t_{synch} data points together.

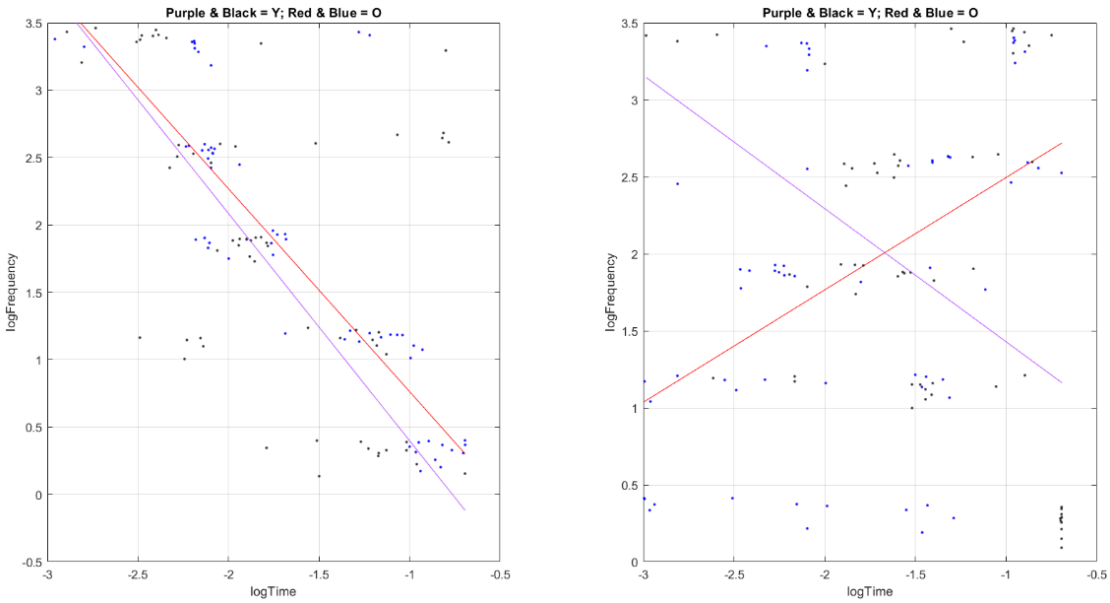

Figure 5.4.2

For the tSSS method, model fitting $t_{synch}G$ with log-log polynomial fits for AO (left side) and AS (right side) conditions per age group (Y = purple line and black dots; O = red line and blue dots) across all sensors' t_{synch} data points together.

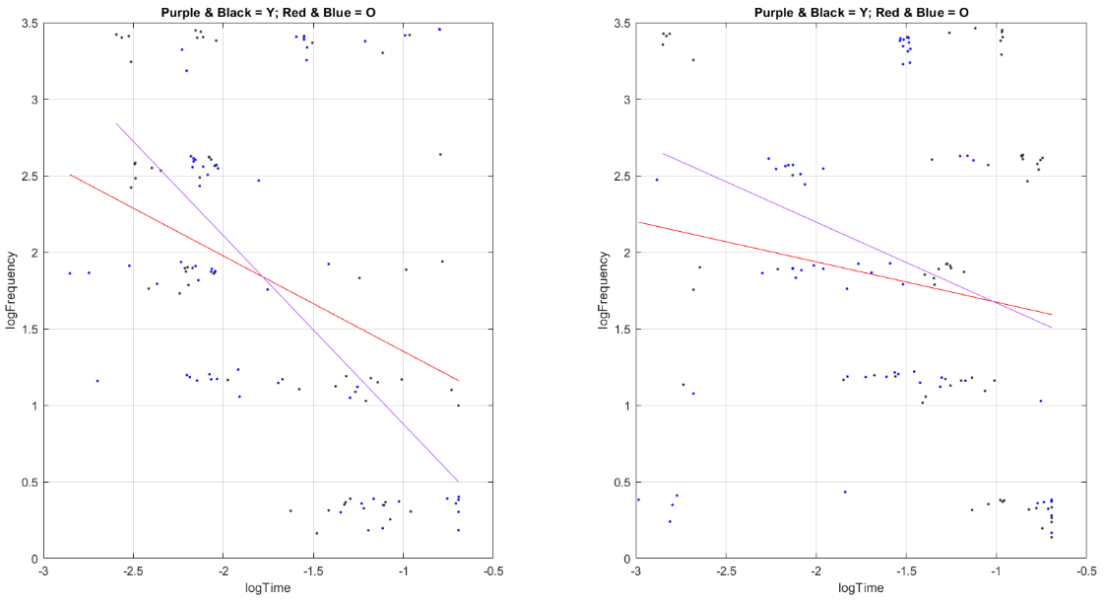

5.3.3 Differences in chronological age, NART-IQ, and cognitive performance between age groups

The mean NART-IQ was 114 (SD = 6.8, Range = 98 to 124), indicating that the sample was generally above average and less varied in premorbid intelligence than the general population. The mean score of cognitive performance on the QMCI was 76 (SD = 9.2, Range 59 to 93), indicating that the sample had normal cognitive functioning. NART-IQ was significantly correlated with cognitive performance (r = .41, p = .006). A set of independent t-tests were run to interrogate the differences in NART-IQ and cognitive performance per age group. There was a significant difference in NART-IQ (t(42) = 3.04, p = .004, d = 0.92) between O (M = 116.55, SD = 6.42) and Y groups (M = 110.81, SD = 6.07), showing that older adults had higher pre-morbid IQ. There was not a significant difference in cognitive performance on the QMCI (t(42) = -1.90, p > .05, d = -0.57) between O (M = 73.18, SD = 9.36) and Y groups (M = 78.27, SD = 8.40). However, this comparison turned significant when controlling for NART-IQ via an ANCOVA, contextualised by the significant correlation between the variables, where the main effect of age group was significant (F(1,41) = 17.83, p < .001, η^2_p = 0.30) such that Y (M = 80.75) had a significantly higher QMCI score than O (M = 70.70) after statistically controlling for pre-morbid IQ. There was also a significant difference in mean RT (t(42) = 4.46, p < .001, d = 1.34) between O (M = 820.11, SD = 199.38) and Y groups (M = 598.48, SD = 120.65), and in raw ISD (t(42) = 3.42, p = .001, d = 1.03) between O (M = 216.99, SD = 73.54) and Y groups (M = 144.89, SD = 66.20). However, this difference disappeared for CV (t(42) = 1.68, p > .05, d = 0.51) and modelled ISD (t(42) = -0.15, p > .05, d = -0.04).

5.3.4 Differences in P3b peaks and t_{synch}G between age groups

Due to differences in SNR and scaling of amplitude between sensor types (Garces, 2017), two separate 2x2 mixed ANOVAs were run to interrogate the differences in P3b amplitude between age groups (O and Y) and estimation methods (SSS and tSSS) for each sensor type of magnetometers and planar gradiometers. For magnetometers, there were no significant main effects of estimation method (F(1,39) = 2.15, p > .05, η^2_p = 0.05) or age group (F(1,39) = 0.54, p > .05, η^2_p = 0.01), and no significant interaction either (F(1,39) = 1.00, p > .05, η^2_p = 0.02). For planar gradiometers, there were also no significant main effects of estimation method (F(1,39) = 1.30, p > .05, η^2_p = 0.03) or age group (F(1,39) = 0.01, p > .05, η^2_p = 0.01), and no significant interaction either (F(1,39) = 1.60, p > .05, η^2_p = 0.04). In summary, there was no significant difference in P3b amplitude for age groups or estimation method, irrespective of sensor type.

Because the differences in scaling between sensor types do not affect peak latency as they do peak amplitude, a 2x2x2 mixed ANOVA was conducted to examine differences in

P3b latency for age group (O and Y), estimation method (SSS and tSSS), and sensor type (Magnetometers and Planar Gradiometers). There was no significant main effects of estimation method ($F(1,78) = 0.05$, $p > .05$, $\eta^2_p = 0.01$) or sensor type ($F(1,78) = 0.52$, $p > .05$, $\eta^2_p = 0.01$), and no significant interactions ($ps > .05$), but there was a significant main effect of age group ($F(1,78) = 14.66$, $p < .001$, $\eta^2_p = 0.16$), with a later peak latency for O ($M = 429.83$, $SD = 68.45$, *95% CI* [409.56, 450.11]) than Y ($M = 374.01$, $SD = 70.05$, *95% CI* [353.24, 394.79]). The main effect descriptive data of the three-way mixed ANOVA are presented visually in Figure 5.5 to clarify the two nonsignificant effects and one significant effect in P3b latency, the latter seen for the age group variable (O versus Y, with a longer latency for O).

Figure 5.5

Line plot visualisations of the nonsignificant estimation method main effect (SSS versus tSSS) and sensor type main effect (Magnetometers/M versus Planar Gradiometers/P), and significant age group main effect (O > Y) on P3b latency, with dots as means and bars as the 95% confidence intervals to show overlaps and differences between conditions.

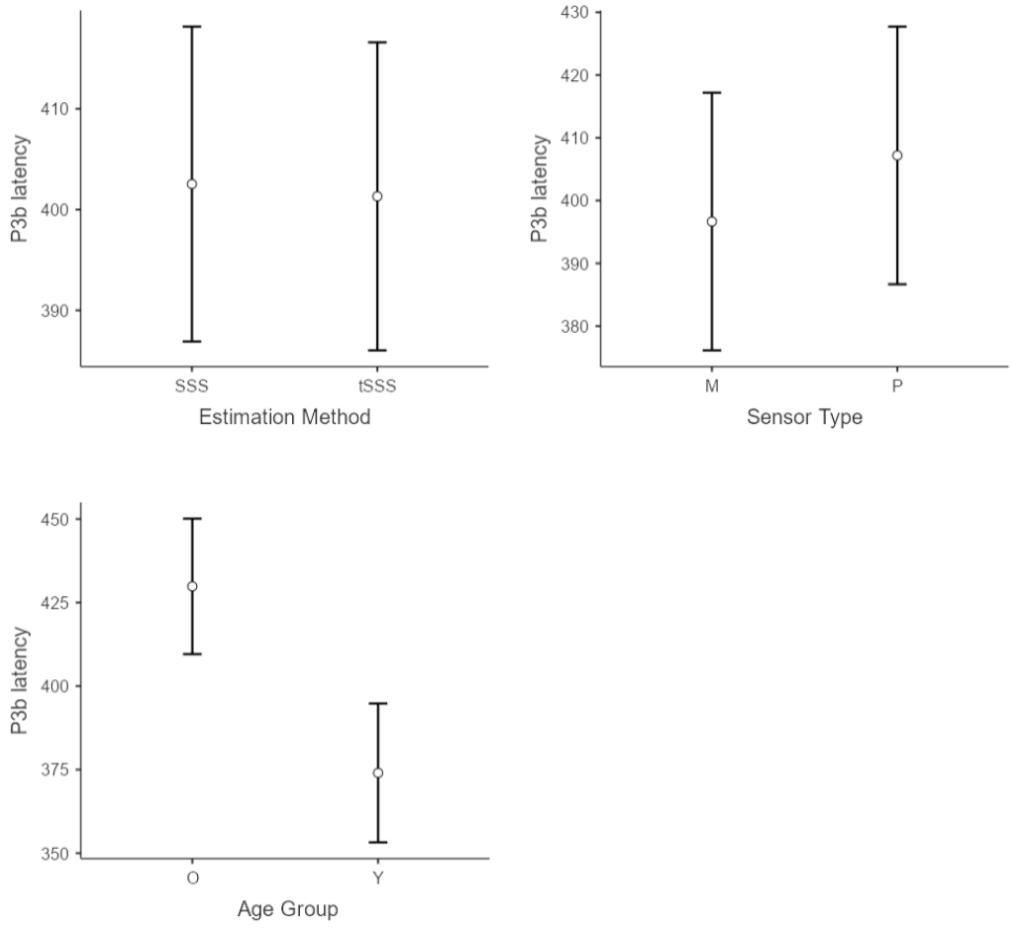

In a 2x2 mixed ANOVA for AOt_{synch}G (Figure 5.6), there was no significant main effects (Figure 5.5.2) of estimation method (F(1,39) = 0.21, p > .05, η^2_p = 0.01) or age group (F(1,39) = 1.37, p > .05, η^2_p = 0.03), and no significant interaction either (F(1,39) = 0.26, p > .05, η^2_p = 0.01), despite visualising a mean change in age group (Figure 5.4.1 and Figure 5.4.2). Notably, the standard deviation of t_{synch}G for the Y groups was much higher than O groups (e.g., O-AO-SSS = 0.29; O-AO-tSSS = 0.28, versus Y-AO-SSS = 0.53; Y-AO-SSS = 0.47). Despite AO being the main focus here, for completeness a 2x2 mixed ANOVA for ASt_{synch}G was also conducted (Figure 5.7). There was no significant main effects of estimation method (F(1,39) = 3.79, p = .059, η^2_p = 0.09) or age group (F(1,39) = 0.270, p > .05, η^2_p = 0.03), and no significant interaction either (F(1,39) = 0.01, p > .05, η^2_p = 0.01). Both the main effect and interaction descriptive data of the two-way mixed ANOVA are presented visually in Figure 5.6 and Figure 5.7 to clarify the nonsignificant effects with wide confidence intervals in both AO-t_{synch}G and AS-t_{synch}G respectively. In summary, there was no significant difference in t_{synch}G for age groups or estimation method. Additionally, a 2x2 mixed ANCOVA controlling for NART-IQ did not alter these significances (ps > .05).

Figure 5.6

Line plot visualisations of the nonsignificant estimation method main effect (SSS versus tSSS) and age group main effect (O and Y) on AO-t_{synch}G, and nonsignificant interaction of estimation method and age group, with dots as means and bars as the 95% confidence intervals to show overlaps between conditions.

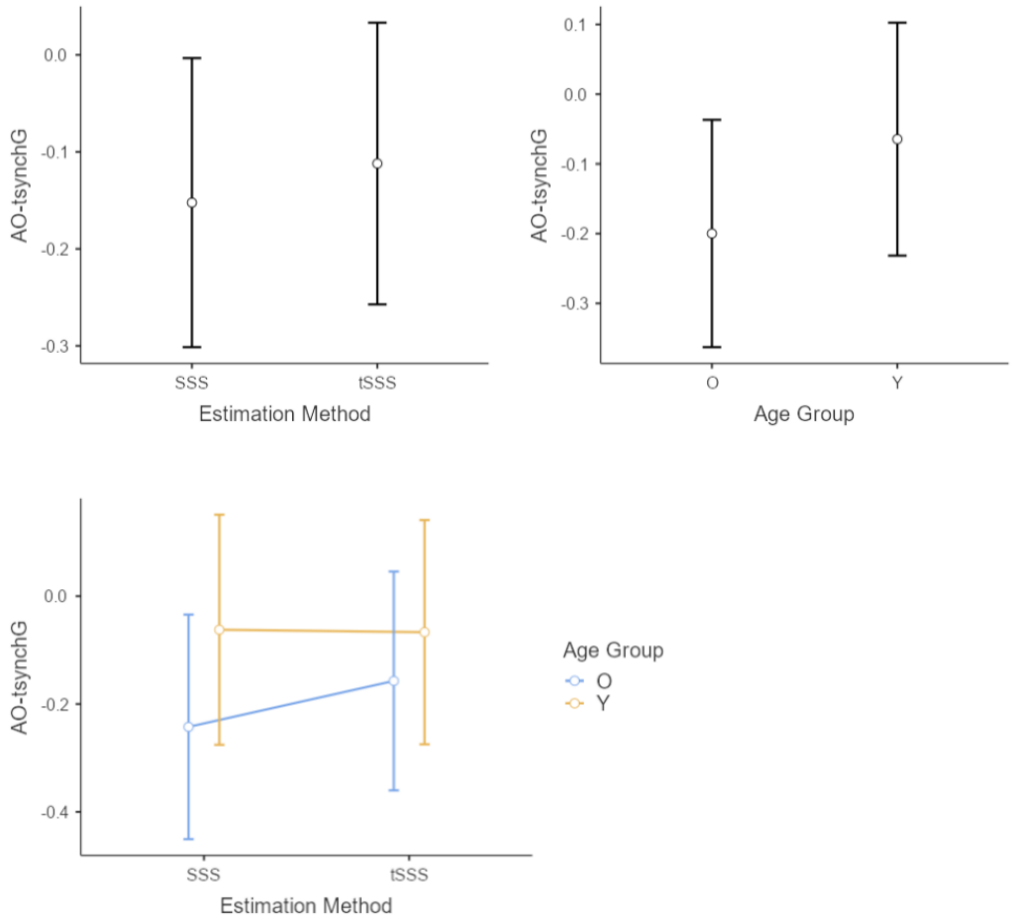

Figure 5.7

Line plot visualisations of the nonsignificant estimation method main effect (SSS versus tSSS) and age group main effect (O and Y) on AS-t_{synch}G, and nonsignificant interaction of estimation method and age group, with dots as means and bars as the 95% confidence intervals to show overlaps between conditions.

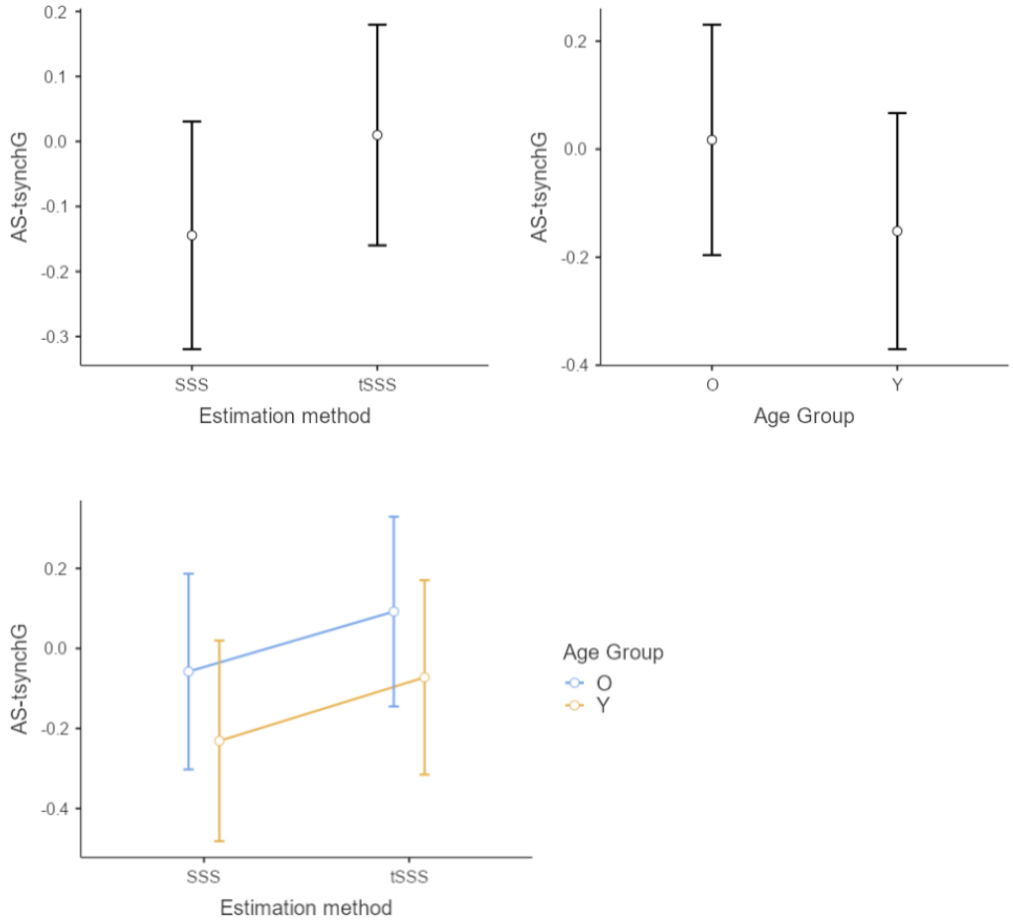

5.4 Discussion

We wanted to apply the FM and new $t_{synch}G$ metric to MEG for the very first time. Our objectives were to determine whether the FM is an empirically credible, alternative explanation of event-related MEG, and whether there is a difference in $t_{synch}G$ between two age groups of healthy young and older adults. The aim was not only to further advance our understanding of event-related MEG, but also our understanding of age-related changes in the brain. Based on findings from Burgess (2012) and Chapter 3, we predicted that changes in instantaneous frequency and PLV would be negatively cross-correlated, with post-stimulus frequency slowing concurrent with increasing PLV. The results of this study provide clear evidence for the negative cross-correlations as predicted, and power curve gradients were accurately fitted across t_{synch} points for the AO condition. Whilst these trends were not as clear in the AS condition, this is likely due to the same innate limitation of the AS condition as outlined in Chapter 3. Namely, the oddball gradient may reflect rigid task demands with naturally more efficient information processing and communication across neural networks, also supported by a ROI dedicated to enhancing the SNR of the P3b component. In contrast, the standard condition's gradient may trend towards zero due to reflecting far less homogenous activity over trials and lower SNR. Overall, these findings are analogous to those in EEG and suggest that the FM and its explanatory mechanism of cross-frequency phase modulation can explain event-related changes recorded in MEG.

Second, we sought to explore the ability to estimate a $t_{synch}G$ metric in MEG using both magnetometers and planar gradiometers together. Based on the FM, the VSH, and the findings from Chapter 3, it was predicted that modelling t_{synch} across ordinal IMFs would follow the same power law curve to reflect the systematic, gradual spread of activity across neural networks of increasing scale (thus decreasing frequency) over time. AO $t_{synch}G$ was successfully estimated in both power law curves and log-log polynomial straight lines for each sensor and across both sensor types of magnetometers and planar gradiometers, irrespective of pre-processing procedures (i.e., SSS or tSSS). The fits were very similar to those seen in the previous EEG studies and show that it is possible to use both sensor types' t_{synch} together to provide a greater number of data points per individual for subsequent modelling of $t_{synch}G$. However, there may be cases where it is better or unavoidable to rely on just planar gradiometers or magnetometers depending on the SNR and nature of the MEG setup, particularly as not all MEG systems comprise planar gradiometers like the Elekta Neuromag® TRIUX. In any case, it could also be beneficial for the number of target IMFs to be increased and/or the number of target downsamples to be increased, with a higher sampling rate and low-pass filter, to further improve SNR and robustness of the $t_{synch}G$ metric. The downside of this change would be an increased computational load, which is

already high for EMD analyses owing to its implementation on trial-level data (Sweeney-Reed & Nasuto, 2007; Sweeney Reed et al., 2018).

There being no significant differences in $t_{synch}G$ between SSS and tSSS suggests it is acceptable to use tSSS where participants, perhaps unwittingly, introduce substantial noise from inside the MEG array (e.g., from dental metalwork). This pre-processing could be particularly beneficial if MEG-age derived from $t_{synch}G$ were to be applied in clinical settings, where metal artefacts may be unavoidable and the thinner MaxShield™ MSR more common. However, deeper evaluation of the impact of MEG data cleaning, including MaxFilter™ and head movement correction, is still recommended within the wider aim of improving SNR. A good starting place would be collecting two groups/conditions (e.g., age-equivalent or repeated measures), comprising very clean versus very noisy data to see how pre-processing of each can affect the outcomes. For example, this could elucidate how a potential significant negative correlation between chronological age and SNR may be accounted for when applying $t_{synch}G$ to detect and track age-related changes. More generally, just like EEG data can be 'overcleaned' (Delorme, 2023), the same risk will no doubt apply to MEG data, and this risk needs careful consideration moving forward.

Finally, we wanted to examine the differences in $t_{synch}G$ and the ERF's P3b component between young adult and older adult age groups. Whilst there was a descriptive difference in the visualisation of grand average $t_{synch}G$s per age group (when averaging across instantaneous frequency and PLV data first), there were no significant differences in the $t_{synch}G$ between age group based on the individual-level data. This is likely in part due to lower SNR in the individual-level $t_{synch}G$ as previously outlined in Chapters 3 and 4, but particularly in the Y group of the current study (evidenced by visualisations and standard deviations). Additionally, there was limited statistical power in the current study due to resource limitations, which can not only lead to type-II errors (Button et al., 2013) but also type-S errors (Gelman & Carlin, 2014), where the sign of the difference is switched compared to the true effect. That said, it may also be the case that $t_{synch}G$ was simply reflecting the near equality between young and older adults in their cognitive and neural states. Just like in chapter 4, the older sample in this study was very healthy and displayed a NART-IQ bias. Therefore, there may have only been relatively minor age-related changes and not across the whole deep structure as measured by $t_{synch}G$. These changes could have been isolated to discrete surface features like P3b latency, and not to such an extent that it impacted $t_{synch}G$ and cognitive performance (evidenced by the older participants remaining in the normal QMCI band). Again, this is particularly pertinent given the methodology and statistical sensitivity of the current study. Overall, these findings, just like the findings in Chapter 4, are inconclusive and support a larger, more diverse sampling strategy in future.

This could comprise an examination of the impact of early life maturational processes (i.e., <18 years) and late life degradation processes (i.e., >80 years) on $t_{synch}G$, which may reveal accentuated or even entirely distinct changes. However, SNR would still need to be improved in parallel, to disentangle the effects of suboptimal SNR from meaningful age-related changes. Future optimisations to methodological and analytical pipelines will be discussed in Chapter 7, as the current findings certainly support a deeper interrogation of $t_{synch}G$.

In summary, there were three broad aims of this thesis, which could be achieved concurrently; namely, 1) to advance our understanding of event-related and resting-state EEG and MEG, 2) to advance our understanding of age-related changes in the brain with EEG and MEG, and 3) to establish EEG and MEG metrics that have the potential to track those age-related changes over time. This MEG study has improved our understanding of event-related changes by suggesting that the FM's explanatory mechanism is applicable to ERFs just like ERPs. It has also taken us a step closer to better understanding age-related changes in the deep structure of event-related MEG, but there are no wholly convincing results yet, likely due to the current suboptimal SNR. Nevertheless, this study serves as another foundation for future studies with larger, more diverse samples and optimised methodology and analysis pipelines. Combining the findings of Chapters 3, 4, and 5 together, we now have a greater understanding of EEG and MEG event-related changes and their age-related changes, plus a new $t_{synch}G$ metric that has the potential to detect and track deleterious age-related changes once optimised.

Chapter 6: Estimating chronological age from the EEG: resting-state oscillatory dynamics in the healthy ageing brain

Declaration of prior use: a substantial portion of this chapter has been submitted as a preprint on PsyArXiv and for publication in the journal Psychophysiology.

6.1 Introduction

There is extensive literature on the effects of ageing on the EEG (as outlined in Chapter 2), which has now been added to by establishing $t_{synch}G$ and how it can be used to estimate EEG-age in the context of event-related paradigms. In this chapter, the focus will turn to resting-state EEG, specifically how amplitude across the broad power spectrum and PAF can be used to estimate chronological age. Amplitude and frequency are distinct metrics but can be compared in their ability to estimate age, with the fact that they are distinct as a reason to make the comparison. The applied motivation for this approach was the same as for the previous work in event-related EEG, that an individual's brain age might act as a proxy of their general brain functioning. Therefore, a discrepancy between chronological age and EEG-estimated age could prove clinically informative by implicating deleterious conditions. Using a resting-state paradigm may be a more participant-friendly approach too, where event-related paradigms could be more difficult to manage and complete from both clinician and patient or community perspectives (Duncan et al., 2009). Sitting at rest could also feed into reduced measurement noise, particularly in an eyes-closed paradigm where the participant simply needs to stay still and awake. Finally, establishing frequency and amplitude metrics of the resting-state brain and how they can be used to estimate EEG-age could allow for further diagnostic triangulation (Hackfort & Birkner, 2011), such as combined with $t_{synch}G$ as a novel phase metric of the event-related brain, in the wider hunt for early and accurate detection of deleterious age-related change.

As outlined in Chapter 2, a mean decline in PAF is arguably the best-established EEG-correlate of increasing age and has been reported not only from the visual inspection of relatively small numbers of EEG recordings (Duffy et al., 1984; Dustman et al., 1993; Hughes & Cayaffa, 1977; Mizukami & Katada, 2018; Obrist, 1954; Stroganova et al., 1999) but also in multiple studies using large sample sizes and automated algorithms (Aurlien et al., 2004; Chiang et al., 2011; Finley et al., 2022; Hashemi et al., 2016; John et al., 1980; Lodder & van Putten, 2011; Merkin et al., 2023; Samson-Dollfuss & Goldberg, 1979). It is a normal brain-ageing phenomenon that likely reflects changes in neural and cognitive integrity, although no specific mechanism or interpretation has been established beyond reasonable doubt. Any relationship between age, neural function, and cognitive performance is likely to be complex and masked by numerous factors, such as those outlined by the

deficit vs benefit ageing models. A couple of advantages of M-PAF compared to other estimates of PAF (e.g., N-PAF, C-PAF, and K-PAF; all outlined in Chapter 2 and with no conclusion forthcoming on which method is best) is it can be readily extended to frequency bands other than alpha and incorporates the 1/f slope, thus both periodic (e.g., traditional oscillatory bands) and aperiodic (e.g., non-oscillatory) components of the EEG power spectrum can be considered (Donoghue et al., 2020). This would allow us a deeper insight into the complex age-related changes in frequency across the spectrum, and potentially offer additional metrics for tracking problematic age-related changes. However, peaks in frequency bands other than alpha are rarely clear and, thus, rarely reported, and peaks that do occur tend to be broader than in alpha. Consequently, age-related changes across the EEG power spectrum are traditionally examined via changes of oscillatory power in pre-defined frequency bands, but the results vary widely and depend on the methodology and statistical approach used by the researchers (Cragg et al., 2011; Dauwels et al., 2010a; Duffy et al., 1993; Gómez et al., 2013; Ishii et al., 2017; Vysata et al., 2012). For example, studies that account for age-related changes in the aperiodic 1/f slope concurrently with oscillatory power have produced contrasting evidence to the traditional approaches, although the findings have not been entirely consistent (Donoghue et al., 2021; Finley et al., 2022; Merkin et al., 2023; Schaworonkow & Voytek, 2021; Trondle et al., 2022).

One way to circumvent the difficult choices required when estimating PAF or oscillatory power in discrete frequency bands is to consider a distinct metric that could improve SNR and provide a robust assessment of age-related changes in the EEG. That metric is a quantification of age-related changes across the broad EEG power spectrum using a multivariate method called PLS regression. In a similar way to how $t_{synch}G$ allows us to study the deep structure of event-related changes in the brain rather than surface features, PLS regression analysis of the broad frequency spectrum is a more holistic, distinct measure of the resting state brain compared to targeting power in discrete frequency bands or PAF. At the time of writing, PLS has not previously been used to examine the broad EEG power spectra (e.g., 0.1 to 45 Hz) with the focused aim of estimating chronological age. This is a gap in the literature because multivariate approaches have advantages that may provide more robust results than conventional approaches, such as PAF, when attempting to match chronological age and brain age. For example, multivariate analyses can use all amplitude information in the broad EEG power spectra (e.g., 0.1 to 45 Hz) dataset at the same time, work when there are no visible peaks in the spectra, and they reduce subjective user input. Interrogating the relationships between PAF and the broad power spectrum with chronological age will provide another foundation for the applied use of EEG-age, but it will also extend our understanding of oscillatory dynamics in the resting state, healthy ageing

brain. In turn, we also wanted to compare proxy measures of general cognitive integrity alongside EEG-estimated age to again probe age-related processes (e.g., dedifferentiation and noise versus reserve) from the same general, system-level perspective as implemented when interpreting event-related EEG in chapters 4 and 5.

Overall, our objective was to use the EEG power-frequency spectrum to estimate chronological age as EEG-age. First, we wanted to compare the well-established variants of PAF on their ability to estimate age. Based on previous evidence, we predicted that PAF would be negatively correlated with chronological age, and we aimed to determine which estimate of PAF (M-PAF, C-PAF, K-PAF, or a variant of N-PAF) correlated most strongly and provided the most accurate estimate of chronological age. Second, we sought to explore the potential of multivariate analyses of the broad EEG spectrum (0.1 to 45 Hz), using PLS as a distinct analytical approach to PAF that has not previously been used to estimate chronological age. Third, we wanted to examine the relationships of PAF age and PLS EEG-age with already established proxy measures of general cognitive integrity. As with the previous chapters, the objectives of this chapter were such that the outcomes will directly inform the aims of this thesis; to better understand resting-state EEG, in and out of the ageing context (aims #1 and #2), and to establish metrics for tracking age-related changes in the brain (aim #3).

6.2 Methods

6.2.1 Participants

This is the same EEG dataset as previously used in Chapters 3 and 4, but now focusing on the resting state data therein instead of the event-related data. As a brief recap of the demographics, sixty healthy adults (24 men, 36 women; 5 left-handed, 55 right-handed) volunteered to participate, which allowed for ten participants per decade of chronological age across six decades (*M* = 49 years, *SD* = 17.9, *Range* = 20 to 78). Having reached our resource limit, a sensitivity power analysis for a univariate negative correlation between PAF and chronological age using Pearson's *r*, with an alpha of .05 and a beta of .2 [.1], calculated a minimum detectable effect size of -.31 [-.37] (calculated using G*Power, version 3.1.9.7; Faul et al., 2009). Participants had a mean of 17 years in formal education (*SD* = 4.0, *Range* = 7 to 27). Fifty-two participants identified as White, seven as Asian, and one as Black, with all participants recruited via Aston University's advertising portals, which includes the ARCHA Panel that comprises older adults from around the UK who volunteer to take part in studies at Aston University. This study received a favourable opinion from AU-REC and was carried out in accordance with the Declaration of Helsinki and the British Psychological Society Code of Human Research Ethics. Written informed consent was obtained from each participant, and they were reimbursed £15 for their participation.

All participants actively reported having no experience of traumatic brain injury, no diagnosis of neurological or psychiatric disorder, and no known cognitive impairment. Participants were screened for depression via the GDS-15 (Sheikh & Yesavage, 1986), as severe depression may confound measures of PAF (Tement et al., 2016; Zhou et al., 2023). Participants were also screened for cognitive impairment via the QMCI (O'Caoimh & Molloy, 2017). As in Chapter 4, we included the QMCI not only as a screening tool, where healthy adults should report scores that are isolated to the normal category, but as our estimate of general cognitive integrity, a proxy measure of dedifferentiation and noise, where higher scores represented higher general brain functioning. Participants also completed the NART (Nelson, 1982; Nelson & Willison, 1991), and, again as in Chapter 4, we converted the raw NART scores to estimates of the Wechsler Adult Intelligence Scale score (WAIS-IV; Wechsler, 2008), called NART-IQ, via a validated conversion, NARTIQ = 126.41 - 0.9775 × NART errors (Bright et al., 2018). NART-IQ was included as an efficient, proxy measure of age-related mechanisms that support cognitive functioning, particularly reserve (Boyle et al., 2021), in contrast to the QMCI as a proxy measure of age-related deficits.

6.2.2 EEG recording

DC-EEG was recorded for 4 minutes while participants were sitting at rest, on a comfortable chair in a quiet room, with their eyes closed. The EEG setup used for data collection is outlined in Chapter 2 of this thesis. With a mean electrode impedance of 15.48 kΩs (*SD* = 13.33, *Range* = 0.01 to 120.50), most electrodes had similar impedances that were less than the reported optimal cut-offs of 40 kΩs (Ferree et al., 2001; i.e., 94% of 3780 electrodes) and 50 kΩs (Kaneko et al., 2021; i.e., 97% of 3780 electrodes) for the high-impedance ANT EEG system. For one participant, one mastoid electrode (M1) reached 120.50 kΩs, although this was still below the workable maximum of 200 kΩs (Ferree et al., 2001).

6.2.3 Data preparation

EEG data were pre-processed and analysed in MATLAB R2019b. DC-EEG recordings can contain long slow trends that deviate substantially from zero in the absence of any artefact. Therefore, the raw data was demeaned and then a time-varying baseline was used (spanning 1025 data points, ± 2.048 seconds), derived from a standard 3rd-order Savitzky-Golay filter (Press & Teukolsky, 1990), and raw data that deviated from the Savitzky-Golay filtered signal by ±120 μV were excluded. The largest possible contiguous segment of artefact-free EEG was selected for each person. Over 100 seconds of EEG was obtained for each person (*M* = 205 seconds, *SD* = 58, *Range* = 103 to 343, with one EEG recording that exceeded 4 minutes) without the need for EOG correction. However, for 12 participants, channels had to be excluded to achieve this target duration and avoid noise-

contamination of the PAF and spectral estimates, to be left with the most reliable estimates possible per participant using the available data. In most cases, fewer than 5 channels were excluded, except for four cases where 6, 7, 9, and 16 channels respectively were excluded. Subsequent agglomeration across channels and/or participants simply used the data that remained. This data preparation was completed without reference to demographics, such as chronological age, but we later checked whether age and length of recording were correlated; they were not (r = -.05, p = .730).

6.2.4 Signal analysis

For the N-PAF and M-PAF methods, an autoregressive power spectral density estimation was used with the covariance method of model order 256 that covers a span of 512 milliseconds (256×2; MATLAB function 'pcov.m'), allowing for the estimation of spectral density values from 0.1 to 45 Hz at a resolution of 0.1 Hz compared to around 0.25 Hz for the Welch method. Frequencies above 45 Hz were excluded from analysis because of their low SNR, including the United Kingdom's 50 Hz mains electricity noise, and frequencies below 0.1 Hz were also excluded. To prevent the highest power values at low frequencies from biasing the statistical analyses, the EEG power spectrum was converted to amplitude by taking the square root and then the logarithm (base 2) to create a $\log_2(amplitude)$ spectrum that was used in subsequent analyses (Burgess, 2019). The K-PAF and C-PAF methods were implemented using an openly accessible MATLAB code called 'restingIAF', which has been shared by Corcoran et al. (2018). For both methods, spectral analysis followed the traditional Welch FFT-method implemented with a 4096-millisecond Hamming-tapered window with 50% overlap. The power spectra were then normalised and smoothed using a 5th-order Savitzky-Golay filter (spanning 11 frequency bins, ± 2.69 Hz).

The N-PAF method was implemented first. This approach involved a simple identification of all peaks in the spectrum between 7 to 13 Hz at each channel for each participant. A peak was defined as any part of the spectrum where the gradient of the amplitude $(\delta A/\delta f)$ changed sign. If more than one peak was identified, the N-PAF was defined as the peak with the highest amplitude. No identifiable peak occurred in <2% of channels (i.e., 67 out of 3780 channels), and these channels were each listed as a missing datum. One way to calculate a univariate estimate of PAF for the N-PAF method is to calculate an average across channels. Consequently, channels are weighted equally regardless of their SNR. Alongside the classic N-PAF method, we also implemented an alternative version of N-PAF that we named the Direct Estimate-PAF (D-PAF). This involved SVD (Harner, 1990) of the channel-by-spectra matrix, to emphasise features of the EEG power spectrum that were consistent across channels in an individual. Spectra were the $\log_2(amplitude)$ values estimated at 0.1 Hz intervals. In the current context, the first

extracted component accounted for a large majority of variance in every participant (*M* = 94% variance, *SD* = 3%, *Range* = 82% to 99%). Post-SVD, the summary measure of PAF was obtained simply by identifying the peak with the highest amplitude in the 7 to 13 Hz range.

K-PAF and C-PAF methods were implemented next, in accordance with the 'restingIAF' code that was shared by Corcoran et al. (2018). The K-PAF approach involved finding the centre-of-gravity (i.e., amplitude-weighted mean frequency) in the alpha range, using a smoothed Welch's EEG spectrum. The bounds of the alpha band were defined when the gradient of the amplitude was equal to zero. The summary estimate of PAF was derived from data across all available channels, with each channel contributing equally. The C-PAF approach also used smoothed EEG spectra, with the peak frequency being defined at each channel (as in N-PAF) before averaging to produce the summary measure. This averaging involved excluding channels with a low amplitude alpha peak, such that the minimum amplitude of a peak would be a standard deviation above the estimate predicted by a regression model of the log-transformed power spectral density. To finish, the SNR-weighted mean of the remaining PAFs was calculated.

Finally, the M-PAF method was implemented in close alignment with the methods used in previously published papers that correlated M-PAF with age (e.g., Chiang et al., 2011; Lodder & van Putten, 2011). It assumed that the EEG power spectrum consists of an aperiodic 1/f slope plus Gaussian distributions representing the peaks of five different periodic frequency bands (i.e., Theta, Alpha, Beta1, Beta2, and Gamma). Specifically, the $\log_2(amplitude)$ spectrum consisted of a $A_0.\frac{1}{f^m} + k$ component, where ***f*** is the frequency raised to the power ***m,*** weighted by a constant, $\boldsymbol{A_0}$, with an offset, ***k***, plus the five frequency bands. These bands were represented by a Gaussian distribution, $A_i e^{\left[-\frac{1}{2}\left(\frac{f-\mu_i}{\sigma_i{}^2}\right)^2\right]}$, with maximum amplitude, $\boldsymbol{A_i}$, mean peak frequency, $\boldsymbol{\mu_i}$ and standard deviation, $\boldsymbol{\sigma_i}$. Combined this gives:

$$log_2 A(f) = A_0.\frac{1}{f^m} + \sum_{i=1}^{5} A_i e^{\left[-\frac{1}{2}\left(\frac{f-\mu_i}{\sigma_i{}^2}\right)^2\right]} + k \quad (6.1)$$

The model was fitted using non-linear least squares (MATLAB function 'fit.m') with conventional constraints: $m < 0$, $0 \leq A_i \leq 10\ log_2(\mu V/Hz)$, peak frequencies, μ_i, to be in the ranges 1-7, 7-13, 13-21, 21-29, and 29-47 Hz, and maximum widths, σ_i, to be 15, 10, 30, 30, and 30 Hz for the five frequency bands respectively. An example fit of this model to an individual's EEG power spectrum is shown in Figure 6.1 (*M* = .995 $R^2_{Adjusted}$, *SD* = .006,

Range = 0.963 to 0.999). The model was not fitted to each channel but, like D-PAF, to the first component of a SVD, so one summary estimate of PAF accounted for all channels. An overview of the procedural differences between the PAF methods is shown in Table 6.1.

Figure 6.1

The model EEG density spectrum. a) shows an individual's observed spectrum compared with the modelled spectrum; b) shows the 1/f slope; c) shows the five Gaussian components representing the theta, alpha, beta1, beta2 and gamma frequency bands.

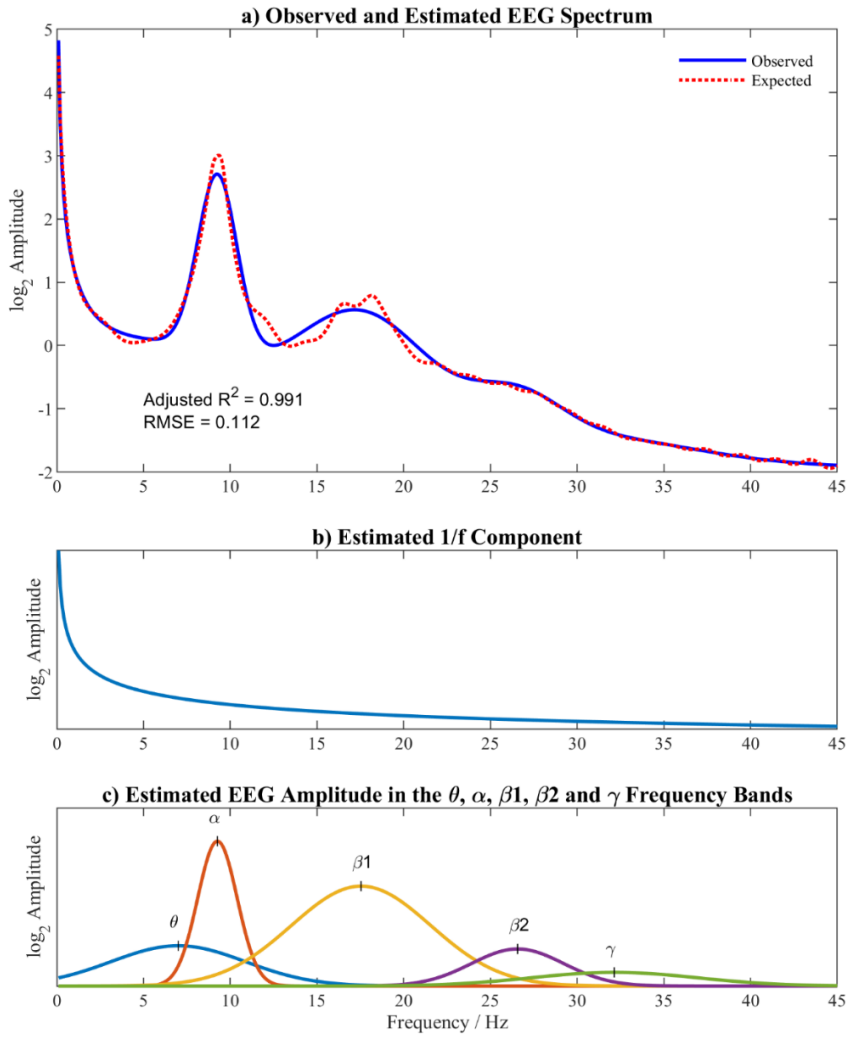

Table 6.1

Differences between PAF estimation methods

	Method name	Spectral analysis	Channel treatment	Peak identification
N-PAF	Naïve-Peak Alpha Frequency (Chiang et al., 2008)	Autoregressive Method (AM; Gersch, 1970)	No averaging	Per channel, the alpha peak with the highest amplitude
D-PAF	Direct Estimate-Peak Alpha Frequency	Autoregressive Method (AM; Gersch, 1970)	Singular Value Decomposition (SVD; Harner, 1990)	The SVD's first-component's alpha peak with the highest amplitude
M-PAF	Modelled-Peak Alpha Frequency (Chiang et al., 2011; Lodder & van Putten, 2011)	Autoregressive Method (AM; Gersch, 1970)	Singular Value Decomposition (SVD; Harner, 1990)	The SVD's first-component's frequency of the Gaussian distribution used to represent the alpha frequency
C-PAF	Corcoran-Peak Alpha Frequency (Corcoran et al., 2018)	Welch-FFT (Welch, 1967)	Weighted-averaging across smoothed EEG spectra-PAF	The SNR-weighted, averaged alpha peak with the highest amplitude
K-PAF	Klimesch-Peak Alpha Frequency (Klimesch et al., 1990, 1993)	Welch-FFT (Welch, 1967)	Averaging across smoothed EEG spectra-PAF with individually defined alpha bands	The amplitude-weighted, averaged mean frequency

The ability of the broad EEG power spectrum of 0.1 to 45 Hz range to predict chronological age (i.e., EEG-age) was assessed using PLS (MATLAB function 'plsregress.m'). The predictor was the first component of the SVD of the channel-by-spectra matrix. The number of PLS factors to be extracted needed to be defined, which was done via permutation testing. Specifically, the significance of each factor was determined by comparing the amount of variance accounted for by each additional factor compared with the percentage of variance accounted for by multiple permutations (1000 times) of the age data. Identification of the most age-responsive components per factor was determined using

recursive weighted-PLS, R-PLS (Rinnan et al., 2014), which iteratively reweights the variables using the regression coefficients calculated by PLS until only a small number of the most important predictors remain. In this way, age-predictive weightings for each part of the EEG spectrum are reduced to a small number of critical frequencies that can be used to predict age nearly as accurately as the full spectrum.

6.3 Results

6.3.1 Correlations between chronological age, NART-IQ, and cognitive performance

The mean NART-IQ was 115 (*SD* = 5.8, *Range* = 102 to 125), indicating that the sample was generally above average and less varied in premorbid intelligence than the general population. There was also a significant positive correlation between NART-IQ and chronological age (r = .54, p < .001), which reflects the high premorbid intelligence (e.g., reserve) of older adult volunteers on the ARCHA Panel. The mean score of cognitive performance on the QMCI was 77.0 (*SD* = 7.4, *Range* = 61 to 93), indicating that the sample had normal cognitive functioning. Age was not significantly correlated with cognitive performance (r = -.18, p > .05), and NART-IQ was not significantly correlated with cognitive performance (r = .12, p > .05).

The mean score of mood on the GDS-15 was 2 (*SD* = 2.6, *Range* = 0 to 11), indicating that the sample was presenting with normal mood on average. Chronological age (r = -.07, p > .05), cognitive performance (r = -.16, p > .05), and NART-IQ (r = -.14, p > .05) were not significantly correlated with mood. Participants had a mean of 17 years in formal education (*SD* = 4.0, *Range* = 7 to 27), and chronological age (r = -.16, p > .05), cognitive performance (r = .01, p > .05), NART-IQ (r = .09, p > .05), and mood (r = -.14, p > .05) were not significantly correlated with years in formal education.

6.3.2 Topographical variation of PAF estimated by the N-PAF method

D-PAF, C-PAF, K-PAF, and M-PAF are methods that aim to summarize PAF across all available channels, so we considered the N-PAF method in isolation because it best estimates PAF at channels separately. Figure 6.2a visualises the topographical distribution of PAF averaged across all participants (*M* = 9.57 Hz, *SD* = 0.16, *Range* = 9.26 to 9.86), with the amplitude at each mean PAF value shown in Figure 6.2b (*M* = 1.22 log2A, *SD* = 0.58, *Range* = -0.58 to 2.15). Maximum power at PAF occurred at right occipital sites for eyes closed at rest. There were significant negative correlations (p < .05, uncorrected for multiple comparisons) between chronological age and PAF at 52 channels (Figure 6.2c), indicating that PAF decreases with increasing age across most channels and with little topographical variation (*M* = .40 *r*, *SD* = 0.01). The largest clusters of negative correlations were at temporoparietal sites, but the maximum correlation coefficient was FT7 (r = -.61, p <

.001). The amplitude at each PAF per channel revealed no significant correlations with age (Figure 6.2d; maximum correlation coefficient of r = .25, p > .05, at TP7). In summary, there was little topographical variation and a consistent correlation between PAF and chronological age.

Figure 6.2

Summary of PAF and amplitude estimated by the N-PAF method, and their relationships with chronological age. a) shows the distribution of PAF, averaged across participants, by topography; b) shows the distribution of amplitude at each PAF, averaged across participants, by topography; c) shows the Pearson's r correlation coefficients between age and PAF by topography; d) shows the Pearson's r correlation coefficients between age and amplitude at each PAF by topography.

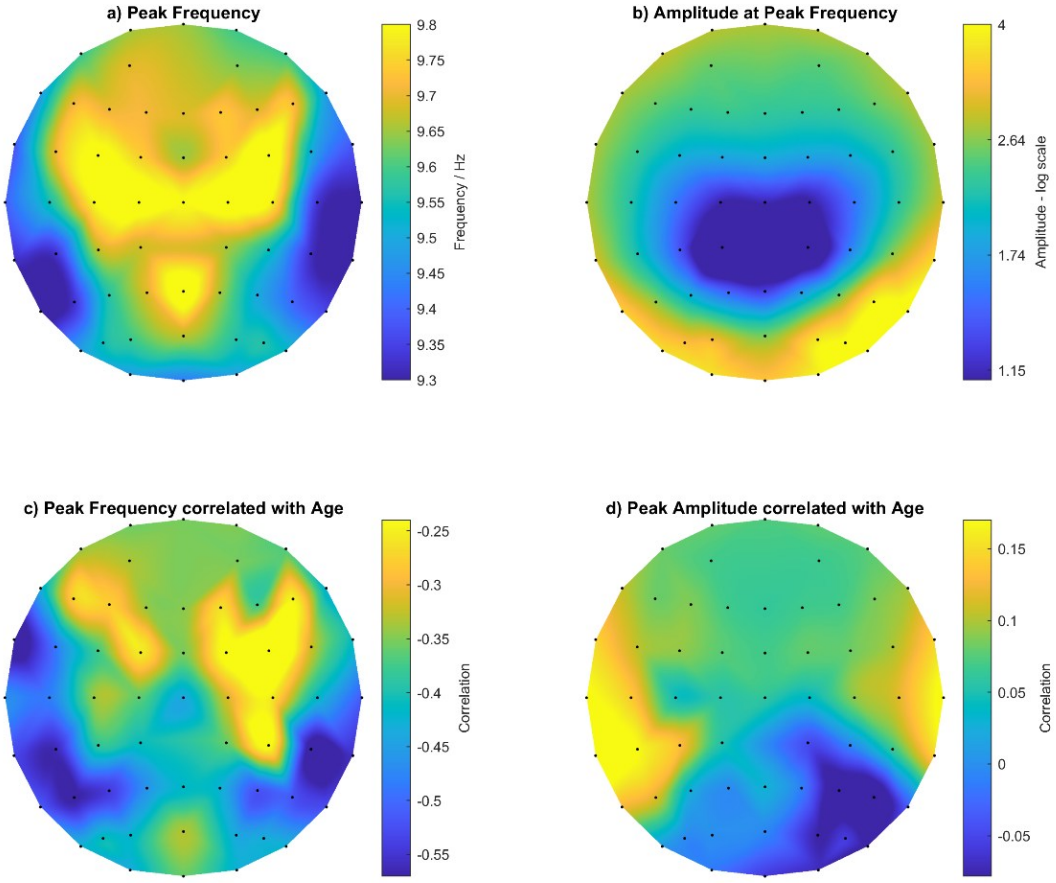

To formally evaluate the importance of topographical variation on N-PAF's estimate of PAF, we estimated the proportion of variance attributable to between-subject (B-S; participants) and within-subject (W-S; channels) factors using the Minimum Norm Quadratic Unbiased Estimator (MINQUE in SPSS Statistics 26.0.0; IBM Corporation, 2021; Rao, 1972) with uniform random effect priors (i.e., scheme 1). B-S factors accounted for 71% of the total

variance in PAF, and W-S factors, which represent the consistency of the topographical distribution of PAF across individuals, accounted for 2% of the variance, which leaves 27% attributable to measurement error. In the current study, accounting for only 2% of the total variance in PAF, W-S variation could be treated as noise (i.e., inconsistent SNR), which is consistent with the little topographical variation shown in Figure 2 and, thus, supports using a single summary value to represent an individual's PAF. The next section will compare four summary measures of PAF, estimated via D-PAF, M-PAF, C-PAF, and K-PAF methods.

6.3.3 Comparing D-PAF, M-PAF, C-PAF, and K-PAF

A comparison of the four methods of estimating PAF is shown in Figure 6.3. Using the D-PAF and M-PAF methods, estimates of PAF were provided for all participants. Using the C-PAF and K-PAF methods, estimates were unavailable for two participants (3% of the total sample) because there were too few channels with sufficiently prominent alpha peaks. A Bland-Altman analysis (Bland & Altman, 1986), which plots the difference in PAF between two methods' estimates against the average PAF of the same two estimates, reveals that the level of agreement in PAF between methods is relatively poor, with wide 95% limits of agreement (±1.96 SD) and constant error (as shown via the bias of the Mean line) in all except the comparison between D-PAF and M-PAF. Indeed, one-sample t-tests of the mean values support that D-PAF and M-PAF methods produced estimates of PAF that are not significantly different from each other, but they are significantly higher than C-PAF, which, in turn, produced significantly higher estimates than K-PAF (D-PAF = M-PAF > C-PAF > K-PAF). Additionally, proportional error is present in all comparisons comprising D-PAF, suggesting greater bias towards D-PAF the higher the average PAF. Given the correlational nature of the study, the distribution of the PAF variables are reported in Table 6.2 and a correlation matrix of PAF methods in Table 6.3.

Figure 6.3

Comparing PAF estimates from the Direct (D-PAF), Corcoran (C-PAF), Klimesch (K-PAF), and Modelled (M-PAF) methods using Bland-Altman analysis

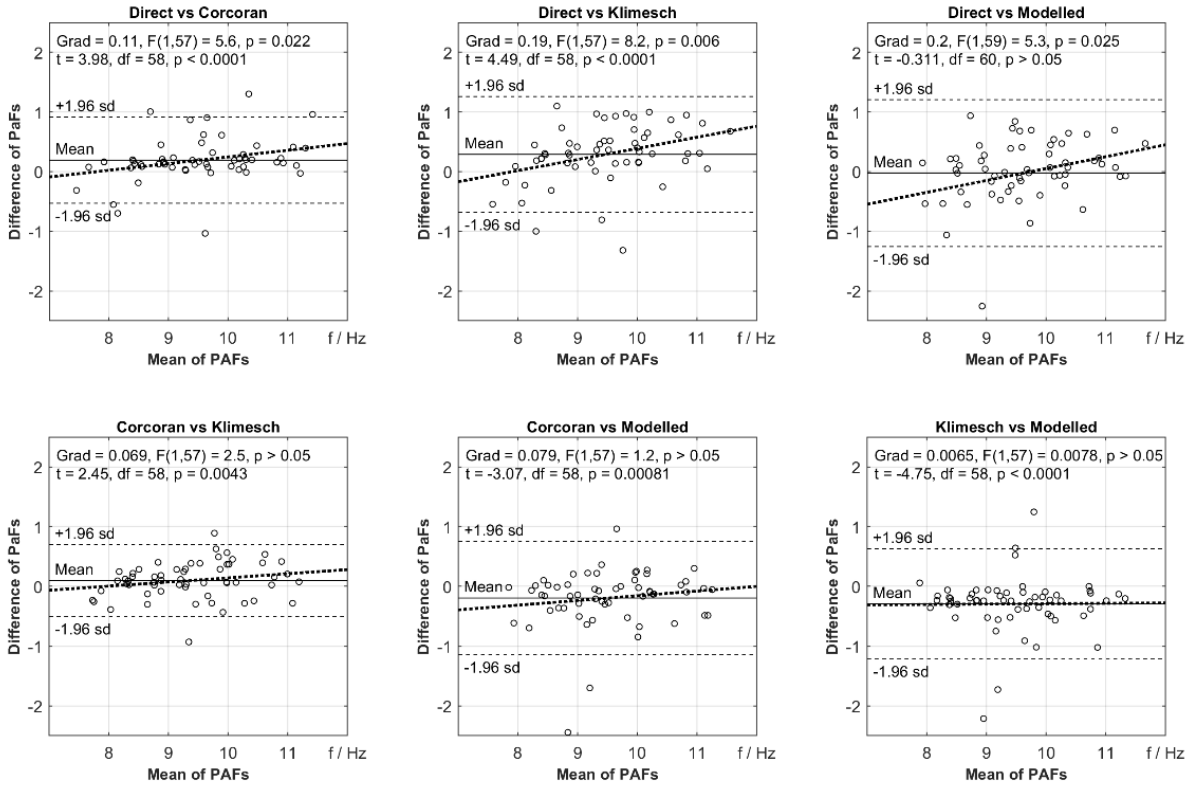

Table 6.2

Distribution of PAF across PAF methods

	M	SD	Range	Shapiro-Wilk W (*p*)
D-PAF	9.50	1.04	7.20 to 11.80	0.99 (> 0.05)
M-PAF	9.63	0.88	7.85 to 11.40	0.98 (> 0.05)
C-PAF	9.42	0.95	7.61 to 11.20	0.97 (> 0.05)
K-PAF	9.32	0.89	7.85 to 11.20	0.97 (> 0.05)

Table 6.3

Pearson's r correlations between PAF methods

	D-PAF	M-PAF	C-PAF	K-PAF
D-PAF	-			
M-PAF	.80*	-		
C-PAF	.94*	.86*	-	
K-PAF	.89*	.86*	.95*	-

Note. *p < .001

6.3.4 Estimating chronological age with PAF

D-PAF, M-PAF, C-PAF, and K-PAF were used to look at the relationship between chronological age and PAF, with chronological age regressed onto each estimate of PAF. In each case, PAF proved to be a significant predictor of age (Figure 6.4), and M-PAF was the most accurate and strongest predictor of age, descriptively, according to root-mean-square error (RMSE) and the correlation coefficient respectively. Using the Glass & Hopkins method (Glass & Hopkins, 1996; IBM Support, 2020) to compare the strengths of correlation coefficients between chronological age and PAF age for each method of estimating PAF, Table 6.4 shows that no method proved significantly stronger than any others (p > .05). The regression of chronological age on M-PAF corresponded with a correlation of r = -.51 (or .51 on M-PAF age) and accounted for approximately 24% of the variance in age (*RMSE* = 15.54). When regressing M-PAF onto chronological age (*RMSE* = 0.76), each decade of chronological age was associated with an expected change of 0.25 Hz in PAF ($PAF = -0.025 \times Age + 10.8$).

Figure 6.4

Scattergrams showing the linear relationship between PAF and chronological age. a) D-PAF, b) C PAF, c) K-PAF, and d) M-PAF; r = Pearson's correlation coefficient; RMSE = Root Mean Squared Error of Estimation; gradients are in years per Hz

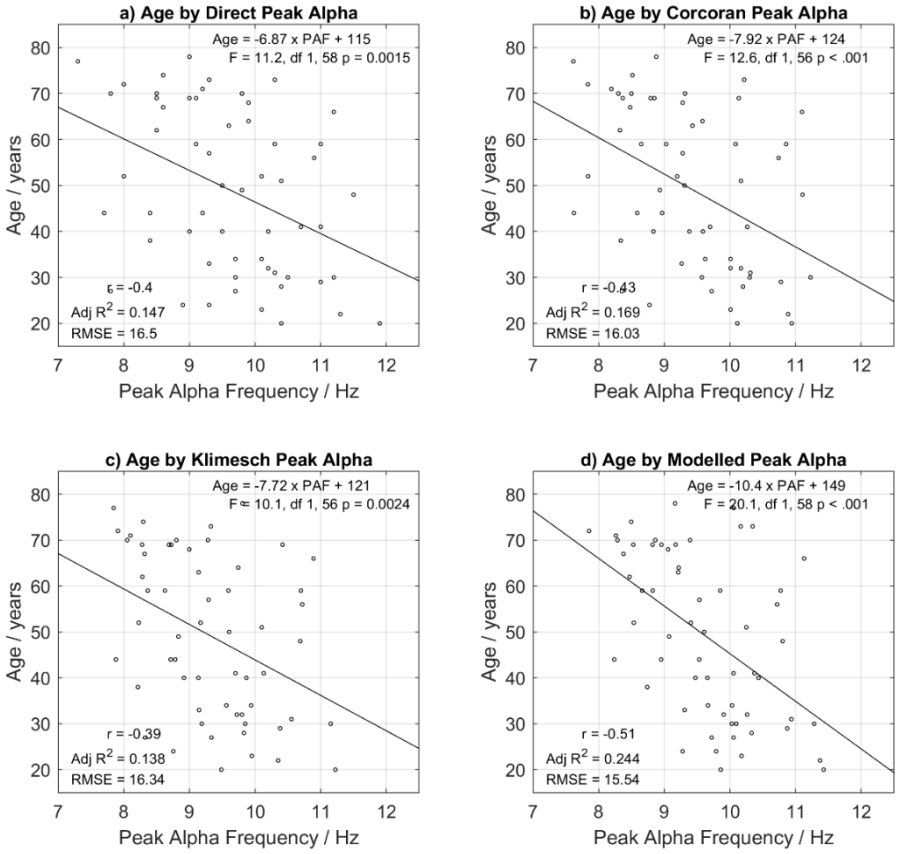

Table 6.4

Differences between correlations of chronological age with PAF age for the PAF methods

	D-PAF	M-PAF	C-PAF	K-PAF
D-PAF	-			
M-PAF	-.11	-		
C-PAF	-.03	.08	-	
K-PAF	.01	.12	.04	-

Note. The values represent the differences between the respective Pearson's *r* correlation coefficients (e.g., D-PAF age – M-PAF age); no method proved significantly stronger than any others ($p > .05$).

The M-PAF method was used to also obtain estimates of peak frequency for theta, beta1, beta2, and gamma, along with the bands' amplitudes and widths. The correlation between the peak frequency, amplitude, and width of each frequency band with chronological age is shown in Table 6.5. The M-PAF approach also allowed for the estimation of the amplitude, A_0, of the $\frac{1}{f^m}$ component (i.e., aperiodic 1/f slope) of the model, the exponent itself, *m*, and the overall offset, k, none of which were significantly correlated with age (r = -.01, -.16 and .02 respectively, p > .05). There was also no significant correlation between the total amplitude (global) in the 0.1 to 45 Hz frequency range and age (r = .21, p > .05).

Table 6.5

Correlations of chronological age with peak frequency, amplitude, and width for the five frequency ranges using the M-PAF method

	Theta	Alpha	Beta1	Beta2	Gamma
Peak frequency	-.21	-.51**	-.47**	-.33**	.08
Amplitude	-.14	.01	.39**	.28*	-.10
Width	-.32*	-.28*	.08	.08	.33*

Note. *p < .05; **p < .01

The correlations of chronological age with peak frequency, amplitude, and width seen in multiple frequency bands show that age-related changes in the EEG power spectrum extend beyond a simple, discrete slowing of the PAF. This finding further supports our examination of the relationship between chronological age and the broad EEG power spectrum of 0.1 to 45 Hz range with PLS.

6.3.5 Estimating chronological age as EEG-age with PLS regression

PLS regression was used to look at the relationship between chronological age and EEG-age. Chronological age was regressed onto the first SVD-extracted component of the EEG spectra. Permutation testing revealed that only two factors, used to derive β-weights, were statistically significant (Figures 6.5a & 6.5d). The β-weights by frequency are shown in Figure 6.5b, with frequencies that were significant in predicting age indicated by the Variable Importance in Projection scores (VIP) being >1 (displayed as a blue circle). Age was most strongly predicted by sections of the EEG spectrum that map onto the low-alpha and beta frequency ranges (positive weightings) contrasted with frequencies in the theta and high-

alpha ranges (negative weightings). Using these weightings, it was possible to estimate expected chronological age based solely on the EEG spectrum (i.e., EEG-age) and statistically compare these estimates with true chronological ages. There was a strong positive, significant correlation between PLS EEG-age and chronological age (r = .69, p < .001; Figure 6.5c), with the RMSE of 13.02 years showing considerably better accuracy than was achieved using the best PAF estimate to predict chronological age (M-PAF method; r = -.51, *RMSE* = 15.54).

Adding PLS EEG-age as an additional predictor of chronological age, alongside M-PAF age, significantly improved the fit of a regression model ($R^2_{Adjusted}$ = .458; R^2_{Change} = .219, $F(1,57) = 23.8$, p < .001). Given the interpretation that PLS-correlates of age comprise more information across the broad EEG spectrum than PAF-correlates of age, we also tested to what extent PLS EEG-age remained significantly correlated with age when the PAF is partialled out (r = .53, p < .001, controlling for PAF-M, PAF-D, PAF-C, and PAF-K). Finally, a BHR comparing a null model including PLS EEG-age with a second model adding in M-PAF age, in attempts to predict chronological age, reported BF_{01} = 3.31. This finding provides substantial evidence in favour of H_0 (Jeffreys, 1961; Wagenmakers et al., 2011) and suggests that EEG-age is the important predictor of chronological age.

Figure 6.5

The prediction of chronological age with EEG-age via PLS analysis of EEG spectra. a) the percentage variance in chronological age accounted for by number of components; b) The factor-weights of the two significant factors (i.e., latent variables) by frequency; c) The two-dimensional β-weights by frequency; d) Chronological age (True Age) by EEG-age (PLS Estimated Age); e) The R-PLS optimal β-weights by frequency; f) Chronological age (True Age) by EEG-age (R-PLS Estimated Age)

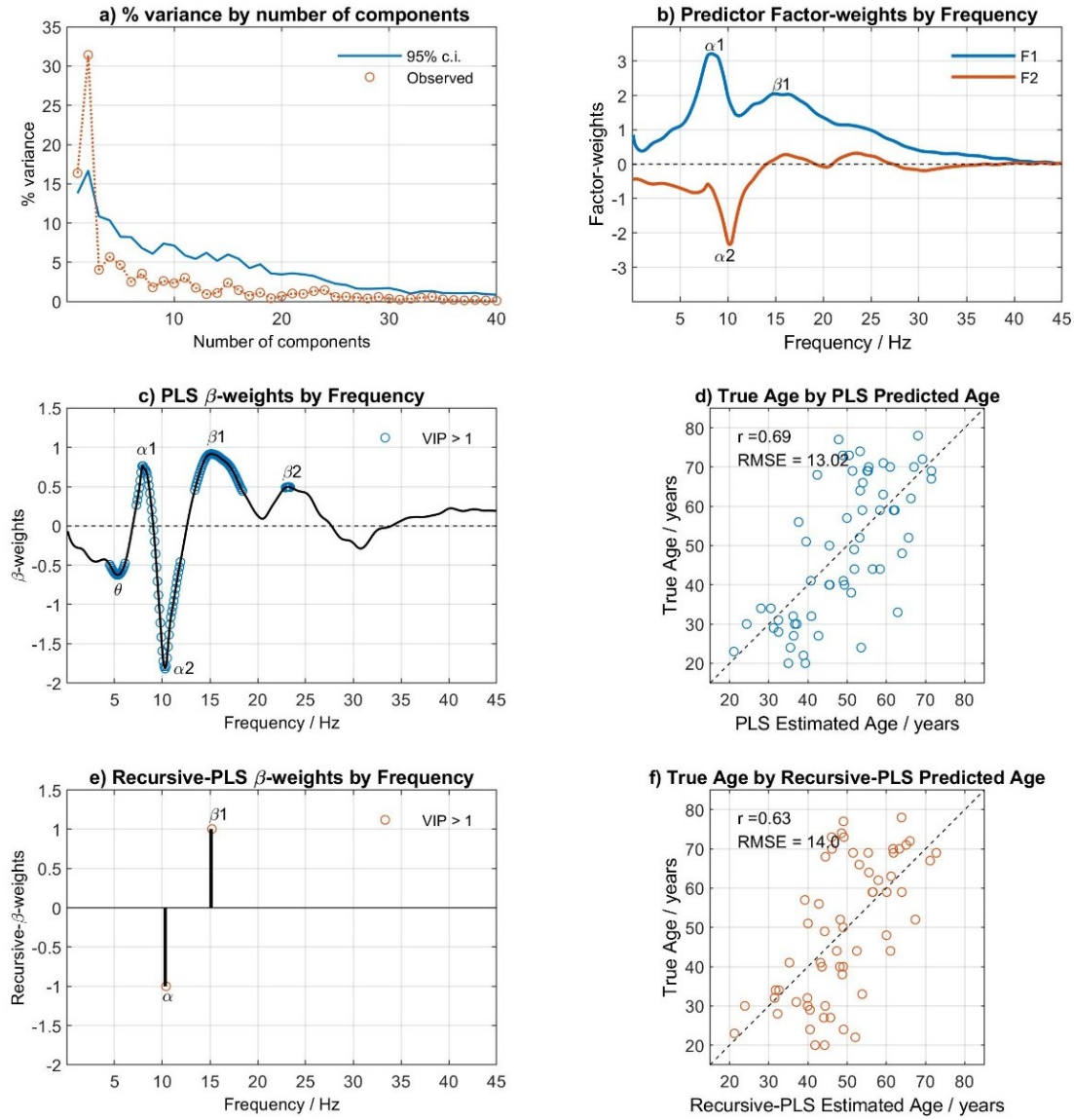

Identification of the most age-responsive components of the full EEG power spectrum was determined using R-PLS. After 14 iterations, a two-component solution (Figure 6.5e), which contrasts power at 10.3 Hz (negative weighting) and 15.1 Hz (positive weighting), significantly correlates with chronological age. The RMSE was only a little less good than the full spectrum (Figure 6.5f; R-PLS EEG-age: r = .62, *RMSE* = 14, versus PLS EEG-age: r = .69, *RMSE* = 13.02). This suggests that the most important predictor of age is the contrast between alpha and beta1. Using regression to predict chronological age with EEG $\log_2(amplitude)$ at 10.3 Hz and 15.1 Hz shows a significant relationship ($F(2,57)$ = 18.75, $p < .001$, $R^2_{Adjusted}$ = .376, RMSE = 14.0) given by:

$$Age = 68.8 - 22.5\, A_{10.3\,Hz} + 44.1\, A_{15.1\,Hz} \quad (6.2)$$

Given the correlational nature of the study, the distribution of the EEG-age variables is presented in Table 6.6 and a correlation matrix of PAF and EEG-age methods in Table 6.7. Comparing the correlations using the Glass & Hopkins method again, the PLS EEG-age methods were consistently significantly more strongly correlated with age than the PAF-age methods (Table 6.8).

Table 6.6

Distribution of EEG-age across PLS methods and M-PAF as the best PAF predictor

	M	SD	Range	Shapiro-Wilk W (p)
EEG-age PLS	49	12.20	20 to 73	0.99 (> 0.05)
EEG-age R-PLS	49	11.30	21 to 73	0.99 (> 0.05)
EEG-age M-PAF	49	9.10	30 to 68	0.98 (> 0.05)

Table 6.7

Pearson's r correlations between PAF and EEG-age methods

	D-PAF	M-PAF	C-PAF	K-PAF	EEG-age PLS	EEG-age R-PLS
D-PAF	-	-	-	-	-	-
M-PAF	.80**	-	-	-	-	-
C-PAF	.94**	.86**	-	-	-	-
K-PAF	.89**	.86**	.95**	-	-	-
EEG-age PLS	-.42**	-.62**	-.45**	-.42*	-	-
EEG-age R-PLS	-.40*	-.52**	-.40*	-.38*	.79**	-

Note. *p < .01; **p < .001

Table 6.8

Differences between correlations of chronological age with brain age for PAF age and PLS EEG-age methods

	D-PAF	M-PAF	C-PAF	K-PAF	PLS	R-PLS
D-PAF	-					
M-PAF	-.11	-				
C-PAF	-.03	.08	-			
K-PAF	.01	.12	.04	-		
PLS	-.28**	-.18*	-.25*	-.29**	-	
R-PLS	-.23*	-.12	-.20	-.24*	.05	-

Note. The values represent the differences between the respective Pearson's *r* correlation coefficients (e.g., D-PAF age – M-PAF age); *p < .05; **p < .01

6.3.6 Correlations between EEG-age, NART-IQ, and cognitive performance

Whilst there were no significant differences in the ability to predict chronological age within the PAF and PLS approaches respectively, M-PAF age and PLS EEG-age were chosen for the final stages of analysis because they produced the most accurate estimates of age, with the lowest RMSE, per approach. It was expected that QMCI would be negatively correlated with age, implicating deleterious age-related changes such as dedifferentiation and noise. In contrast, neither chronological age nor PLS EEG-age was significantly correlated with QMCI, but M-PAF age was significantly correlated with cognitive performance (Table 6.9.1). A BHR was used to evaluate null models against alternative models in predicting chronological age and cognitive functioning with PAF age and PLS EEG-age, to judge the levels of evidence in favour of the null (H0) by using established cut-offs (Jeffreys, 1961; Wagenmakers et al., 2011). The default Jeffreys-Zellner-Siow (JZS) prior with an r scale of 0.354 was used due to this being the first time, at the time of writing, that PLS had been used to estimate EEG-age. A BHR comparing a null model including M-PAF age with a second model adding in PLS EEG-age, in attempts to predict QMCI, reported BF01 = 3.51, providing substantial evidence in favour of H0 (Jeffreys, 1961; Wagenmakers et al., 2011) and suggesting M-PAF age is the important predictor of general cognitive functioning. However, there was a notable inconsistency between EEG-age and M-PAF age in that EEG-age was significantly correlated with NART-IQ (r = .43, p < .001), analogous to the correlation between chronological age and NART-IQ (r = .54, p < .001), but M-PAF age was not significantly correlated with NART-IQ (r = .18, p > .05). To explore these inconsistencies further, partial correlations were run between ages and cognitive performance accounting for NART-IQ (Table 6.9.1). M-PAF age remained significantly correlated with cognitive performance, but PLS EEG-age and chronological age were now also significantly negatively correlated with cognitive performance. Notably, there were no significant differences (p > .05) in the strength of the correlations for each method once NART-IQ had been considered (Table 6.9.2). Indeed, a BHR comparing a null model including M-PAF age and NART-IQ with a second model adding in PLS EEG-age, in attempts to predict QMCI, reported BF01 = 2.56, providing only anecdotal evidence in favour of H0. In summary, these results cannot answer which estimate of brain age is the most strongly correlated with general cognitive functioning.

It was also expected that NART-IQ would positively correlate with QMCI, implicating protective processes that support cognitive functioning, such as reserve. Indeed, NART-IQ and QMCI were significantly positively correlated when controlling for chronological age due to the age-NART-IQ bias (r = .26, p = .047). Additionally, mood and number of years in formal education were not significantly correlated with any of the EEG measures (p > .05),

which is not overly surprising considering the relatively low levels of depression and small effect sizes when using years in education as a predictor variable. To end, when controlling for both NART-IQ and chronological age, M-PAF age remained significantly negatively correlated with cognitive performance (r = -.36, p = .005) but PLS EEG-age was not significantly correlated with cognitive performance (r = -.21, p > .05), which suggests that PAF remains the better estimate of age-matched, general cognitive functioning.

Table 6.9.1

Correlations of M-PAF age, PLS EEG-age, and chronological age (CA) with QMCI

	M-PAF	PLS	CA
QMCI	-.41**	-.25	-.18
QMCI (controlled for NART-IQ)	-.45***	-.33*	-.29*

Note. *p < .05; **p < .01; ***p < .001

Table 6.9.2

Differences between correlations of age with QMCI for M-PAF age, PLS EEG-age, and chronological age (CA), when accounting for NART-IQ

	M-PAF	PLS	CA
M-PAF	-		
PLS	-.12	-	
CA	-.16	-.04	-

Note. The values represent the differences between the respective Pearson's *r* correlation coefficients (e.g., M-PAF age – PLS EEG-age); no method proved significantly stronger than any others (p > .05).

6.4 Discussion

Our objective was to use the EEG power-frequency spectrum to estimate chronological age as EEG-age. First, we compared the well-established variants of PAF on their ability to estimate age. Irrespective of the peak-estimation method used, with the methods varying widely in their pre-specified implementation, PAF was consistently negatively correlated with chronological age, which is consistent with previous evidence that suggests an adult's decline in PAF is a normal brain-ageing phenomenon. We also sought to determine which estimate of PAF (M-PAF, C-PAF, K-PAF, or a variant of N-PAF) correlated most strongly and provided the most accurate estimate of chronological age. Although there were no statistically significant differences in the strength of their correlations with age, the different methods produced estimates of PAF that varied substantially. This is unsurprising given the very different assumptions and procedures required in each case, but it does underline the lack of consensus as to how best to estimate PAF. Our recommendation is, that for the sole purpose of estimating chronological age, the M-PAF method is to be preferred, primarily because M-PAF had the lowest expected error (i.e., highest accuracy) out of the PAF-based estimates of chronological age. Also, due to the use of SVD, M-PAF did not require mass, unweighted averaging across electrode channels, and, due to the use of AMs, M-PAF should be able to interrogate and track fine-grained changes in PAF over time better than other methods. Finally, M-PAF was adapted to provide estimates of other periodic and aperiodic components of the EEG power spectrum, several of which showed age-related correlations that suggest a more extensive, complex pattern of age-related changes than solely a decrease in PAF. We also showed that topographical variation in PAF (i.e., W-S variance) was relatively unimportant, although we still conclude it would be sensible to use multiple, well-defined scalp locations that are likely to show clear alpha peaks, reflecting good SNR, to reduce the standard error of the estimated power spectrum.

We then explored the potential of multivariate analyses of the broad EEG spectrum (0.1 to 45 Hz), using PLS as a distinct analytical approach to PAF that has not previously been used to estimate chronological age. Chronological age was estimated with greater accuracy by PLS than PAF, and with stronger correlations between chronological age and estimated brain age than reported with PAF and in previous attempts to operationalise an EEG-age concept (e.g., Al Zoubi et al., 2018; Sun et al., 2019). Additionally, a contrast between alpha and beta1 appeared to be the most age-responsive aspect of the resting-state EEG spectrum, again indicating extensive, complex patterns of age-related change. The main conclusion thus far is that EEG-age, estimated from the broad EEG power spectrum, can estimate chronological age with an expected error of between 13 to 14 years and substantially better than well-established PAF estimates of age (or indeed the ERP and

t_{synch}G estimates of age in previous chapters). This indicates that EEG-age is a more comprehensive measure of the neural synchronization that underpins the EEG signal and thus, potentially, general brain functioning and integrity. As with previous event-related estimates of EEG-age, it remains to be seen whether this resting-state EEG-age is sufficiently accurate to be useful though, particularly at the individual level where the baseline variability in EEG metrics is greater thus making it more difficult to track meaningful change over time than at the group level (Burgess & Gruzelier, 1993). However, the correlation coefficient between chronological age and PLS EEG-age (r = .69) is the same as the correlation coefficient between scores on the NART and WAIS-IV (Bright et al., 2018), which, given that the NART is a clinically useful and well-established tool, suggests our EEG-age metric may have some utility for tracking general brain functioning.

One of the several advantages of using the broad EEG power spectrum to estimate EEG-age is that it removes the need to define frequency band boundaries of interest and eliminates concerns about the number of identifiable peaks. This means that, in contrast to other methods, an estimate of EEG-age can be obtained in all cases, provided sufficient EEG data has been recorded. Furthermore, using SVD with sophisticated multivariate methods further removes the need to implement mass, unweighted averaging across electrode channels and allows for all information in the EEG spectra dataset to be used at the same time. PLS appears to be an effective and efficient method of analysing the power spectrum in the context of ageing research, reducing subjective decision-making during the analysis of EEG data, and providing a more robust estimate of age than the qualitatively distinct PAF-based approach.

Finally, we wanted to examine the relationship of EEG-age with proxy measures of general cognitive integrity. The relationships between PAF, chronological age, and cognitive functioning were already established, but PLS had not previously been used to estimate EEG-age before. There was a robust negative correlation between general cognitive performance and the best PAF age estimate, M-PAF age (i.e., QMCI positively correlated with PAF itself). This is consistent with previous evidence that suggests lower PAF, thus a higher PAF-estimated brain age even with chronological age-matched samples, likely reflects detrimental changes in neural and cognitive integrity (e.g., dedifferentiation and noise as outlined by the deficit models of ageing). PLS EEG-age and chronological age were both significantly negatively correlated with cognitive performance, as could be expected with an ageing sample, only after statistically controlling for NART-IQ. Furthermore, the strengths of the coefficients were not significantly different from that of the correlation between M-PAF age and cognitive performance. Taken together, these results suggest that the significant negative correlations between age and general cognitive performance were

initially masked by the positive correlation between chronological age and premorbid IQ, which is not overly surprising in this sample of healthy adults who displayed QMCI scores in the normal cognitive functioning range – this is the same outcome and explanation as in chapter 4.

Based on the comparisons between PAF and PLS, PLS EEG-age likely incorporates variance from a wider range of age-related processes. This is a reasonable assertion given PLS analyses consider a different type of information, amplitude from across the EEG power spectrum rather than an isolated alpha-band peak frequency, and, thus, provide a better estimate of chronological age compared to PAF. We know that the EEG power spectrum is a marker of the mass-synchronised action of cortical neurones (Lopes da Silva, 2013) and thus could provide insights into deleterious age-related conditions from a general, system-level perspective (Koenig et al., 2020). Therefore, in a similar way to how ERP components and $t_{synch}G$ were compared, a subset of early neural developments that are damaging to general fluid cognitive functioning (e.g., decreased QMCI), or potentially indicative of future degradation once reaching a critical point, might be spotted and tracked via PAF (e.g., reflecting the deficit model of ageing, such as a transition to wider, less specialised neural networks). In contrast, PLS likely provides a more comprehensive insight into general brain functioning that may reflect both protective (e.g., reserve, benefit model) and deleterious (e.g., dedifferentiation and noise, deficit model) changes in the form of general crystallised and fluid cognition.

The findings of this study should now be confirmed in samples where there is no age-NART-IQ bias, and where QMCI scores are not restricted to the normal cognitive functioning range. Indeed, a limitation of this study is that the sample was not representative of the general population in the UK, let alone elsewhere across the globe. The sample was, on average, less ethnically diverse and more intelligent than normative data, and, as discussed already, this difference in intelligence was particularly marked in older adults. Furthermore, this study purposely followed a general approach to the measurement (QMCI and NART) and interpretation (Koenig et al., 2020) of neural and cognitive integrity, but future studies could measure specific subcategories of fluid and crystallised intelligence (e.g., Ociepka et al., 2023). The proxy measures used in this study were not intended to be exhaustive but to provide a starting point in the interrogation of general brain functioning and cognitive functioning with EEG-age.

Similarly, future studies could provide a systematic, thorough comparison of the different approaches to estimating the PAF and PLS measures. This could include the wide array of different analytical approaches to elucidate specific mechanisms and concrete

reasons for the differences observed within and between PAF and PLS EEG-age. This could also include approaches not covered here, such as other spectral parameterisation algorithms like 'specparam' that may provide a better representation of the non-oscillatory contents of the EEG (Donoghue et al., 2020). This comparison of technical differences would take us a step closer to confirming whether the PLS EEG-age estimate outperforms the PAF-age estimate simply because it uses more data from the EEG spectrum. It might be, for example, that the difference is due to the method of spectral analysis used. That said, our current analyses indicate that the method of spectral analysis, smoothing, and agglomeration made relatively little difference to the PAF-age correlation, which would suggest that the PLS-age correlation is stronger than the PAF-age correlation because PLS uses more information from the EEG-spectrum. In summary, it will be necessary to establish good, large-scale normative data that makes it possible to estimate the EEG-age of individuals across the entire human lifespan, not just adulthood, with high reliability, validity, and precision. This would facilitate the identification of individuals with unusual discrepancies between their EEG-age and the normative EEG-age for their chronological age and condition.

Whilst the idea of using EEG-age as an early-detection biomarker is not new (e.g., Al Zoubi et al., 2018; Sun et al., 2019), our approach to estimating EEG-age already has advantages over previous attempts. We are proposing a specific EEG measure that is simple, quick, relatively cheap, and safe to collect. It requires no behavioural input or active effort from the participant, aside from staying still and awake, and is a relatively objective and stable measurement. It also reduces several subjective analytical decisions on the part of the researcher. Additionally, our study has incorporated a more age-balanced sample of exclusively healthy adults compared to previous approaches to examining EEG-age (e.g., Matoušek & Petersén, 1973; Wackermann & Matoušek, 1998). In summary, although our EEG-age metric has advantages over many of the traditional neuroimaging methodologies and neuropsychological measures, there is a long way to go before it can be used in a clinical setting. That said, we posit that incorporating an optimised version of our EEG-age metric, comprising even simpler, accessible data collection (e.g., fewer EEG electrodes) and robust, reliable analysis (e.g., an automated procedure), would augment these scores and enable detection at an earlier stage (Koenig et al., 2020). As part of optimising EEG-age, it would also be worthwhile to examine the aperiodic 1/f gradient in greater detail and incorporate the most extreme ends of the EEG spectrum, particularly low frequencies (< 0.01 Hz), as this would likely improve the ability of EEG-age to estimate chronological age.

In summary, the three broad aims of this thesis were, 1) to advance our understanding of event-related and resting-state EEG and MEG, 2) to advance our

understanding of age-related changes in the brain with EEG and MEG, and 3) to establish EEG and MEG metrics that have the potential to track those age-related changes over time. This chapter has advanced our understanding of resting-state EEG and the changes seen across the broadband frequency range in healthy ageing, whilst also proposing M-PAF and EEG-age as potential ways to track age-related changes over time. Specifically, we have reported, for the first time, that chronological age was estimated with greater accuracy by a multivariate PLS analysis of the broad EEG power-frequency spectrum (0.1 to 45 Hz) than by PAF. Whilst a restricted sample of healthy adults with a chronological age-NART-IQ bias has limited the scope of the current conclusions, and a thorough comparison of the technical differences within and between the calculations of PAF- and EEG- ages would be valuable, we propose that EEG-age could be refined into a biomarker for neural and cognitive integrity. A discrepancy between resting-state EEG-age and chronological age could prove clinically informative by implicating protective or deleterious age-related change earlier than previously possible.

Chapter 7: General discussion

7.1 An overview of the main findings of this PhD thesis

There were three broad aims of this PhD thesis, which could be achieved concurrently; namely, 1) to advance our understanding of event-related and resting-state EEG and MEG, 2) to advance our understanding of age-related changes in the brain with EEG and MEG, and 3) to establish EEG and MEG metrics that have the potential to track those age-related changes over time. As a summary of the experimental findings presented through chapters 3-6, Chapter 3 provided new empirical support for the FM and its cross-frequency phase modulation mechanism that had been posited to explain event-related changes in the EEG. There are residual unanswered questions, but in its current form the FM provides a very credible account of evoked and induced changes. Certainly, it was convincing enough for application under the principle that all models are wrong, but some are useful. Chapter 4 successfully applied the FM in an ageing context, advancing our understanding of the deep structure of age-related changes in event-related EEG. In turn, Chapter 5 applied the FM in MEG for the very first time and confirmed that the FM could explain event-related changes in the MEG. Overall, chapters 4 and 5 provided further novel empirical evidence that validate the FM and advance our understanding of the ageing human brain, but they too left residual unanswered questions. Particularly pertaining to the meaning of $t_{synch}G$ and its current SNR; it is yet unknown how much of the findings with $t_{synch}G$ can be accounted for by suboptimal SNR as opposed to meaningful age-related changes. In turn, it is unknown whether the reported accuracy of EEG-age is good enough to be useful. Consequently, future research should prioritise optimising the methodological and analytical pipelines underpinning the estimation of $t_{synch}G$, as a prerequisite to establishing EEG-age in the clinic and wider community as a metric that can be used to detect and track deleterious age-related changes. Finally, Chapter 6 extended the hunt for novel brain age metrics to a resting-state paradigm, which proved successful in advancing our understanding of the resting-state, ageing brain. However, there is again residual uncertainty around whether the reported EEG-age is an accurate enough predictor of chronological age to be useful.

As the final analytical contribution to this thesis, a multiple regression analysis was performed comprising a combination of M-PAF, PLS EEG-age and AO-$t_{synch}G$ metrics taken from the same EEG dataset outlined and analysed in Chapters 3, 4, and 6. It produced a significant predictive model ($p < .001$) that accounted for 50% of the variance in age ($r = .72$; *RMSE* = 12.19); specifically, PLS EEG-age and AO-$t_{synch}G$ were significant individual predictors (*ps* < .05*)*, but M-PAF was not ($p > .05$). Taking this one step further to include the

best performing P3b peaks, hierarchical regression was run. First, alongside PLS EEG-age, adding AO-t_{synch}G (F(1,54) = 7.63, p < .01, *adjR2 change* = 0.07) significantly improved the overall model, F(2,54) = 28.51, p < .001, *adjR2* = 0.50, *RMSE* = 12.19, r = .72. Adding M-PAF did not improve the model (F(1,53) = 0.23, p > .05, *adjR2 change* = -0.01), nor did adding P3b SVD peak latency improve the model (F(1,53) = 0.23, p > .05, *adjR2 change* = 0.01). This can be interpreted as t_{synch}G already accounting for the latency component. To end, adding P3b SVD peak amplitude (F(1,53) = 7.63, p < .01, *adjR2 change* = 0.08) significantly improved the model, F(3,53) = 25.52, p < .001, *adjR2* = 0.57, RMSE = 11.18, r = .77. Therefore, the best predictive model, estimating chronological age to just over a decade and accounting for 57% of the variance in chronological age, came when using an EEG-age (i.e., 'brain age') metric that was estimated from all three predictors of PLS EEG-age, AO t_{synch}G, and P3b SVD peak amplitude (i.e., here termed 'modelled EEG-age').

Overall, it remains to be seen whether EEG-age is sufficiently accurate to be useful, particularly at the individual level where the baseline variability in EEG metrics is substantial thus making it more difficult to track meaningful change over time than at the group level (Burgess & Gruzelier, 1993). However, the correlation coefficient between chronological age and PLS EEG-age (r = .69; outlined and discussed in Chapter 6) was already the same as the correlation coefficient between scores on the NART and WAIS-IV (Bright et al., 2018), which, given that the NART is a clinically useful and well-established tool, suggested our EEG-age metric may have some utility for tracking general brain functioning. The correlation coefficient between modelled EEG-age and chronological age (r = .77) is now greater than that for NART and WAIS-IV; this is very promising given the need to further optimise methodology and analytical pipelines as well (Chronological age distribution: M = 49 years, SD = 17.87, *Range* = 20 to 78; Modelled EEG-age distribution: M = 49 years, SD = 13.54, *Range* = 22 to 78). Figure 7.1 provides a scatterplot to visualise the strong positive relationship between modelled EEG-age (comprising PLS EEG-age, AO t_{synch}G, and P3b SVD peak amplitude metrics) and chronological age.

Figure 7.1

A scatterplot visualisation of the strong positive linear relationship between chronological age and modelled EEG-age (r = .77, p < .001), with modelled EEG-age comprising PLS EEG-age, AO $t_{synch}G$, and P3b SVD peak amplitude metrics from chapters 4 and 6.

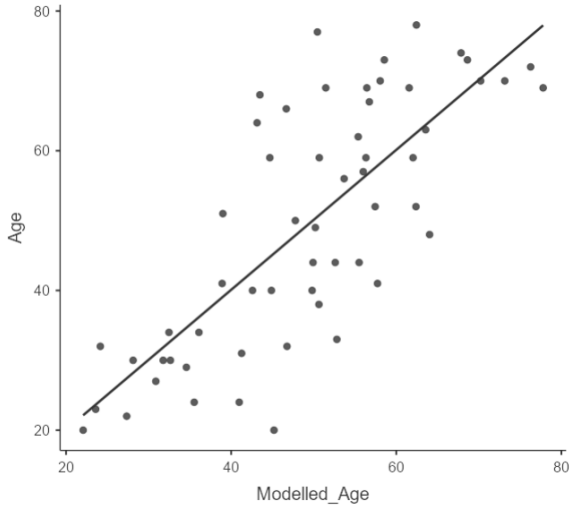

7.2 A look into the future of EEG-age and MEG-age

There is substantial scope for future research projects to build on the foundations set by this thesis, particularly enhancing the SNR of the established metrics underpinning our brain age estimate. This subsection will propose potential targets for future research, but this is not an exhaustive list.

First, EMD can be further refined as an analytical approach for estimating $t_{synch}G$. For example, there are alternative versions of EMD that have been proposed for the purpose of improving the SNR of IMFs, such as Multivariate EMD (Rehman & Mandic, 2010) and Ensemble EMD (Wu & Huang, 2009). Ensemble EMD is a noise-assisted version that performs iterative decomposition over multiple copies of the original signal with added white Gaussian noise, intending to triangulate the decompositions on the true underlying oscillatory functions. Ensemble EMD can produce IMFs that are purported to be less noisy and less liable to mode mixing from both noise and frequency band overlap (Colominas et al., 2014). Furthermore, optimisations are being made to the ensemble EMD algorithm to further reduce issues arising from signal intermittency (e.g., residual noise in IMFs and early modes that often require discarding). These optimisations have been shown to provide superior separation of the IMFs whilst reducing computational load and providing a more complete, cleaner set of decompositions (Al-Baddai et al., 2017; Calvo & Lee, 2024). EMD as an analysis tool is also becoming far more accessible, owing to the release of open-access toolboxes in software such as MATLAB (e.g., EMDLAB is a plug-in extension for

EEGLAB; Al-Subari et al., 2015). These toolboxes may see an increased use and thus further optimisation of EMD as an analysis method of choice in EEG and MEG studies.

Alongside optimising EMD, the modelling procedure used to estimate $t_{synch}G$ could be optimised. For example, an optimisation of the time windows of interest for identifying t_{synch} per IMF, as is already the case for ERP components (Luck, 2014), would be beneficial in reducing early or late outliers that hijack the estimate of t_{synch} and thus bias $t_{synch}G$. This optimisation is also a prerequisite for using area and fractional measures instead of peaks, which could also improve SNR. For example, we could use the fractional area latency of the PLV data per IMF to calculate t_{synch}. This would involve computing the area under the PLV waveform over an accurate, defined latency range, before finding the time point (i.e., t_{synch}) that divides that area into a prespecified fraction (e.g., one-half, called 50% area latency). Fractional area latency has already been shown to improve the SNR of ERP metrics compared to peak estimates (Kiesel et al., 2008), so could support better estimates of t_{synch} and thus $t_{synch}G$. This optimisation could be combined with implementing higher sampling rates and low-pass filters, which could allow for more IMFs but also more downsamples, thus more t_{synch} data points contributing to $t_{synch}G$ and, again, a lesser impact of outliers. In summary, a more robust modelling procedure would help us to disentangle suboptimal SNR from age-related changes when interpreting changes in $t_{synch}G$.

The proposed optimisations to EMD, estimation of t_{synch}, and modelling of $t_{synch}G$ could be combined with further optimisations to data pre-processing. In EEG, a minimalistic approach of combining interpolation of noisy channels alongside refined filtering seems to be optimal (De Cheveigne et al., 2019; Delorme, 2023). However, physiological noise that often disproportionately impacts high frequency such as gamma, including EOG but also muscle and heart artefacts, could be measured and statistically accounted for in more sophisticated ways than Gratton or trial rejection (e.g., Croft & Barry, 2000a, 2000b; Uriguen & Garcia-Zapirain; cf. Delorme, 2023). This would go together with testing more impactful, holistic data cleaning tools like independent components analysis (ICA) and wavelet denoising (WD), which split the complex oscillations into discrete coefficients for removal prior to a reconstruction of the signal. However, these more sophisticated data cleaning tools may rely too much on user input, particularly in clinical settings, and can be detrimental to brain data, potentially including phase, if not used in a careful and considered manner (e.g., Delorme, 2023; Grobbelaar et al., 2022; Montefusco-Siegmund et al., 2013; Thatcher, 2012). When it comes to MEG, greater examination of the impacts of the wide array of interference suppression tools (e.g., SSS vs tSSS) would be beneficial to build on the foundation set by Chapter 5. However, it needs to be remembered that the more sophisticated the procedures get, the harder it becomes to apply them practicably in clinical and community settings.

Improving the SNR of IMFs, particularly high frequency components, could not only improve $t_{synch}G$ estimates but also allow us to better distinguish potential endogenous versus exogenous aspects of the EEG and MEG signals (Polich, 2007). Early exogenous activity, also termed evoked potentials, has historically been interpreted as distinct from event-related potentials, with suggestions that perhaps they are better accounted for by EMs than PRMs (e.g., Jervis et al., 1983; Mazaheri & Jensen, 2006, 2008). Better measurement of the changes in early, high-frequency IMFs would help us to examine these proposals and test their limits in the context of the FM and its explanatory mechanism. These efforts could be further supported by using additional sensors from further optimised ROIs per condition and task, across a range of different paradigms with a range of sensory and task demands. For example, low, medium and high task demands across different senses and cognitive faculties, such as simple auditory stimulation, versus attentional oddball, sustained attention to response, go/no-go, and memory recognition tasks, but also longer resting state recordings to interrogate a wider frequency range. In turn, this could also elucidate whether age-related changes are indeed clearer in tasks with harder task demands, as per the CRUNCH theory of ageing (e.g., Cappell et al., 2010; De Felice & Holland, 2018; Reuter-Lorenz & Cappell, 2008).

SVD was used in the current study as a method of improving SNR, providing a weighted average over the electrode ROIs, and reducing computational load by data reduction. The use of SVD could be further optimised in future, as there are a range of different approaches to implementing SVD that could be formally compared in the context of estimating EEG-age (Falini, 2022); for example, there are several approaches for determining the amount of variance thus components to retain for the reconstruction of the signal. These alternative approaches include visualising the variance accounted for by each component and identifying the knee-bend, or using a majority of variance single component heuristic, or a between 70-90% of variance multicomponent heuristic, or a more sophisticated statistical approach based on the likes of permutation testing to determine a confidence interval threshold for the variance thus components to retain. Alternatively, SVD could be avoided and analysis performed by treating the ROI electrodes as unweighted per participant (i.e., traditional averaging) or by incorporating a multivariate approach (e.g., PLS or mixed effect models). Therefore, research could compare these alternatives, but the downside here is that EMD is computationally heavy and takes a long time without some sort of data reduction (Sweeney-Reed & Nasuto, 2007; Sweeney-Reed et al., 2018).

It would also be worthwhile to interrogate the reliability of t_{synch} and $t_{synch}G$ (e.g., analogous to Burgess & Gruzelier, 1993, and Mcevoy et al., 2000, who reported on the reliability of other EEG metrics). For example, tracking participants' IMFs and $t_{synch}G$ over

time in a longitudinal study with short, medium, and long timepoint checks. At the same time, an interrogation of intra-individual variability of IMFs and $t_{synch}G$ is advised, similar to previous interrogations of how age-related changes in latency variability may underpin changes in other cognitive and neurophysiological metrics. That said, underlying SNR must be improved first.

Moving beyond $t_{synch}G$, there are a range of alternative metrics that the analytical approaches used to test the FM offers to an interested researcher. For example, individual IMFs' t_{synch} could be examined in more detail, particularly if interested in the perspective that the deficit ageing process likely starts at or pivots around a particular IMF(s). There may then be wider grand changes in later life or after certain deleterious age-related changes and/or conditions emerge. This focus on discrete IMFs/t_{synch} would be analogous to examining discrete peaks of ERP components, but with the added value of having the instantaneous frequency data to match alongside to see how they both change with age (e.g., task demands, cognitive integrity, arousal). Alternative measures of general cognitive performance (e.g., see Apostolo et al., 2016) and pre-morbid IQ, also known as fluid and crystallised intelligence (e.g., see Bright & Van der Linde, 2020, and O'Carroll, 2008), could be incorporated at the same time. Or indeed, a focus on more specific types of cognition (e.g., Ociepka et al., 2022, 2023). Thereafter, any links in PLV and instantaneous frequency between different IMFs could be examined with methods like Granger Causality (Granger, 1969), which employs lagged cross-correlations to see whether earlier changes in the initial IMFs statistically forecast later IMFs' changes. That said, this would require a revised approach to examining full head sensor arrays rather than the ROIs that have historically been employed for optimising the SNR of discrete ERP components or ERS/ERD in discrete frequency bands (e.g., Luck, 2014).

Running EEG recordings in a shielded room, such as a Faraday cage, would also aid SNR. But this could be taken further to implementing multimodal MEG-EEG to provide additional insights into cross-neurophysiological event-related changes and resting-state brain activity. This approach would allow for experimental triangulation over time and potentially lead to greater SNR (e.g., Babiloni et al., 2004). At the same time as multimodal imaging, further refinements to the methodology could be made, such as longer time windows (to provide a better perspective on later IMFs/lower frequencies) and more trials that are designed in a way to maximise the SNR per participant (e.g., as outlined for the oddball paradigm in Luck, 2014, Polich, 1996, and Duncan et al., 2009). Consideration of how to apply these approaches in source space rather than solely sensor space could follow, not only to compare differences between the approaches but also in the hopes of improving SNR. For example, we could apply EMD on the virtual electrodes in MEG

(Stapleton-Kotloski et al., 2018). However, there is a wide array of different approaches to implementing source localisation, and it is not confirmed how each approach may affect the phase relations seen in sensor space (Delorme, 2023; Montefusco-Siegmund et al., 2013; Thatcher, 2012). That said, examination of lagged frequency and phase relations across the entire scalp whilst also mapping source activity could be very informative if practicable (Alexander et al., 2013; Klimesch, 2018; Woolnough et al., 2022), such as providing a visualisation of ERP as a travelling wave that decreases in frequency as it spreads across the cortex. In future, optically pumped magnetometers (OPMs) may also provide an alternative, more participant-friendly version of MEG (e.g., MEG sensor arrays that are worn on the head like EEG caps, thus the sensors are closer to the signal source), but there is a way to go before OPMs will have sufficient interference suppression techniques to realise the potential for increased SNR and are widely accessible for research let alone clinical contexts (Seymour et al., 2022). However, there is an important distinction to be made between optimisations in an academic environment, supporting proof-of-principle research, versus optimisations for an applied clinical or even community environment. In applied environments, we would want robust recordings from a minimal number of cheap, easily applied electrodes and simple tasks or resting state paradigms with automated analysis pipelines. As noted earlier, the more sophisticated the procedures get, both methodologically and analytically, the harder it becomes to apply them practicably.

Future research should also recruit a wider number and diversity of samples from healthy, subclinical and clinical ageing populations, whilst also controlling for factors such as pre-morbid IQ (i.e., cognitive reserve) and cognitive performance levels (i.e., varying amounts of ageing deficits). This would enable researchers to determine whether an age-discrepancy score is useful at an early stage of disease and reflects specific problems (e.g., acting as a reliable diagnostic test for Alzheimer's disease) or a general pre-condition brain state that is indicative of a range of potential pathologies. Therefore, as noted, it will be necessary to recruit participants with specific age-related conditions, such as SCI (Reisberg et al., 2010; Stewart, 2012; Yue et al., 2021), MCI (Davis et al., 2018; Gauthier et al., 2006; Geslani et al., 2005; Ritchie, 2004), and established dementia, of varying aetiologies, to determine the practical utility of an age-discrepancy score. In a similar vein, examination of the impact of early life maturational processes (i.e., <18 years) and late life degradation processes (i.e., >80 years) on $t_{synch}G$ would be useful, as it may reveal accentuated or even entirely distinct changes. But again, SNR would still need to be improved in parallel, to disentangle the effects of suboptimal SNR from meaningful age-related changes.

Finally, we could stress test the FM and brain age estimates by exploring the effects of brain stimulation. Variable effects on event-related EEG have been reported so far with a

range of stimulation parameters and sites, using both transcranial magnetic stimulation, TMS that stimulates or inhibits neuronal firing (Chung et al., 2015; Rego et al., 2012), and transcranial alternating current stimulation, tACS that entrains or modulates ongoing oscillations (Feher et al., 2017; Popp et al., 2019). Plasticity-focused TMS or tACS could be applied in attempts to causally alter event-related activity, such as t_{synch}. For example, if brain stimulation were to affect t_{synch}G in alignment with age-related ERP effects (e.g., flatter gradient with delayed latency; Bersani et al., 2015; Rego et al., 2012), it would help to further validate the FM and explain age-related changes in the brain, whilst perhaps even allowing improved mechanistic links to cognitive performance thereafter by asking the question of which brain activity is necessary for normal cognitive performance.

Moving beyond the FM to end, there is a need for a deeper interrogation of potential amplitude changes in event-related EEG and MEG, given the FM cannot account for changes in amplitude between pre-stimulus and post-stimulus periods. The FM will likely need to be amalgamated with other explanatory models and mechanisms to fully explain the complexity of EEG and MEG, in and out of an ageing context. Related to explaining changes and differences in amplitude between conditions or groups, future research should further interrogate the relationship between oscillatory and non-oscillatory activity and their age-related changes, particularly 1/f noise that may well partly explain changes in power (Donoghue et al., 2021; Merkin et al., 2023; Voytek, 2015b). Aperiodic activity was partially considered in Chapter 6, but it can be modelled in several distinct ways, with defined alternatives in the likes of the ‘specparam’ algorithm (Donoghue et al., 2020). Like the variety of PAF estimates that do not well align, the exact underlying model of the aperiodic activity - the 1/f gradient in particular - remains contentious, so we could model several different approaches alongside oscillatory measures in attempts to estimate brain age.

7.3 The overall conclusions of this PhD thesis

With an ageing global population, the number of older adults with deleterious age-related changes in the brain, including dementia, will continue to increase unless we can make progress in the early detection and treatment of such conditions. This thesis has presented a set of research projects that have used EEG and MEG to advance our understanding of oscillatory dynamics in the ageing human brain. First, the Firefly Model (FM) of short-term, event-related oscillatory dynamics was tested. The FM offered an empirically credible, alternative explanation of information processing that relies on systematic oscillatory phase synchronisation and frequency slowing. Second, inspired by the aphorism, ‘All models are wrong, but some are useful’, the FM was used to develop a new phase-based metric – time of synchronisation gradient, tsynchG – for tracking age-related changes in the brain. This tsynchG metric was established as a new EEG-estimate of brain

age, with EEG-age significantly correlating with chronological age, before being estimated in MEG for the first time. Thereafter, long-term, resting-state oscillatory dynamics were examined, with peak alpha frequency (PAF) and alternative amplitude-based EEG-age estimates examined as distinct methods of tracking age-related changes in the brain. Using multivariate methods to analyse the broad EEG power spectrum (0.1 to 45 Hz), the resting-state EEG-age and chronological age were also correlated strongly, and EEG-age was a more accurate estimate and accounted for more variance in chronological age than well-established PAF estimates of age.

In summary, this thesis has introduced new metrics as estimates of 'brain age', framed as markers of general brain functioning that have the potential to detect and track deleterious age-related changes over time. In doing so, this thesis has also offered novel contributions that advance our understanding of event-related and resting-state EEG and MEG, and in turn our understanding of age-related changes in oscillatory dynamics of the human brain. There is significant scope for research projects to build on these foundations. For example, our vision for the future is a reliable, valid, and precise estimate of EEG-age for comparison with chronological age. Therefore, future research needs to focus on refining the methodology and analytical pipelines to maximise SNR of the metrics underpinning estimates of brain age, particularly at the individual level, before applying them beyond healthy ageing. Thereafter, there is hope that EEG-age and MEG-age can be compared with actual chronological age and any discrepancy between the metrics might reflect some age-related condition, based on either protective or deleterious changes in the brain. When it comes to practical application of this brain age metric, EEG is certainly one of the most accessible neuroimaging tools, and it has clear potential for the much sought-after early detection of deleterious changes in the brain, in part due to its outstanding temporal resolution. However, a serious question mark remains over whether EEG can provide a sufficiently accurate brain age estimate to enable a clinically informative comparison with chronological age. There is a long way to go yet, but this thesis offers a promising step in the right direction; towards answering the Alzheimer's Society's (2024a) call for more screening to detect and track deleterious age-related conditions earlier, accurately, and in an accessible way. One hundred years after Hans Berger's first successful EEG recording, it is fair to say that EEG in the year 2024 still offers an irresistible 'window on the mind' and is full of untapped potential.

List of references

Al-Baddai, S., Al-Subari, K., Lang, E., & Ludwig, B. (2017). Optimising approach for sifting process to solve a common type of empirical mode decomposition mode mixing. *International Scholarly and Scientific Research & Innovation, 11*(6), 649-652. https://www.researchgate.net/publication/317845622_Optimizing_Approach_for_Sifting_Process_to_Solve_a_Common_Type_of_EMD_Mode_Mixing

Al-Subari, L., Al-Baddai, S., Tome, A. M., Goldhacker, M., Faltermeier, R., & Lang, E. W. (2015). EMDLAB: A toolbox for analysis of single-trial EEG dynamics using empirical mode decomposition. *Journal of Neuroscience Methods, 253*, 193-205. https://doi.org/10.1016/j.jneumeth.2015.06.020

Al Zoubi, O., Ki Wong, C., Kuplicki, R. T., Yeh, H-W., Mayeli, A., Refai, H., Paulus, M., & Bodurka, J. (2018). Predicting age from brain EEG signals: A machine learning approach. *Frontiers in Aging Neuroscience, 10*, 184. https://doi.org/10.3389/fnagi.2018.00184

Alexander, D. M., Jurica, P., Trengove, C., Nikolaev, A. R., Gepshtein, S., Zvyagintsev, M., Mathiak, K., & Schulze-Bonhage, A., Ruescher, J., Ball, T., & Van Leeuwen, C. (2013). Traveling waves and trial averaging: The nature of single-trial and averaged brain responses in large-scale cortical signals. *NeuroImage, 73*, 95-112. https://doi.org/10.1016/j.neuroimage.2013.01.016

Alin, A., Kurt, S., McIntosh, A. R., Oniz, A., & Ozgoren, M. (2009). Partial least squares analysis in electrical brain activity. *Journal of Data Science, 7*(1), 99-110. https://doi.org/10.6339/JDS.2009.07(1).434

Alzheimer's Society. (2024a). *The economic impact of dementia: module 1*. https://www.alzheimers.org.uk/sites/default/files/2024-05/the-annual-costs-of-dementia.pdf

Alzheimer's Society. (2024b). *The economic impact of dementia: module 4*. https://www.alzheimers.org.uk/sites/default/files/2024-09/Modelling-impacts-early-diagnosis.pdf

Angelakis, E., Lubar, J. F., & Stathopoulou, S. (2004a). Electroencephalographic peak alpha frequency correlates of cognitive traits. *Neuroscience Letters, 371*(1), 60-63. https://doi.org/10.1016/j.neulet.2004.08.041

Angelakis, E., Lubar, J. F., Stathopoulou, S., & Kounios, J. (2004b). Peak alpha frequency: An electroencephalographic measure of cognitive preparedness. *Clinical Neurophysiology, 115*(4), 887-897. https://doi.org/10.1016/j.clinph.2003.11.034

Apostolo, J., Holland, C., O'Connell, M. D. L., Feeney, J., Tabares-Seisdedos, R., Tadros, G., Campos, E., Santos, N., Robertson, D. A., Marcucci, M., Varela-Nieto, I., Crespo-Facorro, B., Vieta, E., Navarro-Pardo, E., Selva-Vera, G., Balanza-Martinez, V., & Cano, A. (2016). Mild cognitive decline: A position statement of the Cognitive Decline Group of the European Innovation Partnership for Active and Healthy Ageing (EIPAHA). *Maturitas, 83*, 83-93. https://doi.org/10.1016/j.maturitas.2015.10.008

Aron, L., Zullo, J., & Yankner, B. A. (2022). The adaptive aging brain. *Current opinion in neurobiology, 72*, 91-100. https://doi.org/10.1016/j.conb.2021.09.009

Aurlien, H., Gjerde, I. O., Aarseth, J. H., Eldøen, G., Karlsen, B., Skeidsvoll, H., & Gilhus, N. E. (2004). EEG background activity described by a large computerized database. *Clinical Neurophysiology, 115*(3), 665-673. https://doi.org/10.1016/j.clinph.2003.10.019

Babiloni, C., Arakaki, X., Azami, H., Bennys, K., Blinowska, K., Bonanni, L., Bujan, A., Carrillo, M. C., Cichocki, A., de Frutos-Lucas, J., Percio, C. D., Dubois, B., Edelmayer, R., Egan, G., Epelbaum, S., Escudero, J., Evans, A., Farina, F., Fargo, K., . . . Guntekin, B. (2021). Measures of resting state EEG rhythms for clinical trials in Alzheimer's disease: Recommendations of an expert panel. *Alzheimer's & Dementia, 17*(9), 1528-1553. https://doi.org/10.1002/alz.12311

Babiloni, F., Babiloni, C., Carducci, F., Romani, G. L., Rossini, P. M., Angelone, L. M., & Cincotti, F. (2004). Multimodal integration of EEG and MEG data: a simulation study with variable signal-to-noise ratio and number of sensors. *Human Brain Mapping, 22*(1), 52-62. https://doi.org/10.1002/hbm.20011

Babiloni, C., Vecchio, F., Lizio, R., Ferri, R., Rodriguez, G., Marzano, N., Frisoni, G. B., & Rossini, P. M. (2011). Resting state cortical rhythms in Mild Cognitive Impairment and Alzheimer's disease: Electroencephalographic evidence. *Journal of Alzheimer's Disease, 26*(s3), 201-214. https://doi.org/10.3233/JAD-2011-0051

Barry, R. J. (2009). Evoked activity and EEG phase resetting in the genesis of auditory Go/NoGo ERPs. *Biological Psychology, 80*(3), 292-299. https://doi.org/10.1016/j.biopsycho.2008.10.009

Barry, R. J., & De Blasio, F. M. (2017). EEG differences between eyes-closed and eyes-open resting remain in healthy ageing. *Biological Psychology, 129*, 293-304. https://doi.org/10.1016/j.biopsycho.2017.09.010

Basar, E. (1999). *Brain functions and oscillations, principles and approaches.* Springer.

Bates, P. B., & Lindenberger, U. (1997). Emergence of a powerful connection between sensory and cognitive functions across the adult life span: A new window to the study of cognitive aging? *Psychology and Aging, 12*(1), 12-21. https://doi.org/10.1037//0882-7974.12.1.12

Batterham, P. J., Bunce, D., Mackinnon, A. J., & Christensen, H. (2014). Intra-individual reaction time variability and all-cause mortality over 17 years: A community-based cohort study. *Age and Ageing, 43*(1), 84-90. https://doi.org/10.1093/ageing/aft116

Bell, K. L., Lister, J. J., Conter, R., Bush, A. L. H., & O'Brien, J. (2021). Cognitive event-related potential responses differentiate older adults with and without probable mild cognitive impairment. *Experimental Aging Research, 47*(2), 145-164. https://doi.org/10.1080/0361073X.2020.1861838

Bells, S., Lefebvre, J., Prescott, S. A., Dockstader, C., Bouffet, E., Skocic, J., Laughlin, S., & Mabbott, D. J. (2017). Changes in white matter microstructure impact cognition by disrupting the ability of neural assemblies to synchronize. *Journal of Neuroscience, 37*(34), 8227-8238. https://doi.org/10.1523/JNEUROSCI.0560-17.2017

Bennington, J. Y., & Polich, J. (1999). Comparisons of P300 from passive and active tasks for auditory and visual stimuli. *International Journal of Psychophysiology, 34*(2), 171-177. https://doi.org/10.1016/S0167-8760(99)00070-7

Berger, H. (1929). Uber das elektrenkephalogramm des menschen. *Archiv fur Psychiatrie und Nervenkrankheiten, 87*, 527-570. https://doi.org/10.1007/BF01797193

Berger, A., & Kiefer, M. (2021). Comparison of different response time outlier exclusion methods: A simulation study. *Frontiers in Psychology, 12*, 675558. https://doi.org/10.3389/fpsyg.2021.675558

Bersani, F. S., Minichino, A., Fattapposta, F., Bernabei, L., Spagnoli, F., Mannarelli, D., Francesconi, M., Pauletti, C., Corrado, A., Vergnani, L., Taddei, I., Biondi, M., & Chiaie, R. D. (2015). Prefrontocerebellar transcranial direct current stimulation increase amplitude and decreases latency of P3b component in patients with euthymic bipolar disorder. *Neuropsychiatric Disease and Treatment, 11*, 2913-2917. https://doi.org/10.2147/NDT.S91625

Bland, J. M., & Altman, D. G. (1986). Statistical methods for assessing agreement between two methods of clinical measurement. *The Lancet, 327*(8476), 307-310. https://doi.org/10.1016/S0140-6736(86)90837-8

Bornkessel, I. D., Fiebach, C. J., Friederici, A. D., & Schlesewsky, M. (2004). "Capacity" reconsidered: Individual differences in language comprehension and individual alpha frequency. *Experimental Psychology, 51*(4), 279-289. https://doi.org/10.1027/1618-3169.51.4.279

Boyle, R., Knight, S. P., de Looze, C., Carey, D., Scarlett, S., Stern, Y., Robertson, I. H., Kenny, R. A., & Whelan, R. (2021). Verbal intelligence is a more robust cross-sectional measure of cognitive reserve than level of education in healthy older adults. *Alzheimer's Research & Therapy, 13*, 128. https://doi.org/10.1186/s13195-021-00870-z

Bright, P., Hale, E., Gooch, V. J., Myhill, T., & van der Linde, I. (2018). The National Adult Reading Test: Restandardisation against the Wechsler Adult Intelligence Scale-Fourth edition. *Neuropsychological Rehabilitation, 28*(6), 1019-1027. https://doi.org/10.1080/09602011.2016.1231121

Bright, P., Jaldow, E., & Kopelman, M. D. (2002). The National Adult Reading Test as a measure of premorbid intelligence: A comparison with estimates derived from demographic variables. *Journal of the International Neuropsychological Society, 8*(6), 847-854. https://doi.org/10.1017/S1355617702860131

Bright, P., & Van der Linde, I. (2020). Comparisons of methods for estimating premorbid intelligence. *Neuropsychological Rehabilitation, 30*(1), 1-14. https://doi.org/10.1080/09602011.2018.1445650

Bruns, A. (2004). Fourier-, Hilbert- and Wavelet-based signal analysis: Are they really different approaches? *Journal of Neuroscience Methods, 137*(2), 321-332. https://doi.org/10.1016/j.jneumeth.2004.03.002

Burgess, A. P. (2012). Towards a unified understanding of event-related changes in the EEG: The Firefly Model of synchronisation through cross-frequency phase modulation. *PLoS ONE, 7*(9), e45630. https://doi.org/10.1371/journal.pone.0045630

Burgess, A. P. (2019). How conventional visual representations of time-frequency analyses bias our perception of EEG/MEG signals and what to do about it. *Frontiers in Human Neuroscience, 13*, 212. https://doi.org/10.3389/fnhum.2019.00212

Burgess, A., & Gruzelier, J. (1993). Individual reliability of amplitude distribution in topographical mapping of EEG. *Electroencephalography and Clinical Neurophysiology, 86*(4), 219-223. https://doi.org/10.1016/0013-4694(93)90101-Z

Button, K. S., Ioannidis, J. P. A., Mokrysz, C., Nosek, B. A., Flint, J., Robinson, E. S. J., & Munafo, M. R. (2013). Power failure: why small sample size undermines the reliability of neuroscience. *Nature Reviews Neuroscience, 14*(5), 365-376. https://doi.org/10.1038/nrn3475

Buzsaki, G., & Draguhn, A. (2004). Neuronal oscillations in cortical networks. *Science, 304*(5679), 1926-1929. https://doi.org/10.1126/science.1099745

Buzsaki, G., Anastassiou, C. A., & Koch, C. (2012). The origin of extracellular fields and currents: EEG ECoG, LFP and Spikes. *Nature Reviews Neuroscience, 13*, 407-420. https://doi.org/10.1038/nrn3241

Byers, A. L., & Yaffe, K. (2011). Depression and risk of developing dementia. *Nature Reviews Neurology, 7*(6), 323-331. https://doi.org/10.1038/nrneurol.2011.60

Cabeza, R., Albert, M., Belleville, S., Craik, F. I. M., Duarte, A., Grady, C. L., Lindenberger, U., Nyberg, L., Park, D. C., Reuter-Lorenz, P. A., Rugg, M. D., Steffener, J., & Rajah, M. N. (2018). Maintenance, reserve and compensation: The cognitive neuroscience of healthy ageing. *Nature Reviews Neuroscience, 19*, 701-710. https://doi.org/10.1038/s41583-018-0068-2

Calvo, M. S., & Lee, H. S. (2024). Enhanced complete ensemble EMD with superior noise handling capabilities: A robust signal decomposition method for power systems analysis. *Engineering Reports, 6*(11), e12862. https://doi.org/10.1002/eng2.12862

Canolty, R. T., & Knight, R. T. (2010). The functional role of cross-frequency coupling. *Trends in Cognitive Sciences, 14*(11), 506-515. https://doi.org/10.1016/j.tics.2010.09.001

Cattell, R. B. (1963). Theory of fluid and crystallised intelligence: A critical experiment. *Journal of Educational Psychology, 54*(1), 1-22. https://doi.org/10.1037/h0046743

Chiang, A. K., Rennie, C. J., Robinson, P. A., Roberts, J. A., Rigozzi, M. K., Whitehouse, R. W., Hamilton, R. J., & Gordon, E. (2008). Automated characterization of multiple alpha peaks in multi-site electroencephalograms. *Journal of Neuroscience Methods, 168*(2), 396-411. https://doi.org/10.1016/j.jneumeth.2007.11.001

Chiang, A. K. I., Rennie, C. J., Robinson, P. A., van Albada, S. J., & Kerr, C. C. (2011). Age trends and sex differences of alpha rhythms including split alpha peaks. *Clinical Neurophysiology, 122*(8), 1505-1517. https://doi.org/10.1016/j.clinph.2011.01.040

Chung, S. W., Rogasch, N. C., Hoy, K. E., & Fitzgerald, P. B. (2015). Measuring brain stimulation induced changes in cortical properties using TMS-EEG. *Brain Stimulation, 8*(6), 1010-1020. https://doi.org/10.1016/j.brs.2015.07.029

Clark, C. R., Veltmeyer, M. D., Hamilton, R. J., Simms, E., Paul, R., Hermens, D., & Gordon, E. (2004). Spontaneous alpha peak frequency predicts working memory performance across the age span. *International Journal of Psychophysiology, 53*(1), 1-9. https://doi.org/10.1016/j.ijpsycho.2003.12.011

Cohen, D. (1972). Magnetoencephalography: Detection of the brain's electrical activity with a superconducting magnetometer. *Science, 175*(4022), 664-666. https://doi.org/10.1126/science.175.4022.664

Cohen, M. X. (2014). *Analysing neural times series data: Theory and practice.* The MIT Press.

Cohen, M. X., & Gulbinaite, R. (2014). Five methodological challenges in cognitive electrophysiology. *NeuroImage, 85*, 702-710. https://doi.org/10.1016/j.neuroimage.2013.08.010

Colominas, M. A., Schlotthauer, G., & Torres, M. E. (2014). Improved complete ensemble EMD: A suitable tool for biomedical signal processing. *Biomedical Signal Processing and Control, 14*, 19-29. https://doi.org/10.1016/j.bspc.2014.06.009

Comerchero, M. D., & Polich, J. (1999). P3a and P3b from typical auditory and visual stimuli. *Clinical Neurophysiology, 110*(1), 24-30. https://doi.org/10.1016/S0168-5597(98)00033-1

Cong, F., Sipola, T., Huttunen-Scott, T., Xu, X., Ristaniemi, T, & Lyytinen, H. (2009). Hilbert-Huang versus Morlet Wavelet transformation on mismatch negativity of children in uninterrupted sound paradigm. *Nonlinear Biomedical Physics, 3*(1), 1-8. https://doi.org/10.1186/1753-4631-3-1

Corcoran, A. W., Alday, P. M., Schlesewsky, M., & Bornkessel-Schlesewsky, I. (2018). Toward a reliable, automated method of individual alpha frequency (IAF) quantification. *Psychophysiology, 55*(7), e13064. https://doi.org/10.1111/psyp.13064

Cragg, L., Kovacevic, N., McIntosh, A. T., Poulsen, C., Martinu, K., Leonard, G., & Paus, T. (2011). Maturation of EEG power spectra in early adolescence: A longitudinal study. *Developmental Science, 14*(5), 935-943. https://doi.org/10.1111/j.1467-7687.2010.01031.x

Cremer, R., & Zeef, E. J. (1987). What kind of noise increases with age? *Journal of Gerontology, 42*(5), 515-518. https://doi.org/10.1093/geronj/42.5.515

Croft, R.J., & Barry, R.J. (2000a). EOG correction of blinks with saccade coefficients: A test and revision of the aligned-artefact average solution. *Clinical Neurophysiology, 111*(3), 444-451. https://doi.org/10.1016/S1388-2457(99)00296-5

Croft, R.J., & Barry, R.J. (2000b). Removal of ocular artefact from the EEG: A review. *Clinical Neurophysiology, 30*(1), 5-19. https://doi.org/10.1016/S0987-7053(00)00055-1

Dauwels, J., Srinivasan, K., Reddy, M. R., Musha, T., Vialatte, F-B., Latchoumane, C., Jeong, J., & Cichocki, A. (2011). Slowing and loss of complexity in Alzheimer's EEG: Two sides of the same coin? *International Journal of Alzheimer's Disease, 2011*, 1-10. https://doi.org/10.4061/2011/539621

Dauwels, J., Vialatte, F., & Cichocki, A. (2010a). Diagnosis of Alzheimer's disease from EEG signals: Where are we standing? *Current Alzheimer Research, 7*(6), 487-505. https://doi.org/10.2174/156720510792231720

Dauwels, J., Vialatte, F., Musha, T., & Cichocki, A. (2010b). A comparative study on synchrony measures for the early diagnosis of Alzheimer's disease based on EEG. *NeuroImage, 49*(1), 668-693. https://doi.org/10.1016/j.neuroimage.2009.06.056

David, O., Kilner, J. M., & Friston, K. J. (2006). Mechanisms of evoked and induced responses in MEG/EEG. *NeuroImage, 31*(4), 1580-1591. https://doi.org/10.1016/j.neuroimage.2006.02.034

Davis, M., O'Connell, T., Johnson, S., Cline, S., Merikle, E., Martenyi, F., & Simpson, K. (2018). Estimating Alzheimer's disease progression rates from normal cognition through mild cognitive impairment and stages of dementia. *Current Alzheimer Research, 15*(8), 777-788. https://doi.org/10.2174/1567205015666180119092427

De Cheveigne, A., & Nelken, I. (2019). Filters: When, why, and how (not) to use them. *Neuron, 102*(2), 280-293. https://doi.org/10.1016/j.neuron.2019.02.039

De Felice, S., & Holland, C. A. (2018). Intra-individual variability across fluid cognition can reveal qualitatively different cognitive styles of the aging brain. *Frontiers in Psychology, 9*, 1973. https://doi.org/10.3389/fpsyg.2018.01973

De Tiege, X., de Beeck, M. O., Funke, M., Legros, B., Parkkonen, L., Goldman, S., & van Bogaert, P. (2008). Recording epileptic activity with MEG in a light-weight magnetic shield. *Epilepsy Research, 82*(2-3), 227-231. https://doi.org/10.1016/j.eplepsyres.2008.08.011

Deary, I. J., Johnson, W, & Starr, J. (2010). Are processing speed tasks biomarkers of cognitive ageing? *Psychology and Aging, 25*(1), 219-228. https://doi.org/10.1037/a0017750

Deary, I. J., Liewald, D., & Nissan, J. (2011). A free, easy-to-use, computer-based simple and four-choice reaction time programme: The Deary-Liewald reaction time task. *Behaviour Research Methods, 43*, 258-268. https://doi.org/10.3758/s13428-010-0024-1

Delorme, A. (2023). EEG is better left alone. *Scientific Reports, 13*, 2372. https://doi.org/10.1038/s41598-023-27528-0

Delorme, A., & Makeig, S. (2004). EEGLAB: An open-source toolbox for analysis of single-trial EEG dynamics including independent component analysis. *Journal of Neuroscience Methods, 134*(1), 9-21. https://doi.org/10.1016/j.jneumeth.2003.10.009

Dementia UK. (2023). *What is dementia? Your dementia questions answered.* https://www.dementiauk.org/information-and-support/about-dementia/what-is-dementia/

Der, G., & Deary, I. J. (2006). Age and sex differences in reaction time in adulthood: Results from the United Kingdom health and lifestyle survey. *Psychology and Aging, 21*, 62-73. https://doi.org/10.1037/a0015515

Dien, J. (1998). Issues in the application of the average reference: Review, critiques, and recommendations. *Behaviour Research Methods, Instruments, & Computers, 30*, 34-43. https://doi.org/10.3758/BF03209414

Doesburg, S. M., Roggeveen, A. B., Kitajo, K., & Ward, L. M. (2008). Large-scale gamma-band phase synchronisation and selective attention. *Cerebral Cortex, 18*(2), 386-396. https://doi.org/10.1093/cercor/bhm073

Donoghue, T., Haller, M., Peterson, E. J., Varma, P., Sebastian, P., Gao, R., Noto, T., Lara, A. H., Wallis, J. D., Knight, R. T., Shestyuk, A., & Voytek, B. (2020). Parameterising neural power spectra into periodic and aperiodic components. *Nature Neuroscience, 23*, 1655-1665. https://doi.org/10.1038/s41593-020-00744-x

Donoghue, T., Schaworonkow, N., & Voytek, B. (2021). Methodological considerations for studying neural oscillations. *European Journal of Neuroscience, 55*(11-12), 3502-3527. https://doi.org/10.1111/ejn.15361

Doppelmayr, M., Klimesch, W., Sauseng, P., Hodlmoser, K., Stadler, W., & Hanslmayr, S. (2005). Intelligence related differences in EEG-bandpower. *Neuroscience Letters, 381*(3), 309-313. https://doi.org/10.1016/j.neulet.2005.02.037

Duffy, F. H., Albert, M. S., McAnulty, G., & Garvey, A. J. (1984). Age-related differences in brain electrical activity of healthy subjects. *Annals of Neurology, 16*(4), 430-438. https://doi.org/10.1002/ana.410160403

Duffy, F. H., McAnulty, G. B., & Albert, M. S. (1993). The pattern of age-related differences in electrophysiological activity of healthy males and females. *Neurobiology of Aging, 14*(1), 73-84. https://doi.org/10.1016/0197-4580(93)90025-7

Duncan, C. C., Barry, R. J., Connolly, J. F., Fischer, C., Michie, P. T., Naatanen, R., Polich, J., Reinvang, I., & Van Petten, C. (2009). Event-related potentials in clinical research: Guidelines for eliciting, recording, and quantifying mismatch negativity, P300, and N400. *Clinical Neurophysiology, 120*(11), 1883-1908. https://doi.org/10.1016/j.clinph.2009.07.045

Dustman, R. E., Shearer, D. E., & Emmerson, R. Y. (1993). EEG and event-related potentials in normal aging. *Progress in Neurobiology, 41*(3), 369-401. https://doi.org/10.1016/0301-0082(93)90005-d

Dykiert, D., Der, G., Starr, J. M., & Deary, I. J. (2012). Age differences in intra-individual variability in simple and choice reaction time: Systematic review and meta-analysis. *PLoS ONE, 7*(10), e45759. https://doi.org/10.1371/journal.pone.0045759

Ebaid, D., & Crewther, S. G. (2020). Time for a systems biological approach to cognitive aging? A critical review. *Frontiers in Aging Neuroscience, 12*, 114. https://doi.org/10.3389/fnagi.2020.00114

Engel, A. K., & Fries, P. (2010). Beta-band oscillations – signalling the status quo? *Current Opinion in Neurobiology, 20*(2), 156-165. https://doi.org/10.1016/j.conb.2010.02.015

Falini, A. (2022). A review on the selection criteria for the truncated SVD in data science applications. *Journal of Computational Mathematics and Data Science, 5*, 100064. https://doi.org/10.1016/j.jcmds.2022.100064

Faul, F., Erdfelder, E., Buchner, A., & Lang, A-G. (2009). Statistical power analyses using G*Power 3.1: Tests for correlation and regression analyses. *Behaviour Research Methods, 41*, 1149-1160. https://doi.org/10.3758/BRM.41.4.1149

Feher, K. D., Nakataki, M., & Morishima, Y. (2017). Phase-dependent modulation of signal transmission in cortical networks through tACS-induced neural oscillations. *Frontiers in Human Neuroscience, 11*, 1-13. https://doi.org/10.3389/fnhum.2017.00471

Fell, J., Dietl, T., Grunwald, T., Kurthen, M., Klaver, P., Trautner, P., Schaler, C., Elger, C. E., & Fernández, G. (2004). Neural bases of cognitive ERPs: More than phase reset. *Journal of Cognitive Neuroscience, 16*(9), 1595–1604. https://doi.org/10.1162/0898929042568514

Fellinger, R., Klimesch, W., Gruber, W., Freunberger, R., & Doppelmayr, M. (2011). Pre-stimulus alpha phase-alignment predicts P1-amplitude. *Brain Research Bulletin, 85*, 417-423. https://doi.org/10.1016/j.brainresbull.2011.03.025

Ferree, T. C., Luu, P., Russell, G. S., & Tucker, D. M. (2001). Scalp electrode impedance, infection risk, and EEG data quality. *Clinical Neurophysiology, 112*(3), 536-544. https://doi.org/10.1016/s1388-2457(00)00533-2

Finley, A. J., Angus, D. J., Knight, E. L., van Reekum, C. M., Lachman, M. E., Davidson, R. J., & Schaefer, S. M. (2024). Resting EEG periodic and aperiodic components predict cognitive decline over 10 years. *Journal of Neuroscience, 44*(13), e1332232024. https://doi.org/10.1523/JNEUROSCI.1332-23.2024

Finley, A. J., Angus, D. J., van Reekum, C. M., Davidson, R. J., & Schaefer, S. M. (2022). Periodic and aperiodic contributions to theta-beta ratios across adulthood. *Psychophysiology, 59*(11), e14113. https://doi.org/10.1111/psyp.14113

Fjell, A. M., Rosquist, H., & Walhovd, K. B. (2009). Instability in the latency of P3a/P3b brain potentials and cognitive function in ageing. *Neurobiology and Aging, 30*(12), 2065-2079. https://doi.org/10.1016/j.neurobiolaging.2008.01.015

Fjell, A. M. Walhovd, K. B., Fischl, B. & Reinvang, I. (2007). Cognitive functiona, P3a/P3b brain potentials, and cortical thickness in aging. *Human Brain Mapping, 28*(11), 1098-1116. https://doi.org/10.1002/hbm.20335

Fjell, A. M., Walhovd, K. B., & Reinvang, I. (2005). Age-dependent changes in distribution of P3a/P3b amplitude and thickness of the cerebral cortex. *NeuroReport, 16*(13), 1451-1454. https://doi.org/10.1097/01.wnr.0000177011.44602.17

Franke, K., & Gaser, C. (2019). Ten years of BrainAGE as a neuroimaging biomarker of brain aging: What insights have we gained? *Frontiers in Neurology, 10*, 789. https://doi.org/10.3389/fneur.2019.00789

Freschl, J., Azizi, L. A., Balboa, L., Kaldy, Z., & Blaser, E. (2022). The development of peak alpha frequency from infancy to adolescence and its role in visual temporal processing: A meta-analysis. *Developmental Cognitive Neuroscience, 57*, 101146. https://doi.org/10.1016/j.dcn.2022.101146

Fuentemilla, L., Marco-Pallares, J., & Grau, C. (2006). Modulation of spectral power and of phase resetting of EEG contributes differentially to the generation of auditory event-related potentials. *NeuroImage, 30*(3), 909-916. https://doi.org/10.1016/j.neuroimage.2005.10.036

Gao, Y., Ge, G., Sheng, Z., & Sang, E. (2008). Analysis and solution to the mode mixing phenomenon in EMD. *Congress on Image and Signal Processing, 5*, 223-227. https://doi.org/10.1109/CISP.2008.193

Garces, P., Lopez-Sanz, D., Maestu, F., & Pereda, E. (2017). Choice of magnetometers and gradiometers after signal space separation. *Sensors, 17*(12), 2926. https://doi.org/10.3390/s17122926

Gauthier, S., Reisberg, B., Zaudig, M., Petersen, R. C., Ritchie, K., Broich, K., Belleville, S., Brodaty, H., Bennett, D., Chertkow, H., Cummings, J. L., de Leon, M., Feldman, H., Ganguli, M., Hampel, H., Scheltens, P., Tierney, M. C., Whitehouse, P., & Winblad, B. (2006). Mild cognitive impairment. *The Lancet, 367*(9518), 1262-1270. https://doi.org/10.1016/S0140-6736(06)68542-5

Geisler, C., Diba, K., Pastalkova, E., Mizuseki, K., Royer, S., & Buzsaki, G. (2010). Temporal delays among place cells determine the frequency of population theta oscillations in the hippocampus. *PNAS, 107*(17), 7957-7962. https://doi.org/10.1073/pnas.0912478107

Gelman, A., & Carlin, J. (2014). Beyond power calculations: assessing type s (sign) and type m (magnitude) errors. *Perspectives on Psychological Science, 9*(6), 641-651. https://doi.org/10.1177/1745691614551642

Gersch, W. (1970). Spectral analysis of EEGs by autoregressive decomposition of time series. *Mathematical Biosciences, 7*(1-2), 205-222. https://doi.org/10.1016/0025-5564(70)90049-0

Geslani, D. M., Tierney, M. C., Herrmann, N., & Szalai, J. P. (2005). Mild cognitive impairment: An operational definition and its conversion rate to Alzheimer's disease. *Dementia and Geriatric Cognitive Disorders, 19*(5-6), 383-389. https://doi.org/10.1159/000084709

Glass, G. V., & Hopkins, K. D. (1996). Chapter 14. In *Statistical Methods in Education and Psychology (3rd Ed.)*. Allyn & Bacon.

Gómez, C., M Pérez-Macías, J., Poza, J., Fernández, A., & Hornero, R. (2013). Spectral changes in spontaneous MEG activity across the lifespan. *Journal of Neural Engineering, 10*(6), 066006. https://doi.org/10.1088/1741-2560/10/6/066006

Gonzalez-Moreno, A., Aurtenetxe, S., Lopez-Garcia, M-E., del Pozo, F., Maestu, F., & Nevado, A. (2014). Signal-to-noise ratio of the MEG signal after preprocessing. *Journal of Neuroscience Methods, 222*, 56-61. https://doi.org/10.1016/j.jneumeth.2013.10.019

Grabner, R. H., Neubauer, A. C. & Stern, E. (2006). Superior performance and neural efficiency: The impact of intelligence and expertise. *Brain Research Bulletin, 69*, 422–439. https://doi.org/10.1016/j.brainresbull.2006.02.009

Grady, C. (2012). The cognitive neuroscience of ageing. *Nature Reviews Neuroscience, 13*, 491-505. https://doi.org/10.1038/nrn3256

Grandy, T. H., Werkle-Bergner, M., Chicherio, C., Lövdén, M., Schmiedek, F., & Lindenberger, U. (2013). Individual alpha peak frequency is related to latent factors of general cognitive abilities. *NeuroImage, 79*, 10-18. https://doi.org/10.1016/j.neuroimage.2013.04.059

Granger, C. W. J. (1969). Investigating causal relations by econometric models and cross-spectral methods. *Econometrica, 37*(3), 424-438. https://doi.org/10.2307%2F1912791

Gratton, G., Coles, M. G. H., & Donchin, E. (1983). A new method for off-line removal of ocular artifact. *Electroencephalography and Clinical Neurophysiology, 55*(4), 468-484. https://doi.org/10.1016/0013-4694(83)90135-9

Grobbelaar, M., Phadikar, S., Ghaderpour, E., Struck, A. E., Sinha, N., Ghosh, R., & Ahmed, M. Z. I. (2022). A survey on denoising techniques of electroencephalogram signals using wavelet transform. *Signals, 3*, 577-586. https://doi.org/10.3390/signals3030035

Hackfort, D., & Birkner, H-A. (2011). Triangulation as a basis for diagnostic judgments. *International Journal of Sport and Exercise Psychology, 1*, 82-94. https://doi.org/10.1080/1612197X.2003.9671705

Haegens, S., Cousijn, H., Wallis, G., Harrison, P. J., & Nobre, A. C. (2014). Inter- and intra-individual variability in alpha peak frequency. *NeuroImage, 92*, 46-55. https://doi.org/10.1016/j.neuroimage.2014.01.049

Hamalainen, M., Hari, R., Ilmoniemi, R. J., Knuutila, J., & Lounasmaa, O. V. (1993). Magnetoencephalography: Theory, instrumentation, and applications to noninvasive studies of working human brain. *Reviews of Modern Physics, 65*, 413. https://doi.org/10.1103/RevModPhys.65.413

Hamalainen, M. S., & Sarvas, J. (1989). Realistic conductivity geometry model of the human head for interpretation of neuromagnetic data. *IEEE Transactions on Biomedical Engineering, 36*(2), 165-171. https://doi.org/10.1109/10.16463

Hanslmayr, S., Klimesch, W., Sauseng, P., Gruber, W., Doppelmayr, M., Freunberger, R., Pecherstorfer, T., & Birbaumer, N. (2007). Alpha phase reset contributes to the generation of ERPs. *Cerebral Cortex, 17*(1), 1–8. https://doi.org/10.1093/cercor/bhj129

Harner, R. N. (1990). Singular value decomposition – A general linear model for analysis of multivariate structure in the electroencephalogram. *Brain Topography, 3*, 43-47. https://doi.org/10.1007/BF01128860

Hashemi, A., Pino, L. J., Moffat, G., Mathewson, K. J., Aimone, C., Bennett, P. J., Schmidt, L. A., & Sekuler, A. B. (2016). Characterizing population EEG dynamics throughout adulthood. *eNeuro, 3*(6), ENEURO.0275-16.2016. https://doi.org/10.1523/ENEURO.0275-16.2016

He, B. J. (2014). Scale-free brain activity: Past, present, and future. *Trends in Cognitive Sciences, 18*(9), 480-487. https://doi.org/10.1016/j.tics.2014.04.003

Hedges, D., Janis, R., Mickelson, S., Keith, C., Bennett, D., & Brown, B. L. (2016). P300 amplitude in Alzheimer's disease: A meta-analysis and meta-regression. *Clinical EEG and Neuroscience, 47*, 48-55. https://doi.org/10.1177/1550059414550567

Hillebrand, A., & Barnes, G. R. (2002). A quantitative assessment of the sensitivity of whole-head MEG to activity in the adult human cortex. *NeuroImage, 16*(3), 638-650. https://doi.org/10.1006/nimg.2002.1102

Hillebrand, A., Singh, K. D., Holliday, I. E., Furlong, P. L., & Barnes, G. R. (2005). A new approach to neuroimaging with magnetoencephalography. *Human Brain Mapping, 25*(2), 199-211. https://doi.org/10.1002/hbm.20102

Hindriks, R., Woolrich, M., Luckhoo, H., Joensson, M., Mohseni, H., Kringelbach, M. L., & Deco, G. (2015). Role of white-matter pathways in coordinating alpha oscillations in resting visual cortex. *NeuroImage, 106*, 328-339. https://doi.org/10.1016/j.neuroimage.2014.10.057

Hofmann, S. M., Beyer, F., Lapuschkin, S., Goltermann, O., Loeffler, M., Müller, K-R., Villringer, A., Samek, W., & Witte, A. V. (2022). Towards the interpretability of deep learning models for multi-modal neuroimaging: Finding structural changes of the ageing brain. *NeuroImage, 261*, 119504. https://doi.org/10.1016/j.neuroimage.2022.119504

Howe, A.S., Bani-Fatemi, A., & De Luca, V. (2014). The clinical utility of the auditory P300 latency subcomponent event-related potential in preclinical diagnosis of patients with mild cognitive impairment and Alzheimer's disease. *Brain and Cognition, 86*, 64-74. https://doi.org/10.1016/j.bandc.2014.01.015

Huang, N. E., Shen, Z., & Long, S. R. (1999). A new view of nonlinear water waves: The Hilbert spectrum. *Annual Review of Fluid Mechanics, 31*, 417-457. https://doi.org/10.1146/annurev.fluid.31.1.417

Huang, N. E., Shen, Z., Long, S. R., Wu, M. C., Shih, H. H., Zheng, Q., Yen, N. C., Tung, C. C., & Liu, H. H. (1998). The empirical mode decomposition and the Hilbert spectrum for nonlinear and non-stationary time series analysis. *Proceedings of the Royal Society A, 454*, 903-995. https://doi.org/10.1098/rspa.1998.0193

Huang, C., Wahlund, L. O., Dierks, T., Julin, P., Winblad, B., & Jelic, V. (2000). Discrimination of Alzheimer's disease and mild cognitive impairment by equivalent EEG sources: A cross-sectional and longitudinal study. *Clinical Neurophysiology, 111*(11), 1961-1967. https://doi.org/10.1016/S1388-2457(00)00454-5

Huettel, S. A., Singerman, J. D., & McCarthy, G. (2001). The effects of aging upon the hemodynamic response measured by functional MRI. *NeuroImage, 13*(1), 161-175. https://doi.org/10.1006/nimg.2000.0675

Hughes, J. R., & Cayaffa, J. J. (1977). The EEG in patients at different ages without organic cerebral disease. *Electroencephalography and Clinical Neurophysiology, 42*(6), 776-784. https://doi.org/10.1016/0013-4694(77)90231-0

Hughes, S. W., & Crunelli, V. (2005). Thalamic mechanisms of EEG alpha rhythms and their pathological implications. *The Neuroscientist, 11*(4), 357-372. https://doi.org/10.1177/1073858405277450

Huffmeijer, R., Bakermans-Kranenburg, M. J., Alink, L. R. A., & Van Ijzendoorn, M. H. (2014). Reliability of event-related potentials: The influence of number of trials and electrodes. *Physiology & Behaviour, 130*, 13-22. https://doi.org/10.1016/j.physbeh.2014.03.008

Huotilainen, M., Winkler, I., Alho, K., Escera, C., Virtanen, J., Ilmoniemi, R. J., Jaaskelainen, L. P., Pekkonen, E., Naatanen, R. (1998). Combined mapping of human auditory EEG and MEG responses. *Electroencephalography and Clinical Neurophysiology, 108*(4), 370-379. https://doi.org/10.1016/S0168-5597(98)00017-3

IBM Corporation. (2021, March 02). *Variance Components Analysis.* IBM Corporation. https://www.ibm.com/docs/en/spss-statistics/26.0.0?topic=statistics-variance-components-analysis

IBM Support. (2020, April 16). *Differences between correlations.* IBM Corporation. https://www.ibm.com/support/pages/differences-between-correlations

International Telecommunication Union (2019, July). *Safe listening guidelines for personal sound amplifiers. https://www.itu.int/rec/T-REC-H.871-201907-I/en*

Ishii, R., Canuet, L., Aoki, Y., Hata, M., Iwase, M., Ikeda, S., Nishida, K., & Ikeda, M. (2017). Healthy and pathological brain aging: From the perspective of oscillations, functional connectivity, and signal complexity. *Neuropsychobiology, 75*(4), 151-161. https://doi.org/10.1159/000486870

Jackson, A. F., & Bolger, D. J. (2014). The neurophysiological bases of EEG and EEG measurement: A review for the rest of us. *Psychophysiology, 51*(11), 1061-1071. https://doi.org/10.1111/psyp.12283

Jausovec, N., & Jausovec, K. (2000). Differences in event-related and induced brain oscillations in the theta and alpha frequency bands related to human intelligence. *Neuroscience Letters, 293*(3), 191-194. https://doi.org/10.1016/S0304-3940(00)01526-3

Jeffreys, H. (1961). *Theory of probability*. Oxford University Press.

Jekel, K., Damian, M., Wattmo, C., Hausner, L., Bullock, R., Connelly, P.J., Dubois, B., Eriksdotter, M., Ewers, M., Graessel, E., Kramberger, M.G., Law, E., Mecocci, P., Molinuevo, J. L., Nygard, L., Olde-Rikkert, M.G.M., Orgogozo, J. M., Pasquier, F., Peres, K., Salmon, E., Sikkes, S. A. M., Sobow, T., Spiegel, R., Tsolaki, M., Winblad, B., & Frolich, L. (2015). Mild cognitive impairment and deficits in instrumental activities of daily living: A systematic review. *Alzheimer's Research & Therapy, 7*, 1-20. https://doi.org/10.1186/s13195-015-0099-0

Jelic, V., Johansson, S-E., Almkvist, O., Shigeta, M., Julin, P., Nordberg, A., Winblad, B., & Wahlund, L-O. (2000). Quantitative electroencephalography in mild cognitive impairment: Longitudinal changes and possible prediction of Alzheimer's disease. *Neurobiology of Aging, 21*(4), 533-540. https://doi.org/10.1016/S0197-4580(00)00153-6

Jervis, B. W., Nichols, M. J., Johnson, T. E., Allen, E., & Hudson, N. R. (1983). A fundamental investigation of the composition of auditory evoked potentials. *IEEE Transactions on Biomedical Engineering, 30*(1), 43-50. https://doi.org/10.1109/TBME.1983.325165

Jessen, F., Amariglio, R. E., Buckley, R. F., Van der Flier, W. M., Han, Y., Molinuevo, J. L., Rabin, L., Rentz, D. M., Rodriguez-Gomez, O., Saykin, A. J., Sikkes, S. A. M., Smart, C. M., Wolfsgruber, S., & Wagner, M. (2020). The characterisation of subjective cognitive decline. *The Lancet, 19*(3), 271-278. https://doi.org/10.1016/S1474-4422(19)30368-0

Jiang, S., Qu, C., Wang, F., Liu, Y., Qiao, Z., Qiu, X., Yang, X., & Yang, Y. (2015) Using event-related potential P300 as an electrophysiological marker for differential diagnosis and to predict the progression of mild cognitive impairment: A meta-analysis. *Neurological Sciences, 36*, 1105-1112. https://doi.org/10.1007/s10072-015-2099-z

Joffe, D., Oakley, D. S., Lucini, F. A., & Palermo, F. X. (2021). *Measurements of EEG alpha peak frequencies over the lifespan: Validating target ranges on an in-clinic platform.* BioRxiv [preprint]. https://doi.org/10.1101/2021.10.06.463353

John, E. R., Ahn, H., Prichep, L., Trepetin, M., Brown, D., & Kaye, H. (1980). Developmental equations for the electroencephalogram. *Science, 210*(4475), 1255-1258. https://doi.org/10.1126/science.7434026

John, E. R., Karmel, B. Z., Corning, W. C., Easton, P., Brown, D., Ahn, H., John, M., Harmony, T., Prichep, L., Toro, A., Gerson, I., Bartlett, F., Thatcher, R., Kaye, H., Valdes, P., & Schwartz, E. (1977). Neurometrics: Numerical taxonomy identifies different profiles of brain functions within groups of behaviourally similar people. *Science, 196*(4297), 1393-1410. https://doi.org/10.1126/science.867036

Jung, T. P., Makeig, S., Westerfield, M., Townsend, J., Courchesne, E., & Sejnowski, T. J. *(1999).* Analysing and visualising single-trial event-related potentials. *Advances in Neural Information Processing Systems, 11*, 118-124.

Jung, T.P., Makeig, S., Westerfield, M., Townsend, J., Courchesne, E., & Sejnowski, T.J. (2001). Analysis and visualisation of single-trial event-related potentials. *Human Brain Mapping, 14*, 166-185. https://doi.org/10.1002/hbm.1050

Jurcak, V., Tsuzuki, D., & Dan, I. (2007). 10/20, 10/10, and 10/5 systems revisited: Their validity as relative head-surface-based positioning systems. *NeuroImage, 34*(4), 1600-1611. https://doi.org/10.1016/j.neuroimage.2006.09.024

Kaneko, N., Yokoyama, H., Masugi, Y., Watanabe, K., & Nakazawa, K. (2021). Phase dependent modulation of cortical activity during action observation and motor imagery of walking: An EEG study. *NeuroImage, 225*, 117486. https://doi.org/10.1016/j.neuroimage.2020.117486

Kiesel, A., Miller, J., Jolicoeur, P., & Brisson, B. (2008). Measurement of ERP latency differences: A comparison of single-participants and jackknife-based scoring methods. *Psychophysiology, 45*(2), 250-274. https://doi.org/10.1111/j.1469-8986.2007.00618.x

Klimesch, W. (1999). EEG alpha and theta oscillations reflect cognitive and memory performance: A review and analysis. *Brain Research Reviews, 29*(2-3), 169-195. https://doi.org/10.1016/S0165-0173(98)00056-3

Klimesch, W. (2018). The frequency architecture of brain and brain body oscillations: An analysis. *European Journal of Neuroscience, 48*(7), 2431-2453. https://doi.org/10.1111/ejn.14192

Klimesch, W., Hanslmayr, S., Sauseng, P., & Gruber, W. R. (2006). Distinguishing the evoked response from phase reset: A comment to Makinen et al. *NeuroImage, 29*, 808-811. https://doi.org/10.1016/j.neuroimage.2005.08.041

Klimesch, W., Hanslmayr, S., Sauseng, P., Gruber, W., & Doppelmayr, M. (2007a). The P1 and traveling alpha waves: Evidence for evoked oscillations. *Journal of Neurophysiology, 97*(2), 1311-1318. https://doi.org/10.1152/jn.00876.2006

Klimesch, W., Sauseng, P., & Hanslmayr, S. (2007b). EEG alpha oscillations: The inhibition timing hypothesis. *Brain Research Reviews, 53*(1), 63-88. https://doi.org/10.1016/j.brainresrev.2006.06.003

Klimesch, W., Sauseng, P., Hanslmayr, S., Gruber, W., & Freunberger, R. (2007c). Event-related phase reorganisation may explain evoked neural dynamics. *Neuroscience and Biobehavioural Reviews, 31*(7), 1003-1016. https://doi.org/10.1016/j.neubiorev.2007.03.005

Klimesch, W., Schimke, H., Ladurner, G., & Pfurtscheller, G. (1990). Alpha frequency and memory performance. *Journal of Psychophysiology, 4*(4), 381-390.

Klimesch, W., Schimke, H., & Pfurtscheller, G. (1993). Alpha frequency, cognitive load and memory performance. *Brain Topography, 5*(3), 241-251. https://doi.org/10.1007/bf01128991

Knyazev, G. G. (2012). EEG delta oscillations as a correlate of basic homeostatic and motivational processes. *Neuroscience & Biobehavioural Reviews, 36*(1), 677-695. https://doi.org/10.1016/j.neubiorev.2011.10.002

Koen, J. D., & Rugg, M. D. (2019). Neural dedifferentiation in the aging brain. *Trends in Cognitive Sciences, 23*(7), 547-559. https://doi.org/10.1016/j.tics.2019.04.012

Koenig, T., Smailovic, U., & Jelic, V. (2020). Past, present and future EEG in clinical workup of dementias. *Psychiatry Research: Neuroimaging, 306*, 111182. https://doi.org/10.1016/j.pscychresns.2020.111182

Kondacs, A., & Szabó, M. (1999). Long-term intra-individual variability of the background EEG in normals. *Clinical Neurophysiology, 110*(10), 1708-1716. https://doi.org/10.1016/S1388-2457(99)00122-4

Krishnan, A., Williams, L. J., McIntosh, A. R., & Abdi, H. (2011). Partial Least Squares (PLS) methods for neuroimaging: A tutorial and review. *NeuroImage, 56*(2), 455-475. https://doi.org/10.1016/j.neuroimage.2010.07.034

Lachaux, J. P., Rodriguez, E., Martinerie, J., & Varela, F. J. (1999). Measuring phase synchrony in brain signals. *Human Brain Mapping, 8*(4), 194-208.

https://doi.org/10.1002/(SICI)1097-0193(1999)8:4%3C194::AID-HBM4%3E3.0.CO;2-C

Lehtinen, M., Forsman, K., Malmivuo, J., & Eskola, H. (1996). Effects of skull and scalp thickness on EEG. *Proceedings of the 1st International Conference on Bioelectromagnetism, 34*, 263-264.

Lindsley, D. B. (1939). A longitudinal study of the occipital alpha rhythm in normal children: Frequency and amplitude standards. *The Journal of Genetic Psychology, 55*, 197-213. https://doi.org/10.1080/08856559.1939.10533190

Livingstone, G., Huntley, J., Sommerlad, A., Ames, D., Ballard, C., Banerjee, S., Brayne, C., Burns, A., Cohen-Mansfield, J., Cooper, C., Costafreda, S. G., Dias, A., Fox, N., Gitlin L. N., Howard, R., Kales, H. C., Kivimaki, M., Larson, E. B., Ogunniyi, A., … Mukadam, N. (2020). Dementia prevention, intervention, and care: 2020 report of the Lancet commission. *The Lancet, 396*(10248), 413-446. https://doi.org/10.1016%2FS0140-6736(20)30367-6

Livingston, G., Huntley, J., Liu, K. Y., Costafreda, S. G., Selbaek, G., Alladi, S., Ames, D., Banerjee, S., Burns, A., Brayne, C., Fox, N. C., Ferri, C. P., Gitlin, L. N., Howard, R., Kales, H. C., Kivimaki, M., Larson, E. B., Nakasujja, N., Rockwood, K., Samus, Q., Shira, K., Singh-Manoux, A., Schneider, L. S., Walsh, S., Yao, Y., Sommerlad, A., & Mukadam, N. (2024). Dementia prevention, intervention, and care: 2024 report of the Lancet standing commission. *The Lancet, 404*(10452), 572-628. https://doi.org/10.1016/S0140-6736(24)01296-0

Lobaugh, N. J., West, R., & McIntosh, A. R. (2001). Spatiotemporal analysis of experimental differences in event-related potential data with partial least squares. *Psychophysiology, 38*(3), 517-530. https://doi.org/10.1017/s0048577201991681

Lodder, S. S., & van Putten, M. J. A. M. (2011). Automated EEG analysis: Characterizing the posterior dominant rhythm. *Journal of Neuroscience Methods, 200*(1), 86-93. https://doi.org/10.1016/j.jneumeth.2011.06.008

Logan, J. M., Sanders, A. L., Snyder, A. Z., Morris, J. C., & Buckner, R. L. (2002). Under-recruitment and nonselective recruitment: Dissociable neural mechanisms associated with aging. *Neuron, 33*(5), 827-840. https://doi.org/10.1016/s0896-6273(02)00612-8

Lonie, J. A., Parra-Rodriguez, M. A., Tierney, K. M., Herrmann, L. L., Donaghey, C., O'Carroll, R. E., & Ebmeier, K. P. (2010). Predicting outcome in mild cognitive

impairment: 4-year follow-up study. *British Journal of Psychiatry, 197*(2), 135-140. https://doi.org/10.1192/bjp.bp.110.077958

Lopes da Silva, F. (2013). EEG and MEG: Relevance to neuroscience. *Neuron, 80*(5), 1112-1128. https://doi.org/10.1016/j.neuron.2013.10.017

Lowet, E., Roberts, M. J., Peter, A., Gips, B., & De Weerd, P. (2017). A quantitative theory of gamma synchronisation in macaque V1. *eLife, 6*, e26642. https://doi.org/10.7554/eLife.26642

Luck, S. J. (2014). *An introduction to the event-related potential technique* (2nd Ed.). The MIT Press.

Luo, J., Bai, J., & Shao, J. (2006). Application of the wavelet transforms on axial strain calculation in ultrasound elastography. *Progress in Natural Science, 16*(9), 942-947. https://doi.org/10.1080/10020070612330093

Lutz, A., Greischar, L. L., Rawlings, N. B., Richard, M., & Davidson, R. J. (2004). Long-term meditators self-induce high-amplitude gamma synchrony during mental practice. *PNAS, 101*(46), 16369-16373. https://doi.org/10.1073/pnas.0407401101

Lyons, R.G. (2011). *Understanding digital signal processing* (3rd Ed.). Prentice Hall.

MacDonald, S. W. S., Li, S-C., & Backman, L. (2009). Neural underpinnings of within-person variability in cognitive functioning. *Psychology and Aging, 24*(4), 792-808. https://doi.org/10.1037/a0017798

Maddrey, A. M., Cullum, C. M., Weiner, M. F., & Filley, C. M. (1996). Premorbid intelligence estimation and level of dementia in Alzheimer's disease. *Journal of the International Neuropsychological Society, 2*(6), 551-555. https://doi.org/10.1017/S1355617700001727

Mahjoory, K., Schoffelen, J-M., Keitel, A., & Gross, J. (2020). The frequency gradient of human resting-state brain oscillations follows cortical hierarchies. *eLife, 9*, e53715. https://doi.org/10.7554/eLife.53715

Makeig, S., Westerfield, M., Jung, T. P., Enghoff, S., Townsend, J., Courchesne, E., & Sejnowski, T. J. (2002). Dynamic brain sources of visual evoked responses. *Science, 295*(5555), 690–694. https://doi.org/10.1126/science.1066168

Makinen, V., Tiitinen, H., & May, P. (2005). Auditory event-related responses are generated independently of on-going brain activity. *NeuroImage, 24*(4), 961-968. https://doi.org/10.1016/j.neuroimage.2004.10.020

Matoušek, M., & Petersén, I. (1973). Automatic evaluation of EEG background activity by means of age-dependent EEG quotients. *Electroencephalography and Clinical Neurophysiology, 35*(6), 603-612. https://doi.org/10.1016/0013-4694(73)90213-7

Mazaheri, A., & Jensen, O. (2006). Posterior alpha activity is not phase-reset by visual stimuli. *PNAS, 103*, 2948-2952. https://doi.org/10.1073/pnas.0505785103

Mazaheri, A., & Jensen, O. (2008). Asymmetric amplitude modulations of brain oscillations generate slow evoked responses. *Journal of Neuroscience, 28*(31), 7781-7787. https://doi.org/10.1523/JNEUROSCI.1631-08.2008

McDonough, I. M., Nolin, S. A., & Visscher, K. M. (2022). 25 years of neurocognitive aging theories: What have we learned? *Frontiers in Aging Neuroscience, 14*, 1002096. https://doi.org/10.3389/fnagi.2022.1002096

McDowell, K., Kerick, S. E., Santa Maria, D. L., & Hatfield, B. D. (2003). Aging, physical activity, and cognitive processing: An examination of P300. *Neurobiology of Aging, 24*(4), 597-606. https://doi.org/10.1016/S0197-4580(02)00131-8

Mcevoy, L. K., Smith, M., & Gevins, A. (2000). Test-retest reliability of cognitive EEG. *Clinical Neurophysiology, 111*(3), 457-463. https://doi.org/10.1016/S1388-2457(99)00258-8

McIntosh, A. R., & Lobaugh, N. J. (2004). Partial least squares analysis of neuroimaging data: Applications and advances. *NeuroImage, 23*(S1), S250-S263. https://doi.org/10.1016/j.neuroimage.2004.07.020

Merkin, A., Sghirripa, S., Graetz, L., Smith, A. E., Hordacre, B., Harris, R., Pitcher, J., Semmler J., Rogasch, N. C., & Goldsworthy, M. (2023). Do age-related differences in aperiodic neural activity explain differences in resting EEG alpha? *Neurobiology of Aging, 121*, 78-87. https://doi.org/10.1016/j.neurobiolaging.2022.09.003

Minami, S., Oishi, H., Takemura, H., & Amano, K. (2020). Inter-individual differences in occipital alpha oscillations correlate with white matter tissue properties of the optic radiation. *eNeuro, 7*(2), ENEURO.0224-0219.2020. https://doi.org/10.1523/ENEURO.0224-19.2020

Mizukami, K., & Katada, A. (2018). EEG frequency characteristics in healthy advanced elderly. *Journal of Psychophysiology, 32*(3), 131-139. https://doi.org/10.1027/0269-8803/a000190

Montefusco-Siegmund, R., Maldonado, P. E., & Devia, C. (2013). Effects of ocular artefact removal through ICA decomposition on EEG phase. *IEEE/EMBS Conference on Neural Engineering, 6*, 1374-1377. https://doi.org/10.1109/NER.2013.6696198

Morimoto, S. S., & Alexopoulos, G. S. (2013). Cognitive deficits in geriatric depression: Clinical correlates and implications for current and future treatment. *Psychiatric Clinics of North America, 36*(4), 517-531. https://doi.org/10.1016/j.psc.2013.08.002

Mushtaq, F., Welke, D., Gallagher, A., Pavlov, Y., Kouara, L., Bosch-Bayard, J., van den Bosch, J., Arvaneh, M., Bland, A., Chaumon, M., Borck, C., He, X., Luck, S., Machizawa, M., Pernet, C., Puce, A., Segalowitz, S., Rogers, C., Awais, M., Babiloni, C., Bailey, N., Baillet, S., Bendall, R., Brady, D., Bringas-Vega, M., Busch, N., Calzada-Reyes, A., Chatard, A., Clayson, P., & Cohen, M. (2024). One hundred years of EEG for brain and behaviour research. *Nature Human Behaviour, 8*(8), 1437-1443. https://doi.org/10.1038/s41562-024-01941-5

Näpflin, M., Wildi, M., & Sarnthein, J. (2007). Test-retest reliability of resting EEG spectra validates a statistical signature of persons. *Clinical Neurophysiology, 118*(11), 2519-2524. https://doi.org/10.1016/j.clinph.2007.07.022

Neda, Z., Ravasz, E., Brechet, Y., Vicsek, T., & Barabasi, A. L. (2000). The sound of many hands clapping. *Nature, 403*, 849-850. https://doi.org/10.1038/35002660

Nelson, H. E. (1982). *National adult reading test (NART): For the assessment of premorbid intelligence in patients with dementia.* NFER-Nelson.

Nelson, H. E., & McKenna, P. (1975). The use of current reading ability in the assessment of dementia. *British Journal of Social and Clinical Psychology, 14*(3), 259-267. https://doi.org/10.1111/j.2044-8260.1975.tb00178.x

Nelson, H. E., & O'Connell, A. (1978). Dementia: The estimation of premorbid intelligence levels using the new adult reading test. *Cortex, 14*(2), 234-244. https://doi.org/10.1016/S0010-9452(78)80049-5

Nelson, H. E., & Willison, J. (1991). *National Adult Reading Test (NART).* NFER-Nelson.

Neto, E., Allen, E. A., Aurlien, H., Nordby, H., & Eichele, T. (2015). EEG spectral features discriminate between Alzheimer's and vascular dementia. *Frontiers in Neurology, 6*, 25. https://doi.org/10.3389/fneur.2015.00025

Neubauer, A. C., Grabner, R. H., Fink, A. & Neuper, C. (2005). Intelligence and neural efficiency: Further evidence of the influence of task content and sex on the brain–IQ

relationship. *Brain Research Cognitive Brain Research, 25*(1), 217–225. https://doi.org/10.1016/j.cogbrainres.2005.05.011

Neubauer, A. C., Grabner, R. H, Freudenthaler, H. H., Beckman, J. F., & Guthke, J. (2004). Intelligence and individual differences in becoming neurally efficient. *Acta Psychologica, 116*, 55-74. https://doi.org/10.1016/j.actpsy.2003.11.005

Neuper, C., & Pfurtscheller, G. (2001). Event-related dynamics of cortical rhythms: Frequency-specific features and functional correlates. *International Journal of Psychophysiology, 43*(1), 41-58. https://doi.org/10.1016/S0167-8760(01)00178-7

Newson, J. J., & Thiagarajan, T. C. (2019). EEG frequency bands in psychiatric disorders: A review of resting state studies. *Frontiers in Human Neuroscience, 12*, 521. https://doi.org/10.3389/fnhum.2018.00521

Obrist, W. D. (1954). The electroencephalogram of normal aged adults. *Electroencephalography and Clinical Neurophysiology, 6*, 235-244. https://doi.org/10.1016/0013-4694(54)90025-5

O'Caoimh, R., Gao, Y., Svendovski, A., Gallagher, P., Eustace, J., & Molloy, D. W. (2017). Comparing approaches to optimise cut-off scores for short cognitive screening instruments in mild cognitive impairment and dementia. *Journal of Alzheimer's Disease, 57*(1), 123-133. https://doi.org/10.3233/JAD-161204

O'Caoimh, R., & Molloy, D. W. (2017). The Quick Mild Cognitive Impairment Screen (Qmci). In A. J. Larner (Ed.), *Cognitive Screening Instruments: A Practical Approach* (pp. 255-272). Springer International Publishing. https://doi.org/10.1007/978-3-319-44775-9_12

O'Carroll, R. (2008). The assessment of premorbid ability: A critical review. *The Neural Basis of Cognition, 1*(1), 83-89. https://doi.org/10.1080/13554799508402350

Ociepka, M., Kalamala, P., & Chuderski, A. (2022). High individual alpha frequency brains run fast, but it does not make them smart. *Intelligence, 92*, 101644. https://doi.org/10.1016/j.intell.2022.101644

Ociepka, M., Kalamala, P., & Chuderski, A. (2023). Take your time: Slow brain rhythms predict fluid intelligence. *Intelligence, 100,* 101780. https://doi.org/10.1016/j.intell.2023.101780

Office for National Statistics. (2024). *National population projections: 2021-based interim.* https://www.ons.gov.uk/peoplepopulationandcommunity/populationandmigration/populationprojections/bulletins/nationalpopulationprojections/2021basedinterim

O'Keefe, J., & Reece, M. L. (1993). Phase relationship between hippocampal place units and the EEG theta rhythm. *Hippocampus, 3*(3), 317-330. https://doi.org/10.1002/hipo.450030307

Olejarczyk, E., Bogucki, P., & Sobieszek, A. (2017). The EEG split alpha peak: Phenomenological origins and methodological aspects of detection and evaluation. *Frontiers in Neuroscience, 11*, 506. https://doi.org/10.3389/fnins.2017.00506

Oostenveld, R., Fries, P., Maris, E., & Schoffelen, J. M. (2011). FieldTrip: Open source software for advanced analysis of MEG, EEG, and invasive electrophysiological data. *Computational Intelligence and Neuroscience, 2011*, 156869. https://doi.org/10.1155/2011/156869

Park, D. C., Polk, T. A., Park, R., Minear, M., Savage, A., & Smith, M. R. (2004). Aging reduces neural specialization in ventral visual cortex. *PNAS, 101*(35), 13091-13095. https://doi.org/10.1073/pnas.0405148101

Park, J., Carp, J., Kennedy, K. M., Rodrigue, K. M., Bischof, G. N., Huang, C-M., Rieck, J. R., Polk, T. A., & Park, D. C. (2014). Neural broadening or neural attenuation? Investigating age-related dedifferentiation in the face network in a large lifespan sample. *The Journal of Neuroscience, 32*(6), 2154-2158. https://doi.org/10.1523/JNEUROSCI.4494-11.2012

Pavlov, Y. G., Adamian, N., Appelhoff, S., Arvaneh, M., Benwell, C. S. Y., Beste, C., Bland, A. R., Bradford, D. E., Bublatzky, F., Busch, N. A., Clayson, P. E., Cruse, D., Czeszumski, A., Dreber, A., Dumas, G., Ehinger, B., Ganis, G., He, X., Hinojosa, J. A., … & Mushtaq, F. (2021). #EEGManyLabs: Investigating the replicability of influential EEG experiments. *Cortex, 144*, 213-229. https://doi.org/10.1016/j.cortex.2021.03.013

Penttilä, M., Partanen, J. V., Soininen, H., & Riekkinen, P. J. (1985). Quantitative analysis of occipital EEG in different stages of Alzheimer's disease. *Electroencephalography and Clinical Neurophysiology, 60*(1), 1-6. https://doi.org/10.1016/0013-4694(85)90942-3

Pesaran, B., Nelson, M. J., & Andersen, R. A. (2008). Free choice activates a decision circuit between frontal and parietal cortex. *Nature, 453*, 406-409. https://doi.org/10.1038/nature06849

Pfurtscheller, G., & Lopes da Silva, F. H. (1999). Event-related EEG/MEG synchronisation and desynchronization: Basic principles. *Clinical Neurophysiology, 110*(11), 1842-1857. https://doi.org/10.1016/S1388-2457(99)00141-8

Pichot, R. E., Henreckson, D. J., Foley, M., & Koen, J. D. (2022). *Neural noise is associated with age-related neural dedifferentiation.* BioRxiv [preprint]. https://doi.org/10.1101/2022.11.17.516990

Picton, T. W. (1992). The P300 wave of the human event-related potential. *Journal of Clinical Neurophysiology, 9*(4), 456-479. https://doi.org/10.1097/00004691-199210000-00002

Pletzer, B., Kerschbaum, H., & Klimesch, W. (2010). When frequencies never synchronise: The golden mean and the resting EEG. *Brain Research, 1335*, 91-102. https://doi.org/10.1016/j.brainres.2010.03.074

Poil, S-S., de Haan, W., van der Flier, W. M., Mansvelder, H. D., Scheltens, P., & Linkenkaer-Hansen, K. (2013). Integrative EEG biomarkers predict progression to Alzheimer's disease at the MCI stage. *Frontiers in Aging Neuroscience, 5*, 58. https://doi.org/10.3389/fnagi.2013.00058

Polich, J. (1996). Meta-analysis of P300 normative ageing studies. *Psychophysiology, 33*(4), 334-353. https://doi.org/10.1111/j.1469-8986.1996.tb01058.x

Polich, J. (1997). EEG and ERP assessment of normal ageing. *Electroencephalography and Clinical Neurophysiology, 104*(3), 244-256. https://doi.org/10.1016/S0168-5597(97)96139-6

Polich, J. (2007). Updating P300: An integrative theory of P3a and P3b. *Clinical Neurophysiology, 118*(10), 2128-2148. https://doi.org/10.1016/j.clinph.2007.04.019

Polich, J., & Criado, J. R. (2006). Neuropsychology and neuropharmacology of P3a and P3b. *International Journal of Psychophysiology, 60*(2), 172-185. https://doi.org/10.1016/j.ijpsycho.2005.12.012

Polich, J., Howard, L., & Starr, A. (1985). Effects of age on the P300 component of the event-related potential from auditory stimuli: Peak definition, variation, and measurement. *Journal of Gerontology, 40*(6), 721-726. https://doi.org/10.1093/geronj/40.6.721

Popa, L. L., Dragos, H., Pantelemon, C. Rosu, O. V., & Strilciuc, S. (2020). The role of quantitative EEG in the diagnosis of neuropsychiatric disorders. *Journal of Medicine and Life, 13*(1). 8-15. https://doi.org/10.25122/jml-2019-0085

Popov, T., Tröndle, M., Baranczuk-Turska, Z., Pfeiffer, C., Haufe, S., & Langer, N. (2023). Test-retest reliability of resting-state EEG in young and older adults. *Psychophysiology*, e14268. Advance online publication. https://doi.org/10.1111/psyp.14268

Popp, F., Dallmer-Zerbe, I., Philipsen, A., & Herrmann, C. S. (2019). Challenges of P300 modulation using transcranial alternating current stimulation (tACS). *Frontiers in Psychology, 10*, 1-14. https://doi.org/10.3389/fpsyg.2019.00476

Porcaro, C., Balsters, J. H., Mantini, D., Robertson, I. H., & Wenderoth, N. (2019). P3b amplitude as a signature of cognitive decline in the older population: An EEG study enhanced by functional source separation. *NeuroImage, 184*, 535-546. https://doi.org/10.1016/j.neuroimage.2018.09.057

Press, W. H., & Teukolsky, S. A. (1990). Savitzky-Golay smoothing filters. *Computers in Physics, 4*(6), 669-672. https://doi.org/10.1063/1.4822961

Prichep, L. S., John, E. R., Ferris, S. H., Rausch, L., Fang, Z., Cancro, R., Torossian, C., & Reisberg, B. (2006). Prediction of longitudinal cognitive decline in normal elderly with subjective complaints using electrophysiological imaging. *Neurobiology of Aging, 27*(3), 471-481. https://doi.org/10.1016/j.neurobiolaging.2005.07.021

Pritchard, W. S. (1992). The brain in fractal time: 1/f-like power spectrum scaling of the human electroencephalogram. *International Journal of Neuroscience, 66*(1-2), 119-129. https://doi.org/10.3109/00207459208999796

Quinn, A. J., Green, G. G. R., & Hymers, M. (2021). Delineating between-subject heterogeneity in alpha networks with Spatio-Spectral Eigenmodes. *NeuroImage, 240*, 118330. https://doi.org/10.1016/j.neuroimage.2021.118330

Rao, C. R. (1972). Estimation of variance and covariance components in linear models. *Journal of the American Statistical Association, 67*(337), 112-115. https://doi.org/10.1080%2F01621459.1972.10481212

Rathee, S., Bhatia, D., Punia, V., & Singh, R. (2020). Peak alpha frequency in relation to cognitive performance. *Journal of Neurosciences in Rural Practice, 11*(3), 416-419. https://doi.org/10.1055/s-0040-1712585

Rego, S. R., Marcolin, M. A., May, G., & Gjini, K. (2012). Effects of transcranial magnetic stimulation on the cognitive event-related potential P300: A literature review. *Clinical EEG and Neuroscience, 43*(4), 285-290. https://doi.org/10.1177/1550059412445657

Rehman, N., & Mandic, D. P. (2010). Multivariate empirical mode decomposition. *Proceedings of the Royal Society A, 466*(2117), 1291-1302. https://doi.org/10.1098/rspa.2009.0502

Reisberg, B., Shulman, M. B., Torossian, C., Leng, L., & Zhu, W. (2010). Outcome over seven years of healthy adults with and without subjective cognitive impairment. *Alzheimer's & Dementia, 6*(1), 11-24. https://doi.org/10.1016/j.jalz.2009.10.002

Reuter-Lorenz, P. A., Marshuetz, C., Jonides, J., Smith, E. E., Hartley, A., & Koeppe, R. (2001). Neurocognitive ageing of storage and executive processes. *European Journal of Cognitive Psychology, 13*(1-2), 257-278. https://doi.org/10.1080/09541440125972

Reuter-Lorenz, P. A., & Park, D. C. (2014). How does it STAC up? Revisiting the scaffolding theory of aging and cognition. *Neuropsychology Review, 24*(3), 355-370. https://doi.org/10.1007/s11065-014-9270-9

Ribary, U., Doesburg, S. M., & Ward, L. M. (2019). Unified principles of thalamocortical network dynamics: A framework for typical/atypical functional connectivity. In S. Supek & C. Aine (Eds.), *Magnetoencephalography* (pp. 1-28). Springer. https://doi.org/10.1007/978-3-030-00087-5_19

Riha, C., Guntensperger, D., Kleinjung, T., & Meyer, M. (2020). Accounting for heterogeneity: Mixed-effects models in resting-state EEG data in a sample of tinnitus sufferers. *Brain Topography, 33*, 413-424. https://doi.org/10.1007/s10548-020-00772-7

Rilling, G., & Flandrin, P. (2008). One or two frequencies? The empirical mode decomposition answers. *IEEE Transactions on Signal Processing, 56*(1), 85-95. https://doi.org/10.1109/TSP.2007.906771

Rinnan, Å., Andersson, M., Ridder, C., & Engelsen, S. B. (2014). Recursive weighted partial least squares (rPLS): An efficient variable selection method using PLS. *Journal of Chemometrics, 28*(5), 439-447. https://doi.org/10.1002/cem.2582

Ritchie, K. (2004). Mild cognitive impairment: An epidemiological perspective. *Dialogues in Clinical Neuroscience, 6*(4), 401-408. https://doi.org/10.31887/DCNS.2004.6.4/kritchie

Ritter, P., & Becker, R. (2009). Detecting alpha rhythm phase reset by phase sorting: Caveats to consider. *NeuroImage, 47*(1), 1-4. https://doi.org/10.1016/j.neuroimage.2009.04.031

Robinson, L., Tang, E., & Taylor, J.P. (2015). Dementia: Timely diagnosis and early intervention. *BMJ*, *350*, h3029. https://doi.org/10.1136/bmj.h3029

Rodriguez-Larios, J., & Alaerts, K. (2019). Tracking transient changes in neural frequency architecture: Harmonic relationships between theta and alpha peaks facilitate cognitive performance. *The Journal of Neuroscience, 39*(32), 6291-6298. https://doi.org/10.1523/JNEUROSCI.2919-18.2019

Salinsky, M. C., Oken, B. S., & Morehead, L. (1991). Test-retest reliability in EEG frequency analysis. *Electroencephalography and Clinical Neurophysiology, 79*(5), 382-392. https://doi.org/10.1016/0013-4694(91)90203-G

Samson-Dollfus, D., & Goldberg, P. (1979). Electroencephalographic quantification by time domain analysis in normal 7--15-year-old children. *Electroencephalography and Clinical Neurophysiology, 46*(2), 147-154. https://doi.org/10.1016/0013-4694(79)90064-6

Sanz-Blasco, R., Ruiz-Sanchez de Leon, J. M., Avila-Villanueva, M., Valenti-Soler, M., Gomez-Ramirez, J., & Fernandez-Blazquez, M. A. (2022). Transition from mild cognitive impairment to normal cognition: Determining the predictors of reversion with multi-state Markov models. *Alzheimer's & Dementia, 18*(6), 1177-1185. https://doi.org/10.1002/alz.12448

Salthouse, T. A. (2010). Selective review of cognitive ageing. *Journal of the International Neuropsychological Society, 16*(5), 754-760. https://doi.org/10.1017/S1355617710000706

Salthouse, T. A. (2016). Little relation of adult age on cognition after controlling general influences. *Developmental Psychology, 52*(10), 1545-1554. https://doi.org/10.1037/dev0000162

Sauseng, P., Klimesch, W., Gruber, W. R., Hanslmayr, S., & Freunberger, R. (2007). Are event-related potential components generated by phase resetting of brain oscillations? A critical discussion. *Neuroscience, 146*(4), 1435-1444. https://doi.org/10.1016/j.neuroscience.2007.03.014

Sayers, B. M., Beagley, H. A., & Henshall, W. R. (1974). The mechanism of auditory evoked EEG responses. *Nature, 247*, 481-483. https://doi.org/10.1038/247481a0

Scally, B., Burke, M. R., Bunce, D., & Delvenne, J-F. (2018). Resting-state EEG power and connectivity are associated with alpha peak frequency slowing in healthy aging. *Neurobiology of Ageing, 71*, 149-155. https://doi.org/10.1016/j.neurobiolaging.2018.07.004

Schaworonkow, N., & Voytek, B. (2021). Longitudinal changes in aperiodic and periodic activity in electrophysiological recordings in the first seven months of life. *Developmental Cognitive Neuroscience, 47*, 100895. https://doi.org/10.1016/j.dcn.2020.100895

Seymour, R. A., Alexander, N. A., Mellor, S., O'Neill, G. C., Tierney, T. M., Barnes, G. R., & Maguire, E. A. (2022). Interference suppression techniques for OPM-based MEG: opportunities and challenges. *NeuroImage, 247*, 118834. https://doi.org/10.1016/j.neuroimage.2021.118834

Shah, A. S., Bressler, S. L., Knuth, K. H., Ding, M., Mehta, A. D., Ulbert, I., & Schroeder, C. E. (2004). Neural dynamics and fundamental mechanisms of event-related brain potentials. *Cerebral Cortex, 14*, 476–483. https://doi.org/10.1093/cercor/bhh009

Sheikh, J. I., & Yesavage, J. A. (1986). Geriatric Depression Scale (GDS): Recent evidence and development of a shorter version. *Clinical Gerontologist: The Journal of Aging and Mental Health, 5*(1-2), 165-173. https://doi.org/10.1300/J018v05n01_09

Siegel, M., Donner, T. H., Oostenveld, R., Fries, P., & Engel, A. K. (2008). Neuronal synchronisation along the dorsal visual pathway reflects the focus of spatial attention. *Neuron, 60*(4), 709-719. https://doi.org/10.1016/j.neuron.2008.09.010

Sims, J. R., Zimmer, J. A., Evans, C. D., Lu, M., Ardayfio, P., Sparks, J., Wessels, A. M., Shcherbinin, S., Wang, H., Nery, E. S. M., Collins, E. C., Solomon, P., Salloway, S., Apostolova, L. G., Hansson, O., Ritchie, C., Brooks, D. A., Mintun, M., & Skovronsky, D. M. (2023). Donanemab in early symptomatic Alzheimer Disease. *JAMA*. Advance online publication. https://doi.org/10.1001/jama.2023.13239

Singer, W. (2018). Neuronal oscillations: Unavoidable and useful? *European Journal of Neuroscience, 48*, 2389-2398. https://doi.org/10.1111/ejn.13796

Snaedal, J., Johannesson, G. H., Gudmundsson, T. E., Blin, N. P., Emilsdottir, A. L., Einarsson, B., & Johnsen, K. (2012). Diagnostic accuracy of statistical pattern recognition of electroencephalogram registration in evaluation of cognitive impairment and dementia. *Dementa and Geriatric Cognitive Disorders, 34*, 51-60. https://doi.org/10.1159/000339996

Soroko, S. I., Shemyakina, N. V., Nagornova, Z. V., & Bekshaev, S. S. (2014). Longitudinal study of EEG frequency maturation and power changes in children on the Russian North. *International Journal of Developmental Neuroscience, 38*(1), 127-137. https://doi.org/10.1016/j.ijdevneu.2014.08.012

Squires, N. K., Squires, K. C., & Hillyard, S. A. (1975). Two varieties of long-latency positive waves evoked by unpredictable auditory stimuli. *Electroencephalography and Clinical Neurophysiology, 38*(4), 387-401. https://doi.org/10.1016/0013-4694(75)90263-1

Stapleton-Kotloski, J. R., Kotloski, R. J., Popli, G., & Godwin, D. W. (2018). Magnetoencephalography: clinical and research practices. *Brain Sciences, 8*(8), 157. https://doi.org/10.3390/brainsci8080157

Stern, Y. (2012). Cognitive reserve in ageing and Alzheimer's disease. *The Lancet: Neurology, 11*(11), 1006-1012. https://doi.org/10.1016/S1474-4422(12)70191-6

Stewart, R. (2012). Subjective cognitive impairment. *Current Opinion in Psychiatry, 25*(6), 445-450. https://doi.org/10.1097/YCO.0b013e3283586fd8

Stroganova, T. A., Orekhova, E. V., & Posikera, I. N. (1999). EEG alpha rhythm in infants. *Clinical Neurophysiology, 110*(6), 997-1012. https://doi.org/10.1016/S1388-2457(98)00009-1

Stolk, A., Todorovic, A., Schoffelen, J-M., & Oostenveld, R. (2013). Online and offline tools for head movement compensation in MEG. *NeuroImage, 68*, 39-48. https://doi.org/10.1016/j.neuroimage.2012.11.047

Sun, H., Paixao, L., Oliva, J. T., Goparaju, B., Carvalho, D. Z., van Leeuwen, K. G., Akeju, O., Thomas, R. J., Cash, S. S., Bianchi, M. T., & Westover, M. B. (2019). Brain age from the electroencephalogram of sleep. *Neurobiology of Aging, 74*, 112-120. https://doi.org/10.1016/j.neurobiolaging.2018.10.016

Surwillo, W. W. (1961). Frequency of the alpha rhythm, reaction time and age. *Nature, 191*, 823-824. https://doi.org/10.1038/191823a0

Sutton, S., Braren, M., Zubin, J., & John, E. R. (1965). Evoked potential correlates of stimulus uncertainty. *Science, 150*(3700), 1187-1188. https://doi.org/10.1126/science.150.3700.1187

Sweeney-Reed, C. M., & Nasuto, S. J. (2007). A novel approach to the detection of synchronisation in EEG based on empirical mode decomposition. *Journal of*

Computational Neuroscience, 23(9), 79-111. https://doi.org/10.1007/s10827-007-0020-3

Sweeney-Reed, C. M., Nasuto, S. J., Vieira, M. F., & Andrade, A. O. (2018). Empirical mode decomposition and its extensions applied to EEG analysis: A review. *Advances in Data Science and Adaptive Analysis, 10*(2), 1840001. https://doi.org/10.1142/S2424922X18400016

Takalo, R., Hytti, H., & Ihalainen, H. (2005). Tutorial on univariate autoregressive spectral analysis. *Journal of Clinical Monitoring and Computing, 19*, 401-410. https://doi.org/10.1007/s10877-005-7089-x

Tales, A., Wilcock, G. K., Phillips, J. E., & Bayer, A. (2014). Is there more to subjective cognitive impairment than meets the eye? A perspective. *Journal of Alzheimer's Diease, 41*, 655-661. https://doi.org/10.3233/jad-132414

Tallon-Baudry, C., & Bertrand, O. (1999). Oscillatory gamma activity in humans and its role in object representation. *Trends in Cognitive Sciences, 3*(4), 151-162. https://doi.org/10.1016/S1364-6613(99)01299-1

Tatum, W. O., Rubboli, G., Kaplan, P. W., Mirsatari, S. M., Radhakrishnan, K., Gloss, D., Caboclo, L. O., Drislane, F. W., Koutroumanidis, M., Schomer, D. L., Trenite, D. K., Cook, M., & Beniczky, S. (2018). Clinical utility of EEG in diagnosing and monitoring epilepsy in adults. *Clinical Neurophysiology, 129*(5), 1056-1082. https://doi.org/10.1016/j.clinph.2018.01.019

Tement, S., Pahor, A., & Jaušovec, N. (2016). EEG alpha frequency correlates of burnout and depression: The role of gender. *Biological Psychology, 114*, 1-12. https://doi.org/10.1016/j.biopsycho.2015.11.005

Thatcher, R. (2012). Coherence, phase differences, phase shift, and phase lock in EEG/ERP analyses. *Developmental Neuropsychology, 37*(6), 476-496. https://doi.org/10.1080/87565641.2011.619241

Trammell, J. P., MacRae, P. G., Davis, G., Bergstedt, D., & Anderson, A. E. (2017). The relationship of cognitive performance and the theta-alpha power ratio is age-dependent: An EEG study of short term memory and reasoning during task and resting-state in healthy young and old adults. *Frontiers in Aging Neuroscience, 9*, 364. https://doi.org/10.3389/fnagi.2017.00364

Trondle, M., Popov, T., Dziemian, S., & Langer, N. (2022). Decomposing the role of alpha oscillations during brain maturation. *eLife, 11*, e77571. https://doi.org/10.7554/eLife.77571

Uriguen, J. A., & Garcia-Zapirain, B. (2015). EEG artefact removal – state-of-the-art and guidelines. *Journal of Neural Engineering, 12*, 031001. https://doi.org/10.1088/1741-2560/12/3/031001

Valdés-Hernández, P. A., Ojeda-González, A., Martínez-Montes, E., Lage-Castellanos, A., Virués-Alba, T., Valdés-Urrutia, L., & Valdes-Sosa, P. A. (2010). White matter architecture rather than cortical surface area correlates with the EEG alpha rhythm. *NeuroImage, 49*(3), 2328-2339. https://doi.org/10.1016/j.neuroimage.2009.10.030

Van Dinteren, R., Arns, M., Jongsma, M. L. A., & Kessels, R. P. C. (2014). P300 development across the lifespan: A systematic review and meta-analysis. *PLoS ONE, 9*(2), e87347. https://doi.org/10.1371/journal.pone.0087347

Van Dyck, C. H., Swanson, C. J., Aisen, P., Bateman, R. J., Chen, C., Gee, M., Kanekiyo, M., Li, D., Reyderman, L., Cohen, S., Froelich, L., Katayama, S., Sabbagh, M., Vellas, B., Watson, D., Dhadda, S., Irizarry, M., Kramer, L. D., & Iwatsubo, T. (2023). Lecanemab in early Alzheimer's disease. *New England Journal of Medicine, 388*(1), 9-21. https://doi.org/10.1056/nejmoa2212948

Van den Broek, S. P., Reinders, F., Donderwinkel, M., & Peters, M. J. (1998). Volume conduction effects in EEG and MEG. *Electroencephalography and Clinical Neurophysiology, 106*(6), 522-534. *https://doi.org/10.1016/S0013-4694(97)00147-8*

Vecchio, F., & Maatta, S. (2011). The use of auditory event-related potentials in Alzheimer's disease diagnosis. *International Journal of Alzheimer's Disease, 2011*, 1-7. https://doi.org/10.4061/2011/653173

Von Stein, A., & Sarnthein, J. (2000). Different frequencies for different scales of cortical integration: From local gamma to long range alpha/theta synchronization. *International Journal of Psychophysiology, 38*(3), 301-313. https://doi.org/10.1016/S0167-8760(00)00172-0

Voytek, B., Kramer, M. A., Case, J., Lepage, K. Q., Tempesta, Z. R., Knight, R. T., & Gazzaley, A. (2015a). Age-related changes in 1/f neural electrophysiological noise. *Journal of Neuroscience, 35*(38), 13257-13265. https://doi.org/10.1523/JNEUROSCI.2332-14.2015

Voytek, B., & Knight, R. T. (2015b). Dynamic network communication as a unifying neural basis for cognition, development, aging, and disease. *Biological Psychiatry, 77*(12), 1089-1097. https://doi.org/10.1016/j.biopsych.2015.04.016

Vrba, J., Robinson, S. E. (2001). Signal processing in magnetoencephalography. *Methods, 25*(2), 249-271. https://doi.org/10.1006/meth.2001.1238

Vysata, O., Kukal, J., Prochazka, A., Pazdera, L., & Valis, M. (2012). Age-related changes in the energy and spectral composition of EEG. *Neurophysiology, 44*(1), 63-67. https://doi.org/10.1007/s11062-012-9268-y

Wackermann, J., & Matoušek, M. (1998). From the 'EEG age' to a rational scale of brain electric maturation. *Electroencephalography and Clinical Neurophysiology, 107*(6), 415-421. https://doi.org/10.1016/S0013-4694(98)00090-X

Wagenmakers, E-J., Wetzels, R., Borsboom, D., & van der Maas, H. L. J. (2011). Why psychologists must change the way they analyse their data: The case of Psi: Comment on Bem (2011). *Journal of Personality and Social Psychology, 100*(3), 426-432. https://psycnet.apa.org/doi/10.1037/a0022790

Walhovd, K. B., Rosquist, H., & Fjell, A. M. (2008). P300 amplitude age reductions are not caused by latency jitter. *Psychophysiology, 45*(4), 545-553. https://doi.org/10.1111/j.1469-8986.2008.00661.x

Wechsler, D. (2008). *Wechsler Adult Intelligence Scale (4th Ed.).* Pearson Assessment.

Weiner, M. W., Veitch, D. P., Miller, M. J., Aisen, P. S., Albala, B., Beckett, L. A., Green, R. C., Harvey, D., Jack Jr, C. R., Jagust, W., Landau, S. M., Morris, J. C., Nosheny, R., Okonkwo, O. C., Perrin, R. J., Petersen, R. C., Rivera-Mindt, M., Saykin, A. J., Shaw, L. M., … Trojanowski, J. Q. (2022). Increasing participant diversity in AD research: Plans for digital screening, blood testing, and a community-engaged approach in the Alzheimer's Disease Neuroimaging Initiative 4. *Alzheimer's & Dementia, 19*(1), 307-317. https://doi.org/10.1002/alz.12797

Welch, P. (1967). The use of fast Fourier transform for the estimation of power spectra: A method based on time averaging over short, modified periodograms. *IEEE Transactions on Audio and Electroacoustics, 15*(2), 70-73. https://doi.org/10.1109/TAU.1967.1161901

Widmann, A., Schroger, E., & Maess, B. (2015). Digital filter design for electrophysiological data – a practical approach. *Journal of Neuroscience Methods, 250*, 34-46. https://doi.org/10.1016/j.jneumeth.2014.08.002

Wold, S., Sjöström, M., & Eriksson, L. (2001). PLS-regression: A basic tool of chemometrics. *Chemometrics and Intelligent Laboratory Systems, 58*(2), 109-130. https://doi.org/10.1016/S0169-7439(01)00155-1

Woodman, G.F. (2010). A brief introduction to the use of event-related potentials (ERPs) in studies of perception and attention. *Attention and Perceptual Psychophysiology, 72*, 2031-2046. https://doi.org/10.3758/BF03196680

Woolnough, O., Forseth, K. J., Rollo, P. S., Roccaforte, Z. J., & Tandon, N. (2022). Event-related phase synchronisation propagates rapidly across human ventral visual cortex. *NeuroImage, 256*, 119262. https://doi.org/10.1016/j.neuroimage.2022.119262

Wu, Z., & Huang, N. E. (2009). Ensemble empirical mode decomposition: A noise-assisted data analysis method. *Advances in Adaptive Data Analysis, 1*, 1–41. https://doi.org/10.1142/S1793536909000047

Yesavage, J. A., Brink, T. L., Rose, T. L., Lum, O., Huang, V., Adey, M., & Leirer, V. O. (1983). Development and validation of a geriatric depression screening scale: A preliminary report. *Journal of Psychiatric Research, 17*(1), 37-49. https://doi.org/10.1016/0022-3956(82)90033-4

Yeung, N., Bogacz, R., Holroyd, C. B., & Cohen, J. D. (2004). Detection of synchronised oscillations in the electroencephalogram: An evaluation of methods. *Psychophysiology, 41*(6), 822-832. https://doi.org/10.1111/j.1469-8986.2004.00239.x

Yue, L., Hu, D., Zhang, H., Wen, J., Wu, Y., Li, W., Sun, L., Li, X., Wang, J., Li, G., Wang, T., Shen, D., & Xiao, S. (2021). Prediction of 7-year's conversion from subjective cognitive decline to mild cognitive impairment. *Human Brain Mapping, 42*(1), 192-203. https://doi.org/10.1002/hbm.25216

Zhadin, M. N. (1984). Rhythmic processes in the cerebral cortex. *Journal of Theoretical Biology, 108*(4), 565-595. https://doi.org/10.1016/S0022-5193(84)80080-6

Zhou, P., Wu, Q., Zhan, L., Guo, Z., Wang, C., Wang, S., Yang, Q., Lin, J., Zhang, F., Liu, L., Lin, D., Fu, W., & Wu, X. (2023). Alpha peak activity in resting-state EEG is associated with depressive score. *Frontiers in Neuroscience, 17*, 1057908. https://doi.org/10.3389/fnins.2023.1057908